Formation and preservation of abiotic organic signatures vs. lipid biomarkers — experimental studies in preparation for the ExoMars 2020 mission

Dissertation

zur Erlangung des mathematisch-naturwissenschaftlichen Doktorgrades

"Doctor rerum naturalium"

der Georg-August-Universität Göttingen

im Promotionsprogramm Geowissenschaften

der Georg-August University School of Science (GAUSS)

vorgelegt von

Helge Mißbach

aus Salzgitter

Göttingen, 2018

"Non est ad astra mollis e terris via"

"There is no easy way from the Earth to the stars"

Seneca the Younger

Preface

This cumulative thesis comprises 5 individual scientific contributions in the form of published articles or prepared manuscripts (Chapters 2 to 6). These contributions are accompanied by an introductory chapter, a general discussion focusing on implications of the results for the ExoMars mission, and a summary outlining the main conclusions of this work (Chapters 1, 7 and 8, respectively).

The following published articles and prepared manuscripts form a part of this thesis (corresponding author marked with *):

Mißbach, H.*, Duda, J.-P., Lünsdorf, N.K., Schmidt, B.C., Thiel, V. (2016). Testing the preservation of biomarkers during experimental maturation of an immature kerogen. *International Journal of Astrobiology* 15, 3, 165–175. (Chapter 2 of this thesis)
Own contribution: Data evaluation, writing of the manuscript.

Mißbach, H.*, Schmidt, B.C., Duda, J.-P., Lünsdorf, N.K., Goetz, W., Thiel, V. (2018). Assessing the diversity of lipids formed via Fischer–Tropsch-type reactions. *Organic Geochemistry* 119, 110–121. (Chapter 3 of this thesis)
Own contribution: Design and implementation of experiments; preparation and analysis of samples; data evaluation; writing of the manuscript.

Duda, J-P.*, Thiel, V., Bauersachs, T., **Mißbach, H.**, Reinhardt, M., Schäfer, N., Van Kranendonk, M.J., Reitner, J. (2018). Ideas and perspectives: hydrothermally driven redistribution and sequestration of early Archaean biomass – the "hydrothermal pump hypothesis". *Biogeosciences* 15, 5, 1535–1548. (Chapter 4 of this thesis)
Own contribution: Implementation of Fischer–Tropsch-type synthesis including sample preparation, GC–MS analyses and data evaluation; proofreading the entire manuscript.

Goesmann, F., Brinckerhoff, W.B., Raulin, F., Goetz, W.*, Danell, R.M., Getty, S.A., Siljeström, S., **Mißbach, H.** et al. (2017) The Mars Organic Molecule Analyzer (MOMA) Instrument: Characterization of Organic Material in Martian Sediments. *Astrobiology* 17, 6–7, 655–685. (Chapter 5 of this thesis)
Own contribution: Design and performance of MOMA-like GC–MS analyses; data evaluation; writing of Section 7.5 "Test experiments on GC–MS prototype system: A case study" (corresponding to Section 5.7.5 of this thesis); proofreading the entire manuscript.

Mißbach, H.*, Steininger, H., Thiel, V., Goetz, W. (in preparation). Investigating the effect of perchlorate on flight-like gas chromatography–mass spectrometry as performed by MOMA onboard the ExoMars 2020 rover. To be submitted to *Icarus*. (Chapter 6 of this thesis)
Own contribution: Sample preparation; design and implementation of the experiments; data evaluation; writing of the manuscript.

Please note that minor language and stylistic features of individual contributions were adapted to the overall style of the thesis.

Abstract

Molecular organic biomarkers have widely been used to track life through Earth's history, and they became increasingly important in the search of potential (remnants of) life on Mars. The Mars Organic Molecule Analyzer (MOMA) instrument will be the key instrument onboard the ExoMars rover (launch in 2020), with the goal to characterize the organic inventory of martian sediments/rocks and the search for signs of life in the form of organic biomarkers. However, this task is potentially facing a series of problems and challenges including, for example, the degradation of organic biomarkers (e.g., by UV and/or particle radiation, thermal stress); mixing of biologically with abiotically derived organic matter (e.g., from meteorites/comets, abiotic synthesis) which requires careful source discrimination; limited capabilities of in situ gas chromatography–mass spectrometry (GC–MS) techniques (as used by MOMA) compared to conventional bench-top methods; the presence of perchlorates in martian soils which can lead to degradation of organic molecules upon heating. Therefore, pre-flight tests and experiments with analog materials can help to enhance the later evaluation of potential biosignatures.

This thesis combines a series of mainly experimental studies aimed at (i) assessing the diversity of biomarker-like lipids from abiotic Fischer–Tropsch-type (FTT) synthesis, (ii) determining the impact of thermal stress on biologically and abiotically derived lipids, (iii) providing reference data to differentiate between biologically and abiotically synthesized lipids in sediments and rocks and (iv) identifying analytical limitations and potential pitfalls of MOMA GC–MS techniques.

In the first study, experimental maturation in gold capsules (300/400 °C, 2 kbar, $2-2400$ h) was performed on isolated kerogen from the Eocene Green River formation to determine the impact of thermal maturation on biological n-alkane distribution patterns and selected lipid biomarkers (pristane, phytane, steranes, hopanes, cheilanthanes). The study revealed major differences in their thermal degradation behavior. Furthermore, it was demonstrated that n-alkane distribution patterns and respective biomarkers withstand thermal maturation at 300 °C for 2400 h, while they quickly degraded at 400 °C (< 48 h, corresponding to a vitrinite reflectance of 1.83% R_O).

The second study addressed abiotic FTT synthesis which yielded a variety of solvent extractable biomarker-like lipids (e.g., linear and methyl-branched alkanes and alkanols, n-alkanoic acids). These showed a unimodal distribution of homologous compounds in contrast to uneven distributions of biologically derived lipids. Thus, a discrimination of abiotically (FTT synthesis) and biologically derived lipids based on their primary distributions is principally possible. However, primary distributions change in the course of thermal maturation which can complicate lipid source discrimination.

In the third study, kerogen from an Archean hydrothermal chert vein (~ 3.5 Ga Dresser Formation, Pilbara Craton, Western Australia) was investigated. Organic matter, cracked from the kerogen via catalytic hydropyrolysis revealed n-alkane homologs with a distinct decrease $> n$-C_{18}. The same n-alkane pattern was observed in recent bacterial biomass from *Anabaena cylindrica*, whereas abiotically derived organics from FTT reactions show unimodal distributions. Based on these observations, a biological origin of the kerogen was inferred. This is furthermore consistent with a low $\delta^{13}C_{TOC}$ value of -32.8 ± 0.3 ‰ and stable carbon isotope values of n-alkanes ranging from -29.4 ‰ to -33.3 ‰.

Moreover, case studies using MOMA-like GC–MS techniques were carried out to test the applicability to different sample types and to assess the impact of perchlorates on these techniques. The studies included pyrolysis, in situ derivatization and thermochemolysis GC–MS analyses on a synthetic and a natural sample with and without Mg-perchlorate (0 wt%, 1 wt%, 10 wt%). It was demonstrated that not every MOMA-like GC–MS technique is applicable to every sample type or organic compound class. For example, pyrolysis was largely affected by perchlorates, while thermochemolysis with tetramethylammonium hydroxide (TMAH) appears to be perchlorate resistant. This underlines that perchlorates in martian soils do not necessarily hamper MOMA-like GC–MS analysis.

Finally, it was demonstrated that the discrimination of biologically from abiotically derived organic materials is principally possible with MOMA-like GC–MS techniques. However, advantages and disadvantages of each technique must be carefully weighed up and complementary analyses of a given sample using different techniques should be considered to minimize method dependent biases. Nonetheless, these studies emphasize that MOMA is principally able to detect potential biomarkers in martian soil or rock samples.

iv

Kurzfassung

Die Analyse organischer Biomarker ist ein wichtiges Werkzeug bei der Rekonstruktion früherer Lebewelten auf der Erde. In den letzten Jahrzehnten hat sich ihr Anwendungsbereich auch auf extraterrestrische Systeme ausgeweitet, so zum Beispiel auf die Suche nach Spuren von Leben auf dem Mars. Das *Mars Organic Molecule Analyzer* (MOMA) Instrument bildet das Hauptinstrument auf dem ExoMars rover, welcher 2020 zum Mars starten wird. MOMAs Aufgabe liegt darin, organische Moleküle im Marsboden oder Gestein zu identifizieren und nach potentiellen Spuren von Leben in Form von organischen Biomarkern zu suchen. Allerdings kann diese durch einige Probleme und Herausforderungen behindert werden, zum Beispiel durch: Zerstörung organischer Biomarker durch UV/kosmische Strahlung oder thermische Prozesse; Vermischung biologischer mit nicht biologischer Organik, z.B. aus Meteoriten/Kometen oder abiotischer Synthese, was eine sorgfältige Unterscheidung erforderlich macht; technische Einschränkungen bei der Analyse organischer Stoffe mittels MOMA Gas Chromatographie–Massenspektrometrie (GC–MS) im Vergleich zur Analyse mit konventionellen Laborverfahren; Perchlorate im Marsboden, die zur Zerstörung organischer Moleküle während der Analyse führen können. Daher ist es wichtig, vorhergehende Teststudien und Experimente durchzuführen, um dadurch die spätere Einordnung potentieller Biosignaturen zu erleichtern.

Diese Arbeit umfasst mehrere überwiegend experimentelle Studien, die darauf abzielten, (i) die Vielfalt biomarkerähnlicher Lipide aus abiotischer Synthese ("Fischer–Tropschtype"; FTT) zu erfassen, (ii) den Einfluss thermischer Reifung auf biotische und abiotische Lipide zu ermitteln, (iii) Referenzdaten zur Unterscheidung biotischer und abiotischer Lipide in Sedimenten und Gesteinen zu erzeugen und (iv) mögliche analytische Limitierungen und Fehlerquellen bei der Nutzung von MOMA GC–MS Techniken zu identifizieren.

Die erste Studie beschäftigte sich mit dem Einfluss thermischer Reifung auf biologische *n*-Alkan Verteilungsmuster und bestimmte Lipid-Biomarker (Pristan, Phytan, Sterane, Hopane, Cheilanthane). Dafür wurde isoliertes Kerogen aus Gestein der Eozänen Green River Formation einer experimentellen thermischen Reifung unterzogen (300/ 400 °C, 2 kbar, 2 – 2400 h). Die Ergebnisse zeigten große Unterschiede im Erhaltungspotential der Lipid-Biomarker auf. Außerdem wurde dargelegt, dass *n*-Alkan Verteilungsmuster sowie die genannten Biomarker eine thermische Reifung bei 300 °C für 2400 h überstehen, während sie bei 400 °C schnell zerstört werden ($<$ 48 h, dies entspricht einer Vitrinitreflexion von 1.83% R_O).

Die zweite Studie behandelte die abiotische FTT Synthese. Die Experimente führten zu einer Reihe von lösungsmittelextrahierbaren, biomarkerähnlichen Lipiden (zum Beispiel lineare und Methyl-verzweigte Alkane und Alkanole, *n*-Alkansäuren). Diese zeigten eine unimodale Verteilung, im Gegensatz zu ungleichmäßigen Verteilungsmustern von Lipiden aus biologischer Quelle. Somit ist eine Unterscheidung von abiotischen und biotischen Lipiden anhand ihrer primären Verteilungsmuster prinzipiell möglich. Jedoch können diese primären Verteilungen homologer Komponenten durch thermische Reifung verändert werden, was eine genaue Feststellung ihrer Herkunft erschweren kann.

In der dritten Studie wurde Kerogen aus der $\sim$ 3,5 Ga alten Dresser Formation (Pilbara Kraton, Westaustralien) untersucht. Dieses stammte aus einem hydrothermalen Gang, der

überwiegend aus Chert besteht. Mittels katalytischer Hydropyrolyse wurden n-Alkane aus dem Kerogen gewonnen. Diese wiesen ein ungleichmäßiges Verteilungsmuster mit einer markanten Verringerung der Intensität von n-Alkanen $> n$-C_{18} auf. Untersuchungen von Bakterien (*Anabaena cylindrica*) mit gleichen Verfahren ergaben das gleiche Verteilungsmuster. Im Gegensatz dazu zeigten abiotische organische Komponenten aus der FTT Synthese eine unimodale Verteilung. Aus diesen Beobachtungen wurde eine biologische Herkunft des Kerogens abgeleitet. Niedrige $\delta^{13}C_{TOC}$ Werte von -32.8 ± 0.3 ‰ und ebenfalls niedrige $\delta^{13}C$ Isotopenwerte der n-Alkane (zwischen -29.4 ‰ und -33.3 ‰) stimmen mit dieser Interpretation überein.

Außerdem wurden mehrere Analogstudien mit MOMA GC–MS Techniken durchgeführt, um ihre generelle Anwendbarkeit für verschiedene Probenarten zu testen und den Einfluss von Perchloraten auf die Analyse zu ermitteln. Dafür wurden eine synthetische und eine natürliche Probe mit und ohne Perchlorat (0 wt%, 1 wt%, 10 wt%) durch MOMA Pyrolyse, in situ Derivatisierung und Thermochemolyse GC–MS Verfahren analysiert. Die Ergebnisse zeigten, dass nicht jede dieser Techniken uneingeschränkt für jede Probenart geeignet ist. Die Pyrolyse wurde zum Beispiel stark durch Perchlorate in den Proben beeinflusst, während bei der Thermochemolyse mit Tetramethylammoniumhydroxid (TMAH) kein Effekt erkennbar war. Dies macht deutlich, dass MOMA GC–MS Analysen nicht unbedingt von Perchloraten in Marsböden behindert werden.

Abschließend wurde aufgezeigt, dass die Unterscheidung biotischer von abiotischer Organik durch MOMA GC–MS möglich ist. Allerdings sollten komplementäre Analysen gleicher Proben durch unterschiedliche Techniken in Erwägung gezogen werden, um umfassende Erkenntnisse über die jeweilige Probe zu erhalten. Insgesamt jedoch untermauern diese Studien, dass MOMA prinzipiell in der Lage sein wird, potentielle organische Biomarker in Marsböden oder Gesteinen zu erkennen.

Contents

List of Figures

List of Tables

Introduction

1.1 Aim of the thesis

This work was organized within the scope of the Mars Organic Molecule Analyzer (MOMA) project. MOMA will be the key instrument onboard the ExoMars rover which is planned to launch in 2020. The main goal of the ExoMars rover mission is to search for biosignatures and therefore, traces of life on the surface of Mars (Vago et al., 2017). Experimental studies and pre-flight tests with analog materials provide the groundwork which is needed for later evaluation of potential biosignatures.

This project was aimed at:

- Assessing the diversity of biomarker-like lipids from abiotic Fischer–Tropsch-type (FTT) synthesis

- Determining the impact of thermal stress on biologically and abiotically (FTT) produced lipids

- Providing reference data to differentiate between biologically and abiotically synthesized lipids in sediments and rocks

- Identifying analytical limitations and potential pitfalls of MOMA gas chromatography–mass spectrometry (GC–MS) techniques

The results of this project form an important prerequisite to facilitate MOMA data interpretation.

1.2 Life on Earth, and beyond? Background and basic definitions

Life is present in a great variety and complexity almost everywhere on Earth today. Despite recent advances in technology, the distribution and diversity of life as well as its impact on the Earth's system is still poorly understood. The same applies to the reconstruction of environmental conditions and the emergence of life on early Earth, which is further hampered by the sparse geological record (Sleep, 2010; see also Section 1.3).

There are many definitions for life as we know it (that is carbon based), often focusing on different properties or processes, but none of which are widely applied (Schulze-Makuch and Irwin, 2008; Westall and Brack, 2018). More recent definitions are:

> "[...]*'life' –in the broad sense of the term – is a complex collective network made out of self-reproducing autonomous agents whose basic organization is instructed by material records generated through the evolutionary-historical process of that collective network.*" (Ruiz-Mirazo et al., 2004, p. 339)

> "[...], *life is a coded and organized entropy generator that can search and evolve to find further appropriate potential energies and materials*" (Russell, 2011, p. 701).

More generally, life or living entities can be defined as self-organizing systems that are more or less isolated from, and in disequilibrium with their surroundings, transform energy, retain a low entropy, and can encode information and transmit it via replication (Schulze-Makuch and Irwin, 2008).

Some basic requirements for life are appropriate temperature conditions (~ -20 to 120 °C; Clarke, 2014), energy sources (e.g., light, chemical energy, energy-rich compounds), the availability of certain elements and nutrients (e.g., C, H, N, O, P, S) and liquid water (Follmann and Brownson, 2009; Cockell et al., 2016; Westall and Brack, 2018). On today's Earth, both energy and bio-essential elements are mainly sourced by the constant interaction between minerals/rocks and fluids (particularly liquid water). Therefore, these processes are also considered important for (the origin of) life (Westall and Brack, 2018).

Life's requirements define the "habitability" of environments. A recent definition by Cockell et al. (2016, p. 90) for a habitable environment is:

> "[...] *'an environment capable of supporting the activity of at least one known organism', where 'activity' (and thus 'living') is metabolic activity allowing for survival, maintenance, growth, or reproduction.*"

In other words, "habitable" does not necessarily imply that life is actually present, even though all the requirements for its existence are fulfilled (Cockell, 2014; Cockell et al., 2016). Following the definition above, (early) Mars and also other planetary bodies in our solar system (e.g., Enceladus, Europa, Titan) are considered habitable. For this reason, they have become targets for exobiological investigations (Chyba and Phillips, 2001; McKay and Smith, 2005; Raulin, 2007; Cockell, 2014; McKay et al., 2014). In search of life on Mars, the early Earth is commonly used as an analog, as environmental conditions in the early history of both planets (Hadean – Archean; pre-Noachian – Hesperian; see Fig. 1.1 for a definition of these time periods) are thought to have been similar on a regional scale (McKay, 2010; Westall et al., 2015; see also Sections 1.3 and 1.4).

1.3 Early Earth

1.3.1 Crustal evolution

The geological record of the early Earth is scarce. Soon after the proto-Earth was accreted, it collided with a Mars-sized object, leading to the formation of the Moon ~ 4.45 Ga ago (Zahnle et al., 2007; Jacobson et al., 2014; see also Fig. 1.1). After the collision, the Earth had a well mixed magma ocean from which a mafic proto-crust was probably formed by ~ 4.4 Ga (Zahnle et al., 2007; Van Kranendonk et al., 2012; Valley et al., 2014; Kamber, 2015). This age corresponds to the age of the oldest dated detrital zircons found in Archean rocks from the Jack Hills greenstone belt, Yilgarn Craton, Australia (Froude et al., 1983; Wilde et al., 2001; Valley et al., 2014; see also Figs. 1.1, 1.2). The first crust probably had high recycling rates and was episodically melted by impacts so that the overall preservation potential was very low (Kamber et al., 2003; Zahnle et al., 2007;
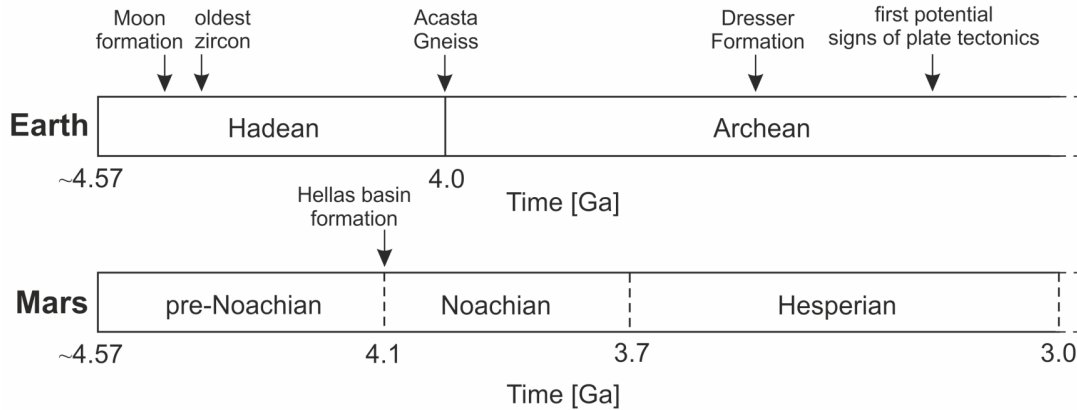
Figure 1.1: Major time periods and events on early Earth and Mars. The Hadean–Archean boundary is marked by the age of the oldest rocks on Earth (Acasta Gneiss, Slave Craton, Canada; Bowring and Williams, 1999; Van Kranendonk et al., 2012; Mojzsis et al., 2014). Other ages: Moon formation ~ 4.45 Ga (Jacobson et al., 2014); oldest zircon, Jack Hills greenstone belt, Yilgarn Craton, Australia, 4.374 Ga (Valley et al., 2014); Dresser Formation, Pilbara Craton, Australia, ~ 3.49 Ga (Van Kranendonk, 2006); first potential signs of plate tectonics, $\sim 3.2-3.0$ Ga (Heubeck and Lowe, 1994; Van Kranendonk, 2010; Van Kranendonk et al., 2010, 2012). Boundaries of the Noachian and Hesperian periods are estimated, largely based on crater counting (Hartmann and Neukum, 2001; Carr and Head, 2010).

Van Kranendonk et al., 2012; Kamber, 2015). Additionally, a complete mantle overturn in the Hadean could have led to an overall exchange of the first crust (Griffin et al., 2014; Kamber, 2015).

The oldest crustal remains and also the oldest dated rocks on Earth are from the Acasta Gneiss complex, Slave Craton, Canada (~ 4 Ga, Hadean–Archean boundary, Figs. 1.1 and 1.2; Bowring and Williams, 1999; Mojzsis et al., 2014). Well preserved Paleoarchean crustal remains were found in the Pilbara Craton (Australia) and the Kaapvaal Craton (South Africa) with an age of $3.5-3.2$ Ga (Fig. 1.2). They mainly consist of mafic to ultramafic rocks with bits of felsic rocks, cherts and some clastic sedimentary rocks (Van Kranendonk et al., 2012). Overall, the preservation potential of the Archean crust increased compared to the Hadean, due to a stabilization of the lithosphere at the Hadean–Archean boundary and a formation of cratonic nuclei (Kamber, 2015). Extensive volcanism and volcanic resurfacing were common in the Archean (Kamber, 2010; Van Kranendonk, 2010; Kröner et al., 2013). Whether plate tectonics were already present in the (early) Archean is under debate (see review by Korenaga, 2013). Locally restricted plate tectonics could have commenced between 3.2 and 3.0 Ga (Heubeck and Lowe, 1994; Van Kranendonk, 2010; Van Kranendonk et al., 2010, 2012; see also Fig. 1.1).

1.3.2 Volatiles and climate

At least a part of the volatiles on Earth (including water and carbon compounds) were probably delivered by small bodies (i.e., comets or meteorites), possibly until the late Hadean/early Archean (Chyba, 1990; Morbidelli et al., 2000; Botta and Bada, 2002; Zahnle et al., 2007; Shaw, 2008; Altwegg et al., 2014; Marty et al., 2016). On the other

Figure 1.2: Schematic map showing localities of some of the oldest rocks on Earth. (1) Slave Craton, (2) Nuvvuagittuq belt and (3) Saglek Block, Canada; (4) Itsaq Gneiss Complex (including the Isua supracrustal belt), Greenland; (5) Kaapvaal Craton, South Africa; (6) Pilbara Craton and (7) Yilgarn Craton, Western Australia.

hand, early Earth also lost part of its volatiles due to mixing of the magma ocean, outgassing and impact events prior to 4 Ga (Nisbet and Sleep, 2001; Shaw, 2008). Within millions of years after the Moon forming impact, a first ocean could have formed from condensation of water vapour (Zahnle, 2006; Elkins-Tanton, 2011). The early ocean's water temperature would have been largely controlled by endogenic heating and the atmospheric composition, further influenced by volcanic/hydrothermal activity and impacts (Nisbet and Sleep, 2001; Zahnle, 2006).

In the long term, a warm climate was necessary to maintain liquid water on Earth. Problematically, the Sun's luminosity was too low in Earth's early history (only 70 % of today's value; Gough, 1981) to deliver enough energy ("faint-young-Sun paradox"; Kasting, 1993; Nisbet and Sleep, 2001; Sagan and Chyba, 1997; Feulner, 2012). To counteract this, the greenhouse effect of the early Earth's atmosphere had to be stronger and/or the albedo had to be lower (Kasting, 1993; Shaw, 2008; Rosing et al., 2010). In this context, a massive CO_2 greenhouse was suggested as a solution to maintain warm surface temperatures (Walker et al., 1981; Hessler et al., 2004; Shaw, 2008, and references therein). However, atmospheric CO_2 contents might not have been high enough due to removal by weathering processes (e.g., reaction of basalt with CO_2 followed by carbonate formation; Sleep and Zahnle, 2001; Zahnle, 2006) but geological evidence of this is scarce (Shaw, 2008).

It has been suggested that other gas components, such as higher amounts of H_2 and N_2 (Wordsworth and Pierrehumbert, 2013), or even methane (Pavlov et al., 2000; Lazar et al., 2012), could have principally led to greenhouse warming. Methane could have been produced in hydrothermal systems (Etiope and Sherwood Lollar, 2013; Konn et al., 2015; Etiope et al., 2016), with the contribution of H_2 and catalyzing minerals from serpentinization (i.e., the interaction of fluids with mafic rocks/minerals at elevated temperatures and pressures, see equation 3.1 as an example; Berndt et al., 1996; Sleep et al., 2004; McCollom and Bach, 2009; Russell et al., 2010; Lazar et al., 2012). There is plenty of evidence that hydrothermal activity was still wide-ranging in the Archean due to the presence of

liquid water and high volcanic activity (Baross and Hoffman, 1985; Hofmann, 2011; Van Kranendonk et al., 2012; Djokic et al., 2017; Westall and Brack, 2018; Chapter 4 of this thesis).

1.3.3 Emergence of life

The oldest suggested remnants of life (≥ 3.7 Ga) were found in Greenland and Canada (e.g., Isua supracrustal belt, Nuvvuagittuq belt, Saglek block; see Fig. 1.2) in the form of carbon isotopic fingerprints, microbial structures and microfossils (Schidlowski et al., 1979; Schidlowski, 2001; Nutman et al., 2016; Dodd et al., 2017; Hassenkam et al., 2017; Tashiro et al., 2017), but all of these remain controversial. First widely accepted evidence for biological activity (stromatolites, microfossils, molecular organic biosignatures) were found in Archean rocks of the Pilbara Craton in Australia (e.g., 3.49 Ga Dresser Formation and ~ 3.4 Ga Strelley Pool Formation; Walter et al., 1980; Lowe, 1980; Van Kranendonk, 2006; Marshall et al., 2007; Van Kranendonk et al., 2008; Sugitani et al., 2010; Duda et al., 2016; Chapter 4 of this thesis; see also Figs. 1.1 and 1.2) and in the Barberton greenstone belt, Kaapvaal Craton, South Africa (e.g., ~ 3.2 Ga Moodies group; Noffke et al., 2006; Heubeck, 2009; Homann et al., 2015). Following Darwinistic reasoning, the origin of life has to predate these first instances. However, it remains unclear when life actually emerged on Earth which is at least partially due to the scarce geological record and the vague definition of life (see Section 1.2). It is considered that the first important steps could have happened in the late Hadean, as there, potentially, was liquid water (in oceans), all the necessary molecular ingredients and enough energy (Blair Hedges, 2002; Bada, 2004; Pascal et al., 2006; Pearce et al., 2017; Westall and Brack, 2018).

Organic molecules considered important for the formation of life (e.g., amino acids, fatty acids, acetic acid) could have been delivered to Earth via meteorites, comets or interplanetary dust particles (Chyba and Sagan, 1992; Ehrenfreund and Charnley, 2000; Deamer et al., 2002; Dass et al., 2016, and references therein). Another possibility could have been the in situ production of these molecules on Earth via abiotic synthesis (Bada, 2004; Follmann and Brownson, 2009; Dass et al., 2016). This could have happened through electrical discharge in the atmosphere (Miller, 1953, 1955; Bada, 2013) or reactions on catalytic surfaces related to hydrothermal activity in the early water bodies, like for example carbon fixation (Huber and Wächtershäuser, 1997) or Fischer–Tropsch-type (FTT) synthesis (Fischer, 1935; Shock and Schulte, 1998; McCollom et al., 1999; Holm and Charlou, 2001; McCollom and Seewald, 2007; Proskurowski et al., 2008; Chapter 3 of this thesis; see also reviews covering prebiotic chemistry by Follmann and Brownson, 2009; Dass et al., 2016).

Many different models exist on how life formed, ranging from life directly evolving from simple molecules (e.g., CO_2, CO) via a series of autocatalytic reactions, to continuous polymerization and finally (spontaneous) replication in a "prebiotic soup" (Bada, 2004; Follmann and Brownson, 2009; Dass et al., 2016). In any case, an initial accumulation of organic molecules is considered necessary for further reactions (Deamer et al., 2002; Pascal et al., 2006; Martin et al., 2008; Westall et al., 2013; Deamer and Georgiou, 2015; Westall and Brack, 2018). Different accumulation mechanisms are discussed, for example:

- temperature gradients in the pores of hydrothermal vent systems which can serve as

small reaction chambers with reactive surfaces (Baross and Hoffman, 1985; Braun and Libchaber, 2004; Baaske et al., 2007; Martin et al., 2008; Budin et al., 2009; Westall et al., 2013)

- adsorption to mineral surfaces (e.g., iron-sulfur or clay minerals) that potentially also promote polymerization reactions (Paecht-Horowitz, 1976; Wächtershäuser, 1988; Russell et al., 1994; Ferris et al., 1996; Huber and Wächtershäuser, 1997; Russell and Hall, 1997; Orgel, 1998; Hanczyc et al., 2003; Ferris, 2005; Brasier et al., 2011; Cleaves II et al., 2012)

- wet–dry cycles, e.g., in warm ponds with or without connection to hydrothermal fields (Deamer and Georgiou, 2015; Ross and Deamer, 2016; Pearce et al., 2017)

- evaporation and (geo-)chromatographic effects in intertidal areas (Wing and Bada, 1991; Cleaves II et al., 2012; Stüeken et al., 2013; Westall et al., 2013).

The concentration of molecules allows increased reaction with each other which could, in principle, lead to the formation of vesicles and/or more complex molecules via polymerization reactions (Orgel, 1998; Deamer et al., 2002; Hanczyc et al., 2003; Budin et al., 2009; Follmann and Brownson, 2009). Vesicles can then either include readily formed more complex molecules (peptides or even RNA?; Hanczyc et al., 2003; Bada, 2004; Follmann and Brownson, 2009) or serve as a protected environment for the formation and development of these more complex compounds (Deamer et al., 2002; Damer and Deamer, 2015). Potentially, the first living entities were solely based on RNA ("RNA-World" Gilbert, 1986; Orgel, 2004).

It is neither clear whether first life was thermophilic or mesophilic, nor whether it was heterotrophic or autotrophic. However, it was most likely chemotrophic and evolved under anaerobic conditions (Nisbet and Sleep, 2001; Follmann and Brownson, 2009; Martin and Sousa, 2016). The evolution of photosynthesis decoupled life from local energy supplies and it had the ability to expand into other areas of the planet, given that there was light, water and CO_2 (Nisbet and Sleep, 2001; Martin and Sousa, 2016). Cyanobacteria might have been active before ~ 2.5 Ga, as it is assumed that they produced the oxygen responsible for the Great Oxidation Event ($\sim 2.5 - 2.3$ Ga Lyons et al., 2014; Schirrmeister et al., 2015, 2016).

1.4   Early Mars

1.4.1   Crustal evolution

Early Mars, like early Earth, probably had a magma ocean in the beginning. Yet, the overall cooling of the planet probably happened faster because it is smaller and further away from the Sun (Elkins-Tanton, 2012; Vago et al., 2017). The bulk of the mostly basaltic (McSween et al., 2009) martian crust was probably immediately formed when the planet cooled (Nimmo and Tanaka, 2005). The evolution of Mars in the pre-Noachian (Fig. 1.1) remains ambiguous. It is assumed that many basin forming impacts happened during that time (Frey, 2006). Furthermore, it is believed that the hemispheric dichotomy of Mars (i.e., the division between the southern and the northern hemisphere, indicated

by a difference in crustal thickness) formed in the pre-Noachian, potentially via a large impact (Watters et al., 2007; Andrews-Hanna et al., 2008; Nimmo et al., 2008; Carr and Head, 2010). The dichotomy is also expressed by the different topography of the northern and southern hemisphere (southern highlands vs. northern lowlands; Watters et al., 2007; Fig. 1.3).
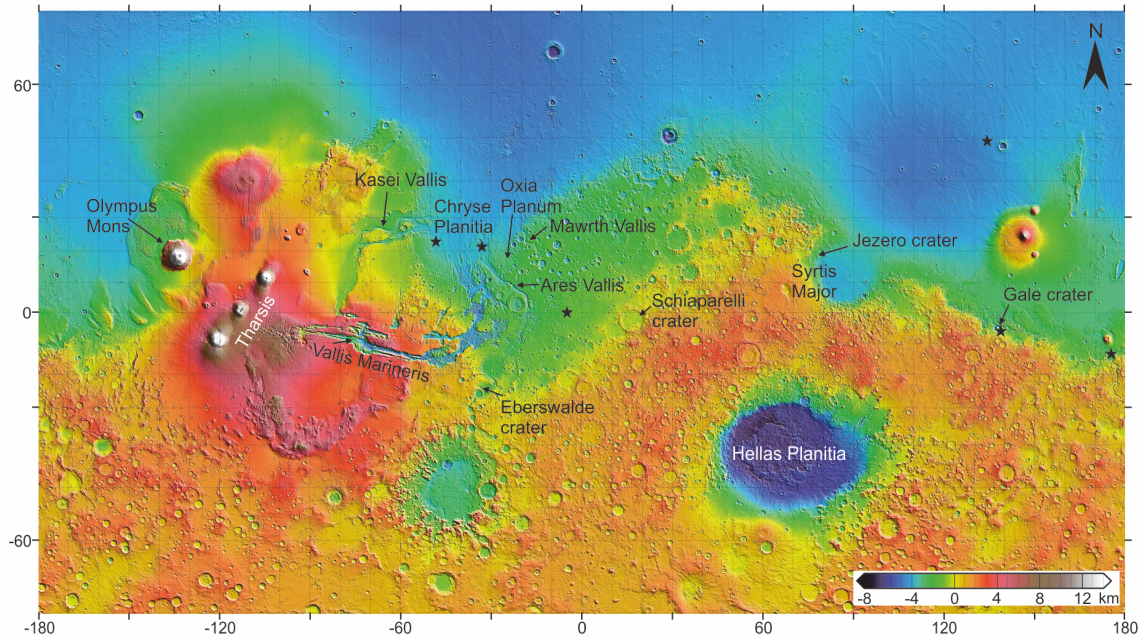
Figure 1.3: Topographic map of Mars. Elevation is indicated by colors (see scale in the bottom right). Stars mark landing sites of some current/past surface missions. Image modified, original image credit: NASA/GSFC (2000), https://attic.gsfc.nasa.gov/mola/images/mercat_med.jpg.

The beginning of the Noachian is marked by the formation of the Hellas basin via a large impact ("Hellas Planitia", possibly ~ 4.1 Ga, Figs. 1.1, 1.3; Frey, 2006; Carr and Head, 2010). Impact rates remained high until the late Noachian (Hartmann and Neukum, 2001). The majority of volcanic activity at this time was probably focused on the formation of Tharsis, a large and topographically very high volcanic region in the western hemisphere of Mars, consisting of 3 main shield volcanoes (Scott and Tanaka, 1986; Phillips et al., 2001; Williams et al., 2008; Fig. 1.3). Besides this, only a few (probably basaltic) Noachian volcanic deposits were identified (Mustard et al., 2005; Squyres et al., 2007; Flahaut et al., 2012).

In the Hesperian (Fig. 1.1), the cratering rate was low (Carr and Head, 2010). At the same time, episodic but widespread volcanism led to the formation of lava plains, large feeder-dike systems and small shield volcanoes, resurfacing about 30% of Mars (Head et al., 2002, 2006; Carr and Head, 2010). This is comparable to widespread volcanic activity on the Archean Earth (see Section 1.3). Although most of the crust on Mars has a mafic composition (McSween et al., 2009), some geological structures of presumably Hesperian age are suspected to contain felsic rocks (e.g., at Syrtis Major and Gale crater, Fig. 1.3; Wray et al., 2013; Sautter et al., 2015, respectively).

It is unlikely that plate tectonics were active on Mars (van Thienen et al., 2004). However, some morphological features (ridges, grabens, potential faults) indicate former

tectonic activity. Most of these features formed early in Mars' history (pre-Noachian–Noachian) and are largely related to volcanic activity (Plescia and Saunders, 1982; Anderson et al., 2001; Connerney et al., 2005; Kronberg et al., 2007; Golombek and Phillips, 2010).

1.4.2   Volatiles, water activity and climate

Volatiles on Mars could have been (at least partly) delivered via meteorites and comets, as also suggested for Earth (Chyba, 1990; see also Section 1.3.2). Most of the volatiles (including water) initially present from planetary accretion probably degassed when the magma ocean solidified, and a smaller fraction later on via volcanic outgassing, both leading to a steam atmosphere (Elkins-Tanton, 2011; Grott et al., 2011). Decreasing temperatures possibly led to the collapse of this steam atmosphere and formation of an early surface ocean soon after the planet had cooled (Elkins-Tanton, 2011). However, later impacts may have caused a loss of volatiles and, potentially, an early atmosphere (Melosh and Vickery, 1989; Jakosky and Phillips, 2001; Barabash et al., 2007). Furthermore, they could have evaporated the potential early ocean by severely raising the surface temperatures (Segura et al., 2002; Carr and Head, 2010).

Liquid water activity on Noachian Mars is evidenced by morphological and mineralogical features. For example, a huge quantity of valley networks (Gulick, 2001; Fassett and Head, 2008a,b; Lasue et al., 2013) and also some deltas (e.g., in Eberswalde crater and Jezero crater, Fig. 1.3; Mangold et al., 2012; Schon et al., 2012, respectively) were probably formed by fluvial activity. Furthermore, widespread occurrences of phyllosilicates and sulphates in Noachian terranes most likely originate from weathering of basalt in the presence of water (Poulet et al., 2005; Bibring et al., 2006; Mustard et al., 2008; Ehlmann et al., 2011).

In the Hesperian, surface water activity declined as indicated by fewer abundances of valley networks (restricted to Hesperian aged volcanoes) and lower weathering rates (Fassett and Head, 2007; Carr and Head, 2010; Andrews-Hanna and Lewis, 2011). From the late Hesperian onwards, large outflow channels (up to tens of kilometers wide and thousands of kilometers long; Carr, 1996) were probably formed by liquid water, sourced by groundwater flows or lava–ice interactions (e.g., Kasei Vallis, Ares Vallis, see Fig. 1.3; Carr and Head, 2010; Lasue et al., 2013; Rodriguez et al., 2015; Cassanelli and Head, 2018). The presence of valley networks and large outflow channels as indicators of fluvial activity and possible flood-like events during the Hesperian led to the conclusion that there could have been a long standing ocean or large water body on Mars (Baker et al., 1991; Parker et al., 1993; Clifford and Parker, 2001), but this remains controversial (see reviews by Carr and Head, 2010; Lasue et al., 2013).

It is still under intense debate whether Mars was "cold and dry", "cold and wet" or "warm and wet" (Fairén, 2010; Wordsworth et al., 2015; Davis et al., 2016; Wordsworth, 2016; Luo et al., 2017; Shaw, 2017, 2018; Salese et al., 2016; Batalha et al., 2016, 2018). Nevertheless, it is likely that the solar energy that early Mars received was lower than for Earth because of the larger distance to the sun, leading to the problem of how liquid water could have existed (Vago et al., 2017). The martian atmosphere during the Noachian and Hesperian probably mainly consisted of CO_2, with minor contributions of H_2O and CH_4 from hydrothermal processes (Pavlov et al., 2000; Schulte et al., 2006; Shaw, 2008;

Wordsworth, 2016; Vago et al., 2017). These atmospheric compositions, however, were not sufficient to maintain a warm climate (Wordsworth et al., 2013; Wordsworth, 2016; Vago et al., 2017). The effect of a lower albedo to counteract the low energy input from the Sun (as suggested for early Earth; Rosing et al., 2010) is most likely not applicable to Mars (Fairén et al., 2012). Still, one possible explanation is that surface temperatures were episodically raised by impact events, volcanic heating, and related hydrothermal activity (Carr, 1996; Abramov and Kring, 2005; Cousins and Crawford, 2011; Lasue et al., 2013; Osinski et al., 2013; Wordsworth et al., 2013; Halevy and Head III, 2014; Wordsworth, 2016; Vago et al., 2017). Dissolved ions from weathering processes may additionally have depressed the melting point of the water (Fairén et al., 2009).

1.4.3   Life on Mars?

The martian surface today is considered uninhabitable (McKay, 2010; Oehler and Allen, 2012). However, it is assumed that early Mars was habitable, although it may have been a "punctuated habitability" with limited connectivity between spatially and temporally restricted habitable systems (McKay, 2010; Westall et al., 2013, 2015; Cockell, 2014). The most probable time for possible development of life was in the Noachian, because there is evidence for widespread liquid surface water and there could have been hydrothermal activity. Furthermore, the lateral connectivity between possible habitats would have been the highest (Westall et al., 2015; Vago et al., 2017).

Important prebiotic molecules could have been delivered (via meteorites, comets or interplanetary dust particles) or produced by in situ processes as discussed for Earth (see Section 1.3.3). Settings for the potential origin of life on Mars could have been similar to those on Earth. Possible settings are hydrothermal systems, warm ponds or small lakes, but probably not tidal areas (Westall et al., 2013, 2015; see also Section 1.3.3). Besides hydrothermal systems related to volcanic activity, impact related hydrothermal systems could have been important for the origin of life on Mars as well (Carr, 1996; Abramov and Kring, 2005; Carr and Head, 2010; Cousins and Crawford, 2011; Osinski et al., 2013). Additionally, it was recently hypothesized that potential life on Mars entirely originated in the subsurface and never colonized surface areas (Michalski et al., 2018).

In summary, surface conditions were not stable enough for a long lasting evolution of microorganisms, so that they could have only reached an early stage of evolution (e.g., no photosynthesis). That means that life could have existed (or still exists) on Mars in the form of chemotrophs that lived (or live) in surface or subsurface areas (Westall et al., 2013, 2015; Vago et al., 2017).

1.5   Tracing life through space and time

The first surface mission to Mars was the Viking mission in 1976. The landers conducted biology experiments and GC–MS analysis of martian soils searching for extant/extinct life (Biemann et al., 1976, 1977; Levin and Straat, 1976, 1977). After Viking, several missions followed investigating martian geology and/or searching for (remnants of) life. Recently, the first organic molecules in martian soil were detected by the Sample Analysis at Mars (SAM) instrument onboard the Curiosity rover (Freissinet et al., 2015), but as yet,

no direct traces of life have been detected.

Potential life on Mars could have left traces (biosignatures) similar to those found in Archean rocks on Earth, including microfossils, macroscale morphological features (e.g., stromatolites), stable isotope signatures (e.g., depletion in $\delta^{13}C$ values) or organic biomarkers (Simoneit et al., 1998; Cady et al., 2003; Summons et al., 2008; Westall, 2008; Cady and Noffke, 2009; Westall and Cavalazzi, 2011; Vago et al., 2017). However, the biogenicity of such signatures in Archean (and also younger) rocks was often questioned in the last two decades because they can, at least up to a certain degree, also be produced abiotically (Brasier et al., 2002; van Zuilen et al., 2002; Lindsay et al., 2005; De Gregorio et al., 2011; Grosch and McLoughlin, 2014; Davies et al., 2016). Therefore, more than one indication may be necessary to verify the biogenicity of a potential biosignature. Furthermore, it is essential to consider the geological context (Westall et al., 2015; Vago et al., 2017).

The ExoMars rover will determine the geological environment, and search for biosignatures in the form of macroscale morphological features and biomarkers by using a variety of different instruments (e.g., MOMA, Raman Laser Spectrometer or MicrOmega; see Vago et al., 2017 for a detailed description of the ExoMars rover's objectives, payload and capabilities). MOMA is specialized to detect organics (including biomarkers) by using laser desorption mass spectrometry (LDMS) and different GC–MS techniques (see Chapter 5).

1.5.1   Organic biomarkers

Organic biomarkers are compounds that are specific for certain (groups of) organisms and derive from functional biomolecules (Peters et al., 2005). During diagenesis, these functional biomolecules undergo chemical conversion (usually including defunctionalization and reduction), resulting in more stable structures which still bear characteristic features of their parent molecule (Summons et al., 2008). Lipids are the most common biomarkers because they are relatively stable under a variety of environmental conditions. Furthermore, they are present in every organism (e.g., in the form of membrane lipids) and are relatively source specific due to characteristic structural differences (Brocks and Summons, 2003; Peters et al., 2005; Summons et al., 2008). Lipid biomarkers furthermore show certain traits that underline their biological origin, such as for example, repeating subunits (e.g., isoprene, acetate; Fig. 1.4a), structural isomer/homolog preferences and/or uneven distribution patterns of homologous compounds (Fig. 1.4b). Their chemical analysis is usually conducted by means of GC–MS, as this technique combines both separation of organic compounds (gas chromatography) and identification of these via mass spectral fingerprints (mass spectrometry; Summons et al., 2008). Some examples for typical lipid biomarker compounds are presented in Figure 1.4c.

1.5.2   Key challenges and study approaches

Lipid biomarkers can be preserved over geological timescales (Brocks and Summons, 2003). Still, their preservation potential is influenced by a variety of parameters. If not buried by sediments under anoxic conditions, lipids can easily be oxidized and/or biodegraded (at least on Earth), both resulting in their decomposition and possibly complete

a) Repeating subunits

Isoprene
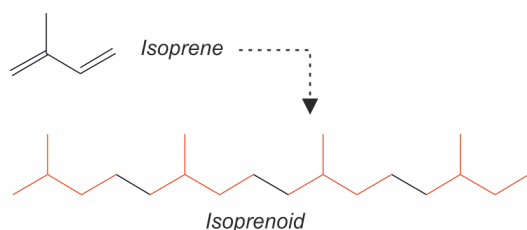
Isoprenoid

b) Preferences/uneven distributions

Intensity

*

Retention time
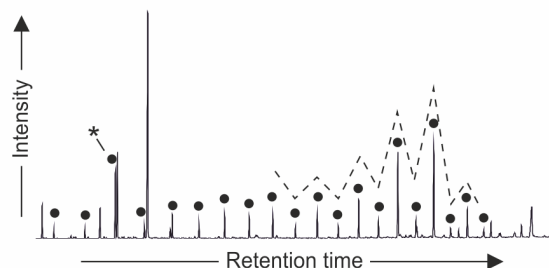
c) Some examples of typical lipid biomarkers

Acyclic isoprenoids

Pristane

Phytane

Cyclic isoprenoids

Cholestane (steroid)

C_{30} hopane (hopanoid)
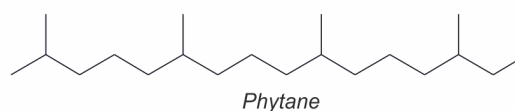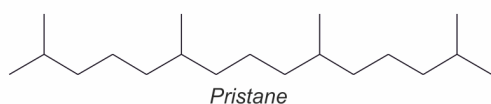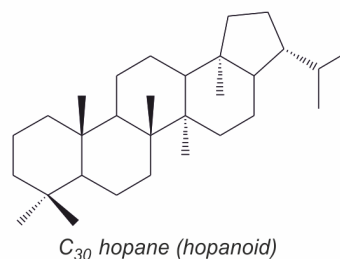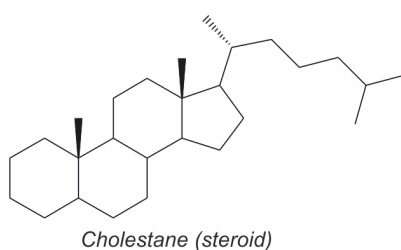
Figure 1.4: Lipid biomarker characteristics and examples. (**a**) The isoprene molecule and its appearance as a repeating subunit in an isoprenoid. (**b**) Examples for a single homolog preference (∗) and an uneven distribution pattern (dashed line). Black dots denote compounds of a homologous series. (**c**) Structural formulas of some typical lipid biomarkers.

destruction of the biosignature (Peters et al., 2005). Furthermore, high temperatures can severely affect biomarker preservation (Brocks and Summons, 2003; Peters et al., 2005). On the surface of Mars, preservation of organic matter is restricted by UV and particle radiation (Oró and Holzer, 1979; Pavlov et al., 2012; Poch et al., 2014). Chapter 2 of this thesis addresses the impact of thermal maturation on the preservation of lipid biomarkers. Experimental maturation (hydrous pyrolysis) of an immature kerogen (i.e., the fraction of organic matter that is insoluble in common organic solvents, acids and bases; Durand, 1980) in gold capsules was carried out at 300 and 400 °C and 2 kbar for certain time intervals (between 2 and 2400 h). Biomarker contents of maturation products were subsequently extracted and determined by GC–MS.

   Another problem when searching for biomarkers in Archean rocks or martian samples is the potential organic input from abiotic sources, such as meteorites (Chyba and Sagan, 1992) and/or in situ processes (e.g., production of lipids via FTT synthesis; Fischer, 1935; McCollom et al., 1999; Holm and Charlou, 2001; McCollom and Seewald, 2007). In this case, careful discrimination of biologically and abiotically derived organic

matter is essential to pinpoint life. Chapter 3 illustrates the variety of biomarker-like lipids produced via FTT synthesis, and discusses criteria for their distinction from biologically derived lipids. FTT synthesis was conducted in stainless steel reactors by heating an oxalic acid solution mixed with montmorillonite to 175 °C for 3 days. Solvent extracted reaction products and extraction residues were analyzed using GC–MS, combustion infrared detection, attenuated total reflectance Fourier transform infrared spectroscopy and pyrolysis-GC–MS.

The potential impact of contamination and the syngeneity of biomarkers has to be carefully assessed, especially when Archean rocks or martian samples are analyzed. Organic matter is syngenetic if it was deposited together with the host rock, meaning that they must have the same age (Oehler and Cady, 2014). Bitumen (i.e., soluble fraction of organic matter, as opposed to kerogen; Durand, 1980) can migrate and is thus susceptible to contamination (Brocks et al., 2008; Brocks, 2011; Oehler and Cady, 2014). Kerogen, on the other hand, is immobile and therefore mostly syngenetic with the host rock (Brocks et al., 2003a,b; Oehler and Cady, 2014). However, kerogen can also be subject to contamination and therefore a thorough preparation of the material is required. Chapter 4 describes the investigation of an Archean kerogen and discusses evidence for its syngeneity and biogenicity. Key analytical approaches for this study were petrographical investigations (including Raman spectroscopy) of the host rock as well as molecular analysis (e.g., catalytic hydropyrolysis, GC–MS) of the isolated kerogen and organic reference materials (cyanobacterial biomass and FTT reaction products).

All instruments onboard the ExoMars rover have to work autonomously and with restricted energy supplies. Thus, the in situ analysis of organic compounds by the MOMA GC–MS (see Chapter 5) is limited compared to conventional bench-top preparation and GC–MS analysis which leads to a series of challenges: (i) Only bulk analysis can be conducted by the MOMA instrument, meaning that fractionation of compound classes (aliphatics, aromatics, etc.) or kerogen isolation is not possible. This potentially complicates the detection of single compounds (in case of coelution); (ii) As an injection of solvent extracts is not possible, organics have to be thermally volatilized. This can lead to analytical by-products from thermal decomposition of organic molecules; (iii) Perchlorates in the martian soil (Hecht et al., 2009; Kounaves et al., 2010, 2014) can lead to the oxidation and chlorination of organic compounds during thermal volatilization (Navarro-González et al., 2010, 2011; Steininger et al., 2012; Sephton et al., 2014); (iv) Not all of the different MOMA GC–MS techniques (4 in total) are applicable to every potential class of organic compounds. Chapter 5 provides a general introduction in the MOMA instrument, while Chapter 6 assesses advantages and limitations of different MOMA GC–MS techniques. A flight analog system was used to perform MOMA-like GC–MS measurements on a natural sample and a standard mix in the laboratory environment. Finally, the implications of the main results of this study for ExoMars research are discussed in Chapter 7.

References

Abramov, O. and Kring, D. A. (2005). Impact-induced hydrothermal activity on early Mars. *Journal of Geophysical Research: Planets*, 110, E12S09.

Altwegg, K., Balsiger, H., Bar-Nun, A., Berthelier, J. J., Bieler, A., Bochsler, P., Briois, C., Calmonte, U., Combi, M., De Keyser, J., Eberhardt, P., Fiethe, B., Fuselier, S., Gasc, S., Gombosi, T. I., Hansen, K. C., Hässig, M., Jäckel, A., Kopp, E., Korth, A., LeRoy, L., Mall, U., Marty, B., Mousis, O., Neefs, E., Owen, T., Rème, H., Rubin, M., Sémon, T., Tzou, C.-Y., Waite, H., and Wurz, P. (2014). 67P/Churyumov-Gerasimenko, a Jupiter family comet with a high D/H ratio. *Science*, 1261952.

Anderson, R. C., Dohm, J. M., Golombek, M. P., Haldemann, A. F. C., Franklin, B. J., Tanaka, K. L., Lias, J., and Peer, B. (2001). Primary centers and secondary concentrations of tectonic activity through time in the western hemisphere of Mars. *Journal of Geophysical Research: Planets*, 106, 20563–20585.

Andrews-Hanna, J. C. and Lewis, K. W. (2011). Early Mars hydrology: 2. Hydrological evolution in the Noachian and Hesperian epochs. *Journal of Geophysical Research: Planets*, 116, E02007.

Andrews-Hanna, J. C., Zuber, M. T., and Banerdt, W. B. (2008). The Borealis basin and the origin of the martian crustal dichotomy. *Nature*, 453, 1212–1215.

Baaske, P., Weinert, F. M., Duhr, S., Lemke, K. H., Russell, M. J., and Braun, D. (2007). Extreme accumulation of nucleotides in simulated hydrothermal pore systems. *Proceedings of the National Academy of Sciences of the United States of America*, 104, 9346–9351.

Bada, J. L. (2004). How life began on Earth: a status report. *Earth and Planetary Science Letters*, 226, 1–15.

Bada, J. L. (2013). New insights into prebiotic chemistry from Stanley Miller's spark discharge experiments. *Chemical Society Reviews*, 42, 2186–2196.

Baker, V. R., Strom, R. G., Gulick, V. C., Kargel, J. S., Komatsu, G., and Kale, V. S. (1991). Ancient oceans, ice sheets and the hydrological cycle on Mars. *Nature*, 352, 589–594.

Barabash, S., Fedorov, A., Lundin, R., and Sauvaud, J.-A. (2007). Martian Atmospheric Erosion Rates. *Science*, 315, 501–503.

Baross, J. A. and Hoffman, S. E. (1985). Submarine hydrothermal vents and associated gradient environments as sites for the origin and evolution of life. *Origins of life and evolution of the biosphere*, 15, 327–345.

Batalha, N. E., Kopparapu, R. K., Haqq-Misra, J., and Kasting, J. F. (2016). Climate cycling on early Mars caused by the carbonate–silicate cycle. *Earth and Planetary Science Letters*, 455, 7–13.

Batalha, N. E., Kopparapu, R. K., Haqq-Misra, J., and Kasting, J. F. (2018). Reply to Shaw. *Earth and Planetary Science Letters*, 484, 415–417.

Berndt, M. E., Allen, D. E., and Seyfried, W. E. (1996). Reduction of CO_2 during serpentinization of olivine at 300 °C and 500 bar. *Geology*, 24, 351–354.

Bibring, J.-P., Langevin, Y., Mustard, J. F., Poulet, F., Arvidson, R., Gendrin, A., Gondet, B., Mangold, N., Pinet, P., Forget, F., Berthé, M., Bibring, J.-P., Gendrin, A., Gomez, C., Gondet, B., Jouglet, D., Poulet, F., Soufflot, A., Vincendon, M., Combes, M., Drossart, P., Encrenaz, T., Fouchet, T., Merchiorri, R., Belluci, G., Altieri, F., Formisano, V., Capaccioni, F., Cerroni, P., Coradini, A., Fonti, S., Korablev, O., Kottsov, V., Ignatiev, N., Moroz, V., Titov, D., Zasova, L., Loiseau, D., Mangold, N., Pinet, P., Douté, S., Schmitt, B., Sotin, C., Hauber, E., Hoffmann, H., Jaumann, R., Keller, U., Arvidson, R., Mustard, J. F., Duxbury, T., Forget, F., and Neukum, G. (2006). Global Mineralogical and Aqueous Mars History Derived from OMEGA/Mars Express Data. *Science*, 312, 400–404.

Biemann, K., Oró, J., Toulmin, P., Orgel, L. E., Nier, A. O., Anderson, D. M., Simmonds, P. G., Flory, D., Diaz, A. V., Rushneck, D. R., and Biller, J. A. (1976). Search for Organic and Volatile Inorganic Compounds in Two Surface Samples from the Chryse Planitia Region of Mars. *Science*, 194, 72–76.

Biemann, K., Oró, J., Toulmin, P., Orgel, L. E., Nier, A. O., Anderson, D. M., Simmonds, P. G., Flory, D., Diaz, A. V., Rushneck, D. R., Biller, J. E., and Lafleur, A. L. (1977). The search for organic substances and inorganic volatile compounds in the surface of Mars. *Journal of Geophysical Research*, 82, 4641–4658.

Blair Hedges, S. (2002). The origin and evolution of model organisms. *Nature Reviews Genetics*, 3, 838–849.

Botta, O. and Bada, J. L. (2002). Extraterrestrial Organic Compounds in Meteorites. *Surveys in Geophysics*, 23, 411–467.

Bowring, S. A. and Williams, I. S. (1999). Priscoan 4.00–4.03 Ga orthogneisses from northwestern Canada. *Contributions to Mineralogy and Petrology*, 134, 3–16.

Brasier, M. D., Green, O. R., Jephcoat, A. P., Kleppe, A. K., Van Kranendonk, M. J., Lindsay, J. F., Steele, A., and Grassineau, N. V. (2002). Questioning the evidence for Earth's oldest fossils. *Nature*, 416, 76–81.

Brasier, M. D., Matthewman, R., McMahon, S., and Wacey, D. (2011). Pumice as a Remarkable Substrate for the Origin of Life. *Astrobiology*, 11, 725–735.

Braun, D. and Libchaber, A. (2004). Thermal force approach to molecular evolution. *Physical Biology*, 1, P1.

Brocks, J. J. (2011). Millimeter-scale concentration gradients of hydrocarbons in Archean shales: Live-oil escape or fingerprint of contamination? *Geochimica et Cosmochimica Acta*, 75, 3196–3213.

Brocks, J. J., Buick, R., Logan, G. A., and Summons, R. E. (2003a). Composition and syngeneity of molecular fossils from the 2.78 to 2.45 billion-year-old Mount Bruce Supergroup, Pilbara Craton, Western Australia. *Geochimica et Cosmochimica Acta*, 67, 4289–4319.

Brocks, J. J., Grosjean, E., and Logan, G. A. (2008). Assessing biomarker syngeneity using branched alkanes with quaternary carbon (BAQCs) and other plastic contaminants. *Geochimica et Cosmochimica Acta*, 72, 871–888.

Brocks, J. J., Love, G. D., Snape, C. E., Logan, G. A., Summons, R. E., and Buick, R. (2003b). Release of bound aromatic hydrocarbons from late Archean and Mesoproterozoic kerogens via hydropyrolysis. *Geochimica et Cosmochimica Acta*, 67, 1521–1530.

Brocks, J. J. and Summons, R. E. (2003). Biomarkers for Early Life. In W. H. Schlesinger (Ed.), *Biogeochemistry*. Elsevier, Oxford, pp. 63–115.

Budin, I., Bruckner, R. J., and Szostak, J. W. (2009). Formation of Protocell-like Vesicles in a Thermal Diffusion Column. *Journal of the American Chemical Society*, 131, 9628–9629.

Cady, S. L., Farmer, J. D., Grotzinger, J. P., Schopf, J. W., and Steele, A. (2003). Morphological Biosignatures and the Search for Life on Mars. *Astrobiology*, 3, 351–368.

Cady, S. L. and Noffke, N. (2009). Geobiology: evidence for early life on Earth and the search for life on other planets. *GSA Today*, 19, 4–10.

Carr, M. H. (1996). Water erosion on Mars and its biologic implications. *Endeavour*, 20, 56–60.

Carr, M. H. and Head, J. W. (2010). Geologic history of Mars. *Earth and Planetary Science Letters*, 294, 185–203.

Cassanelli, J. P. and Head, J. W. (2018). Formation of outflow channels on Mars: Testing the origin of Reull Vallis in Hesperia Planum by large-scale lava-ice interactions and top-down melting. *Icarus*, 305, 56–79.

Chyba, C. F. (1990). Impact delivery and erosion of planetary oceans in the early inner Solar System. *Nature*, 343, 129–133.

Chyba, C. F. and Phillips, C. B. (2001). Possible ecosystems and the search for life on Europa. *Proceedings of the National Academy of Sciences of the United States of America*, 98, 801–804.

Chyba, C. F. and Sagan, C. (1992). Endogenous production, exogenous delivery and impact-shock synthesis of organic molecules: an inventory for the origins of life. *Nature*, 355, 125–132.

Clarke, A. (2014). The thermal limits to life on Earth. *International Journal of Astrobiology*, 13, 141–154.

References

Cleaves II, H. J., Michalkova Scott, A., Hill, F. C., Leszczynski, J., Sahai, N., and Hazen, R. (2012). Mineral-organic interfacial processes: potential roles in the origins of life. *Chem. Soc. Rev.*, 41, 5502–5525.

Clifford, S. M. and Parker, T. J. (2001). The Evolution of the Martian Hydrosphere: Implications for the Fate of a Primordial Ocean and the Current State of the Northern Plains. *Icarus*, 154, 40–79.

Cockell, C. S. (2014). Trajectories of Martian Habitability. *Astrobiology*, 14, 182–203.

Cockell, C. S., Bush, T., Bryce, C., Direito, S., Fox-Powell, M., Harrison, J. P., Lammer, H., Landenmark, H., Martin-Torres, J., Nicholson, N., Noack, L., O'Malley-James, J., Payler, S. J., Rushby, A., Samuels, T., Schwendner, P., Wadsworth, J., and Zorzano, M. P. (2016). Habitability: A Review. *Astrobiology*, 16, 89–117.

Connerney, J. E. P., Acuña, M. H., Ness, N. F., Kletetschka, G., Mitchell, D. L., Lin, R. P., and Reme, H. (2005). Tectonic implications of Mars crustal magnetism. *Proceedings of the National Academy of Sciences of the United States of America*, 102, 14970–14975.

Cousins, C. R. and Crawford, I. A. (2011). Volcano-Ice Interaction as a Microbial Habitat on Earth and Mars. *Astrobiology*, 11, 695–710.

Damer, B. and Deamer, D. W. (2015). Coupled Phases and Combinatorial Selection in Fluctuating Hydrothermal Pools: A Scenario to Guide Experimental Approaches to the Origin of Cellular Life. *Life*, 5, 872–887.

Dass, A. V., Hickman-Lewis, K., Brack, A., Kee, T. P., and Westall, F. (2016). Stochastic Prebiotic Chemistry within Realistic Geological Systems. *ChemistrySelect*, 1, 4906–4926.

Davies, N. S., Liu, A. G., Gibling, M. R., and Miller, R. F. (2016). Resolving MISS conceptions and misconceptions: A geological approach to sedimentary surface textures generated by microbial and abiotic processes. *Earth-Science Reviews*, 154, 210–246.

Davis, J. M., Balme, M., Grindrod, P. M., Williams, R. M. E., and Gupta, S. (2016). Extensive Noachian fluvial systems in Arabia Terra: Implications for early Martian climate. *Geology*, 44, 847–850.

De Gregorio, B. T., Sharp, T. G., Rushdi, A. I., and Simoneit, B. R. T. (2011). Bugs or Gunk? Nanoscale Methods for Assessing the Biogenicity of Ancient Microfossils and Organic Matter. In S. D. Golding and M. Glikson (Eds.), *Earliest Life on Earth: Habitats, Environments and Methods of Detection*. Springer Netherlands, Dordrecht, pp. 239–289.

Deamer, D., Dworkin, J. P., Sandford, S. A., Bernstein, M. P., and Allamandola, L. J. (2002). The First Cell Membranes. *Astrobiology*, 2, 371–381.

Deamer, D. W. and Georgiou, C. D. (2015). Hydrothermal Conditions and the Origin of Cellular Life. *Astrobiology*, 15, 1091–1095.

Djokic, T., Van Kranendonk, M. J., Campbell, K. A., Walter, M. R., and Ward, C. R. (2017). Earliest signs of life on land preserved in ca. 3.5 Ga hot spring deposits. *Nature Communications*, 8, 15263.

Dodd, M. S., Papineau, D., Grenne, T., Slack, J. F., Rittner, M., Pirajno, F., O'Neil, J., and Little, C. T. S. (2017). Evidence for early life in Earth's oldest hydrothermal vent precipitates. *Nature*, 543, 60–64.

Duda, J.-P., Van Kranendonk, M. J., Thiel, V., Ionescu, D., Strauss, H., Schäfer, N., and Reitner, J. (2016). A Rare Glimpse of Paleoarchean Life: Geobiology of an Exceptionally Preserved Microbial Mat Facies from the 3.4 Ga Strelley Pool Formation, Western Australia. *PLoS One*, 11, 1–18.

Durand, B. (1980). Sedimentary organic matter and kerogen. Definition and quantitative importance of kerogen. In B. Durand (Ed.), *Kerogen*. Éditions Technip, Paris, pp. 13–34.

Ehlmann, B. L., Mustard, J. F., Murchie, S. L., Bibring, J.-P., Meunier, A., Fraeman, A. A., and Langevin, Y. (2011). Subsurface water and clay mineral formation during the early history of Mars. *Nature*, 479, 53–60.

Ehrenfreund, P. and Charnley, S. B. (2000). Organic Molecules in the Interstellar Medium, Comets, and Meteorites: A Voyage from Dark Clouds to the Early Earth. *Annual Review of Astronomy and Astrophysics*, 38, 427–483.

Elkins-Tanton, L. T. (2011). Formation of early water oceans on rocky planets. *Astrophysics and Space Science*, 332, 359–364.

Elkins-Tanton, L. T. (2012). Magma Oceans in the Inner Solar System. *Annual Review of Earth and Planetary Sciences*, 40, 113–139.

Etiope, G. and Sherwood Lollar, B. (2013). Abiotic Methane on Earth. *Reviews of Geophysics*, 51, 276–299.

Etiope, G., Vadillo, I., Whiticar, M. J., Marques, J. M., Carreira, P. M., Tiago, I., Benavente, J., Jiménez, P., and Urresti, B. (2016). Abiotic methane seepage in the Ronda peridotite massif, southern Spain. *Applied Geochemistry*, 66, 101–113.

Fairén, A. G. (2010). A cold and wet Mars. *Icarus*, 208, 165–175.

Fairén, A. G., Davila, A. F., Gago-Duport, L., Amils, R., and McKay, C. P. (2009). Stability against freezing of aqueous solutions on early Mars. *Nature*, 459, 401–404.

Fairén, A. G., Haqq-Misra, J. D., and McKay, C. P. (2012). Reduced albedo on early Mars does not solve the climate paradox under a faint young Sun. *A&A*, 540, A13.

Fassett, C. I. and Head, J. W. (2007). Valley formation on martian volcanoes in the Hesperian: Evidence for melting of summit snowpack, caldera lake formation, drainage and erosion on Ceraunius Tholus. *Icarus*, 189, 118–135.

Fassett, C. I. and Head, J. W. (2008a). The timing of martian valley network activity: Constraints from buffered crater counting. *Icarus*, 195, 61–89.

Fassett, C. I. and Head, J. W. (2008b). Valley network-fed, open-basin lakes on Mars: Distribution and implications for Noachian surface and subsurface hydrology. *Icarus*, 198, 37–56.

Ferris, J. P. (2005). Mineral Catalysis and Prebiotic Synthesis: Montmorillonite-Catalyzed Formation of RNA. *Elements*, 1, 145–149.

Ferris, J. P., Hill Jr, A. R., Liu, R., and Orgel, L. E. (1996). Synthesis of long prebiotic oligomers on mineral surfaces. *Nature*, 381, 59–61.

Feulner, G. (2012). The faint young Sun problem. *Reviews of Geophysics*, 50, RG2006.

Fischer, F. (1935). Die Synthese der Treibstoffe (Kogaisin) und Schmieröle aus Kohlenoxyd und Wasserstoff bei Gewöhnlichem Druck. *Brennstoff Chemie*, 16, 1–11.

Flahaut, J., Quantin, C., Clenet, H., Allemand, P., Mustard, J. F., and Thomas, P. (2012). Pristine Noachian crust and key geologic transitions in the lower walls of Valles Marineris: Insights into early igneous processes on Mars. *Icarus*, 221, 420–435.

Follmann, H. and Brownson, C. (2009). Darwin's warm little pond revisited: from molecules to the origin of life. *Naturwissenschaften*, 96, 1265–1292.

Freissinet, C., Glavin, D. P., Mahaffy, P. R., Miller, K. E., Eigenbrode, J. L., Summons, R. E., Brunner, A. E., Buch, A., Szopa, C., Archer, P. D., Franz, H. B., Atreya, S. K., Brinckerhoff, W. B., Cabane, M., Coll, P., Conrad, P. G., Des Marais, D. J., Dworkin, J. P., Fairén, A. G., François, P., Grotzinger, J. P., Kashyap, S., ten Kate, I. L., Leshin, L. A., Malespin, C. A., Martin, M. G., Martin-Torres, F. J., McAdam, A. C., Ming, D. W., Navarro-González, R., Pavlov, A. A., Prats, B. D., Squyres, S. W., Steele, A., Stern, J. C., Sumner, D. Y., Sutter, B., Zorzano, M. P., and the MSL Science Team (2015). Organic molecules in the Sheepbed Mudstone, Gale Crater, Mars. *Journal of Geophysical Research: Planets*, 120, 495–514.

Frey, H. V. (2006). Impact constraints on, and a chronology for, major events in early Mars history. *Journal of Geophysical Research: Planets*, 111, E08S91.

Froude, D. O., Ireland, T. R., Kinny, P. D., Williams, I. S., Compston, W., Williams, I. R., and Myers, J. S. (1983). Ion microprobe identification of 4,100–4,200 Myr-old terrestrial zircons. *Nature*, 304, 616–618.

Gilbert, W. (1986). Origin of life: The RNA world. *Nature*, 319, 618.

Golombek, M. P. and Phillips, R. J. (2010). Mars tectonics. In T. R. Watters and R. A. Schultz (Eds.), *Planetary Tectonics*. Cambridge University Press, New York, pp. 183–232.

Gough, D. O. (1981). Solar Interior Structure and Luminosity Variations. In V. Domingo (Ed.), *Physics of Solar Variations*. Springer Netherlands, Dordrecht, pp. 21–34.

Griffin, W. L., Belousova, E. A., O'Neill, C., O'Reilly, S. Y., Malkovets, V., Pearson, N. J., Spetsius, S., and Wilde, S. A. (2014). The world turns over: Hadean–Archean crust–mantle evolution. *Lithos*, 189, 2–15.

Grosch, E. G. and McLoughlin, N. (2014). Reassessing the biogenicity of Earth's oldest trace fossil with implications for biosignatures in the search for early life. *Proceedings of the National Academy of Sciences of the United States of America*, 111, 8380–8385.

Grott, M., Morschhauser, A., Breuer, D., and Hauber, E. (2011). Volcanic outgassing of CO_2 and H_2O on Mars. *Earth and Planetary Science Letters*, 308, 391–400.

Gulick, V. C. (2001). Origin of the valley networks on Mars: A hydrological perspective. *Geomorphology*, 37, 241–268.

Halevy, I. and Head III, J. W. (2014). Episodic warming of early Mars by punctuated volcanism. *Nature Geoscience*, 7, 865–868.

Hanczyc, M. M., Fujikawa, S. M., and Szostak, J. W. (2003). Experimental Models of Primitive Cellular Compartments: Encapsulation, Growth, and Division. *Science*, 302, 618–622.

Hartmann, W. K. and Neukum, G. (2001). Cratering Chronology and the Evolution of Mars. In R. Kallenbach, J. Geiss, and W. K. Hartmann (Eds.), *Chronology and Evolution of Mars*. Springer Netherlands, Dordrecht, pp. 165–194.

Hassenkam, T., Andersson, M. P., Dalby, K. N., Mackenzie, D. M. A., and Rosing, M. T. (2017). Elements of Eoarchean life trapped in mineral inclusions. *Nature*, 548, 78–81.

Head, J. W., Kreslavsky, M. A., and Pratt, S. (2002). Northern lowlands of Mars: Evidence for widespread volcanic flooding and tectonic deformation in the Hesperian Period. *Journal of Geophysical Research: Planets*, 107, 3–29.

Head, J. W., Wilson, L., Dickson, J., and Neukum, G. (2006). The Huygens-Hellas giant dike system on Mars: Implications for Late Noachian–Early Hesperian volcanic resurfacing and climatic evolution. *Geology*, 34, 285–288.

Hecht, M. H., Kounaves, S. P., Quinn, R. C., West, S. J., Young, S. M. M., Ming, D. W., Catling, D. C., Clark, B. C., Boynton, W. V., Hoffman, J., DeFlores, L. P., Gospodinova, K., Kapit, J., and Smith, P. H. (2009). Detection of Perchlorate and the Soluble Chemistry of Martian Soil at the Phoenix Lander Site. *Science*, 325, 64–67.

Hessler, A. M., Lowe, D. R., Jones, R. L., and Bird, D. K. (2004). A lower limit for atmospheric carbon dioxide levels 3.2 billion years ago. *Nature*, 428, 736–738.

Heubeck, C. (2009). An early ecosystem of Archean tidal microbial mats (Moodies Group, South Africa, ca. 3.2 Ga). *Geology*, 37, 931–934.

Heubeck, C. and Lowe, D. R. (1994). Depositional and tectonic setting of the Archean Moodies Group, Barberton Greenstone Belt, South Africa. *Precambrian Research*, 68, 257–290.

Hofmann, A. (2011). Archaean hydrothermal systems in the Barberton greenstone belt and their significance as a habitat for early life. In S. D. Golding and M. Glikson (Eds.), *Earliest Life on Earth: Habitats, Environments and Methods of Detection*. Springer, Dordrecht, pp. 51–78.

Holm, N. G. and Charlou, J. L. (2001). Initial indications of abiotic formation of hydrocarbons in the Rainbow ultramafic hydrothermal system, Mid-Atlantic Ridge. *Earth and Planetary Science Letters*, 191, 1–8.

Homann, M., Heubeck, C., Airo, A., and Tice, M. M. (2015). Morphological adaptations of 3.22 Ga-old tufted microbial mats to Archean coastal habitats (Moodies Group, Barberton Greenstone Belt, South Africa). *Precambrian Research*, 266, 47–64.

Huber, C. and Wächtershäuser, G. (1997). Activated Acetic Acid by Carbon Fixation on (Fe, Ni)S Under Primordial Conditions. *Science*, 276, 245–247.

Jacobson, S. A., Morbidelli, A., Raymond, S. N., O'Brien, D. P., Walsh, K. J., and Rubie, D. C. (2014). Highly siderophile elements in Earth's mantle as a clock for the Moon-forming impact. *Nature*, 508, 84–87.

Jakosky, B. M. and Phillips, R. J. (2001). Mars' volatile and climate history. *Nature*, 412, 237–244.

Kamber, B. S. (2010). Archean mafic–ultramafic volcanic landmasses and their effect on ocean–atmosphere chemistry. *Chemical Geology*, 274, 19–28.

Kamber, B. S. (2015). The evolving nature of terrestrial crust from the Hadean, through the Archaean, into the Proterozoic. *Precambrian Research*, 258, 48–82.

Kamber, B. S., Collerson, K. D., Moorbath, S., and Whitehouse, M. J. (2003). Inheritance of early Archaean Pb-isotope variability from long-lived Hadean protocrust. *Contributions to Mineralogy and Petrology*, 145, 25–46.

Kasting, J. F. (1993). Earth's Early Atmosphere. *Science*, 259, 920–926.

Konn, C., Charlou, J. L., Holm, N. G., and Mousis, O. (2015). The Production of Methane, Hydrogen, and Organic Compounds in Ultramafic-Hosted Hydrothermal Vents of the Mid-Atlantic Ridge. *Astrobiology*, 15, 381–399.

Korenaga, J. (2013). Initiation and Evolution of Plate Tectonics on Earth: Theories and Observations. *Annual Review of Earth and Planetary Sciences*, 41, 117–151.

Kounaves, S. P., Chaniotakis, N. A., Chevrier, V. F., Carrier, B. L., Folds, K. E., Hansen, V. M., McElhoney, K. M., O'Neil, G. D., and Weber, A. W. (2014). Identification of the perchlorate parent salts at the Phoenix Mars landing site and possible implications. *Icarus*, 232, 226–231.

Kounaves, S. P., Hecht, M. H., Kapit, J., Gospodinova, K., DeFlores, L., Quinn, R. C., Boynton, W. V., Clark, B. C., Catling, D. C., Hredzak, P., Ming, D. W., Moore, Q., Shusterman, J., Stroble, S., West, S. J., and Young, S. M. M. (2010). Wet Chemistry

experiments on the 2007 Phoenix Mars Scout Lander mission: Data analysis and results. *Journal of Geophysical Research: Planets*, 115, E00E10.

Kronberg, P., Hauber, E., Grott, M., Werner, S. C., Schäfer, T., Gwinner, K., Giese, B., Masson, P., and Neukum, G. (2007). Acheron Fossae, Mars: Tectonic rifting, volcanism, and implications for lithospheric thickness. *Journal of Geophysical Research: Planets*, 112, E04005.

Kröner, A., Elis Hoffmann, J., Xie, H., Wu, F., Münker, C., Hegner, E., Wong, J., Wan, Y., and Liu, D. (2013). Generation of early Archaean felsic greenstone volcanic rocks through crustal melting in the Kaapvaal, craton, southern Africa. *Earth and Planetary Science Letters*, 381, 188–197.

Lasue, J., Mangold, N., Hauber, E., Clifford, S., Feldman, W., Gasnault, O., Grima, C., Maurice, S., and Mousis, O. (2013). Quantitative Assessments of the Martian Hydrosphere. *Space Science Reviews*, 174, 155–212.

Lazar, C., McCollom, T. M., and Manning, C. E. (2012). Abiogenic methanogenesis during experimental komatiite serpentinization: Implications for the evolution of the early Precambrian atmosphere. *Chemical Geology*, 326, 102–112.

Levin, G. V. and Straat, P. A. (1976). Viking Labeled Release Biology Experiment: Interim Results. *Science*, 194, 1322–1329.

Levin, G. V. and Straat, P. A. (1977). Recent results from the Viking Labeled Release Experiment on Mars. *Journal of Geophysical Research*, 82, 4663–4667.

Lindsay, J. F., Brasier, M. D., McLoughlin, N., Green, O. R., Fogel, M., Steele, A., and Mertzman, S. A. (2005). The problem of deep carbon—An Archean paradox. *Precambrian Research*, 143, 1–22.

Lowe, D. R. (1980). Stromatolites 3,400-Myr old from the Archean of Western Australia. *Nature*, 284, 441–443.

Luo, W., Cang, X., and Howard, A. D. (2017). New Martian valley network volume estimate consistent with ancient ocean and warm and wet climate. *Nature Communications*, 8, 15766.

Lyons, T. W., Reinhard, C. T., and Planavsky, N. J. (2014). The rise of oxygen in Earth's early ocean and atmosphere. *Nature*, 506, 307–315.

Mangold, N., Kite, E. S., Kleinhans, M. G., Newsom, H., Ansan, V., Hauber, E., Kraal, E., Quantin, C., and Tanaka, K. (2012). The origin and timing of fluvial activity at Eberswalde crater, Mars. *Icarus*, 220, 530–551.

Marshall, C. P., Love, G. D., Snape, C. E., Hill, A. C., Allwood, A. C., Walter, M. R., Van Kranendonk, M. J., Bowden, S. A., Sylva, S. P., and Summons, R. E. (2007). Structural characterization of kerogen in 3.4 Ga Archaean cherts from the Pilbara Craton, Western Australia. *Precambrian Research*, 155, 1–23.

Martin, W., Baross, J., Kelley, D., and Russell, M. J. (2008). Hydrothermal vents and the origin of life. *Nature Reviews Microbiology*, 6, 805–814.

Martin, W. F. and Sousa, F. L. (2016). Early Microbial Evolution: The Age of Anaerobes. *Cold Spring Harbor Perspectives in Biology*, 8, a018127.

Marty, B., Avice, G., Sano, Y., Altwegg, K., Balsiger, H., Hässig, M., Morbidelli, A., Mousis, O., and Rubin, M. (2016). Origins of volatile elements (H, C, N, noble gases) on Earth and Mars in light of recent results from the ROSETTA cometary mission. *Earth and Planetary Science Letters*, 441, 91–102.

McCollom, T. M. and Bach, W. (2009). Thermodynamic constraints on hydrogen generation during serpentinization of ultramafic rocks. *Geochimica et Cosmochimica Acta*, 73, 856–875.

McCollom, T. M., Ritter, G., and Simoneit, B. R. T. (1999). Lipid Synthesis Under Hydrothermal Conditions by Fischer–Tropsch-Type Reactions. *Origins of Life and Evolution of Biospheres*, 29, 153–166.

McCollom, T. M. and Seewald, J. S. (2007). Abiotic Synthesis of Organic Compounds in Deep-Sea Hydrothermal Environments. *Chemical Reviews*, 107, 382–401.

McKay, C. P. (2010). An Origin of Life on Mars. *Cold Spring Harbor Perspectives in Biology*, 2, a003509.

McKay, C. P., Anbar, A. D., Porco, C., and Tsou, P. (2014). Follow the Plume: The Habitability of Enceladus. *Astrobiology*, 14, 352–355.

McKay, C. P. and Smith, H. D. (2005). Possibilities for methanogenic life in liquid methane on the surface of Titan. *Icarus*, 178, 274–276.

McSween, H. Y., Taylor, G. J., and Wyatt, M. B. (2009). Elemental Composition of the Martian Crust. *Science*, 324, 736–739.

Melosh, H. J. and Vickery, A. M. (1989). Impact erosion of the primordial atmosphere of Mars. *Nature*, 338, 487–489.

Michalski, J. R., Onstott, T. C., Mojzsis, S. J., Mustard, J., Chan, Q. H. S., Niles, P. B., and Johnson, S. S. (2018). The Martian subsurface as a potential window into the origin of life. *Nature Geoscience*, 11, 21–26.

Miller, S. L. (1953). A production of amino acids under possible primitive earth conditions. *Science*, 117, 528–529.

Miller, S. L. (1955). Production of some organic compounds under possible primitive earth conditions. *Journal of the American Chemical Society*, 77, 2351–2361.

Mojzsis, S. J., Cates, N. L., Caro, G., Trail, D., Abramov, O., Guitreau, M., Blichert-Toft, J., Hopkins, M. D., and Bleeker, W. (2014). Component geochronology in the polyphase ca. 3920 Ma Acasta Gneiss. *Geochimica et Cosmochimica Acta*, 133, 68–96.

Morbidelli, A., Chambers, J., Lunine, J. I., Petit, J. M., Robert, F., Valsecchi, G. B., and Cyr, K. E. (2000). Source regions and timescales for the delivery of water to the Earth. *Meteoritics & Planetary Science*, 35, 1309–1320.

Mustard, J. F., Murchie, S. L., Pelkey, S. M., Ehlmann, B. L., Milliken, R. E., Grant, J. A., Bibring, J.-P., Poulet, F., Bishop, J., Dobrea, E. N., Roach, L., Seelos, F., Arvidson, R. E., Wiseman, S., Green, R., Hash, C., Humm, D., Malaret, E., McGovern, J. A., Seelos, K., Clancy, T., Clark, R., Marais, D. D., Izenberg, N., Knudson, A., Langevin, Y., Martin, T., McGuire, P., Morris, R., Robinson, M., Roush, T., Smith, M., Swayze, G., Taylor, H., Titus, T., and Wolff, M. (2008). Hydrated silicate minerals on Mars observed by the Mars Reconnaissance Orbiter CRISM instrument. *Nature*, 454, 305–309.

Mustard, J. F., Poulet, F., Gendrin, A., Bibring, J.-P., Langevin, Y., Gondet, B., Mangold, N., Bellucci, G., and Altieri, F. (2005). Olivine and Pyroxene Diversity in the Crust of Mars. *Science*, 307, 1594–1597.

NASA/GSFC (2000). https://attic.gsfc.nasa.gov/mola/images/mercat_med.jpg.

Navarro-González, R., Vargas, E., de la Rosa, J., Raga, A. C., and McKay, C. P. (2010). Reanalysis of the Viking results suggests perchlorate and organics at midlatitudes on Mars. *Journal of Geophysical Research: Planets*, 115, E12010.

Navarro-González, R., Vargas, E., de la Rosa, J., Raga, A. C., and McKay, C. P. (2011). Correction to "Reanalysis of the Viking results suggests perchlorate and organics at midlatitudes on Mars". *Journal of Geophysical Research: Planets*, 116, E08011.

Nimmo, F., Hart, S. D., Korycansky, D. G., and Agnor, C. B. (2008). Implications of an impact origin for the martian hemispheric dichotomy. *Nature*, 453, 1220–1224.

Nimmo, F. and Tanaka, K. (2005). Early crustal evolution of Mars. *Annual Review of Earth and Planetary Sciences*, 33, 133–161.

Nisbet, E. G. and Sleep, N. H. (2001). The habitat and nature of early life. *Nature*, 409, 1083–1091.

Noffke, N., Eriksson, K. A., Hazen, R. M., and Simpson, E. L. (2006). A new window into Early Archean life: Microbial mats in Earth's oldest siliciclastic tidal deposits (3.2 Ga Moodies Group, South Africa). *Geology*, 34, 253–256.

Nutman, A. P., Bennett, V. C., Friend, C. R. L., Van Kranendonk, M. J., and Chivas, A. R. (2016). Rapid emergence of life shown by discovery of 3,700-million-year-old microbial structures. *Nature*, 537, 535–538.

Oehler, D. Z. and Allen, C. C. (2012). Focusing the search for biosignatures on Mars: facies prediction with an example from Acidalia Planitia. In J. P. Grotzinger and R. E. Milliken (Eds.), *Sedimentary Geology of Mars, SEPM Special Publication 102*. Society for Sedimentary Geology, Tulsa, Oklahoma, pp. 183–194.

Oehler, D. Z. and Cady, S. L. (2014). Biogenicity and Syngeneity of Organic Matter in Ancient Sedimentary Rocks: Recent Advances in the Search for Evidence of Past Life. *Challenges*, 5, 260–283.

Orgel, L. E. (1998). Polymerization on the Rocks: Theoretical Introduction. *Origins of life and evolution of the biosphere*, 28, 227–234.

Orgel, L. E. (2004). Prebiotic Chemistry and the Origin of the RNA World. *Critical Reviews in Biochemistry and Molecular Biology*, 39, 99–123.

Oró, J. and Holzer, G. (1979). The photolytic degradation and oxidation of organic compounds under simulated Martian conditions. *Journal of Molecular Evolution*, 14, 153–160.

Osinski, G. R., Tornabene, L. L., Banerjee, N. R., Cockell, C. S., Flemming, R., Izawa, M. R. M., McCutcheon, J., Parnell, J., Preston, L. J., Pickersgill, A. E., Pontefract, A., Sapers, H. M., and Southam, G. (2013). Impact-generated hydrothermal systems on Earth and Mars. *Icarus*, 224, 347–363.

Paecht-Horowitz, M. (1976). Clays as possible catalysts for peptide formation in the prebiotic era. *Origins of life*, 7, 369–381.

Parker, T. J., Gorsline, D. S., Saunders, R. S., Pieri, D. C., and Schneeberger, D. M. (1993). Coastal geomorphology of the Martian northern plains. *Journal of Geophysical Research: Planets*, 98, 11061–11078.

Pascal, R., Boiteau, L., Forterre, P., Gargaud, M., Lazcano, A., Lopez-Garcia, P., Maurel, M.-C., Moreira, D., Pereto, J., Prieur, D., and Reisse, J. (2006). 5. Prebiotic Chemistry – Biochemistry – Emergence of Life (4.4–2 Ga). *Earth, Moon, and Planets*, 98, 153–203.

Pavlov, A. A., Kasting, J. F., Brown, L. L., Rages, K. A., and Freedman, R. (2000). Greenhouse warming by CH_4 in the atmosphere of early Earth. *Journal of Geophysical Research: Planets*, 105, 11981–11990.

Pavlov, A. A., Vasilyev, G., Ostryakov, V. M., Pavlov, A. K., and Mahaffy, P. (2012). Degradation of the organic molecules in the shallow subsurface of Mars due to irradiation by cosmic rays. *Geophysical Research Letters*, 39, L13202.

Pearce, B. K. D., Pudritz, R. E., Semenov, D. A., and Henning, T. K. (2017). Origin of the RNA world: The fate of nucleobases in warm little ponds. *Proceedings of the National Academy of Sciences of the United States of America*, 114, 11327–11332.

Peters, K. E., Walters, C. C., and Moldowan, J. M. (2005). *The Biomarker Guide - Part I - Biomarkers and Isotopes in the Environment and Human History*. Cambridge University Press, New York.

Phillips, R. J., Zuber, M. T., Solomon, S. C., Golombek, M. P., Jakosky, B. M., Banerdt, W. B., Smith, D. E., Williams, R. M. E., Hynek, B. M., Aharonson, O., and Hauck II, S. A. (2001). Ancient Geodynamics and Global-Scale Hydrology on Mars. *Science*, 291, 2587–2591.

Plescia, J. B. and Saunders, R. S. (1982). Tectonic history of the Tharsis Region, Mars. *Journal of Geophysical Research: Solid Earth*, 87, 9775–9791.

Poch, O., Kaci, S., Stalport, F., Szopa, C., and Coll, P. (2014). Laboratory insights into the chemical and kinetic evolution of several organic molecules under simulated Mars surface UV radiation conditions. *Icarus*, 242, 50–63.

Poulet, F., Bibring, J.-P., Mustard, J. F., Gendrin, A., Mangold, N., Langevin, Y., Arvidson, R. E., Gondet, B., Gomez, C., and Team, T. O. (2005). Phyllosilicates on Mars and implications for early martian climate. *Nature*, 438, 623–627.

Proskurowski, G., Lilley, M. D., Seewald, J. S., Früh-Green, G. L., Olson, E. J., Lupton, J. E., Sylva, S. P., and Kelley, D. S. (2008). Abiogenic Hydrocarbon Production at Lost City Hydrothermal Field. *Science*, 319, 604–607.

Raulin, F. (2007). Question 2: Why an Astrobiological Study of Titan Will Help Us Understand the Origin of Life. *Origins of Life and Evolution of Biospheres*, 37, 345–349.

Rodriguez, J. A. P., Kargel, J. S., Baker, V. R., Gulick, V. C., Berman, D. C., Fairén, A. G., Linares, R., Zarroca, M., Yan, J., Miyamoto, H., and Glines, N. (2015). Martian outflow channels: How did their source aquifers form, and why did they drain so rapidly? *Scientific Reports*, 5, 13404.

Rosing, M. T., Bird, D. K., Sleep, N. H., and Bjerrum, C. J. (2010). No climate paradox under the faint early Sun. *Nature*, 464, 744–747.

Ross, D. S. and Deamer, D. W. (2016). Dry/Wet Cycling and the Thermodynamics and Kinetics of Prebiotic Polymer Synthesis. *Life*, 6, 28.

Ruiz-Mirazo, K., Peretó, J., and Moreno, A. (2004). A Universal Definition of Life: Autonomy and Open-Ended Evolution. *Origins of life and evolution of the biosphere*, 34, 323–346.

Russell, M. J. (2011). Origin of Life. In J. Reitner and V. Thiel (Eds.), *Encyclopedia of Geobiology*. Springer Science & Business Media, Dordrecht, pp. 701–716.

Russell, M. J., Daniel, R. M., Hall, A. J., and Sherringham, J. A. (1994). A hydrothermally precipitated catalytic iron sulphide membrane as a first step toward life. *Journal of Molecular Evolution*, 39, 231–243.

Russell, M. J. and Hall, A. J. (1997). The emergence of life from iron monosulphide bubbles at a submarine hydrothermal redox and pH front. *Journal of the Geological Society*, 154, 377–402.

Russell, M. J., Hall, A. J., and Martin, W. (2010). Serpentinization as a source of energy at the origin of life. *Geobiology*, 8, 355–371.

Sagan, C. and Chyba, C. F. (1997). The Early Faint Sun Paradox: Organic Shielding of Ultraviolet-Labile Greenhouse Gases. *Science*, 276, 1217–1221.

Salese, F., Ansan, V., Mangold, N., Carter, J., Ody, A., Poulet, F., and Ori, G. G. (2016). A sedimentary origin for intercrater plains north of the Hellas basin: Implications for climate conditions and erosion rates on early Mars. *Journal of Geophysical Research: Planets*, 121, 2239–2267.

Sautter, V., Toplis, M. J., Wiens, R. C., Cousin, A., Fabre, C., Gasnault, O., Maurice, S., Forni, O., Lasue, J., Ollila, A., Bridges, J. C., Mangold, N., Le Mouélic, S., Fisk, M., Meslin, P.-Y., Beck, P., Pinet, P., Le Deit, L., Rapin, W., Stolper, E. M., Newsom, H., Dyar, D., Lanza, N., Vaniman, D., Clegg, S., and Wray, J. J. (2015). In situ evidence for continental crust on early Mars. *Nature Geoscience*, 8, 605–609.

Schidlowski, M. (2001). Carbon isotopes as biogeochemical recorders of life over 3.8 Ga of Earth history: evolution of a concept. *Precambrian Research*, 106, 117–134.

Schidlowski, M., Appel, P. W. U., Eichmann, R., and Junge, C. E. (1979). Carbon isotope geochemistry of the 3.7 x 109-yr-old Isua sediments, West Greenland: implications for the Archaean carbon and oxygen cycles. *Geochimica et Cosmochimica Acta*, 43, 189–199.

Schirrmeister, B. E., Gugger, M., Donoghue, P. C. J., and Smith, A. (2015). Cyanobacteria and the Great Oxidation Event: evidence from genes and fossils. *Palaeontology*, 58, 769–785.

Schirrmeister, B. E., Sanchez-Baracaldo, P., and Wacey, D. (2016). Cyanobacterial evolution during the Precambrian. *International Journal of Astrobiology*, 15, 187–204.

Schon, S. C., Head, J. W., and Fassett, C. I. (2012). An overfilled lacustrine system and progradational delta in Jezero crater, Mars: Implications for Noachian climate. *Planetary and Space Science*, 67, 28–45.

Schulte, M., Blake, D., Hoehler, T., and McCollom, T. (2006). Serpentinization and Its Implications for Life on the Early Earth and Mars. *Astrobiology*, 6, 364–376.

Schulze-Makuch, D. and Irwin, L. N. (2008). *Life in the universe: expectations and constraints*. Springer Science & Business Media, Berlin, Heidelberg.

Scott, D. H. and Tanaka, K. L. (1986). *Geologic map of the western equatorial region of Mars*. Technical report.

Segura, T. L., Toon, O. B., Colaprete, A., and Zahnle, K. J. (2002). Environmental Effects of Large Impacts on Mars. *Science*, 298, 1977–1980.

Sephton, M. A., Lewis, J. M. T., Watson, J. S., Montgomery, W., and Garnier, C. (2014). Perchlorate-induced combustion of organic matter with variable molecular weights: Implications for Mars missions. *Geophysical Research Letters*, 41, 7453–7460.

Shaw, G. H. (2008). Earth's atmosphere — Hadean to early Proterozoic. *Chemie der Erde - Geochemistry*, 68, 235–264.

Shaw, G. H. (2017). Comment on "Extensive Noachian fluvial systems in Arabia Terra: Implications for early Martian climate" by Davis et al. *Geology*, 45, e409–e409.

Shaw, G. H. (2018). Comment on "Climate cycling on early Mars caused by the carbonate–silicate cycle" by Batalha et al. *Earth and Planetary Science Letters*, 484, 412–414.

Shock, E. L. and Schulte, M. D. (1998). Organic synthesis during fluid mixing in hydrothermal systems. *Journal of Geophysical Research: Planets*, 103, 28513–28527.

Simoneit, B. R. T., Summons, R. E., and Jahnke, L. L. (1998). Biomarkers as Tracers for Life on Early Earth and Mars. *Origins of life and evolution of the biosphere*, 28, 475–483.

Sleep, N. H. (2010). The Hadean–Archaean Environment. *Cold Spring Harbor Perspectives in Biology*, 2, a002527.

Sleep, N. H., Meibom, A., Fridriksson, T., Coleman, R. G., and Bird, D. K. (2004). H_2-rich fluids from serpentinization: Geochemical and biotic implications. *Proceedings of the National Academy of Sciences of the United States of America*, 101, 12818–12823.

Sleep, N. H. and Zahnle, K. J. (2001). Carbon dioxide cycling and implications for climate on ancient Earth. *Journal of Geophysical Research: Planets*, 106, 1373–1399.

Squyres, S. W., Aharonson, O., Clark, B. C., Cohen, B. A., Crumpler, L., de Souza, P. A., Farrand, W. H., Gellert, R., Grant, J., Grotzinger, J. P., Haldemann, A. F. C., Johnson, J. R., Klingelhöfer, G., Lewis, K. W., Li, R., McCoy, T., McEwen, A. S., McSween, H. Y., Ming, D. W., Moore, J. M., Morris, R. V., Parker, T. J., Rice, J. W., Ruff, S., Schmidt, M., Schröder, C., Soderblom, L. A., and Yen, A. (2007). Pyroclastic Activity at Home Plate in Gusev Crater, Mars. *Science*, 316, 738–742.

Steininger, H., Goesmann, F., and Goetz, W. (2012). Influence of magnesium perchlorate on the pyrolysis of organic compounds in Mars analogue soils. *Planetary and Space Science*, 71, 9–17.

Stüeken, E. E., Anderson, R. E., Bowman, J. S., Brazelton, W. J., Colangelo-Lillis, J., Goldman, A. D., Som, S. M., and Baross, J. A. (2013). Did life originate from a global chemical reactor? *Geobiology*, 11, 101–126.

Sugitani, K., Lepot, K., Nagaoka, T., Mimura, K., Kranendonk, M. V., Oehler, D. Z., and Walter, M. R. (2010). Biogenicity of Morphologically Diverse Carbonaceous Microstructures from the ca. 3400 Ma Strelley Pool Formation, in the Pilbara Craton, Western Australia. *Astrobiology*, 10, 899–920.

Summons, R. E., Albrecht, P., McDonald, G., and Moldowan, J. M. (2008). Molecular Biosignatures. *Space Science Reviews*, 135, 133–159.

Tashiro, T., Ishida, A., Hori, M., Igisu, M., Koike, M., Méjean, P., Takahata, N., Sano, Y., and Komiya, T. (2017). Early trace of life from 3.95 Ga sedimentary rocks in Labrador, Canada. *Nature*, 549, 516–518.

Vago, J. L., Westall, F., Pasteur Instrument Teams, L. S. S. W. G., Other, C., Coates, A. J., Jaumann, R., Korablev, O., Ciarletti, V., Mitrofanov, I., Josset, J.-L., De Sanctis, M. C., Bibring, J.-P., Rull, F., Goesmann, F., Steininger, H., Goetz, W., Brinckerhoff, W., Szopa, C., Raulin, F., Edwards, H. G. M., Whyte, L. G., Fairén, A. G., Bridges, J., Hauber, E., Ori, G. G., Werner, S., Loizeau, D., Kuzmin, R. O., Williams, R. M. E., Flahaut, J., Forget, F., Rodionov, D., Svedhem, H., Sefton-Nash, E., Kminek, G., Lorenzoni, L., Joudrier, L., Mikhailov, V., Zashchirinskiy, A., Alexashkin, S., Calantropio, F., Merlo, A., Poulakis, P., Witasse, O., Bayle, O., Bayón, S., Meierhenrich, U., Carter, J., García-Ruiz, J. M., Baglioni, P., Haldemann, A., Ball, A. J., Debus, A., Lindner, R., Haessig, F., Monteiro, D., Trautner, R., Voland, C., Rebeyre, P., Goulty, D., Didot, F., Durrant, S., Zekri, E., Koschny, D., Toni, A., Visentin, G., Zwick, M., van Winnendael, M., Azkarate, M., Carreau, C., and the ExoMars Project Team (2017). Habitability on Early Mars and the Search for Biosignatures with the ExoMars Rover. *Astrobiology*, 17, 471–510.

Valley, J. W., Cavosie, A. J., Ushikubo, T., Reinhard, D. A., Lawrence, D. F., Larson, D. J., Clifton, P. H., Kelly, T. F., Wilde, S. A., Moser, D. E., and Spicuzza, M. J. (2014). Hadean age for a post-magma-ocean zircon confirmed by atom-probe tomography. *Nature Geoscience*, 7, 219–223.

Van Kranendonk, M. J. (2006). Volcanic degassing, hydrothermal circulation and the flourishing of early life on Earth: A review of the evidence from c. 3490–3240 Ma rocks of the Pilbara Supergroup, Pilbara Craton, Western Australia. *Earth-Science Reviews*, 74, 197–240.

Van Kranendonk, M. J. (2010). Two types of Archean continental crust: Plume and plate tectonics on early Earth. *American Journal of Science*, 310, 1187–1209.

Van Kranendonk, M. J., Altermann, W., Beard, B. L., Hoffman, P. F., Johnson, C. M., Kasting, J. F., Melezhik, V. A., Nutman, A. P., Papineau, D., and Pirajno, F. (2012). A chronostratigraphic division of the Precambrian: possibilities and challenges. In F. M. Gradstein, J. G. Ogg, M. D. Schmitz, and G. M. Ogg (Eds.), *The Geologic Time Scale*. Elsevier, Boston, pp. 299–392.

Van Kranendonk, M. J., Hugh Smithies, R., Hickman, A. H., Wingate, M. T. D., and Bodorkos, S. (2010). Evidence for Mesoarchean (~ 3.2 Ga) rifting of the Pilbara Craton: The missing link in an early Precambrian Wilson cycle. *Precambrian Research*, 177, 145–161.

Van Kranendonk, M. J., Philippot, P., Lepot, K., Bodorkos, S., and Pirajno, F. (2008). Geological setting of Earth's oldest fossils in the ca. 3.5 Ga Dresser Formation, Pilbara Craton, Western Australia. *Precambrian Research*, 167, 93–124.

van Thienen, P., Vlaar, N. J., and van den Berg, A. P. (2004). Plate tectonics on the terrestrial planets. *Physics of the Earth and Planetary Interiors*, 142, 61–74.

van Zuilen, M. A., Lepland, A., and Arrhenius, G. (2002). Reassessing the evidence for the earliest traces of life. *Nature*, 418, 627–630.

Wächtershäuser, G. (1988). Before enzymes and templates: theory of surface metabolism. *Microbiological Reviews*, 52, 452–484.

Walker, J. C. G., Hays, P. B., and Kasting, J. F. (1981). A negative feedback mechanism for the long-term stabilization of Earth's surface temperature. *Journal of Geophysical Research: Oceans*, 86, 9776–9782.

Walter, M. R., Buick, R., and Dunlop, J. S. R. (1980). Stromatolites 3,400–3,500 Myr old from the North Pole area, Western Australia. *Nature*, 284, 443–445.

Watters, T. R., McGovern, P. J., and Irwin III, R. P. (2007). Hemispheres Apart: The Crustal Dichotomy on Mars. *Annual Review of Earth and Planetary Sciences*, 35, 621–652.

Westall, F. (2008). Morphological Biosignatures in Early Terrestrial and Extraterrestrial Materials. *Space Science Reviews*, 135, 95–114.

Westall, F. and Brack, A. (2018). The Importance of Water for Life. *Space Science Reviews*, 214, 50.

Westall, F. and Cavalazzi, B. (2011). Biosignatures in Rocks. In J. Reitner and V. Thiel (Eds.), *Encyclopedia of Geobiology*. Springer Netherlands, Dordrecht, pp. 189–201.

Westall, F., Foucher, F., Bost, N., Bertrand, M., Loizeau, D., Vago, J. L., Kminek, G., Gaboyer, F., Campbell, K. A., Bréhéret, J.-G., Gautret, P., and Cockell, C. S. (2015). Biosignatures on Mars: What, Where, and How? Implications for the Search for Martian Life. *Astrobiology*, 15, 998–1029.

Westall, F., Loizeau, D., Foucher, F., Bost, N., Betrand, M., Vago, J., and Kminek, G. (2013). Habitability on Mars from a Microbial Point of View. *Astrobiology*, 13, 887–897.

Wilde, S. A., Valley, J. W., Peck, W. H., and Graham, C. M. (2001). Evidence from detrital zircons for the existence of continental crust and oceans on the Earth 4.4 Gyr ago. *Nature*, 409, 175–178.

Williams, J.-P., Nimmo, F., Moore, W. B., and Paige, D. A. (2008). The formation of Tharsis on Mars: What the line-of-sight gravity is telling us. *Journal of Geophysical Research: Planets*, 113, E10011.

Wing, M. R. and Bada, J. L. (1991). Geochromatography on the parent body of the carbonaceous chondrite Ivuna. *Geochimica et Cosmochimica Acta*, 55, 2937–2942.

Wordsworth, R., Forget, F., Millour, E., Head, J. W., Madeleine, J.-B., and Charnay, B. (2013). Global modelling of the early martian climate under a denser CO_2 atmosphere: Water cycle and ice evolution. *Icarus*, 222, 1–19.

Wordsworth, R. and Pierrehumbert, R. (2013). Hydrogen-Nitrogen Greenhouse Warming in Earth's Early Atmosphere. *Science*, 339, 64–67.

References

Wordsworth, R. D. (2016). The Climate of Early Mars. *Annual Review of Earth and Planetary Sciences*, 44, 381–408.

Wordsworth, R. D., Kerber, L., Pierrehumbert, R. T., Forget, F., and Head, J. W. (2015). Comparison of "warm and wet" and "cold and icy" scenarios for early Mars in a 3-D climate model. *Journal of Geophysical Research: Planets*, 120, 1201–1219.

Wray, J. J., Hansen, S. T., Dufek, J., Swayze, G. A., Murchie, S. L., Seelos, F. P., Skok, J. R., Irwin III, R. P., and Ghiorso, M. S. (2013). Prolonged magmatic activity on Mars inferred from the detection of felsic rocks. *Nature Geoscience*, 6, 1013–1017.

Zahnle, K. J. (2006). Earth's Earliest Atmosphere. *Elements*, 2, 217–222.

Zahnle, K. J., Arndt, N., Cockell, C. S., Halliday, A., Nisbet, E., Selsis, F., and Sleep, N. H. (2007). Emergence of a Habitable Planet. *Space Science Reviews*, 129, 35–78.

Testing the preservation of biomarkers during experimental maturation of an immature kerogen

Helge Mißbach, Jan-Peter Duda, Nils Keno Lünsdorf, Burkhard C. Schmidt, Volker Thiel

Abstract

Lipid biomarkers have been extensively applied for tracing organisms and evolutionary processes through Earth's history. They have become especially important for the reconstruction of early life on Earth and, potentially, for the detection of life in the extraterrestrial realm. However, it is not always clear how exactly biomarkers reflect a paleoecosystem as their preservation may be influenced by increasing temperatures (T) and pressures (P) during burial. While a number of biomarker indices reflecting thermal maturity have been established, it is often less well constrained to which extent biomarker ratios used for paleoreconstructions are compromised by T and P processes. In this study we conducted hydrous pyrolysis of Green River Shale (GRS) kerogen in gold capsules for $2-2400$ h at 300 °C to assess the maturation behavior of several compounds used as life tracers and for the reconstruction of paleoenvironments (*n*-alkanes, pristane, phytane, gammacerane, steranes, hopanes and cheilanthanes). Lignite samples were matured in parallel with the GRS kerogen to obtain exact vitrinite reflectance data at every sampling point. Our experiment confirms the applicability of biomarker-based indices and ratios as maturity indicators (e.g., total cheilanthanes/hopanes ratio; sterane and hopane isomerization indices). However, several biomarker ratios that are commonly used for paleoreconstructions (e.g., pristane/phytane, pristane/*n*-C_{17}, phytane/*n*-C_{18} and total steranes/hopanes) were considerably affected by differences in the thermal degradation behavior of the respective compounds. Short-term experiments (48 h) performed at 400 °C also revealed that biomarkers $>C_{15}$ (especially steranes and hopanes) and 'biological' chain length preferences for *n*-alkanes are vanished at a vitrinite reflectance between 1.38 and 1.83% R_O. Our data highlight that 'thermal taphonomy' effects have to be carefully considered in the interpretation of biomarkers in ancient rocks and, potentially, extraterrestrial materials.

Keywords: biomarker ratios, closed system pyrolysis, gas chromatography–mass spectrometry, Green River Shale, maturity indicators, vitrinite reflectance, thermal degradation.

2.1 Introduction

Lipid biomarkers are molecular fossils that originate from biological precursor compounds (e.g., Peters et al., 2005a; Brocks et al., 2016). Ever since Treibs (1936) first discovered chlorophyll-derived porphyrins in ca. 230 Ma old Triassic oil shales, biomarkers have been extensively applied for tracing organisms and evolutionary processes through Earth's history and for the reconstruction of past environments. Effective biomarkers should be source-specific, resistant against thermal and biodegradation, and analyzable in natural samples with routine techniques (e.g., Brocks and Summons, 2003; Peters et al., 2005a). Therefore lipids are particularly important, because they fulfill these essential demands and their hydrocarbon skeletons have a high potential for preservation over geological timescales (e.g., Brocks and Summons, 2003; Summons, 2014). Given that the record of body fossils shows huge gaps due to taphonomic effects and the fact that many organisms did not produce preservable hard parts, organic biomarkers may provide a complementary record of past ecosystems independent from the body fossil record (e.g., Hallmann et al., 2011; Brocks et al., 2016). In that respect, biomarkers have become instrumental for the reconstruction of early Life on Earth and, potentially, for the detection of life in the extraterrestrial realm (e.g., Brocks and Summons, 2003; Brocks and Pearson, 2005; Hallmann et al., 2011; Summons, 2014; Olcott Marshall and Cestari, 2015).

Despite the wide use of biomarkers for paleoreconstructions, however, it is not always clear how exactly they reflect a paleoecosystem. For instance, commonly less than 1% of organic matter produced in a marine environment is introduced into the sediment due to abiotic oxidation and intensive microbial reprocessing in the water column and on the sea floor by aerobic and anaerobic respiration (e.g., Hedges and Keil, 1995; Peters et al., 2005a; Middelburg and Meysman, 2007; Vandenbroucke and Largeau, 2007). Furthermore, microbially-driven processes observed in microbial mat settings may also profoundly affect the biomarker inventory (i.e., the 'mat seal effect'; Pawlowska et al., 2013; Blumenberg et al., 2015). During later stages biomarkers are additionally influenced by increasing temperatures (T) and pressures (P). While biomarkers undergo major structural changes during catagenesis (corresponding to temperatures of $50-150$ °C; Tissot and Welte, 1984; Brocks and Summons, 2003; Peters et al., 2005a), they are almost entirely decomposed during metagenesis and metamorphism (corresponding to temperatures of $150-200$ °C and >200 °C, respectively; Tissot and Welte, 1984). High fluid and/or gas pressures, in contrast, may retard the thermal destruction of organic matter (Price, 1993). For the decomposition of biomarkers, geological time is commonly considered as an essential factor in addition to temperature (Tissot and Welte, 1984; Peters et al., 2005b); however, the effect of geological time as a major controlling parameter has also been questioned (Price, 1983, 1993). Further geological factors that influence the preservation of biomarkers are the heating rate and mineralogy, especially the adsorption of carbon compounds onto clay mineral surfaces and mineral catalysts that promote the degradation of hydrocarbons (e.g., Mango, 1996; Mango and Hightower, 1997; Kennedy et al., 2002; Brocks and Summons, 2003). While many studies focused on the generation, expulsion and migration of petroleum hydrocarbons, it is as yet often poorly constrained as to which extent individual organic compounds are affected by these processes, and whether changing P/T conditions cause shifts in relative abundances and ratios of selected biomarkers.

The main portion of organic matter in sediments and rocks is present in the form of 'kerogen', i.e., macromolecules insoluble in usual organic solvents, acids and bases (as opposed to the solvent-soluble 'bitumen' fraction; Durand, 1980). Based on estimations, about 10^{16} tonnes of C are bound to kerogen, compared with only 10^{12} tonnes of living biomass (Durand, 1980; Vandenbroucke and Largeau, 2007). Kerogen formation is still not fully understood, but essentially includes selective preservation of biomacromolecules and polymerization (especially polycondensation) and immobilization processes of organic molecules during early diagenesis (e.g., Durand, 1980; De Leeuw et al., 2006; Vandenbroucke and Largeau, 2007; Hallmann et al., 2011). As macromolecular-bound lipid moieties are more resistant against microbial degradation and thermal overprint than the free molecules, kerogen may facilitate the preservation of biomarkers (e.g., Love et al., 1995; Killops and Killops, 2005; Hallmann et al., 2011). Due to their solid state nature, kerogen particles may remain immobile in the sedimentary environment over geological time scales, and thus are considered syngenetic to the host rock (e.g., Brocks et al., 2003a,b; Love et al., 2008). Kerogen bound biomarkers are therefore commonly used in the reconstruction of Precambrian ecosystems (e.g., Love et al., 2009; Duda et al., 2014; Brocks et al., 2016). However, it is still poorly known how P and T affect the biomarkers that are bound into the kerogen. Therefore maturation experiments could help to better understand these processes.

Numerous earlier maturation experiments have been conducted on the Green River Shale (GRS) (e.g., Burnham and Singleton, 1983; Evans and Felbeck Jr, 1983; Huizinga et al., 1988; Ruble et al., 2001). The GRS comprises relatively immature oil source rocks that contain most lipid biomarker classes regularly used for paleoreconstructions (e.g., Burnham et al., 1982; Evans and Felbeck Jr, 1983). Not surprisingly, biomarkers in the GRS bitumen have been extensively investigated (e.g., Eglinton and Douglas, 1988; Collister et al., 1992; Schoell et al., 1994; Koopmans et al., 1997; Ruble et al., 2001), also as possible analogue studies for current and future Mars missions (Olcott Marshall and Cestari, 2015). The natural bitumen (i.e., geologically produced) has been reported to contain the major portion of the total steranes and hopanes in the GRS. Another minor portion can be released from kerogen via pyrolysis, showing somewhat different distributions of single steranes and hopanes (Eglinton and Douglas, 1988). However, maturation experiments have been mostly focused on petroleum generation from the host rock and changes in the bulk kerogen composition, but so far surprisingly few comprehensive studies exist on the fate of distinct kerogen-bound biomarkers (e.g., Eglinton and Douglas, 1988; Monthioux and Landais, 1989; Peters et al., 1990; Price, 1993).

This study aims at assessing the behavior of selected kerogen-bound hydrocarbon biomarkers, namely *n*-alkanes, pristane, phytane, gammacerane, steranes, hopanes and cheilanthanes, whose presence and ratios are commonly used as life tracers and for the reconstruction of paleoenvironments and evolutionary processes (Peters et al., 2005a,b). By conducting hydrous pyrolysis of the GRS kerogen in closed gold capsules at elevated pressures and for different time intervals and temperature regimes, we evaluated the stability of selected compounds, or compound classes, in relation to each other. Our findings reveal major differences in the preservation of biomarkers along the maturation pathway. This 'thermal taphonomy' has potentially wide implications for their interpretation in ancient rocks and, potentially, extraterrestrial materials.

2.2 Materials and methods

2.2.1 Samples and maturation experiments

The material used for experimental maturation was an oil shale from the Eocene Green River Formation in Eastern Utah (White River Mine located within BLM Oil Shale Research, Development, and Demonstration Lease UTU-84087). Bituminous brown coal samples (SM20; Gruber and Sachsenhofer, 2001) from the Noric Depression (Eastern Alps) were maturated in parallel to the GRS samples (same autoclave, separate gold capsules), to obtain exact vitrinite reflectance values for each maturation step.

The ground GRS rock sample was 3 x extracted with dichloromethane (DCM). The hydrocarbon fraction prepared from the resulting total extract (Section 2.2.2) was used as the untreated reference (0 h). Kerogen was isolated from the pre-extracted GRS using hydrochloric acid and hydrofluoric acid (see e.g., review by Durand and Nicaise, 1980). The residue was homogenized with a mortar and again 3 x extracted with DCM to remove residual bitumen. The dried kerogen (ca. 10 mg) was sealed into gold capsules (3.0 mm outer diameter, 2.6 mm inner diameter, 15 mm length) by arc welding using a Lampert™ tungsten inert gas impulse micro welding device. Extensive heating of the sample during welding was avoided by wrapping the capsule in wet tissue paper. Samples were maturated at 300 °C and 2 kbar for 2 to 2400 h (100 days). Four additional short duration experiments at 400 °C (2, 5, 24 and 48 h) were performed to check for the upper limit of biomarker preservation. Experiments with 2 – 720 h durations were carried out in rapid-quench cold seal pressure vessels (CSPV) enabling a fast heating and cooling of the samples within a few seconds (see Schmidt et al., 2013 for technical details). The 2400 h duration experiments were conducted in conventional CSPV with slower heating and cooling rates (see Le Bayon et al., 2012 for technical details).

2.2.2 Extraction and fractionation

After maturation, the capsules were opened using a metal spike, forceps and scissors, which were thoroughly cleaned between the samples using acetone. About 2/3 of the material was then extracted 4 x with each 2 mL of an *n*-hexane/DCM mixture (1:1, V:V; 20 min ultrasonication). The resulting extracts were combined and carefully reduced using N_2. The extracts were never completely dried before the next step of processing to avoid a major loss of low-boiling compounds (Ahmed and George, 2004). Extracts were dried onto a small amount of silica gel and fractionated by column chromatography (diameter: 1.5 cm, height: 8 cm, Merck silica gel 60). Saturated hydrocarbons were eluted with 3 mL *n*-hexane. The resulting saturated hydrocarbon fractions were reduced to 1 mL and analysed by gas chromatography–mass spectrometry (GC–MS).

2.2.3 GC–MS and vitrinite reflectance

GC–MS analyses were carried out using a Thermo Fisher Trace 1300 Series GC coupled to a Thermo Fisher Quantum XLS Ultra MS. The GC was equipped with a capillary column (Phenomenex Zebron ZB-1MS/Phenomenex Zebron ZB-5, 30 m, 0.1 μm film thickness, inner diameter 0.25 mm). Fractions were injected into a splitless injector and

transferred to the GC column at 270 °C. The carrier gas was He with a flow rate of 1.5 mL/min. The GC oven temperature was ramped 80 °C (1 min) to 310 °C at 5 °C/min (held 20 min). Electron ionization mass spectra were recorded in full scan mode at 70 eV electron energy with a mass range of m/z 50 – 600 and a scan time of 0.42 s.

To determine vitrinite reflectance of the reference coal samples, samples were embedded into epoxy and afterwards cut, abraded (four steps; P400 to P2500), and polished (diamond and alumina slurries, four steps, grain sizes 9 – 0.05 μm, each step 5 min). After polishing the minimum and maximum reflectance of vitrinites have been measured in linear polarized light at 546 nm using a SpectraVision PMT system (A.S. & Co.) consisting of a Zeiss Axio Imager.A2m microscope (Carl Zeiss Microscopy, LLC, New York, United States) with an attached Zeiss MCS CCD/UVNIR spectrometer. Fifteen measurements on random grains were made for each sample. Standard deviations were generally < 0.08%.

2.3   Results and discussion

The hydrocarbon fraction of the untreated GRS bitumen (0 h) contains n-alkanes, acyclic (e.g., pristane and phytane) and cyclic (e.g., steranes and terpanes) isoprenoids as well as some other biomarkers that are not in the focus of this study (e.g., carotenoids; Fig. 2.1). The 300 °C experiment covers a maturity range from immature (0.49% R_O, untreated sample 0 h) to the main catagenetic stage (1.21% R_O, 2400 h) thus being well suited to track continuous changes in the biomarker inventory with increasing maturity. The 400 °C experiment conducted to check for the upper limit of biomarker preservation represents a maturity range between 1.19% R_O (2 h) and 1.83% R_O (48 h).
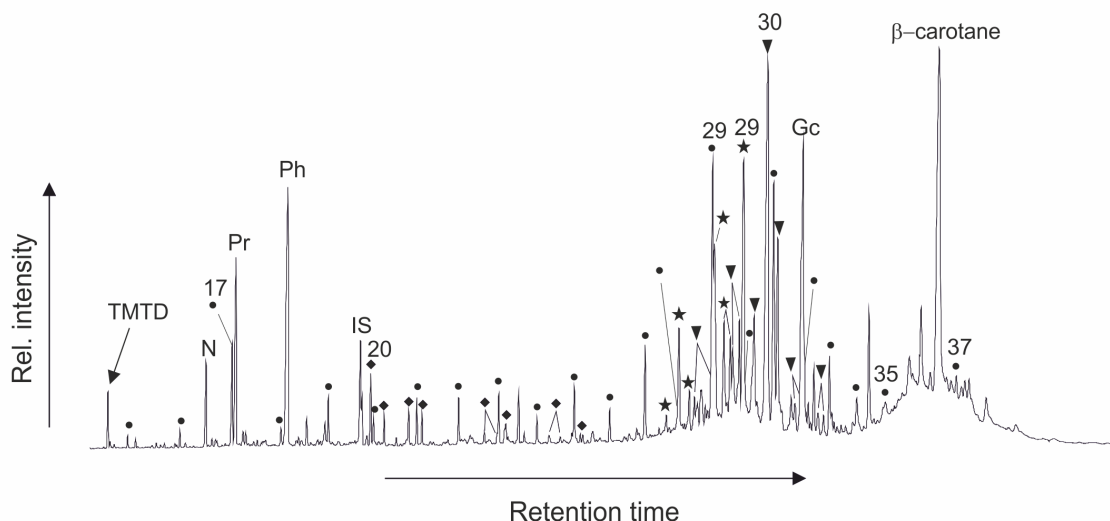
Figure 2.1: GC–MS chromatogram (total ion current, TIC) of Green River Shale bitumen (untreated). Numbers refer to number of carbon atoms. Filled circles denote n-alkanes, stars denote steranes, triangles denote hopanes, diamonds denote cheilanthanes; TMTD,2,6,10 trimethyltridecane; N, norpristane; Pr, pristane; Ph, phytane; Gc, gammacerane; IS, internal standard (eicosane d42 10 mg/L).

2.3.1   *n*-Alkanes

n-Alkanes in the original GRS bitumen have chain lengths from *n*-C_{15} to *n*-C_{37}. They show a bimodal distribution with maxima at *n*-C_{17}, and *n*-C_{29}/*n*-C_{31} (Fig. 2.2). In the long-chain range, *n*-alkanes exhibit a clear odd-over-even predominance as reflected by a carbon preference index (CPI) of 3.6 (calculated after Bray and Evans, 1961; Table 2.1). *n*-C_{17} is common in extant cyanobacteria and algae and its predominance in the short-chain range can be attributed to planktonic photoautotrophs (e.g., Blumer et al., 1971; Hoffmann et al., 1987; Jacobson et al., 1988). The also abundant long chain *n*-alkanes with a pronounced odd-over-even predominance in the range of *n*-C_{27} to *n*-C_{33} are commonly explained by inputs of epicuticular leaf waxes derived from higher land plants (Eglinton and Hamilton, 1967). The *n*-alkane distribution found in the GRS bitumen is thus well in line with a high-productivity lacustrine environment (e.g., Tissot et al., 1978; Horsfield et al., 1994). During experimental maturation, this original *n*-alkane distribution is profoundly altered. While the distinct maximum at *n*-C_{17} and the odd-over-even predominance in the high molecular weight range become less pronounced (Fig. 2.2, 24 – 2400 h), the CPI decreases from 3.6 (0 h) to 1.4 after 2400 h (1.21% R_O, Table 2.1). It should be noted that these experimental data reflect a lag of the CPI with respect to vitrinite reflectance, as a CPI-value approaching 1 is generally expected at $\sim 0.9\%$ R_O (i.e., peak oil window; Peters et al., 2005b). In our experiment, the 'biological' chain length preferences of *n*-alkanes are completely vanished only after 48 h at 400 °C (corresponding to 1.83% R_O, not shown). Possible reasons for this mismatch between biomarkers and vitrinite reflectance are discussed below. Nevertheless, our results underline that the source-specific features of individual *n*-alkane chain lengths gradually disappear with increasing maturity (Tissot et al., 1978; Price, 1993; Peters et al., 2005a).

2.3.2   Acyclic isoprenoids

Acyclic isoprenoids in the GRS bitumen include 2,6,10-trimethyltridecane (C_{16}), norpristane (C_{18}), pristane (C_{19}) and phytane (C_{20}) (Figs. 2.1, 2.2). The pristane/phytane ratio (Pr/Ph) is 0.3, while the pristane/*n*-C_{17} (Pr/*n*-C_{17}) and phytane/*n*-C_{18} (Ph/*n*-C_{18}) ratios are 1.4 and 26.5, respectively (Table 2.1). Pristane and phytane are biomarkers that mainly originate from phytol, the corresponding alcohol to the phytyl side chain of chlorophyll (Brocks and Summons, 2003; Peters et al., 2005b). However, pristane can also derive from tocopherols (E vitamins; Goossens et al., 1984), while phytane can derive from archaeols (i.e., ether lipid compounds from Archaea; Brocks and Summons, 2003). Pristane in oils and bitumens can furthermore originate from cracking of isoprenoid moieties that are bound to the kerogen matrix (Larter et al., 1979; Goossens et al., 1988a,b). However, given the type of environment (see above), chlorophyll and/or tocopherols are likely to be the major precursors for these isoprenoids in the GRS.

Pr/Ph ratios are commonly used for the reconstruction of paleoredox conditions in ancient settings (e.g., Blumenberg et al., 2012; Yamada et al., 2014; Tulipani et al., 2015; Luo et al., 2015; Naeher and Grice, 2015), as phytol is preferentially transformed to pristane under oxic conditions and to phytane under anoxic conditions (Didyk et al., 1978; Peters et al., 2005b). However, the Pr/Ph ratio is also affected by thermal maturity (Ten Haven et al., 1987; Peters et al., 2005b). Our data show that the Pr/Ph ratio increases until
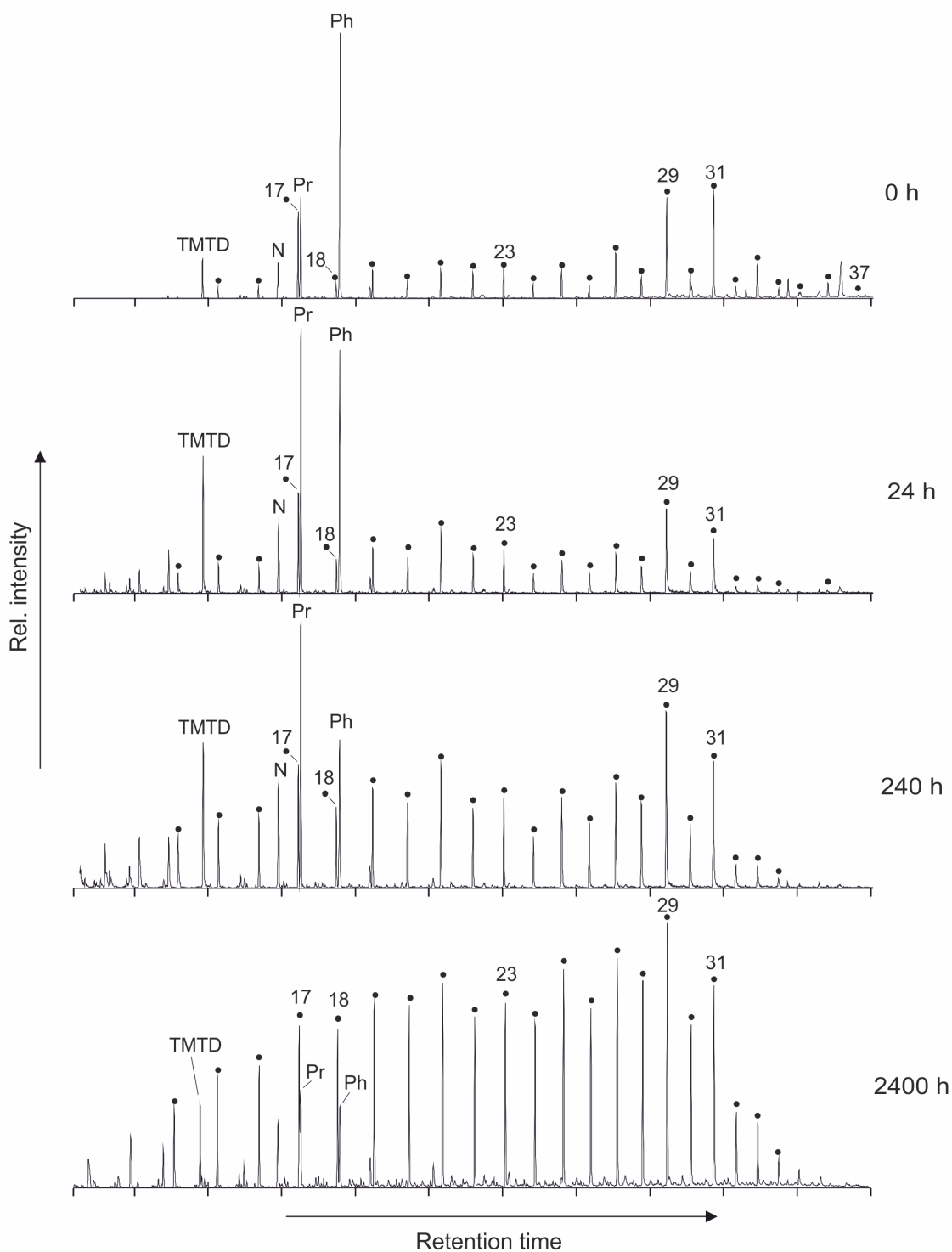
Figure 2.2: GC–MS chromatograms (*n*-alkanes and isoprenoids, *m/z* 85) of Green River Shale bitumen (untreated, 0 h) and experimentally maturated Green River Shale kerogens (300 °C; 24, 240 and 2400 h, respectively). Numbers refer to number of carbon atoms; filled circles denote *n*-alkanes; TMTD, 2,6,10 trimethyl-tridecane; N, norpristane; Pr, pristane; Ph, phytane.

a maturation time of 240 h, but then decreases (Fig. 2.3a). This change in the evolution of Pr/Ph ratios could be due to a preferential release of pristane from kerogen during early catagenesis (Peters et al., 2005b).

The Pr/n-C_{17} and Ph/n-C_{18} ratios are used to assess the impact of biodegradation and thermal maturation on bitumens (e.g., Hieshima and Pratt, 1991; Meredith et al., 2000; Peters et al., 2005a,b; Blumenberg et al., 2012). Both ratios typically increase due to biodegradation (Peters et al., 2005a,b) and decrease with increasing maturity (Alexander et al., 1981; Ten Haven et al., 1987; Peters et al., 2005b). As expected, our data also show a decrease in Ph/n-C_{18} over time, albeit with a somewhat steeper drop of the ratio before 100 h (Fig. 2.3b). This could be explained by a time lag between the formation of phytane and n-C_{18} from kerogen; phytane is dominantly generated during earliest maturation whereas a pronounced formation of n-C_{18} occurs at higher maturities. This effect may be influenced by heating rate (Burnham et al., 1982) or kerogen composition.

The impact of maturity on Pr/n-C_{17} seems to be more complex as the ratio initially increases, summits at 48 h and then decreases with further maturation time (Fig. 2.3b). In natural samples, an increase of the Pr/n-C_{17} ratio may result from preferential biodegradation of the n-alkane (Peters et al., 2005b), which can be excluded here. Instead, the observed phenomenon may be explained by a higher release of pristane relative to n-C_{17} from the kerogen during early maturation (e.g., from tocopherol or other isoprenoid moieties; Larter et al., 1979; Goossens et al., 1984, 1988b). This is in line with the observed initial increase of the Pr/Ph ratio (Fig. 2.3a). Taken together our data suggest a more reliable applicability of Ph/n-C_{18} as a maturity indicator, while that of Pr/n-C_{17} is restricted.

Table 2.1: Biomarker ratios, indices and corresponding vitrinite reflectances (VR) of Green River Shale bitumen and experimentally matured kerogens (300 °C).

Maturation time (hours)	0	2	5	10	24	48	120	240	360	720	2400
CPI	3.6	2.6	2.8	2.7	2.6	2.6	2.2	2.0	1.8	1.7	1.4
VR (% R_O) mean	0.49	0.69	0.64	0.73	0.79	0.85	0.89	0.92	0.96	1.03	1.21
VR (% R_O) SD	0.03	0.05	0.03	0.05	0.04	0.04	0.02	0.06	0.03	0.04	0.04
Pristane/phytane	0.3	0.4	0.5	0.7	1.1	1.2	1.5	1.7	1.6	1.5	1.1
Pristane/n-C_{17}	1.4	1.8	2.0	2.8	3.5	4.8	3.6	2.9	2.7	1.4	0.9
Phytane/n-C_{18}	26.5	28.0	21.0	13.7	9.9	9.3	4.4	2.6	2.4	1.2	0.8
Total steranes/hopanes	0.4	0.3	0.3	0.2	0.2	0.2	0.2	0.1	0.1	0.1	0.1
Total cheilanthanes/hopanes	0.1	0.2	0.2	0.2	0.3	0.3	0.4	0.4	0.4	0.4	1.0
C_{29} 20S/(20S + 20R)	0.23	0.23	0.23	0.23	0.27	0.29	0.38	0.41	0.48	0.53	0.59
C_{31} 22S/(22S + 22R)	0.37	0.37	0.38	0.41	0.45	0.52	0.55	0.56	0.60	0.56	0.55
C_{32} 22S/(22S + 22R)	0.45	0.22	0.26	0.31	0.35	0.43	0.48	0.56	0.57	0.58	0.58
Gammacerane index	4.5	4.1	4.2	4.3	4.2	4.5	4.5	4.6	4.3	4.8	5.3

All ratios and indices were calculated from peak integrals: Isoprenoids and n-alkanes, m/z 85; steranes, m/z 217; hopanes and cheilanthanes, m/z 191. CPI, carbon preference index (after Bray and Evans, 1961); SD, standard deviation ($n = 15$); Gammacerane index = $10 \times$ gammacerane/(gammacerane + C_{30} hopane).

2.3.3 Cyclic isoprenoids

Cyclic isoprenoids in the GRS bitumen include steranes, hopanes, gammacerane and cheilanthanes (Fig. 2.1). The 20S and 20R isomers of C_{27} to C_{29} steranes are abundant

(Figs. 2.1, 2.4). Hopanes range from C_{27} to C_{32}, with the C_{30} pseudohomolog being particularly abundant (Figs. 2.1, 2.4). For all homohopanes (i.e., hopanes $> C_{30}$), both 22S and 22R isomers are present (Fig. 2.4). Cheilanthanes range from C_{20} to C_{26} (Fig. 2.4). All these compounds are useful biosignatures. While steranes derive from sterols, which control the permeability and rigidity of eukaryotic cell membranes (e.g., Brocks and Summons, 2003; Peters et al., 2005b), hopanes mainly originate from bacteriohopanepolyols (C_{35}), which are lipids in some groups of bacteria (Rohmer et al., 1984; Brocks and Pearson, 2005). The pentacyclic triterpenoid gammacerane (C_{30}) derives from tetrahymanol (Ten Haven et al., 1989), which has various biological sources but is particularly abundant in anoxygenic phototrophs (*Rhodopseudomonas palustris*; Kleemann et al., 1990; Eickhoff et al., 2013) and bacterivorous ciliates (Harvey and McManus, 1991; Sinninghe Damsté et al., 1995). Cheilanthanes are tricyclic terpanes (usually C_{19} to C_{45}, rarely up to C_{54}) that were applied as biomarkers in many studies (Moldowan et al., 1983; De Grande et al., 1993; Brocks and Summons, 2003; Brocks and Pearson, 2005; Peters et al., 2005b, and references therein). The actual source of cheilanthanes is still unknown but it has been suggested that the precursor lipids originate from eukaryotic algae (e.g., Brocks and Summons, 2003; Brocks and Pearson, 2005).

The total steranes/hopanes ratio (St/H) is commonly used to evaluate relative inputs of eukaryotic and prokaryotic biomass (e.g., Brocks et al., 1999; Peters et al., 2005b; Love et al., 2009; Blumenberg et al., 2012; Flannery and George, 2014). However, it is known that this ratio may change through taphonomic processes (Pawlowska et al., 2013; Blumenberg et al., 2015). Also thermal maturation appears to be critical, leading to a decreasing St/H ratio (Requejo, 1994; Norgate et al., 1999). In our 300 °C experiment, the St/H ratio shows a four-fold decrease from 0.4 to 0.1, testifying a strong impact of maturity in the range of 0.49 – 1.21% R_O (Table 2.1, Fig. 2.3c). At even higher maturities, in the 400 °C experiment, a point was reached where steranes were entirely decomposed, whereas hopanes were still present (St/H = 0 at 1.38% R_O). This different behavior of steranes and hopanes has to be considered in addition to taphonomic processes in paleoenvironmental studies, particularly in ancient rocks of higher maturities.

Further biomarker based maturity proxies include the total cheilanthanes/hopanes ratio (Chei/H) as well as isomerization indices of homohopanes (22S/(22S + 22R)) and steranes (20S/(20S + 20R)) (e.g., Rullkötter et al., 1986; Summons et al., 1988; Brocks et al., 1999, 2016; Ruble et al., 2001; Peters et al., 2005b; Blumenberg et al., 2012). Chei/H depends on maturity as cheilanthanes are more resistant to thermal maturation than hopanes and are preferentially released from the kerogen with increasing maturity (Aquino Neto et al., 1981; Peters et al., 1990). In our 300 °C experiment, this is confirmed by a continuous increase of the Chei/H ratio from 0.1 to 1.0 (Fig. 2.3d, Table 2.1). In the case of homohopane and sterane isomerization, the biological R-configuration is progressively transferred to the S-configuration during maturation, thus leading to a relative increase of the S isomers (Brocks and Summons, 2003; Peters et al., 2005b; Hallmann et al., 2011). In our experiment, sterane and hopane isomerization consistently increased with maturation time, as expected (Fig. 2.3e). Thermal equilibrium values (22S/(22S + 22R) hopanes: 0.57 – 0.62, 20S/(20S + 20R) steranes: 0.52 – 0.55; Peters et al., 2005b) were reached after 360 h (hopanes) and 720 h (steranes), which in our experiments correspond to 0.96 and 1.03% R_O, respectively (Table 2.1). Thus, a shift can be seen between our experimental data and published biomarker equilibrium values, as full isomerization in geological sys-
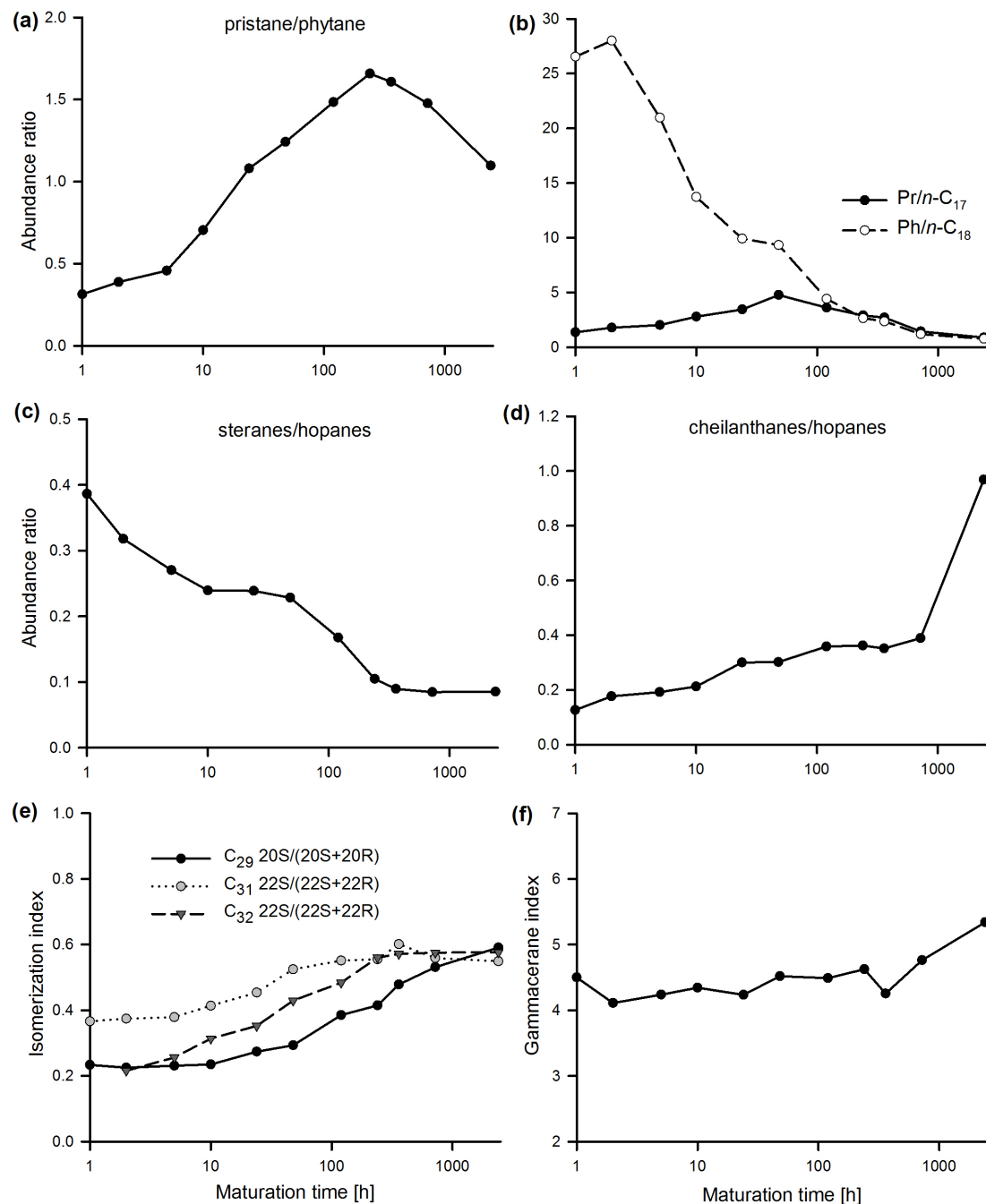
Figure 2.3: Evolution of biomarker-based ratios and indices of untreated (0 h) and experimentally maturated (2 – 2400 h) Green River Shale samples (see also Table 2.1). Please note that the untreated Green River Shale bitumen is always plotted at 1 h (instead of 0 h) due to the logarithmic scale. Gammacerane index $= 10 \times$ gammacerane/(gammacerane $+ C_{30}$ hopane). Pr, pristane; Ph, phytane.

tems is expected at roughly 0.6 and 0.8% R_O, respectively (Peters et al., 2005b). This mismatch may, to some degree, be due to differences in the maturation behavior between the two samples (lignite versus GRS), as well as a lack of resolution due to the setting of time intervals for the experiments. On the other hand, it is commonly observed that vitrinite reflectance data and biomarkers may give different results regarding thermal maturity, with variations of $\pm 0.1\%$ R_O being common (Peters et al., 2005b). Although both vitrinite reflectance and biomarker indicators are controlled by thermal stress (temperature and time), biomarkers may be additionally influenced by other effects. For example, the CPI is also affected by organic matter input (source effect) and biodegradation, while isomerization indices might be influenced by selective thermal decomposition of individual isomers, and/or fast reverse reactions (see Peters et al., 2005b for a detailed discussion). Therefore the comparability of short-term experimental data to natural samples is limited.
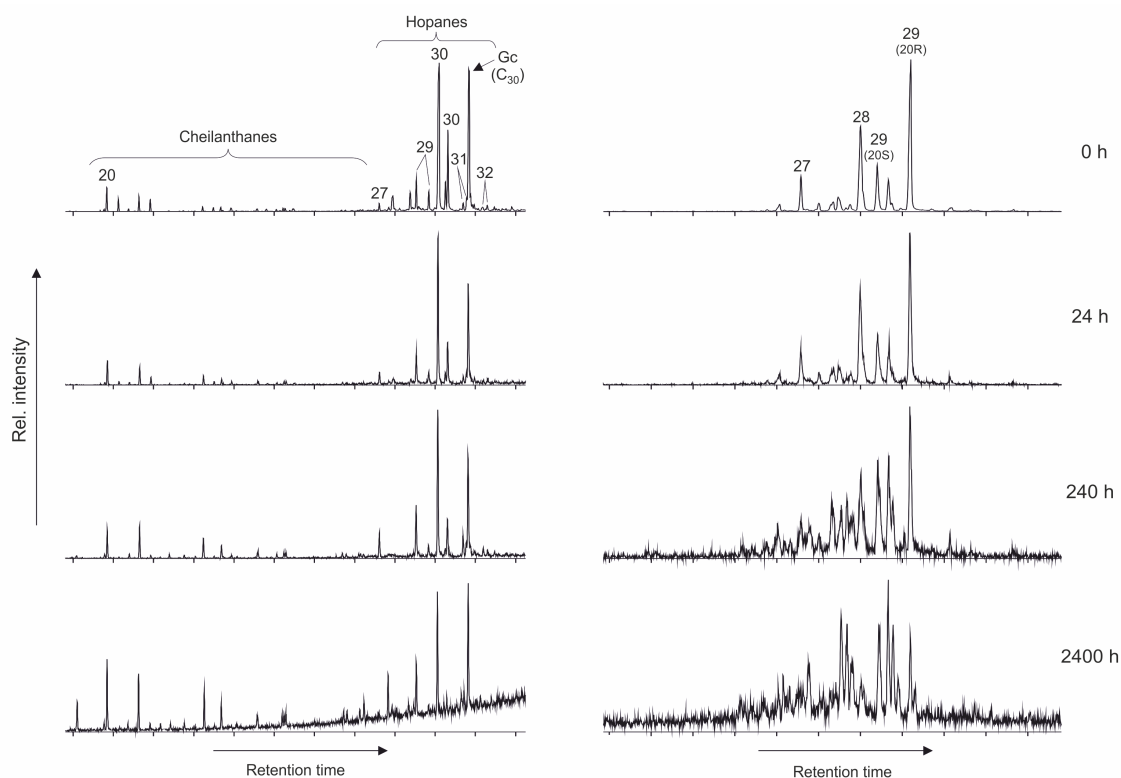
Figure 2.4: GC–MS chromatograms of terpanes (*m/z* 191, left side) and steranes (*m/z* 217, right side) in the Green River Shale bitumen (untreated, 0 h) and experimentally matured Green River Shale kerogens (300 °C; 24, 240 and 2400 h, respectively). Numbers refer to number of carbon atoms. Gc, gammacerane.

The pronounced occurrence of gammacerane and a high gammacerane index (i.e., $10 \times Gc/(Gc + C_{30}$ hopane)) are highly specific indicators for water column stratification and, potentially, increased salinity (Sinninghe Damsté et al., 1995; Peters et al., 2005b). Our data show that the gammacerane index varies little in the course of the 300 °C experiment (Fig. 2.3f), underlining that this proxy is barely affected by maturation processes.

41

2.3.4   When are the biomarkers gone?

The 400 °C experiment ($1.19 - 1.83\%$ R_O) provides information on the overall thermal stability of biomarkers beyond the diagenetic/catagenetic stages. Among the biomarkers investigated in this study, steranes turned out as the thermally least stable compounds. While traces of steranes were still present at the end of the 300 °C experiment (1.19% R_O, Fig. 2.4), these molecules were completely destroyed after 5 h at 400 °C, corresponding to 1.38% R_O (Fig. 2.5). In contrast, hopanes, cheilanthanes and gammacerane were shown to be thermally more stable (in accordance with e.g., Eglinton and Douglas, 1988). In our experiment, traces were still present after 24 h at 400 °C (1.67% R_O), while these compounds were no longer detected after 48 h, corresponding to 1.83% R_O (Fig. 2.5).

It has been postulated that in the range of $1.35 - 2.0\%$ R_O all biomarkers $> C_{15}$ are destroyed (Tissot and Welte, 1984), which is in good accordance with our results. As this range represents the end of catagenesis (~ 150 °C in natural systems), the preservation of biomarkers in Precambrian rocks that experienced extensive metamorphism should be the exception (see e.g., French et al., 2015). Yet, it has been shown that sedimentary rocks may still contain hydrocarbons (and biomarkers) $> C_{15}$ even if they experienced burial metamorphism (i.e., > 200 °C, $> 4\%$ R_O; e.g., Price, 1993; Brocks and Summons, 2003, and references therein). This implies that the preservation of biomarkers in natural systems is also influenced by further parameters such as lithology (grain size), reaction kinetics, presence of water, and fluid pressures (Price, 1993). This stresses the need for further maturation experiments in which these parameters are considered.

2.4   Conclusions

Our experimental maturation performed on kerogen from the Eocene Green River Shale study confirms the applicability of biomarker-based indices and ratios as maturity indicators (e.g., total cheilanthanes/hopanes ratio; sterane and hopane isomerization indices). However, the data also demonstrate that several biomarker ratios that are commonly used for paleobiological and environmental interpretations (e.g., pristane/phytane, pristane/n-C_{17}, phytane/n-C_{18} and total steranes/hopanes) are profoundly biased by differences in the thermal degradation behavior and therefore have to be used only upon consideration of the thermal history of the sample. In particular, a strong relative increase of pristane versus phytane during the early maturation stages indicates different sources and mechanisms of formation for these compounds and gives rise to major shifts in the pristane/n-C_{17} and phytane/n-C_{18} ratios. Likewise, the ratio of eukaryote-derived steranes versus bacterial-derived hopanes strongly decreases in the course of maturation, indicating that steranes are considerably more susceptible to thermal degradation than hopanes. On the basis of the presence or relative abundance of steranes (total steranes/hopanes ratio), organic matter contributions of eukaryotes to ancient sediments may therefore be underestimated. On the other hand, bacterial hopanes and gammacerane (derived from anoxygenic bacteria and/or bacterivorous ciliates) showed very similar stability, so that the gammacerane index remained virtually unaffected by thermal maturation. In our experiment, biomarkers $> C_{15}$ (especially steranes and hopanes) and 'biological' chain length preferences for n-alkanes were completely vanished at 1.83% R_O. However, a systematic shift was observed between measured vitrinite reflectances and molecular ma-
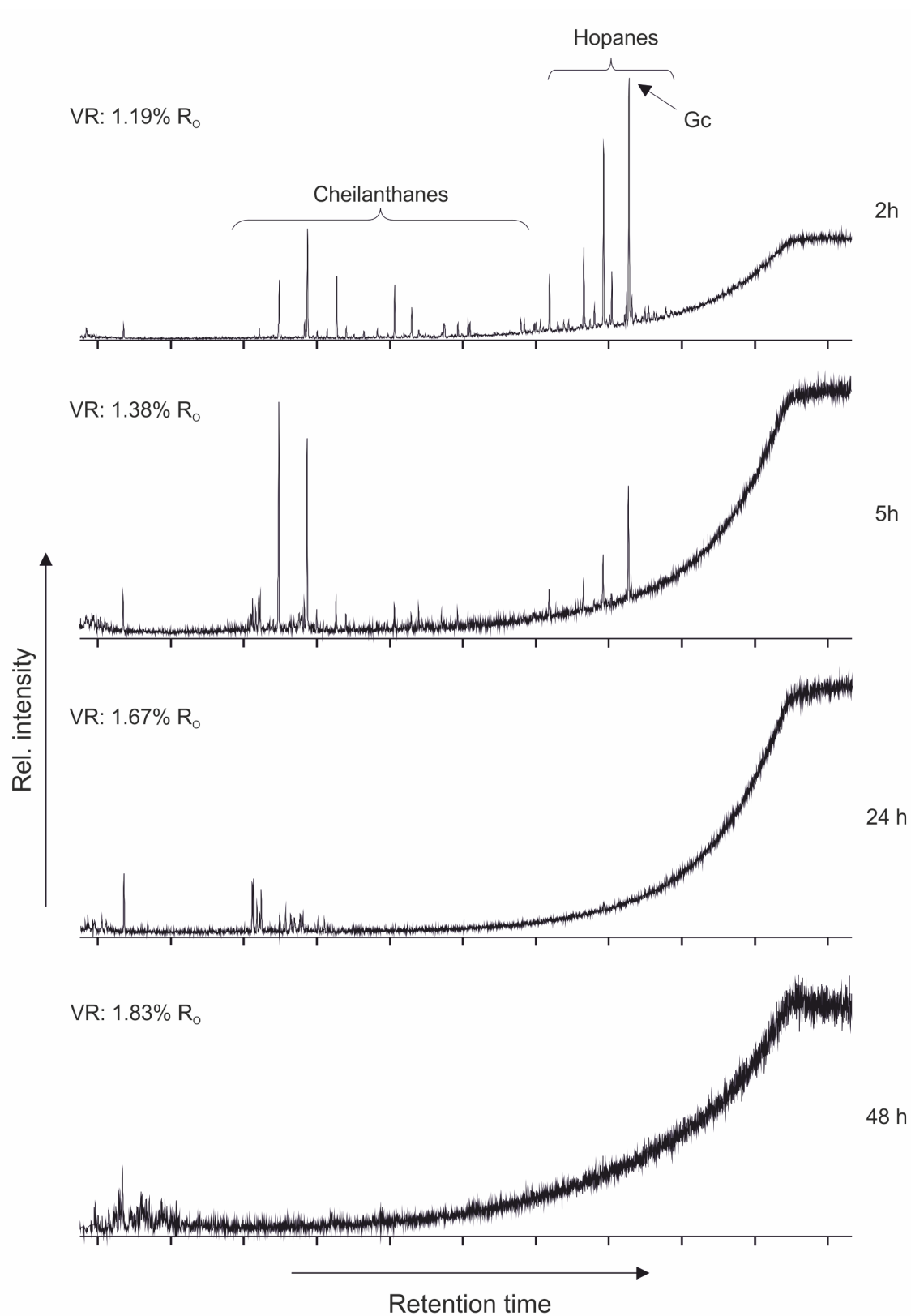
Figure 2.5: GC–MS chromatograms (terpanes, *m/z* 191) of experimentally matured Green River Shale kerogens (400 °C; 2, 5, 24 and 48 h) with corresponding vitrinite reflectance (VR). Gc, Gammacerane.

turity indicators, resulting in R_O values consistently higher than expected for a given biomarker ratio. Summarizing, our study nevertheless underlines the value of maturation experiments for assessing the influence of thermal stress on individual biomarkers, or biomarker ratios. More such experiments have to be performed to improve our ability of assessing the impact of maturation on organic matter in ancient rocks and, potentially, extraterrestrial materials. Future studies should also employ different P/T regimes and matrix minerals for a better estimation of their impact on the preservation of individual biomarkers.

Acknowledgements

References

Ahmed, M. and George, S. C. (2004). Changes in the molecular composition of crude oils during their preparation for GC and GC–MS analyses. *Organic Geochemistry*, 35, 137–155.

Alexander, R., Kagi, R. I., and Woodhouse, G. W. (1981). Geochemical correlation of Windalia oil and extracts of Winning Group (Cretaceous) potential source rocks, Barrow Subbasin, Western Australia. *AAPG bulletin*, 65, 235–250.

Aquino Neto, F. R., Trendel, J. M., Restle, A., Connan, J., and Albrecht, P. A. (1981). Occurrence and formation of tricyclic and tetracyclic terpanes in sediments and petroleums. *Advances in Organic Geochemistry*, 10, 659–667.

Blumenberg, M., Thiel, V., and Reitner, J. (2015). Organic matter preservation in the carbonate matrix of a recent microbial mat – Is there a 'mat seal effect'? *Organic Geochemistry*, 87, 25–34.

Blumenberg, M., Thiel, V., Riegel, W., Kah, L. C., and Reitner, J. (2012). Biomarkers of black shales formed by microbial mats, Late Mesoproterozoic (1.1 Ga) Taoudeni Basin, Mauritania. *Precambrian Research*, 196–197, 113–127.

Blumer, M., Guillard, R. R. L., and Chase, T. (1971). Hydrocarbons of marine phytoplankton. *Marine Biology*, 8, 183–189.

Bray, E. E. and Evans, E. D. (1961). Distribution of *n*-paraffins as a clue to recognition of source beds. *Geochimica et Cosmochimica Acta*, 22, 2–15.

Brocks, J. J., Buick, R., Logan, G. A., and Summons, R. E. (2003a). Composition and syngeneity of molecular fossils from the 2.78 to 2.45 billion-year-old Mount Bruce Supergroup, Pilbara Craton, Western Australia. *Geochimica et Cosmochimica Acta*, 67, 4289–4319.

Brocks, J. J., Jarrett, A. J. M., Sirantoine, E., Kenig, F., Moczydłowska, M., Porter, S., and Hope, J. (2016). Early sponges and toxic protists: possible sources of cryostane, an age diagnostic biomarker antedating Sturtian Snowball Earth. *Geobiology*, 14, 129–149.

Brocks, J. J., Logan, G. A., Buick, R., and Summons, R. E. (1999). Archean molecular fossils and the early rise of eukaryotes. *Science*, 285, 1033–1036.

Brocks, J. J., Love, G. D., Snape, C. E., Logan, G. A., Summons, R. E., and Buick, R. (2003b). Release of bound aromatic hydrocarbons from late Archean and Mesoproterozoic kerogens via hydropyrolysis. *Geochimica et Cosmochimica Acta*, 67, 1521–1530.

Brocks, J. J. and Pearson, A. (2005). Building the biomarker tree of life. *Reviews in Mineralogy and Geochemistry*, 59, 233–258.

Brocks, J. J. and Summons, R. E. (2003). Biomarkers for Early Life. In W. H. Schlesinger (Ed.), *Biogeochemistry*. Elsevier, Oxford, pp. 63–115.

Burnham, A. K., Clarkson, J. E., Singleton, M. F., Wong, C. M., and Crawford, R. W. (1982). Biological markers from Green River kerogen decomposition. *Geochimica et Cosmochimica Acta*, 46, 1243–1251.

Burnham, A. K. and Singleton, M. F. (1983). High-pressure pyrolysis of Green River oil shale. In *ACS Symp. Ser. (United States)*, Lawrence Livermore National Lab., CA.

Collister, J. W., Summons, R. E., Lichtfouse, E., and Hayes, J. M. (1992). An isotopic biogeochemical study of the Green River oil shale. *Organic Geochemistry*, 19, 265–276.

De Grande, S. M. B., Aquino Neto, F. R., and Mello, M. R. (1993). Extended tricyclic terpanes in sediments and petroleums. *Organic Geochemistry*, 20, 1039–1047.

De Leeuw, J. W., Versteegh, G. J. M., and van Bergen, P. F. (2006). Biomacromolecules of algae and plants and their fossil analogues. In J. Rozema, R. Aerts, and H. Cornelissen (Eds.), *Plants and Climate Change*. Springer Netherlands, Dordrecht, pp. 209–233.

Didyk, B. M., Simoneit, B. R. T., Brassell, S. C., and Eglinton, G. (1978). Organic geochemical indicators of palaeoenvironmental conditions of sedimentation. *Nature*, 272, 216–222.

Duda, J.-P., Blumenberg, M., Thiel, V., Simon, K., Zhu, M., and Reitner, J. (2014). Geobiology of a palaeoecosystem with Ediacara-type fossils: The Shibantan Member (Dengying Formation, South China). *Precambrian Research*, 255, 48–62.

Durand, B. (1980). Sedimentary organic matter and kerogen. Definition and quantitative importance of kerogen. In B. Durand (Ed.), *Kerogen*. Éditions Technip, Paris, pp. 13–34.

Durand, B. and Nicaise, G. (1980). Procedures for kerogen isolation. In B. Durand (Ed.), *Kerogen*. Éditions Technip, Paris, pp. 35–53.

Eglinton, G. and Hamilton, R. J. (1967). Leaf epicuticular waxes. *Science*, 156, 1322–1335.

Eglinton, T. I. and Douglas, A. G. (1988). Quantitative study of biomarker hydrocarbons released from kerogens during hydrous pyrolysis. *Energy & Fuels*, 2, 81–88.

Eickhoff, M., Birgel, D., Talbot, H. M., Peckmann, J., and Kappler, A. (2013). Oxidation of Fe(II) leads to increased C-2 methylation of pentacyclic triterpenoids in the anoxygenic phototrophic bacterium Rhodopseudomonas palustris strain TIE-1. *Geobiology*, 11, 268–278.

Evans, R. J. and Felbeck Jr, G. T. (1983). High temperature simulation of petroleum formation—I. The pyrolysis of Green River Shale. *Organic Geochemistry*, 4, 135–144.

Flannery, E. N. and George, S. C. (2014). Assessing the syngeneity and indigeneity of hydrocarbons in the ~1.4 Ga Velkerri Formation, McArthur Basin, using slice experiments. *Organic Geochemistry*, 77, 115–125.

French, K. L., Hallmann, C., Hope, J. M., Schoon, P. L., Zumberge, J. A., Hoshino, Y., Peters, C. A., George, S. C., Love, G. D., and Brocks, J. J. (2015). Reappraisal of hydrocarbon biomarkers in Archean rocks. *Proceedings of the National Academy of Sciences of the United States of America*, 112, 5915–5920.

Goossens, H., de Lange, F., de Leeuw, J. W., and Schenck, P. A. (1988a). The Pristane Formation Index, a molecular maturity parameter. Confirmation in samples from the Paris Basin. *Geochimica et Cosmochimica Acta*, 52, 2439–2444.

Goossens, H., de Leeuw, J. W., Schenck, P. A., and Brassell, S. C. (1984). Tocopherols as likely precursors of pristane in ancient sediments and crude oils. *Nature*, 312, 440–442.

Goossens, H., Due, A., de Leeuw, J. W., van de Graaf, B., and Schenck, P. A. (1988b). The Pristane Formation Index, a new molecular maturity parameter. A simple method to assess maturity by pyrolysis/evaporation-gas chromatography of unextracted samples. *Geochimica et Cosmochimica Acta*, 52, 1189–1193.

Gruber, W. and Sachsenhofer, R. F. (2001). Coal deposition in the Noric Depression (Eastern Alps): raised and low-lying mires in Miocene pull-apart basins. *International Journal of Coal Geology*, 48, 89–114.

Hallmann, C., Kelly, A. E., Gupta, S. N., and Summons, R. E. (2011). Reconstructing deep-time biology with molecular fossils. In M. Laflamme, D. J. Schiffbauer, and Q. S. Dornbos (Eds.), *Quantifying the Evolution of Early Life: Numerical Approaches to the Evaluation of Fossils and Ancient Ecosystems*. Springer Netherlands, Dordrecht, pp. 355–401.

Harvey, H. R. and McManus, G. B. (1991). Marine ciliates as a widespread source of tetrahymanol and hopan-3β-ol in sediments. *Geochimica et Cosmochimica Acta*, 55, 3387–3390.

Hedges, J. I. and Keil, R. G. (1995). Sedimentary organic matter preservation: an assessment and speculative synthesis. *Marine Chemistry*, 49, 81–115.

Hieshima, G. B. and Pratt, L. M. (1991). Sulfur/carbon ratios and extractable organic matter of the Middle Proterozoic Nonesuch Formation, North American Midcontinent rift. *Precambrian Research*, 54, 65–79.

Hoffmann, C. F., Foster, C. B., Powell, T. G., and Summons, R. E. (1987). Hydrocarbon biomarkers from Ordovician sediments and the fossil alga *Gloeocapsomorpha prisca* Zalessky 1917. *Geochimica et Cosmochimica Acta*, 51, 2681–2697.

Horsfield, B., Curry, D. J., Bohacs, K., Littke, R., Rullkötter, J., Schenk, H. J., Radke, M., Schaefer, R. G., Carroll, A. R., Isaksen, G., and Witte, E. G. (1994). Organic geochemistry of freshwater and alkaline lacustrine sediments in the Green River Formation of the Washakie Basin, Wyoming, U.S.A. *Organic Geochemistry*, 22, 415–440.

Huizinga, B. J., Aizenshtat, Z. A., and Peters, K. E. (1988). Programmed pyrolysis-gas chromatography of artificially matured Green River kerogen. *Energy & Fuels*, 2, 74–81.

Jacobson, S. R., Hatch, J. R., Teerman, S. C., and Askin, R. A. (1988). Middle Ordovician Organic Matter Assemblages and Their Effect on Ordovician-Derived Oils: GEOLOGIC NOTE. *AAPG bulletin*, 72, 1090–1100.

Kennedy, M. J., Pevear, D. R., and Hill, R. J. (2002). Mineral Surface Control of Organic Carbon in Black Shale. *Science*, 295, 657–660.

Killops, S. D. and Killops, V. J. (2005). *Introduction to organic geochemistry*. 2. edition, Blackwell Publishing Ltd, Oxford.

Kleemann, G., Poralla, K., Englert, G., Kjøsen, H., Liaaen-Jensen, S., Neunlist, S., and Rohmer, M. (1990). Tetrahymanol from the phototrophic bacterium *Rhodopseudomonas palustris*: first report of a gammacerane triterpene from a prokaryote. *Microbiology*, 136, 2551–2553.

Koopmans, M. P., de Leeuw, J. W., and Sinninghe Damsté, J. S. (1997). Novel cyclised and aromatised diagenetic products of β-carotene in the Green River Shale. *Organic Geochemistry*, 26, 451–466.

Larter, S. R., Solli, H., Douglas, A. G., de Lange, F., and de Leeuw, J. W. (1979). Occurrence and significance of prist-1-ene in kerogen pyrolysates. *Nature*, 279, 405–408.

Le Bayon, R., Buhre, S., Schmidt, B. C., and Ferreiro Mählmann, R. (2012). Experimental organic matter maturation at 2 kbar: Heat-up effect to low temperatures on vitrinite reflectance. *International Journal of Coal Geology*, 92, 45–53.

Love, G. D., Grosjean, E., Stalvies, C., Fike, D. A., Grotzinger, J. P., Bradley, A. S., Kelly, A. E., Bhatia, M., Meredith, W., Snape, C. E., Bowring, S. A., Condon, D. J., and Summons, R. E. (2009). Fossil steroids record the appearance of Demospongiae during the Cryogenian period. *Nature*, 457, 718–721.

Love, G. D., Snape, C. E., Carr, A. D., and Houghton, R. C. (1995). Release of covalently-bound alkane biomarkers in high yields from kerogen via catalytic hydropyrolysis. *Organic Geochemistry*, 23, 981–986.

Love, G. D., Stalvies, C., Grosjean, E., Meredith, W., and Snape, C. E. (2008). Analysis of molecular biomarkers covalently bound within Neoproterozoic sedimentary kerogen. In P. H. Kelley and R. K. Bambach (Eds.), *From Evolution to Geobiology: Research Questions Driving Paleontology at the Start of a New Century. Paleontological Society Papers Vol. 14*. The Paleontological Society, pp. 67–83.

Luo, G., Hallmann, C., Xie, S., Ruan, X., and Summons, R. E. (2015). Comparative microbial diversity and redox environments of black shale and stromatolite facies in the Mesoproterozoic Xiamaling Formation. *Geochimica et Cosmochimica Acta*, 151, 150–167.

Mango, F. D. (1996). Transition metal catalysis in the generation of natural gas. *Organic Geochemistry*, 24, 977–984.

Mango, F. D. and Hightower, J. (1997). The catalytic decomposition of petroleum into natural gas. *Geochimica et Cosmochimica Acta*, 61, 5347–5350.

Meredith, W., Kelland, S. J., and Jones, D. M. (2000). Influence of biodegradation on crude oil acidity and carboxylic acid composition. *Organic Geochemistry*, 31, 1059–1073.

Middelburg, J. J. and Meysman, F. J. R. (2007). Burial at Sea. *Science*, 316, 1294–1295.

Moldowan, J. M., Seifert, W. K., and Gallegos, E. J. (1983). Identification of an extended series of tricyclic terpanes in petroleum. *Geochimica et Cosmochimica Acta*, 47, 1531–1534.

Monthioux, M. and Landais, P. (1989). Natural and artificial maturation of coal: Non-hopanoid biomarkers. *Chemical Geology*, 77, 71–85.

Naeher, S. and Grice, K. (2015). Novel 1H-Pyrrole-2,5-dione (maleimide) proxies for the assessment of photic zone euxinia. *Chemical Geology*, 404, 100–109.

Norgate, C. M., Boreham, C. J., and Wilkins, A. J. (1999). Changes in hydrocarbon maturity indices with coal rank and type, Buller Coalfield, New Zealand. *Organic Geochemistry*, 30, 985–1010.

Olcott Marshall, A. and Cestari, N. A. (2015). Biomarker Analysis of Samples Visually Identified as Microbial in the Eocene Green River Formation: An Analogue for Mars. *Astrobiology*, 15, 770–775.

Pawlowska, M. M., Butterfield, N. J., and Brocks, J. J. (2013). Lipid taphonomy in the Proterozoic and the effect of microbial mats on biomarker preservation. *Geology*, 41, 103–106.

Peters, K. E., Moldowan, J. M., and Sundararaman, P. (1990). Effects of hydrous pyrolysis on biomarker thermal maturity parameters: Monterey Phosphatic and Siliceous members. *Organic Geochemistry*, 15, 249–265.

Peters, K. E., Walters, C. C., and Moldowan, J. M. (2005a). *The Biomarker Guide - Part I - Biomarkers and Isotopes in the Environment and Human History*. Cambridge University Press, New York.

Peters, K. E., Walters, C. C., and Moldowan, J. M. (2005b). *The Biomarker Guide - Part II - Biomarkers and Isotopes in Petroleum Exploration and Earth History*. Cambridge University Press, New York.

Price, L. C. (1983). Geologic time as a parameter in organic metamorphism and vitrinite reflectance as an absolute paleogeothermometer. *Journal of Petroleum Geology*, 6, 5–37.

Price, L. C. (1993). Thermal stability of hydrocarbons in nature: Limits, evidence, characteristics, and possible controls. *Geochimica et Cosmochimica Acta*, 57, 3261–3280.

Requejo, A. G. (1994). Maturation of petroleum source rocks–II. Quantitative changes in extractable hydrocarbon content and composition associated with hydrocarbon generation. *Organic Geochemistry*, 21, 91–105.

Rohmer, M., Bouvier-Nave, P., and Ourisson, G. (1984). Distribution of hopanoid triterpenes in prokaryotes. *Journal of General Microbiology*, 130, 1137–1150.

Ruble, T. E., Lewan, M. D., and Philp, R. P. (2001). New insights on the Green River petroleum system in the Uinta basin from hydrous pyrolysis experiments. *AAPG bulletin*, 85, 1333–1371.

Rullkötter, J., Meyers, P. A., Schaefer, R. G., and Dunham, K. W. (1986). Oil generation in the Michigan Basin: A biological marker and carbon isotope approach. *Organic Geochemistry*, 10, 359–375.

Schmidt, B. C., Blum-Oeste, N., and Flagmeier, J. (2013). Water diffusion in phonolite melts. *Geochimica et Cosmochimica Acta*, 107, 220–230.

Schoell, M., Hwang, R. J., Carlson, R. M. K., and Welton, J. E. (1994). Carbon isotopic composition of individual biomarkers in gilsonites (Utah). *Organic Geochemistry*, 21, 673–683.

Sinninghe Damsté, J. S., Kenig, F., Koopmans, M. P., Köster, J., Schouten, S., Hayes, J. M., and de Leeuw, J. W. (1995). Evidence for gammacerane as an indicator of water column stratification. *Geochimica et Cosmochimica Acta*, 59, 1895–1900.

Summons, R. E. (2014). The exceptional preservation of interesting and informative biomolecules. In M. Laflamme, J. D. Schiffbauer, and S. A. F. Darroch (Eds.), *Reading and Writing of the Fossil Record: Preservational Pathways to Exceptional Fossilization. The Paleontological Society Papers Vol. 20*. The Paleontological Society, pp. 217–236.

Summons, R. E., Brassell, S. C., Eglinton, G., Evans, E., Horodyski, R. J., Robinson, N., and Ward, D. M. (1988). Distinctive hydrocarbon biomarkers from fossiliferous sediment of the Late Proterozoic Walcott Member, Chuar Group, Grand Canyon, Arizona. *Geochimica et Cosmochimica Acta*, 52, 2625–2637.

Ten Haven, H. L., de Leeuw, J. W., Rullkötter, J., and Sinninghe Damsté, J. S. (1987). Restricted utility of the pristane/phytane ratio as a palaeoenvironmental indicator. *Nature*, 330, 641–643.

Ten Haven, H. L., Rohmer, M., Rullkötter, J., and Bisseret, P. (1989). Tetrahymanol, the most likely precursor of gammacerane, occurs ubiquitously in marine sediments. *Geochimica et Cosmochimica Acta*, 53, 3073–3079.

Tissot, B. P., Deroo, G., and Hood, A. (1978). Geochemical study of the Uinta Basin: formation of petroleum from the Green River formation. *Geochimica et Cosmochimica Acta*, 42, 1469–1485.

Tissot, B. P. and Welte, D. H. (1984). *Petroleum Formation and Occurrence*. 2. edition, Springer, Berlin, Heidelberg.

Treibs, A. (1936). Chlorophyll- und Häminderivate in organischen Mineralstoffen. *Angewandte Chemie*, 49, 682–686.

Tulipani, S., Grice, K., Greenwood, P. F., Haines, P. W., Sauer, P. E., Schimmelmann, A., Summons, R. E., Foster, C. B., Böttcher, M. E., Playton, T., and Schwark, L. (2015). Changes of palaeoenvironmental conditions recorded in Late Devonian reef systems from the Canning Basin, Western Australia: A biomarker and stable isotope approach. *Gondwana Research*, 28, 1500–1515.

Vandenbroucke, M. and Largeau, C. (2007). Kerogen origin, evolution and structure. *Organic Geochemistry*, 38, 719–833.

Yamada, K., Ueno, Y., Yamada, K., Komiya, T., Han, J., Shu, D., Yoshida, N., and Maruyama, S. (2014). Molecular fossils extracted from the Early Cambrian section in the Three Gorges area, South China. *Gondwana Research*, 25, 1108–1119.

Assessing the diversity of lipids formed via Fischer–Tropsch-type reactions

(published in *Organic Geochemistry*)

Helge Mißbach, Burkhard C. Schmidt, Jan-Peter Duda, Nils Keno Lünsdorf, Walter Goetz, Volker Thiel

Abstract

Lipid biomarkers are commonly used for tracking life through Earth's history and are also gaining in importance in the search for extraterrestrial life. However, some lipids may also be formed in situ via abiotic Fischer–Tropsch-type (FTT) reactions. These processes have been considered as a source of prebiotic organic matter. Here we report on a FTT synthesis experiment performed under hydrothermal conditions, focusing on more complex, previously undescribed FTT reaction products that may potentially mimic biological signals. The experiment was carried out in stainless steel reactors by heating aqueous solutions of oxalic acid mixed with montmorillonite to 175 °C for 3 days. Organic extracts of the products and extraction residues were analyzed by gas chromatography–mass spectrometry (GC–MS) and combustion-infrared detection, attenuated total reflectance Fourier transform infrared spectroscopy and pyrolysis GC–MS. FTT reactions led to a number of biomarker-like lipids such as linear and methyl-branched alkanes and alkanols as well as *n*-alkanoic acids. However, FTT reactions a priori produce unimodal chain length distributions and isomeric mixtures of methyl-branched compounds, as opposed to biolipids which typically show preferences of individual homologs and/or isomers. Experimental maturation of an immature kerogen demonstrated how these biological signatures may pass into unimodal distributions similar to FTT reaction products by thermal overprint. Therefore, discrimination of biologically derived compounds from FTT organics may become increasingly problematic with ongoing thermal maturation. Extraction residues of FTT reaction products contained organic material, possibly in the form of an organic polymer. However, it remains to be tested whether these residual organics can evolve into kerogen-like material.

Keywords: Fischer–Tropsch-type synthesis, abiotic synthesis, lipids, experimental maturation, gas chromatography–mass spectrometry, Fourier transform infrared spectroscopy.

3.1 Introduction

Lipid biomarkers retain specific structural characteristics over geological time scales which make them essential for tracking life through Earth's history and, potentially, providing evidence for its presence in the extraterrestrial realm (Brocks and Summons, 2003; Brocks

and Pearson, 2005; Peters et al., 2005a,b; Summons et al., 2008; Summons, 2014; Westall et al., 2015). However, simple building blocks of lipids can also be formed via abiotic processes such as Fischer–Tropsch-type (FTT) synthesis, which has been considered as an important source of prebiotic organic matter on the early Earth (see reviews by McCollom and Seewald, 2007; McCollom, 2013; Konn et al., 2015). Furthermore, abiotic organic matter is present in meteorites and thus can be introduced to Earth and other extraterrestrial environments (Chyba and Sagan, 1992; Summons et al., 2008). Earlier claims for an abiotic formation of major petroleum quantities in the Earth's crust, however, have not been confirmed so far (see Höök et al., 2010; Ahmed et al., 2014 for a discussion).

In ancient rocks, the discrimination of biological from abiotic organic matter is severely hampered by alteration during diagenesis and catagenesis. These processes cause a progressive loss of the distinctive traits of biomarkers, such as functional groups, double bonds, carbon chain length preferences, and methylation patterns (Brocks and Summons, 2003; Peters et al., 2005b; Hallmann et al., 2011; Mißbach et al., 2016). Particularly the sources of organic matter in very old (e.g., Archean) rocks are often ambiguous. Consequently, the utility of organic compounds as clear-cut fingerprints of life on the early Earth, and possibly beyond, has been challenged over the last few decades (van Zuilen et al., 2002; Lindsay et al., 2005; McCollom and Seewald, 2007; De Gregorio et al., 2011).

Fischer–Tropsch synthesis was discovered by Franz Fischer and Hans Tropsch in the 1920s. It was originally intended for producing hydrocarbons from coal gasification products (Fischer and Tropsch, 1926; Fischer, 1935) and is now widely applied for industrial synthesis of a variety of lipids (e.g., lubricants and fuels). Because of its economic relevance, Fischer–Tropsch synthesis has been extensively studied with respect to reaction efficiencies and product refinements (Anderson, 1984; Schulz, 1999; Dry, 2002). Geoscientists developed an increasing interest in FTT processes after detecting potential abiotic hydrocarbons in different geological settings (e.g., oceanic hydrothermal vents, ophiolites) and in meteorites (Gelpi and Oró, 1970; Simoneit et al., 1988; Abrajano et al., 1990; Cronin and Pizzarello, 1990; Ferris, 1992; Holm and Charlou, 2001; Etiope and Sherwood Lollar, 2013; Konn et al., 2015). Over the last two decades, FTT processes were intensively studied as they represent a possible source for lipids as basic building blocks of life on the prebiotic Earth (Simoneit, 2004; Martin et al., 2008; Proskurowski et al., 2008; McCollom, 2013; Konn et al., 2015).

In geological settings, FTT reactions could be linked to the hydrothermal reaction between olivine (and/or pyroxene) and H_2O, resulting in the formation of serpentine, brucite, magnetite, and H_2 (i.e., serpentinization; reaction 3.1). The H_2 then may react with CO_2 from various sources to produce CH_4 and, potentially, more complex hydrocarbons (reaction 3.2).

$$(\text{Mg}, \text{Fe})_2\text{SiO}_4 + a\,\text{H}_2\text{O} \longrightarrow 0.5\,\text{Mg}_3\text{Si}_2\text{O}_5(\text{OH})_4 + x\,\text{Mg(OH)}_2 + y\,\text{Fe}_3\text{O}_4 + z\,\text{H}_2 \quad (3.1)$$

$$\quad\quad\; \textit{Olivine} \quad\quad\quad\quad\quad\quad \textit{Serpentine} \quad\quad \textit{Brucite} \quad\; \textit{Magnetite}$$

$$n\,\text{CO}_2 + (2\,n + m/2)\text{H}_2 \longrightarrow C_nH_m + 2\,n\,\text{H}_2\text{O} \quad\quad\quad\quad (3.2)$$

First experiments corroborated the possible abiotic formation of CH_4 under hydrothermal conditions (Berndt et al., 1996). Subsequent studies revealed that FTT synthesis under hydrothermal conditions (water-saturated, temperatures of $100-400$ °C) and in the

presence of catalysts (e.g., magnetite, Ni–Fe alloys) can yield a variety of lipids over a broad range of carbon chain lengths, including alkanes, alcohols and alkanoic acids (Horita and Berndt, 1999; McCollom et al., 1999; Rushdi and Simoneit, 2001; Foustoukos and Seyfried, 2004; McCollom and Seewald, 2006; Taran et al., 2007; Sharma et al., 2009; McCollom, 2013; Fu et al., 2015). Some of these compounds are regularly used as biomarkers for specific (groups of) organisms and paleoreconstructions (Brocks and Summons, 2003; Peters et al., 2005a,b), making a clear distinction between biologically and abiotically derived lipids necessary. However, the diversity of lipids potentially formed via FTT reactions has not been appraised in detail so far.

Kerogen (i.e., the portion of organic matter that is insoluble in organic solvents, acids and bases; Durand, 1980) is considered crucial for the preservation of lipids over geological time scales as its macromolecular structure protects the bound components against microbial degradation and, at least to a certain degree, thermal maturation (Love et al., 1995, 2008; Brocks et al., 2003; Lockhart et al., 2008; Hallmann et al., 2011). Conceivably, functionalized FTT reaction products may undergo condensation reactions by forming covalent cross-links, but reported evidence on this is scarce. FTT reactions can produce thin macromolecular organic coatings on grain surfaces in the laboratory, but these coatings have so far not been characterized on a molecular level (Nuth III et al., 2008). Furthermore, it is known that abiotic condensation reactions of FTT reaction products can lead to the formation of more complex compounds (e.g., acylglycerols, $> C_{120}$ waxes; Rushdi and Simoneit, 2006; Simoneit et al., 2007; De Klerk and Furimsky, 2010). All these observations suggest that organics derived from FTT reactions may be transformed into kerogens and preserved over geological time scales, but as yet no study did, to the best of our knowledge, explicitly investigate the formation of such "FTT-kerogens" under hydrothermal conditions.

In the present study we aimed at appraising the diversity of lipids formed via FTT reactions under hydrothermal conditions, using a well-established experimental setup (McCollom et al., 1999; Rushdi and Simoneit, 2001) and gas chromatography–mass spectrometry (GC–MS) for analysis. Special emphasis was placed on a detailed documentation of methyl-branched FTT reaction products as some of these compounds may interfere with structurally similar lipids from biological sources. We further checked for the formation of kerogen-like, insoluble products using combustion–infrared detection, attenuated total reflectance Fourier transform infrared spectroscopy (ATR–FTIR) and open system pyrolysis coupled to gas chromatography–mass spectrometry (Py-GC–MS). Based on our findings, we discuss implications on the utility of lipids as fingerprint of life on early Earth, and possibly beyond.

3.2 Methods

3.2.1 FTT synthesis

FTT synthesis under hydrothermal conditions was carried out according to McCollom et al. (1999) and Rushdi and Simoneit (2001; and references therein), with minor changes to the setup and the experimental conditions. Briefly, oxalic acid was used as a surrogate for CO, CO_2 and H_2, because handling these gases at elevated pressures and temperatures

is difficult and can lead to a serious hazard in a laboratory environment. Oxalic acid decays under elevated temperatures (i.e., $230 - 750\,°C$) to form a mixture of CO, CO_2 and H_2 and water (Morgan et al., 1992). Aqueous oxalic acid is decomposed during heating, according to reaction (3.3) (Crossey, 1991).

$$C_2H_2O_4 \longrightarrow CH_2O_2 + CO_2 \tag{3.3}$$

Formic acid from reaction (3.3) decomposes under elevated temperatures, and without catalysts, according to reaction (3.4) and (3.5) (Yu and Savage, 1998; Bröll et al., 1999; Wakai et al., 2004).

$$CH_2O_2 \longleftrightarrow CO + H_2O \tag{3.4}$$

$$CH_2O_2 \longleftrightarrow CO_2 + H_2 \tag{3.5}$$

Under hydrothermal conditions, reaction (3.5) is probably favored, delivering H_2 and CO_2 in equimolar amounts (Akiya and Savage, 1998; Yu and Savage, 1998) which then are available as reactants for the FTT reactions. However, it has also been reported that, under most conditions, CO is the main product from these reactions (Wakai et al., 2004). Formic acid is present in many geological fluids, e.g., from marine hydrothermal systems or springs (Martens, 1990; Kawamura and Nissenbaum, 1992; Amend et al., 1998; Zeng and Liu, 2000; Lang et al., 2010; McDermott et al., 2015), and is known as an intermediate in the "water-gas shift reaction" (reaction 6) which, in principle, combines reactions (4) and (5) (Elliott et al., 1983; Martens, 1990; Bröll et al., 1999; Yoshida et al., 2004; Yasaka et al., 2006).

$$CO_2 + H_2 \longleftrightarrow CH_2O_2 \longleftrightarrow CO + H_2O \tag{3.6}$$

In our experiments, 2.5 g oxalic acid dihydrate (suprapur®, Merck KGaA) and 1 g montmorillonite (K10, Sigma Aldrich) were mixed with ~ 8 mL ultrapure water and filled into a Morey-type stainless steel reactor (Fig. 3.1). The inner walls of the reactor itself and the montmorillonite function as a catalyst for the FTT reactions. Montmorillonite is thought to adsorb (remove) the products from the reaction mixture, thus driving the reaction towards the product side according to the *Le Châtelier* principle. According to earlier studies, the reaction also works without montmorillonite, but addition of the clay mineral increases the product yield (see McCollom et al.,1999 for a more detailed description). The reactor was sealed with a pressure seal that has an integrated capillary. This capillary was furthermore connected to a high pressure needle valve (max. 4 kbar; SITEC-Sieber Engineering AG) and an electrical high pressure sensor (max. 7 kbar; tecsis GmbH; Fig. 3.1). Capillaries, valve and pressure sensor were flooded with ultrapure water first (ca. 3 mL), so that initially no headspace was left in the system. The reactor and pressure seal were placed horizontally in an oven and heated to $175\,°C$ in approx. 3 h. This temperature was selected i) to be consistent with earlier studies, ii) to yield high amounts of organics and iii) because it is in the temperature range of modern and Archean hydrothermal systems (D'Amore and Panichi, 1980; McCollom et al., 1999; Rushdi and Simoneit, 2001; Harris et al., 2009). The pressure inside the reactor was not adjustable. Due to the decomposition of oxalic acid and the thermal expansion of water, it increased from atmospheric pressure to between 1.0 and 1.6 kbar upon heating. After the heating

phase (ca. 3 h), the pressure stayed constant or slowly increased during the remaining time. The total duration of the experiments was 66 to 74 h. At the end, the whole setup was cooled to room temperature with compressed air (< 15 min). In total, eight individual experiments were carried out under identical conditions.
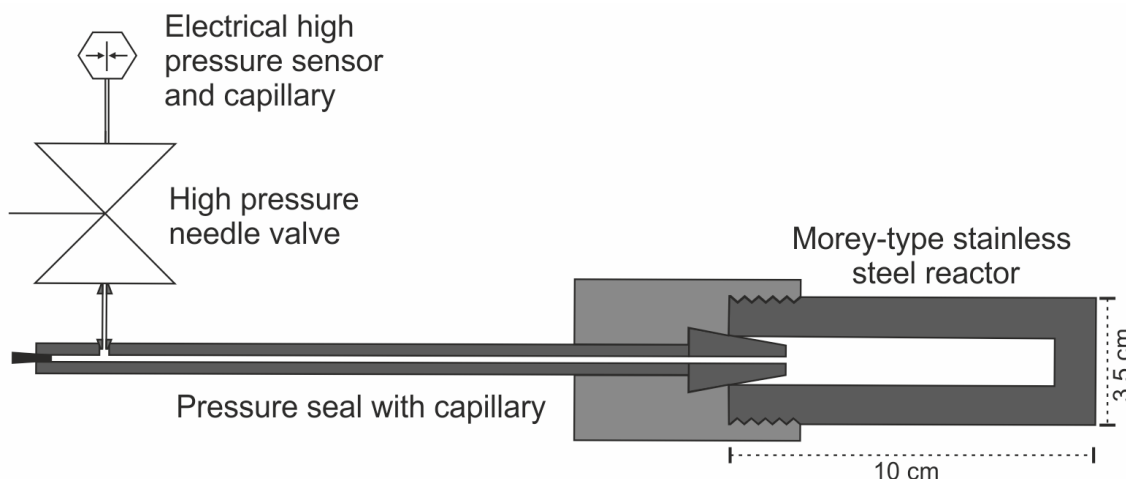
Figure 3.1: Morey-type stainless steel reactor used for Fischer–Tropsch-type synthesis experiments.

Prior to each experiment, the high pressure equipment was completely dissembled and extensively cleaned in three steps. The first step included mechanical cleaning using a soap detergent/water mixture and a brush as well as intensive flushing with deionized and ultraclean water. In the second step, all parts were treated with acetone in an ultrasonic bath and again extensively rinsed with acetone. In the third step, the reactor and the pressure seal were heated to 550 °C for 3 h to remove any potential residual organic contaminants.

Montmorillonite was extracted (4 x) with dichloromethane (DCM) prior to use. Furthermore, extracts of all reactants (i.e., oxalic acid dihydrate, ultrapure water, montmorillonite) were tested for contamination via gas chromatography–mass spectrometry (GC–MS). Additionally, blank experiments were carried out using only water and montmorillonite.

3.2.2   Extraction and fractionation of FTT reaction products

Glassware, pipettes, sea sand and silica gel used for the following extraction and fractionation steps were cleaned at 550 °C (> 3 h). Spatula, forceps and other metal equipment were intensively rinsed with acetone prior to use. All solvents used had $> 99.9\%$ purity initially, and were additionally distilled.

After quenching of the FTT synthesis experiment, the reaction mixtures were released through the high pressure valve into a 22 mL glass vial. Solid materials were transferred to the same vial by using spatula and Pasteur pipettes. The obtained products (FTT reaction mixtures and solid residues) were extracted with 10 mL DCM (4 x, ultrasonication) and the extracts were combined. Montmorillonite was removed by centrifugation and filtration through sea sand. Fluid and solid extraction residues were kept for further analysis

(see Section 3.2.5). The DCM extracts were reduced to 1 mL using rotation evaporation (40 °C, 670 mbar). A 20% aliquot (200 μL) of the total extract was derivatized for 50 min at 70 °C using 200 μL trimethylchlorosilane/N,O-bis(trimethylsilyl)trifluoroacetamide (TMCS/BSTFA, 0.5/9.5, V/V, Sigma Aldrich/Supelco). The extract was then carefully dried using a gentle stream of N_2. 200 μL of an internal standard of known concentration (n-eicosane d42, 4 mg/L, in n-hexane) were added prior to GC–MS measurements.

Another 150 μL of the total extract were deposited on silica gel for fractionation by column chromatography (diameter: 1.5 cm, height: 8 cm, 0.7 g dry silica gel; only conducted for selected samples, see Table A.1 for details). Hydrocarbons (fraction F1) were eluted using 3 mL n-hexane/DCM (4/1; V/V), alcohols and ketones (fraction F2) with 3 mL DCM/ethyl actetate (9/1; V/V) and the polar fraction (F3) with DCM/MeOH (1/1; V/V). After column fractionation, F1 was carefully reduced (close to dryness), dissolved in 50 μL n-hexane and analyzed by GC–MS. F2 was derivatized as described above, dissolved in 100 μL n-hexane and analyzed by GC–MS. F3 was carefully reduced to near-dryness using N_2 and transesterified with a mixture of TMCS/MeOH (2/9; V/V) for 90 min at 80 °C. The reaction mixture was extracted with 1 mL portions of n-hexane (3 x). The n-hexane extracts were combined, reduced to 1 mL and analyzed by GC–MS.

Concentration of samples with N_2 was performed with great caution and samples were never completely dried, unless an internal standard was used for quantification. In that case, the N_2 flow was stopped immediately after the solvents were completely evaporated. Nevertheless, a loss of low boiling compounds should be considered (see Ahmed and George, 2004 for a detailed discussion of this analytical problem).

3.2.3   Isolation and experimental maturation of reference material

Isolated kerogen from the Eocene Green River Formation (Green River Shale; BLM Oil Shale Research, Development, and Demonstration Lease UTU-84087) was used as reference material in this study. The Green River Shale contains high amounts of well precharacterized, relatively immature biogenic organic matter and is therefore ideally suited for maturation experiments demonstrating the progressive thermal alteration of biomarker distributions.

For a detailed description of the following experimental procedure see also Mißbach et al. (2016). The rock sample was crushed, powdered and extracted with DCM (3 x). Kerogen was isolated from the pre-extracted rock powder using hydrochloric and hydrofluoric acid (Durand and Nicaise, 1980) and again extracted with DCM (3 x). 10 mg of dried kerogen and 10 μL water were sealed into gold capsules and experimentally matured at 300 °C/400 °C and 2 kbar for up to 240 h. Capsules were subsequently opened and 2/3 of the maturation product were extracted with 2 mL n-hexane/DCM (4 x; 1/1, V/V; 20 min ultrasonication). Aliphatic hydrocarbons from the extracts were obtained by column chromatography (diameter: 1.5 cm, height: 8 cm, 0.7 g silica gel) by using 3 mL n-hexane as eluent. The resulting aliphatic hydrocarbon fractions were prepared for GC–MS analyses. The remaining 1/3 of the material were used for other analysis (not part of this study).

3.2.4 GC–MS analyses of solvent-extracted FTT reaction products and reference material

GC–MS analyses were carried out using a Thermo Fischer Trace 1310 gas chromatograph coupled to a Thermo Fischer Quantum XLS Ultra mass spectrometer. The GC was equipped with a fused silica column (Phenomenex Zebron ZB-5, 30 m, 0.25 μm film thickness, inner diameter 0.25 mm). Fractions were injected into a splitless injector and transferred to the column at 270 °C. Helium was used as carrier gas at a flow rate of 1.5 mL/min. The GC oven temperature was ramped from 80 °C (isotherm for 1 min) to 310 °C (isotherm for 20 min) at 5 °C/min. Mass spectra were recorded in full scan mode (m/z 50 to 600) using an electron energy of 70 eV and a scan time of 0.42 s.

Alcohols and carboxylic acids were analyzed as their trimethylsilyl (TMS) derivatives (key fragments m/z 75 and m/z 117, respectively). Most of the compounds were identified by comparing representative mass spectra and key fragments (Figs. 3.2, A.1; Table 3.1) with published data (NIST mass spectral library; Rushdi and Simoneit, 2001). Selected n-alkan-1-ols, n-alkan-2-ols and n-alkanoic acids were identified by comparison with commercially available standards. Methylalkanes were identified by their elution order (Kissin, 1987) and mass spectral characteristics (i.e., key fragments that are slightly elevated as compared to n-alkanes depending on the position of the methyl group; Summons, 1987; Fig. A.1).

Table 3.1: Summary of Fischer–Tropsch-type (FTT) synthesis products including carbon number ranges, carbon preference index (CPI), relative abundance and major key fragments used for identification.

Compound	Homolog range[1]	CPI (SD)[2]	Relative abundance [a.u.] (SD)[4]	Key fragments (m/z)[5]
n-Alkanes	$C_{11}-C_{41}$	1.04 (0.05)	20.6 (4.6)	85
Methylalkanes	$C_{12}-C_{36}$	n.d.	4.0 (1.7)	85
n-Alkan-1-ols	C_7-C_{38}	0.88(0.06)	100	$73 < 75$, M -15
n-Alkan-2-ols	C_8-C_{38}	1.00 (0.06)	6.2 (1.4)	$73 > 75$, 117, M -15
n-Alkan-3-ols	C_8-C_{24}	n.d.	1.3 (0.2)	$73 > 75$, 131, M -15
2-Methylalkan-1-ols	C_8-C_{35}	n.d.	13.8 (2.7)	$73 < 75$, 103, M -15
n-Alkanoic acids	C_7-C_{26}	0.74[3] (0.06)	13.6 (4.5)	$73 > 75$, 117, 129, M -15
n-Alkyl formates	C_8-C_{31}	1.02 (0.12)	14.6 (3.1)	69, 83, M -46, M -18

[1] Showing the maximum homolog range observed from all experiments. For information on ranges in individual experiments see Table A.1.
[2] CPI is given as the median of eight individual FTT synthesis experiments with the corresponding standard deviation (SD). n.d.: not determined.
[3] Low CPI value probably due to contamination with n-C_{16} and n-C_{18} alkanoic acids from TMCS derivatization reagent.
[4] Relative abundance of the compounds is given in arbitrary units [a.u.], normalized to n-alkan-1-ols (100); the value displays the median of eight individual FTT synthesis experiments with the corresponding standard deviation (SD).
[5] Mass spectral fragments and fragment intensity distributions used for identification. "M" denotes the mass of the molecular ion.

Carbon preference index (CPI) values were defined as follows:
$\sum (C_{13}-C_{35})_{odd} / \sum (C_{12}-C_{34})_{even}$ for n-alkanes;
$\sum (C_9-C_{25})_{odd} / \sum (C_8-C_{24})_{even}$ for n-alkan-1-ols;
$\sum (C_{11}-C_{25})_{odd} / \sum (C_{10}-C_{24})_{even}$ for n-alkan-2-ols;
$\sum (C_9-C_{21})_{odd} / \sum (C_8-C_{20})_{even}$ for n-alkanoic acids;

$\sum (C_9 - C_{19})_{odd}/ \sum (C_{10} - C_{20})_{even}$ for *n*-alkyl formates.
CPI is given as the median of eight individual FTT synthesis experiments.

3.2.5   Analysis of FTT synthesis extraction residues

Fluid and solid extraction residues of the FTT reaction mixture were separated and analyzed using combustion–infrared detection, ATR–FTIR and Py-GC–MS. Both residues were freeze-dried (-54 °C, $600 - 800$ mbar; Christ Alpha 1–4 LDplus) in separate glass vials covered with aluminum foil.

Carbon content was determined by combustion–infrared detection using a Leco RC612 multiphase carbon/hydrogen analyzer. The oven temperature was ramped from 120 °C to 990 °C at 50 °C/min. Carbon was measured as CO_2 by infrared detection. Oxalic acid dihydrate was analyzed as a reference.

ATR–FTIR measurements were conducted in the mid infrared region using a Bruker Vertex 70 FTIR spectrometer and a Bruker Platinum ATR unit with diamond as ATR crystal. ATR spectra were recorded in 32 scans in the range of 400 to 4000 cm^{-1} using a Globar light source, a KBr beamsplitter and a DLaDTGS detector. Additionally to the analysis of the extraction residues, oxalic acid dihydrate, pure montmorillonite (precleaned) and an organic extract were analyzed as references. The bands in the FTIR spectra were determined by comparison with published data (Socrates, 2004; Riaz and Ashraf, 2014).

Py-GC–MS analyses were performed in two steps (340 °C, 560 °C, each 10 s) using a Pyrola 2000 (PYROLab, Sweden) pyrolyzer device coupled to a Varian CP-3800 GC and a Varian 1200L MS. A separate GC-run was obtained for each pyrolysis step. The GC was equipped with a fused silica column (Phenomenex Zebron ZB-1 HT, inner diameter 0.32 mm, length 30 m, film thickness 0.1 μm). Helium was used as carrier gas at a flow rate of 1.4 mL/min. The GC oven temperature was ramped from 30 °C (isotherm for 5 min) at 10 °C/min to 330 °C (isotherm for 13 min). Mass spectra were recorded using full scan mode (*m/z* 40 to 500 for $1 - 5$ min; *m/z* 50 to 500 for $5 - 45$ min) using an electron energy of 70 eV and a scan time of 0.5 s. Additional Py-GC–MS runs were carried out to scan for (highly volatile) low molecular weight products only, conducting a series of pyrolysis with different temperatures (340 °C, 400 °C, 560 °C) at an oven temperature of 30 °C and a smaller mass range in full scan mode (*m/z* 15 to 180). Blank runs were performed before and after each analysis to keep track of (cross-)contamination.

3.3   Results

3.3.1   Solvent extractable FTT reaction products

The DCM-extracts of all single reactants (i.e., oxalic acid dihydrate, ultrapure water, montmorillonite) as well as blank experiments (i.e., FTT synthesis experiments without oxalic acid) showed minor traces of contamination, mostly siloxanes (GC column, septum bleeding), phthalates (e.g., from plasticizers), *n*-C_{16} and *n*-C_{18} alkanoic acids from the TMCS derivatization reagent, by-products (e.g., certain disilylated compounds) from TMCS/BSTFA derivatization and various unknown cyclic components. Apart from the
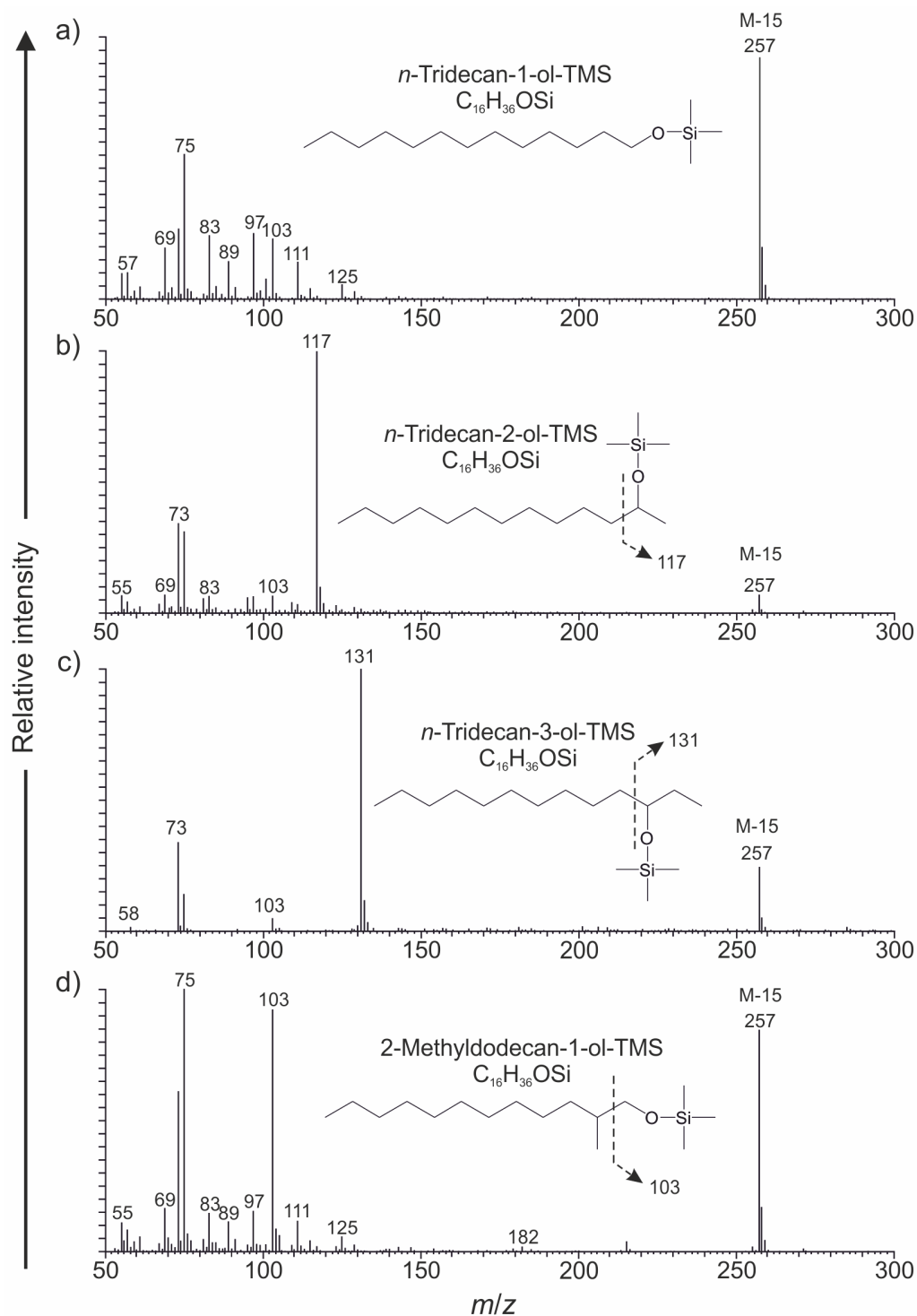
Figure 3.2: Representative mass spectra of selected compounds resulting from Fischer–Tropsch-type reactions. TMS: trimethylsilyl. (**a**) *n*-tridecan-1-ol as TMS ether, (**b**) *n*-tridecan-2-ol as TMS ether, (**c**) *n*-tridecan-3-ol as TMS ether, (**d**) 2-methyldodecan-1-ol as TMS ether (tentative), (**e**) *n*-dodecanoic acid as TMS ester, (**f**) *n*-tridecyl formate. See also Fig. A.1.
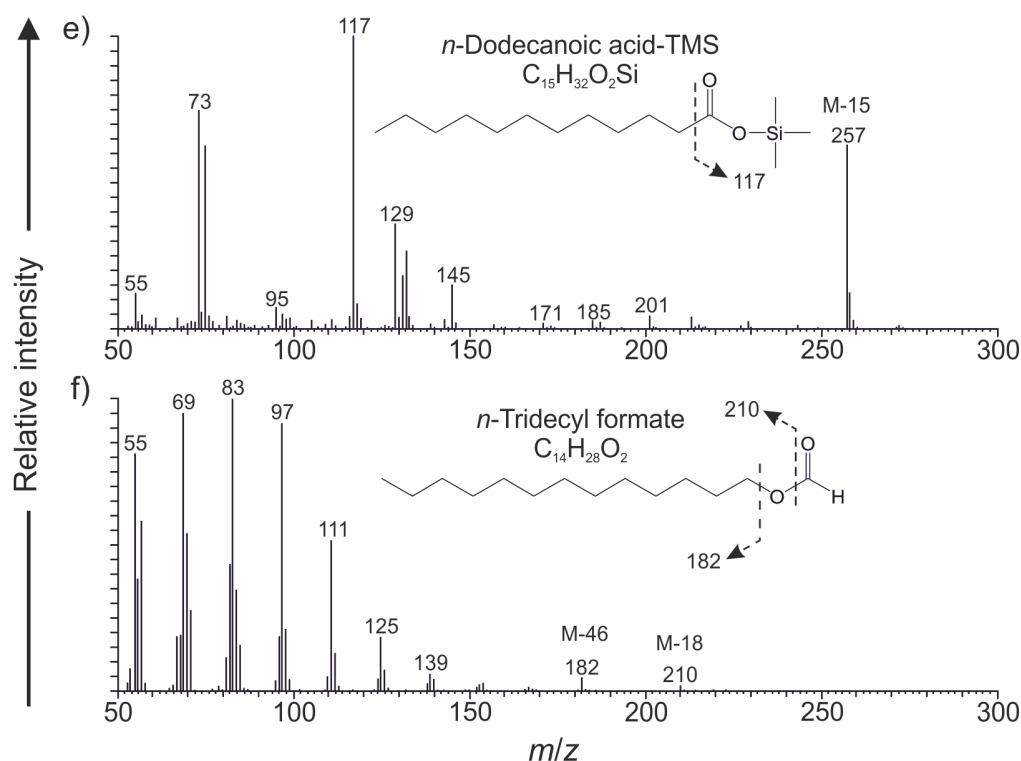
Figure 3.2: Continued.

n-C$_{16}$ and n-C$_{18}$ alkanoic acids, the blank extracts did not contain any compounds that were present in the FTT reaction products.

All FTT synthesis experiments yielded homologous series of acyclic alkanes, alcohols (linear and methyl-branched moieties, respectively), n-alkanoic acids, and n-alkyl formates (Fig. 3.3). Functionalized moieties, particularly alcohols, were the most abundant compounds (Table 3.1). The homolog ranges varied between the individual experiments. In the following, only the overall maximum homolog ranges are given (for ranges from individual experiments see Table A.1). All compound classes exhibited a unimodal distribution without predominance of single moieties as reflected by CPIs of ~ 1. n-Alkan-1-ols revealed a slightly lower value (0.88; Table 3.1). The larger offset observed for n-alkanoic acids (CPI of 0.74) is due to contamination with n-C$_{16}$ and n-C$_{18}$ alkanoic acids from the TMCS derivatization reagent (introduced after FTT synthesis, determined by blank analysis; see above).

Alkanes were dominated by linear homologs with chain lengths ranging from C$_{11}$ to C$_{41}$. Furthermore, monomethylalkanes and traces of dimethylalkanes were detected (Figs. 3.4, A.1; Table 3.1). The monomethylalkanes are comprised of complex isomeric mixtures, with the abundances of individual isomers generally decreasing from the terminal (2-methyl-) towards the mid-chain branching positions (Fig. 3.4).

Alcohols were dominated by n-alkan-1-ols ranging from C$_7$ to C$_{38}$ (Fig. 3.3). Minor concentrations of n-alkan-2-ols and n-alkan-3-ols were also present, ranging from C$_8$ to C$_{38}$ and C$_8$ to C$_{24}$, respectively (Figs. 3.2a – c, 3.3; Table 3.1). The products further contained various other (most probably methyl-branched) alkanol varieties, including compounds tentatively interpreted as 2-methylalkan-1-ols (i.e., with the methyl group lo-
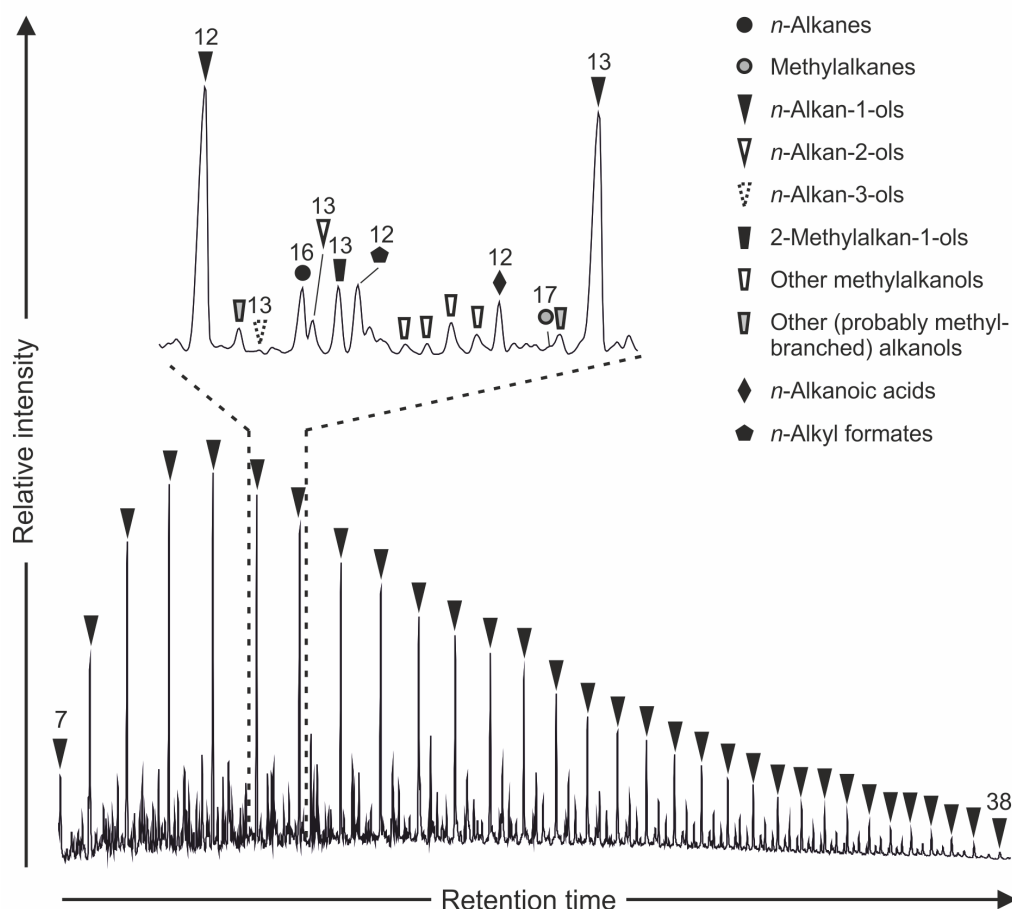
Figure 3.3: GC–MS chromatogram (total ion current) of a derivatized total extract resulting from Fischer–Tropsch-type reactions under hydrothermal conditions. Numbers refer to number of carbon atoms. n-Alkanols and n-alkanoic acids were analyzed as TMS derivatives. The chromatogram is dominated by $C_7 - C_{38}$ n-alkan-1-ols. The enlarged portion of the chromatogram illustrates the structural diversity of further FTT synthesis products.

cated at the functional end of the molecule; Figs. 3.2d, 3.3). Methylalkanols with methyl groups close to the non-functional end (ω-end) of the molecules have also been identified ("other methylalkanols" in Fig. 3.3).

n-Alkanoic acids were present in all samples and showed chain lengths from C_7 to C_{26} (Figs. 3.2e, 3.3; Table 3.1). Unlike the alcohols, no methyl-branched alkanoic acids were found. n-Alkyl formates ranged from C_8 to C_{31} (Figs. 3.2f, 3.3; Table 3.1). No cyclic or aromatic hydrocarbons were observed in any of the experiments.

3.3.2 Extraction residues

Extraction of the FTT reaction mixtures with DCM led to a fluid and a solid extraction residue. The fluid extraction residue was an aqueous, deep black solution. Freeze drying this solution was leading to a thick black coating in the glass vial. The solid extraction residue largely consisted of montmorillonite.

Combustion–infrared detection revealed the presence of organic carbon in both the
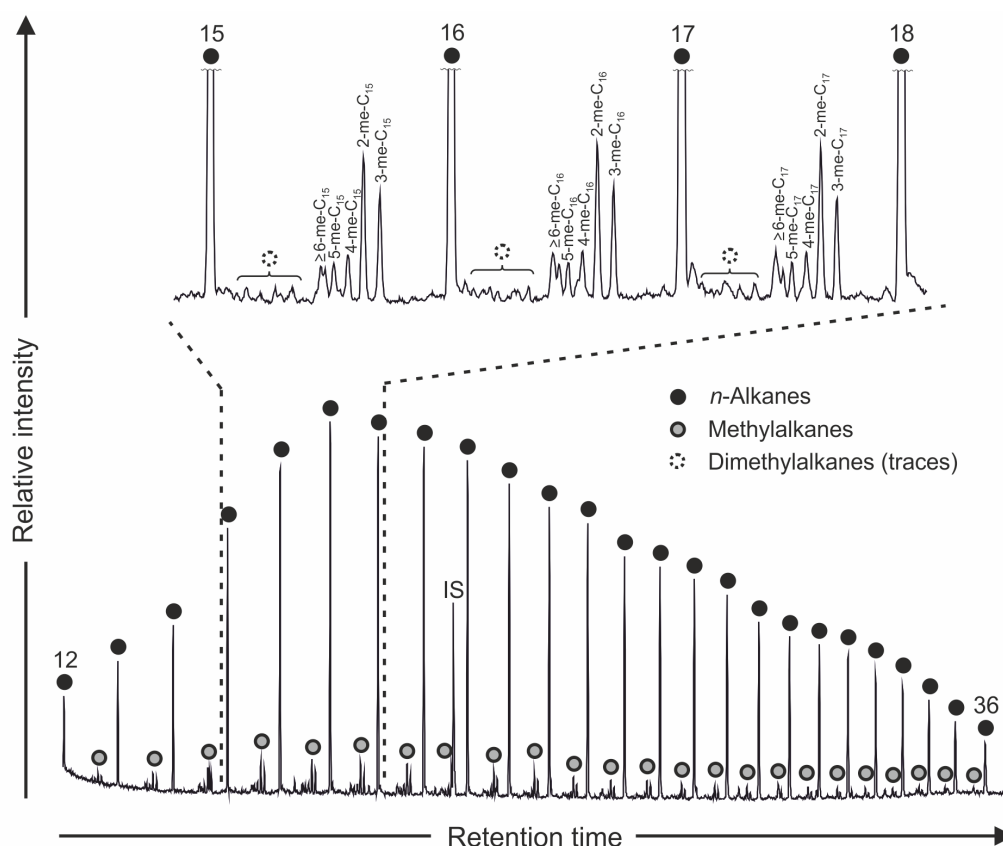
Figure 3.4: Partial GC–MS chromatogram (total ion current) of the hydrocarbon fraction (F1) resulting from Fischer–Tropsch-type reactions under hydrothermal conditions. Numbers refer to number of carbon atoms. IS: internal standard (*n*-eicosane d42).

fluid extraction residue (ca. 15 wt%) and the solid extraction residue (ca. 6 wt%). Both residues produced a major peak at 300 °C (Fig. A.2). Oxalic acid dihydrate produced only one peak at 183 °C (Fig. A.2).

ATR–FTIR revealed that the fluid extraction residue differs from the organic extract and also from pure oxalic acid (Figs. A.3a, e and b, respectively). The spectrum of the fluid extraction residue shows a very broad band between 3600 and 2700 cm^{-1} and a strong band at 1600 cm^{-1} (Fig. A.3a) which are suggesting the presence of O–H and C=O bonds, respectively. Furthermore, there are two absorption bands at 1369 cm^{-1} and 1305 cm^{-1} which might indicate C–O or C–C bonds. A weak absorption at ca. 2900 cm^{-1} might be related to C–H bonds. The solid extraction residue shows a strong band at 1071 cm^{-1} (Fig. A.3c) that is slightly shifted to a major peak in the montmorillonite spectrum (1031 cm^{-1}; Fig. A.3d). Additional bands in the solid extraction residue spectrum occur at 3347 cm^{-1} and 1617 cm^{-1} and might correspond to O–H and C=O bonds, respectively.

Upon pyrolysis, neither the fluid nor the solid extraction residue released any high molecular weight organic compounds that may have been formed during the FTT process. However, all fluid extraction residues yielded low molecular weight products (CO_2, CO and formic acid; Fig. A.4). Pyrolysis of the solid extraction residues only produced CO_2 and CO, but no formic acid.

3.4 Discussion

3.4.1 Variability of FTT reaction products and comparison with previous studies

The nature and distribution of synthesized compounds are in good overall agreement with previous studies. The *n*-alkan-1-ols, for example, are dominating the FTT reaction products in 175 °C experiments (McCollom et al., 1999; Rushdi and Simoneit, 2001; McCollom and Seewald, 2007; McCollom, 2013; Fig. 3.3; Table 3.1). Minor differences in the compound abundances and homolog ranges between individual experiments of this study are possibly due to losses of analytes during the preparation procedure, or slight variations between different experiments (e.g., temperature and pressure). No direct correlation between the duration of the experiments and the variation of the homolog ranges was observed (Table A.1). The observed CPI values close to 1 indicate that homologous series were formed by addition of single carbon units (Rushdi and Simoneit, 2001).

One notable difference to other studies, however, is the virtual absence of *n*-alkenes, *n*-alkanones and *n*-alkanals in the FTT reaction products formed in our experiments. *n*-Alkenes and *n*-alkanals observed in previous experiments were interpreted as possible intermediates in the formation of *n*-alkanes and *n*-alkanols, respectively (Rushdi and Simoneit, 2001), although, other studies did not report the formation of *n*-alkanals (cf. McCollom et al., 1999). We assume that differences in the experimental setup and conditions, specifically the lower concentrations of oxalic acid (McCollom et al., 1999: ca. 3.2 mol/L; Rushdi and Simoneit, 2001: ca. 3.7 mol/L; this study: ca. 1.5 mol/L), different reactor design and initial absence of headspace in the reactor (completely flooded reactor in this study) might have promoted a more complete formation of end member products in our FTT synthesis experiments. Furthermore, the presence of montmorillonite (this study, McCollom et al., 1999; absent in Rushdi and Simoneit, 2001) and its catalytic influence might have an essential impact on which compounds are formed. More systematic experiments would be necessary to test these assumptions.

3.4.2 Diversity of lipid-biomarker-like FTT reaction products

3.4.2.1 Alkanes

n-Alkanes are ubiquitous in sedimentary rocks of any geological age. Whereas most individual homologs are unspecific, particular *n*-alkane distribution patterns can point towards a biological source (Brocks and Summons, 2003; Peters et al., 2005b, and references therein; see also discussion in Section 3.4.2.5). Likewise, individual methylalkanes can show certain source specificity. For instance, 6-, 7- and 8-methylheptadecanes are universally synthesized de novo by cyanobacteria (Fehler and Light, 1970; Coates et al., 2014). Methylalkanes may further derive from the decarboxylation of linear and methyl-branched fatty acid precursors (Kissin, 1987; Summons, 1987; Thiel et al., 1999). Examples are terminally (*iso-*, *anteiso-*) and mid-chain methyl-branched fatty acids synthesized by various bacteria (Dowling et al., 1986; Thiel et al., 1999). Not surprisingly, (sub-) recent microbial mats are characterized by abundant mid-chain- and terminally branched monomethyl- and dimethylalkanes (Robinson and Eglinton, 1990; Shiea et al.,

1990; Kenig et al., 1995; Kenig, 2000; Parenteau et al., 2014). Long-chain methylalkanes may also derive from epicuticular leaf waxes of higher land plants (Eglinton and Hamilton, 1967; Pautler et al., 2010) and from insect waxes (Kenig et al., 1995). Abundant $C_{19} - C_{26}$ mid-chain methylalkanes ("x-peaks") are commonly observed in bitumens and kerogen pyrolysates from late Precambrian to Cambrian sedimentary units (Klomp, 1986; Fowler and Douglas, 1987; Höld et al., 1999; Love et al., 2008). The biological source of these compounds is still not clear, but they may derive from non-photosynthetic sulfur-oxidizing bacteria (Love et al., 2008).

Previous studies reported the formation of monomethyl- and dimethylalkanes by FTT synthesis in the gas phase (Studier et al., 1968; Nooner et al., 1976) and under hydrothermal conditions (McCollom et al., 1999; Rushdi and Simoneit, 2001). However, no isomer distributions of these compounds from experiments under hydrothermal conditions have so far been documented. Detailed examination of our FTT products revealed isomeric mixtures of 2- and 3-methylalkanes (*iso-* and *anteiso*-alkanes, respectively; Figs. 3.4, A.1) and further mid-chain methyl-branched isomers in decreasing abundances, but no predominances of individual methylalkanes such as "x-peaks". Similar distributions have been observed in crude oils and have been explained by thermal cracking of organic matter and clay-catalyzed conversion of α-olefins into methylalkanes (Kissin, 1987). These observations underline that only the predominance of certain isomers of methylalkanes, rather than their occurrence in random distributions, will show sufficient specificity to account for a biological source (cf. Peters et al., 2005b).

3.4.2.2 Alcohols

Linear and methyl-branched alkanols and alkenols are synthesized by many organisms as building blocks of more complex lipids (Rizzo, 2014). In sediments, these compounds commonly derive from wax esters (e.g., from the storage lipids of zooplankton) and from the waxes of higher land plants (Eglinton and Hamilton, 1967; Lee and Hirota, 1973; Fukushima and Ishiwatari, 1984; Pearson et al., 2001). *n*-Alkanols have therefore frequently been applied as biomarkers in recent and subrecent sediments. In biologically derived materials, these compounds typically show a strong even-over-odd predominance, as opposed to FTT reaction products, and a preference of *n*-alkan-1-ols over other isomers, which is similar to FTT reaction products (Ficken et al., 1998; Meyers, 2003; Treignier et al., 2006; Fig. 3.3).

Iso-, *anteiso*-alkanols (i.e., alkanols with a methyl group at the ω-2 or ω-3 carbon) and secondary alkanols (i.e., alkan-2-ols, alkan-3-ols) are common in recent sediments where they most probably derive from in situ microbial synthesis (Sever and Parker, 1969; Cranwell, 1980, 1984; Mudge and Norris, 1997). Likewise, short-chain methylalkanols with the methyl group attached at the functional end of the molecule (e.g., 2-methyldodecan-1-ol and 2-methylhexadecan-1-ol) have been observed in bacteria, algae and higher land plants (Condurso et al., 2006; Ercolini et al., 2009; Effmert et al., 2012; Sameza et al., 2014; Shobier et al., 2016).

n-Alkanols as well as methyl-branched and secondary alkanol moieties were also reported as products from FTT synthesis under hydrothermal conditions (McCollom et al., 1999; Rushdi and Simoneit, 2001). Indeed, detailed observation of our FTT reaction products uncovered a great variety of these compounds (Fig. 3.3). 2-methylalkan-1-ols were

the dominating methylalkanols in this study (Figs. 3.2d, 3.3). Given that only individual 2-methylalkan-1-ols occur as specific biological products (see above), the observed appearance as a homologous series with relatively high abundances is probably a characteristic trait of abiotic formation pathways.

3.4.2.3   Alkanoic acids

Alkanoic acids are essential building blocks of bacterial and eukaryotic cells. Therefore, these compounds are widely occurring and show an extensive structural variety (e.g., saturated, unsaturated, linear and methyl-branched moieties) depending on their exact biological sources and functions. While linear alkanoic acids are widespread in nature, some structural isomers are probably indicative for certain groups of organisms (e.g., methyl-branched alkanoic acids produced by bacteria; Kaneda, 1991; Killops and Killops, 2005, and references therein). FTT synthesis in our study revealed the exclusive formation of linear moieties (Figs. 3.2e, 3.3). The absence of methyl-branched or unsaturated homologs is in line with findings from earlier experiments (McCollom et al., 1999; Rushdi and Simoneit, 2001). Consequently, methylated and/or unsaturated varieties of alkanoic acids may generally be regarded as indicative for a biological origin of these compounds.

3.4.2.4   Aromatic compounds

Polycyclic aromatic hydrocarbons (PAHs) commonly derive from biological precursors (e.g., carotenoids), and are additionally produced through thermal overprint (+ combustion) of these molecules (Simoneit, 1998, 2002, and references therein). However, PAHs were also found in meteorites where they clearly originate from abiotic synthesis (McKay et al., 1996; Becker et al., 1997; Clemett et al., 1998). Furthermore, these compounds have been reported from high temperature FTT synthesis products (> 350 °C; Studier et al., 1972; Nooner et al., 1976; Nooner and Oró, 1979; Rushdi and Simoneit, 2001) and from siderite decomposition at 300 °C in the presence of water (McCollom, 2003). Our FTT reaction products did not contain any alicyclic and/or aromatic compounds. Therefore higher reaction temperatures or further thermal maturation are probably essential for the production of cyclic components from FTT synthesis products, but this has to be tested in further experiments.

3.4.2.5   Predominance of homologs and isomers vs. unimodal distribution patterns

Biosynthesis of lipids typically involves the combination of repeating sub-units (e.g., acetate, isoprene) and modification of these products by desaturation-, reduction-, methylation- or decarboxylation reactions. As a consequence, biologically derived lipids typically exhibit preferences of distinctive homologs. Biologically derived n-alkanes, for instance, mostly show an odd-over-even predominance (due to decarboxylation from fatty acid precursors), and a restriction to certain chain lengths (e.g., n-C$_{17}$ for cyanobacteria; Coates et al., 2014; n-C$_{25}$ – C$_{33}$ for epicuticular leaf waxes; Eglinton and Hamilton, 1967; Peters et al., 2005b; Summons et al., 2008). Likewise, biogenic n-alkanols and n-alkanoic acids are typically dominated by even-numbered carbon chains (Eglinton and Hamilton, 1967; Summons et al., 2008), and exhibit a preference of short-chain (C$_{12}$ – C$_{24}$, marine biota) and/or long-chain homologs (C$_{22}$ – C$_{32}$, land plants; Eglinton and Hamilton, 1967;

Robinson et al., 1984; Rielley et al., 1991; Volkman et al., 1999). Products deriving from FTT synthesis, in contrast, always form homologs and isomers without any pre-dominances (McCollom et al., 1999; Rushdi and Simoneit, 2001; McCollom, 2013; this study). These different primary distributions have to be considered for the interpretation of lipid biomarkers in materials, where contributions from abiotic organic matter cannot be excluded (e.g., Archean rocks, hydrothermal/serpentinization and potentially extraterrestrial settings). The latter is especially important for upcoming space missions aimed at analyzing Mars surface samples with GC–MS (e.g., ExoMars 2020; Goesmann et al., 2017; Vago et al., 2017).

Problematically, distinctive carbon chain length preferences characteristic for biology or isomer distributions are successively reduced during thermal maturation (Brocks and Summons, 2003; Peters et al., 2005b; Mißbach et al., 2016; Fig. A.5). Defunctionalization and thermal cracking of n-alkyl chains typically results in (i) a unimodal distribution of n-alkane homologs and (ii) isomeric mixtures of methylalkanes (Kissin, 1987). Beyond a certain degree of thermal maturation, biologically derived organic matter may therefore exhibit distribution patterns similar to FTT products (Fig. 3.5, cf. Fig. A.5). As a consequence, the distinction of biologically from abiotically derived compounds solely based on GC–MS data may be severely hampered in thermally mature rocks. Stable carbon isotopes may offer an additional approach to pinpoint a biological source of organic matter (Sherwood Lollar et al., 2002; Sangély et al., 2007; Konn et al., 2015). However, some studies revealed that a depletion in ^{13}C (considered as a biological signature in carbon compounds) can also be obtained by an abiotic formation of organic matter or graphite (van Zuilen et al., 2002, 2003; Horita, 2005; McCollom and Seewald, 2006; Konn et al., 2015).

3.4.3   Testing the presence and composition of macromolecular FTT reaction products

The incorporation of lipids into macromolecular organic material (i.e., kerogen) is considered essential for the preservation of biomarkers over geological timescales (Love et al., 1995; Hallmann et al., 2011; Summons, 2014). The FTT reaction products from this study include a variety of functionalized compounds which are potentially important for kerogen formation (Fig. 3.3). It is therefore crucial to explore whether organics deriving from FTT synthesis may undergo polycondensation reactions to form "abiotic kerogens" (cf. De Gregorio et al., 2011).

Combustion–infrared detection revealed the presence of organic materials in the fluid and the solid extraction residues (Fig. A.2). Infrared spectra of this organic material evidence the presence of O–H and C=O bonds (Figs. A.3a, c), while Py-GC–MS experiments only yielded low molecular weight products (Fig. A.4). Consequently, the residual organic material likely consists of organic polymers which are composed of small functionalized molecules, possibly oxalic acid and some diol species such as, for example, methanediol. Methanediol can be formed via the decomposition of formic acid, with formaldehyde as an intermediate (i.e., formaldehyde–methanediol equilibrium; Gibson, 1969; Morooka et al., 2005; Matubayasi et al., 2007). The polymerization reactions in water could have then been catalyzed by montmorillonite (cf. Huang et al., 2008; Nagendrappa, 2011). However, the exact nature of this potential polymer has to be further
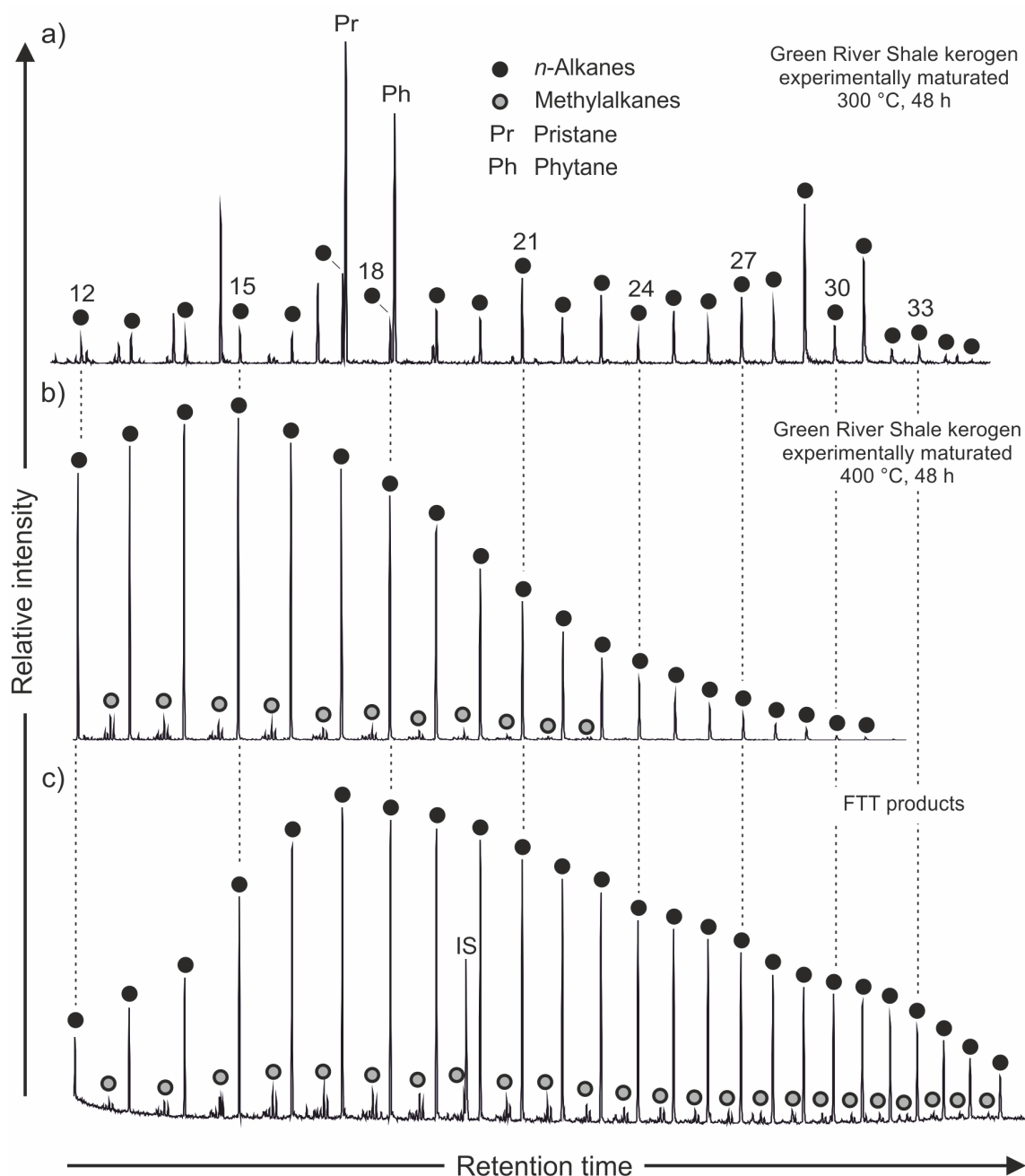
Figure 3.5: Partial mass chromatograms (*m/z* 85) of the aliphatic hydrocarbon fractions from experimentally maturated Green River Shale kerogen (**a**: 48 h at 300 °C; **b**: 48 h at 400 °C); (**c**) partial total ion current chromatogram of the hydrocarbons (F1) from Fischer–Tropsch-type reactions under hydrothermal conditions (cf. Fig. 3.4). Numbers refer to number of carbon atoms. IS, internal standard (*n*-eicosane d42). Note the odd-over-even predominance of *n*-alkane homologs in (**a**) which are distinctively different to the unimodal distribution in (**b**) and (**c**). See Fig. A.5 for a more detailed overview on the effect of thermal alteration on hydrocarbon distributions.

elucidated, and it remains to be tested whether such materials, comprised of small functionalized molecules, can evolve into larger and more complex (insoluble) macromolecular networks resembling biological kerogens. Furthermore, it is unclear if the black color of the fluid extraction residue is due to residual organics. It might also be explained by the dissolution of iron oxides in aqueous oxalic acid solutions (Panias et al., 1996).

3.4.4 Applicability of FTT synthesis experiments to natural systems

The applicability of FTT synthesis experiments for understanding natural systems is limited. For instance, the catalyst present in most experiments (i.e., the stainless steel reactor wall) is more suitable than natural catalysts with respect to concentration and purity. Furthermore, earlier studies suggested that the FTT reactions in these stainless steel reactors probably take place in H_2 rich vapor bubbles (or a gas phase) which form on the surface of the catalyst and not in an aqueous solution (McCollom and Seewald, 2001, 2003, 2007; McCollom, 2013). Together, this probably leads to a faster production and higher yields of organic compounds than it would be expected from natural hydrothermal systems (McCollom and Seewald, 2001; McCollom, 2013, 2016, and references therein). Nevertheless, Ni and Cr bearing minerals that are present in serpentinization environments can help to effectively overcome kinetic barriers and might accelerate hydrocarbon formation in natural settings. Awaruite (a natural Ni–Fe alloy) or Ni-sulfides have been shown to be effective catalysts in the formation of CH_4, ammonium, and even activated acetic acid in reducing environments, while Cr bearing minerals (e.g., chromite) have the potential to catalyze the production of larger hydrocarbons (Huber and Wächtershäuser, 1997; Horita and Berndt, 1999; Foustoukos and Seyfried, 2004; Smirnov et al., 2008; Lazar et al., 2012; review by McCollom, 2013).

The early Archean crust contained a variety of mafic to ultramafic rocks and thus, the amount of catalyzing (e.g., Ni or Cr bearing) minerals was possibly higher than today (Van Kranendonk, 2010; Lazar et al., 2012; Van Kranendonk et al., 2012, and references therein). The production of lipids via FTT synthesis could therefore have been more widespread and effective during Archean times (Lazar et al., 2012). Abiotic lipid production could have been further promoted by higher concentrations of H_2 in the early atmosphere (and oceans) (Kasting, 1993; Tian et al., 2005; Wordsworth and Pierrehumbert, 2013). In recent settings, FTT reactions may account for a locally restricted and slow production of CH_4, and possibly larger hydrocarbons, particularly in shallow serpentinization environments where a separate gas phase or H_2 rich vapor bubbles can be formed (Etiope and Sherwood Lollar, 2013; McCollom, 2013, 2016; Konn et al., 2015; Etiope et al., 2016).

3.5 Conclusions

(i) Fischer–Tropsch-type (FTT) synthesis under hydrothermal conditions leads to a variety of biomarker-like lipids, e.g., linear and methyl-branched alkanes and alkanols as well as *n*-alkanoic acids. No cyclic or aromatic compounds were found. The results of this study are well in line with earlier investigations although the lack of *n*-alkenes and *n*-alkanals in our experiment suggests a more complete formation of end member products.

(ii) Biologically derived lipids usually show the predominance of individual homologs and isomers, while organics deriving from FTT reactions always exhibit a unimodal distribution and isomeric mixtures. Thus, primary distributions should generally allow distinguishing between biologically and abiotically derived lipids.

(iii) Thermal maturation can transform biologically-inherited predominances into unimodal distributions but not vice versa. Hence, discrimination of biologically derived organic compounds and FTT reaction products becomes more difficult with increasing thermal maturity.

(iv) Extraction residues of FTT reaction products contained organic material, possibly in the form of a polymer comprised of oxalic acid and diol species. Whether or not these residual organics can evolve into more complex (insoluble) kerogen-like material remains to be tested.

Acknowledgements

References

Abrajano, T. A., Sturchio, N. C., Kennedy, B. M., Lyon, G. L., Muehlenbachs, K., and Bohlke, J. K. (1990). Geochemistry of reduced gas related to serpentinization of the Zambales ophiolite, Philippines. *Applied Geochemistry*, 5, 625–630.

Ahmed, M. and George, S. C. (2004). Changes in the molecular composition of crude oils during their preparation for GC and GC–MS analyses. *Organic Geochemistry*, 35, 137–155.

Ahmed, M., Lehnert, O., Fuentes, D., and Meinhold, G. (2014). Origin of oil and bitumen in the Late Devonian Siljan impact structure, central Sweden. *Organic Geochemistry*, 68, 13–26.

Akiya, N. and Savage, P. E. (1998). Role of water in formic acid decomposition. *AIChE Journal*, 44, 405–415.

Amend, J. P., Amend, A. C., and Valenza, M. (1998). Determination of volatile fatty acids in the hot springs of Vulcano, Aeolian Islands, Italy. *Organic Geochemistry*, 28, 699–705.

References

Anderson, R. B. (1984). *The Fischer-Tropsch Synthesis*. Academic Press, London.

Becker, L., Glavin, D. P., and Bada, J. L. (1997). Polycyclic aromatic hydrocarbons (PAHs) in Antarctic Martian meteorites, carbonaceous chondrites, and polar ice. *Geochimica et Cosmochimica Acta*, 61, 475–481.

Berndt, M. E., Allen, D. E., and Seyfried, W. E. (1996). Reduction of CO_2 during serpentinization of olivine at 300 °C and 500 bar. *Geology*, 24, 351–354.

Brocks, J. J., Buick, R., Logan, G. A., and Summons, R. E. (2003). Composition and syngeneity of molecular fossils from the 2.78 to 2.45 billion-year-old Mount Bruce Supergroup, Pilbara Craton, Western Australia. *Geochimica et Cosmochimica Acta*, 67, 4289–4319.

Brocks, J. J. and Pearson, A. (2005). Building the biomarker tree of life. *Reviews in Mineralogy and Geochemistry*, 59, 233–258.

Brocks, J. J. and Summons, R. E. (2003). Biomarkers for Early Life. In W. H. Schlesinger (Ed.), *Biogeochemistry*. Elsevier, Oxford, pp. 63–115.

Bröll, D., Kaul, C., Krämer, A., Krammer, P., Richter, T., Jung, M., Vogel, H., and Zehner, P. (1999). Chemistry in Supercritical Water. *Angewandte Chemie International Edition*, 38, 2998–3014.

Chyba, C. F. and Sagan, C. (1992). Endogenous production, exogenous delivery and impact-shock synthesis of organic molecules: an inventory for the origins of life. *Nature*, 355, 125–132.

Clemett, S. J., Dulay, M. T., Gillette, J. S., Chillier, X. D. F., Mahajan, T. B., and Zare, R. N. (1998). Evidence for the extraterrestrial origin of polycyclic aromatic hydrocarbons in the Martian meteorite ALH84001. *Faraday Discussions*, 109, 417–436.

Coates, R. C., Podell, S., Korobeynikov, A., Lapidus, A., Pevzner, P., Sherman, D. H., Allen, E. E., Gerwick, L., and Gerwick, W. H. (2014). Characterization of Cyanobacterial Hydrocarbon Composition and Distribution of Biosynthetic Pathways. *PLoS One*, 9, e85140.

Condurso, C., Verzera, A., Romeo, V., Ziino, M., Trozzi, A., and Ragusa, S. (2006). The leaf volatile constituents of *Isatis tinctoria* by solid-phase microextraction and gas chromatography/mass spectrometry. *Planta medica*, 72, 924–928.

Cranwell, P. A. (1980). Branched/cyclic alkanols in lacustrine sediments (Great Britain): Recognition of *iso-* and *anteiso*-branching and stereochemical analysis of homologous alkan-2-ols. *Chemical Geology*, 30, 15–26.

Cranwell, P. A. (1984). Lipid geochemistry of sediments from Upton Broad, a small productive lake. *Organic Geochemistry*, 7, 25–37.

Cronin, J. R. and Pizzarello, S. (1990). Aliphatic hydrocarbons of the Murchison meteorite. *Geochimica et Cosmochimica Acta*, 54, 2859–2868.

Crossey, L. J. (1991). Thermal degradation of aqueous oxalate species. *Geochimica et Cosmochimica Acta*, 55, 1515–1527.

D'Amore, F. and Panichi, C. (1980). Evaluation of deep temperatures of hydrothermal systems by a new gas geothermometer. *Geochimica et Cosmochimica Acta*, 44, 549–556.

De Gregorio, B. T., Sharp, T. G., Rushdi, A. I., and Simoneit, B. R. T. (2011). Bugs or Gunk? Nanoscale Methods for Assessing the Biogenicity of Ancient Microfossils and Organic Matter. In S. D. Golding and M. Glikson (Eds.), *Earliest Life on Earth: Habitats, Environments and Methods of Detection*. Springer Netherlands, Dordrecht, pp. 239–289.

De Klerk, A. and Furimsky, E. (2010). *Catalysis in the refining of Fischer-Tropsch syncrude*. Royal Society of Chemistry, Cambridge.

Dowling, N. J. E., Widdel, F., and White, D. C. (1986). Phospholipid Ester-linked Fatty Acid Biomarkers of Acetate-oxidizing Sulphate-reducers and Other Sulphide-forming Bacteria. *Microbiology*, 132, 1815–1825.

Dry, M. E. (2002). The Fischer–Tropsch process: 1950–2000. *Catalysis Today*, 71, 227–241.

Durand, B. (1980). Sedimentary organic matter and kerogen. Definition and quantitative importance of kerogen. In B. Durand (Ed.), *Kerogen*. Éditions Technip, Paris, pp. 13–34.

Durand, B. and Nicaise, G. (1980). Procedures for kerogen isolation. In B. Durand (Ed.), *Kerogen*. Éditions Technip, Paris, pp. 35–53.

Effmert, U., Kalderás, J., Warnke, R., and Piechulla, B. (2012). Volatile Mediated Interactions Between Bacteria and Fungi in the Soil. *Journal of Chemical Ecology*, 38, 665–703.

Eglinton, G. and Hamilton, R. J. (1967). Leaf epicuticular waxes. *Science*, 156, 1322–1335.

Elliott, D. C., Hallen, R. T., and Sealock, L. J. (1983). Aqueous Catalyst Systems for the Water-Gas Shift Reaction. 2. Mechanism of Basic Catalysis. *Industrial & Engineering Chemistry Product Research and Development*, 22, 431–435.

Ercolini, D., Russo, F., Nasi, A., Ferranti, P., and Villani, F. (2009). Mesophilic and Psychrotrophic Bacteria from Meat and Their Spoilage Potential In Vitro and in Beef. *Applied and Environmental Microbiology*, 75, 1990–2001.

Etiope, G. and Sherwood Lollar, B. (2013). Abiotic Methane on Earth. *Reviews of Geophysics*, 51, 276–299.

Etiope, G., Vadillo, I., Whiticar, M. J., Marques, J. M., Carreira, P. M., Tiago, I., Benavente, J., Jiménez, P., and Urresti, B. (2016). Abiotic methane seepage in the Ronda peridotite massif, southern Spain. *Applied Geochemistry*, 66, 101–113.

Fehler, S. W. G. and Light, R. J. (1970). Biosynthesis of hydrocarbons in Anabaena variabilis. Incorporation of [methyl-^{14}C] and [methyl-^{2}H$_2$] Methionine into 7- and 8-methyl-heptadecanes. *Biochemistry*, 9, 418–422.

Ferris, J. P. (1992). Chapter 6 Chemical markers of prebiotic chemistry in hydrothermal systems. *Origins of Life and Evolution of Biospheres*, 22, 109–134.

Ficken, K. J., Street-Perrott, F. A., Perrott, R. A., Swain, D. L., Olago, D. O., and Eglinton, G. (1998). Glacial/interglacial variations in carbon cycling revealed by molecular and isotope stratigraphy of Lake Nkunga, Mt. Kenya, East Africa. *Organic Geochemistry*, 29, 1701–1719.

Fischer, F. (1935). Die Synthese der Treibstoffe (Kogaisin) und Schmieröle aus Kohlenoxyd und Wasserstoff bei Gewöhnlichem Druck. *Brennstoff Chemie*, 16, 1–11.

Fischer, F. and Tropsch, H. (1926). Über die direkte Synthese von Erdöl-Kohlenwasserstoffen bei gewöhnlichem Druck (Erste Mitteilung). *Berichte der deutschen chemischen Gesellschaft (A and B Series)*, 59, 830–831.

Foustoukos, D. I. and Seyfried, W. E. (2004). Hydrocarbons in Hydrothermal Vent Fluids: The Role of Chromium-Bearing Catalysts. *Science*, 304, 1002–1005.

Fowler, M. G. and Douglas, A. G. (1987). Saturated hydrocarbon biomarkers in oils of Late Precambrian age from Eastern Siberia. *Organic Geochemistry*, 11, 201–213.

Fu, Q., Socki, R. A., and Niles, P. B. (2015). Evaluating reaction pathways of hydrothermal abiotic organic synthesis at elevated temperatures and pressures using carbon isotopes. *Geochimica et Cosmochimica Acta*, 154, 1–17.

Fukushima, K. and Ishiwatari, R. (1984). Acid and alcohol compositions of wax esters in sediments from different environments. *Chemical Geology*, 47, 41–56.

Gelpi, E. and Oró, J. (1970). Organic compounds in meteorites—IV. Gas chromatographic-mass spectrometric studies on the isoprenoids and other isomeric alkanes in carbonaceous chondrites. *Geochimica et Cosmochimica Acta*, 34, 981–994.

Gibson, H. W. (1969). Chemistry of formic acid and its simple derivatives. *Chemical Reviews*, 69, 673–692.

Goesmann, F., Brinckerhoff, W. B., Raulin, F., Goetz, W., Danell, R. M., Getty, S. A., Siljeström, S., Mißbach, H., Steininger, H., Arevalo, R. D., Buch, A., Freissinet, C., Grubisic, A., Meierhenrich, U. J., Pinnick, V. T., Stalport, F., Szopa, C., Vago, J. L., Lindner, R., Schulte, M. D., Brucato, J. R., Glavin, D. P., Grand, N., Li, X., van Amerom, F. H. W., and the Moma Science Team (2017). The Mars Organic Molecule Analyzer (MOMA) Instrument: Characterization of Organic Material in Martian Sediments. *Astrobiology*, 17, 655–685.

Hallmann, C., Kelly, A. E., Gupta, S. N., and Summons, R. E. (2011). Reconstructing deep-time biology with molecular fossils. In M. Laflamme, D. J. Schiffbauer, and Q. S. Dornbos (Eds.), *Quantifying the Evolution of Early Life: Numerical Approaches to the*

Evaluation of Fossils and Ancient Ecosystems. Springer Netherlands, Dordrecht, pp. 355–401.

Harris, A. C., White, N. C., McPhie, J., Bull, S. W., Line, M. A., Skrzeczynski, R., Mernagh, T. P., and Tosdal, R. M. (2009). Early Archean Hot Springs above Epithermal Veins, North Pole, Western Australia: New Insights from Fluid Inclusion Microanalysis. *Economic Geology*, 104, 793–814.

Höld, I. M., Schouten, S., Jellema, J., and Sinninghe Damsté, J. S. (1999). Origin of free and bound mid-chain methyl alkanes in oils, bitumens and kerogens of the marine, Infracambrian Huqf Formation (Oman). *Organic Geochemistry*, 30, 1411–1428.

Holm, N. G. and Charlou, J. L. (2001). Initial indications of abiotic formation of hydrocarbons in the Rainbow ultramafic hydrothermal system, Mid-Atlantic Ridge. *Earth and Planetary Science Letters*, 191, 1–8.

Höök, M., Bardi, U., Feng, L., and Pang, X. (2010). Development of oil formation theories and their importance for peak oil. *Marine and Petroleum Geology*, 27, 1995–2004.

Horita, J. (2005). Some perspectives on isotope biosignatures for early life. *Chemical Geology*, 218, 171–186.

Horita, J. and Berndt, M. E. (1999). Abiogenic Methane Formation and Isotopic Fractionation Under Hydrothermal Conditions. *Science*, 285, 1055–1057.

Huang, T.-k., Wang, R., Shi, L., and Lu, X.-x. (2008). Montmorillonite K-10: An efficient and reusable catalyst for the synthesis of quinoxaline derivatives in water. *Catalysis Communications*, 9, 1143–1147.

Huber, C. and Wächtershäuser, G. (1997). Activated Acetic Acid by Carbon Fixation on (Fe, Ni)S Under Primordial Conditions. *Science*, 276, 245–247.

Kaneda, T. (1991). *Iso-* and *anteiso*-fatty acids in bacteria: biosynthesis, function, and taxonomic significance. *Microbiological Reviews*, 55, 288–302.

Kasting, J. F. (1993). Earth's Early Atmosphere. *Science*, 259, 920–926.

Kawamura, K. and Nissenbaum, A. (1992). High abundance of low molecular weight organic acids in hypersaline spring water associated with a salt diapir. *Organic Geochemistry*, 18, 469–476.

Kenig, F. (2000). $C_{16}-C_{29}$ homologous series of monomethylalkanes in the pyrolysis products of a Holocene microbial mat. *Organic Geochemistry*, 31, 237–241.

Kenig, F., Sinninghe Damsté, J. S., Kock-van Dalen, A. C., Rijpstra, W. I. C., Huc, A. Y., and de Leeuw, J. W. (1995). Occurrence and origin of mono-, di-, and trimethylalkanes in modern and Holocene cyanobacterial mats from Abu Dhabi, United Arab Emirates. *Geochimica et Cosmochimica Acta*, 59, 2999–3015.

References

Killops, S. D. and Killops, V. J. (2005). *Introduction to organic geochemistry*. 2. edition, Blackwell Publishing Ltd, Oxford.

Kissin, Y. V. (1987). Catagenesis and composition of petroleum: Origin of *n*-alkanes and isoalkanes in petroleum crudes. *Geochimica et Cosmochimica Acta*, 51, 2445–2457.

Klomp, U. C. (1986). The chemical structure of a pronounced series of *iso*-alkanes in South Oman crudes. *Organic Geochemistry*, 10, 807–814.

Konn, C., Charlou, J. L., Holm, N. G., and Mousis, O. (2015). The Production of Methane, Hydrogen, and Organic Compounds in Ultramafic-Hosted Hydrothermal Vents of the Mid-Atlantic Ridge. *Astrobiology*, 15, 381–399.

Lang, S. Q., Butterfield, D. A., Schulte, M., Kelley, D. S., and Lilley, M. D. (2010). Elevated concentrations of formate, acetate and dissolved organic carbon found at the Lost City hydrothermal field. *Geochimica et Cosmochimica Acta*, 74, 941–952.

Lazar, C., McCollom, T. M., and Manning, C. E. (2012). Abiogenic methanogenesis during experimental komatiite serpentinization: Implications for the evolution of the early Precambrian atmosphere. *Chemical Geology*, 326, 102–112.

Lee, R. F. and Hirota, J. (1973). Wax Esters in Tropical Zooplankton and Nekton and the Geographical Distribution of Wax Esters in Marine Copepods. *Limnology and Oceanography*, 18, 227–239.

Lindsay, J. F., Brasier, M. D., McLoughlin, N., Green, O. R., Fogel, M., Steele, A., and Mertzman, S. A. (2005). The problem of deep carbon—An Archean paradox. *Precambrian Research*, 143, 1–22.

Lockhart, R. S., Meredith, W., Love, G. D., and Snape, C. E. (2008). Release of bound aliphatic biomarkers via hydropyrolysis from Type II kerogen at high maturity. *Organic Geochemistry*, 39, 1119–1124.

Love, G. D., Snape, C. E., Carr, A. D., and Houghton, R. C. (1995). Release of covalently-bound alkane biomarkers in high yields from kerogen via catalytic hydropyrolysis. *Organic Geochemistry*, 23, 981–986.

Love, G. D., Stalvies, C., Grosjean, E., Meredith, W., and Snape, C. E. (2008). Analysis of molecular biomarkers covalently bound within Neoproterozoic sedimentary kerogen. In P. H. Kelley and R. K. Bambach (Eds.), *From Evolution to Geobiology: Research Questions Driving Paleontology at the Start of a New Century. Paleontological Society Papers Vol. 14*. The Paleontological Society, pp. 67–83.

Martens, C. S. (1990). Generation of short chain acid anions in hydrothermally altered sediments of the Guaymas Basin, Gulf of California. *Applied Geochemistry*, 5, 71–76.

Martin, W., Baross, J., Kelley, D., and Russell, M. J. (2008). Hydrothermal vents and the origin of life. *Nature Reviews Microbiology*, 6, 805–814.

Matubayasi, N., Morooka, S., Nakahara, M., and Takahashi, H. (2007). Chemical equilibrium of formaldehyde and methanediol in hot water: Free-energy analysis of the solvent effect. *Journal of Molecular Liquids*, 134, 58–63.

McCollom, T. M. (2003). Formation of meteorite hydrocarbons from thermal decomposition of siderite ($FeCO_3$). *Geochimica et Cosmochimica Acta*, 67, 311–317.

McCollom, T. M. (2013). Laboratory simulations of abiotic hydrocarbon formation in Earth's deep subsurface. *Reviews in Mineralogy and Geochemistry*, 75, 467–494.

McCollom, T. M. (2016). Abiotic methane formation during experimental serpentinization of olivine. *Proceedings of the National Academy of Sciences of the United States of America*, 113, 13965–13970.

McCollom, T. M., Ritter, G., and Simoneit, B. R. T. (1999). Lipid Synthesis Under Hydrothermal Conditions by Fischer–Tropsch-Type Reactions. *Origins of Life and Evolution of Biospheres*, 29, 153–166.

McCollom, T. M. and Seewald, J. S. (2001). A reassessment of the potential for reduction of dissolved CO_2 to hydrocarbons during serpentinization of olivine. *Geochimica et Cosmochimica Acta*, 65, 3769–3778.

McCollom, T. M. and Seewald, J. S. (2003). Experimental constraints on the hydrothermal reactivity of organic acids and acid anions: I. Formic acid and formate. *Geochimica et Cosmochimica Acta*, 67, 3625–3644.

McCollom, T. M. and Seewald, J. S. (2006). Carbon isotope composition of organic compounds produced by abiotic synthesis under hydrothermal conditions. *Earth and Planetary Science Letters*, 243, 74–84.

McCollom, T. M. and Seewald, J. S. (2007). Abiotic Synthesis of Organic Compounds in Deep-Sea Hydrothermal Environments. *Chemical Reviews*, 107, 382–401.

McDermott, J. M., Seewald, J. S., German, C. R., and Sylva, S. P. (2015). Pathways for abiotic organic synthesis at submarine hydrothermal fields. *Proceedings of the National Academy of Sciences of the United States of America*, 112, 7668–7672.

McKay, D. S., Gibson, E. K., Thomas-Keprta, K. L., Vali, H., Romanek, C. S., Clemett, S. J., Chillier, X. D. F., Maechling, C. R., and Zare, R. N. (1996). Search for Past Life on Mars: Possible Relic Biogenic Activity in Martian Meteorite ALH84001. *Science*, 273, 924–930.

Meyers, P. A. (2003). Applications of organic geochemistry to paleolimnological reconstructions: a summary of examples from the Laurentian Great Lakes. *Organic Geochemistry*, 34, 261–289.

Mißbach, H., Duda, J.-P., Lünsdorf, N. K., Schmidt, B. C., and Thiel, V. (2016). Testing the preservation of biomarkers during experimental maturation of an immature kerogen. *International Journal of Astrobiology*, 15, 165–175.

Morgan, G. B., Chou, I. M., and Pasteris, J. D. (1992). Speciation in experimental C-O-H fluids produced by the thermal dissociation of oxalic acid dihydrate. *Geochimica et Cosmochimica Acta*, 56, 281–294.

Morooka, S., Wakai, C., Matubayasi, N., and Nakahara, M. (2005). Hydrothermal Carbon–Carbon Bond Formation and Disproportionations of C1 Aldehydes: Formaldehyde and Formic Acid. *The Journal of Physical Chemistry A*, 109, 6610–6619.

Mudge, S. M. and Norris, C. E. (1997). Lipid biomarkers in the Conwy Estuary (North Wales, U.K.): a comparison between fatty alcohols and sterols. *Marine Chemistry*, 57, 61–84.

Nagendrappa, G. (2011). Organic synthesis using clay and clay-supported catalysts. *Applied Clay Science*, 53, 106–138.

Nooner, D. W., Gibert, J. M., Gelpi, E., and Oró, J. (1976). Closed system Fischer-Tropsch synthesis over meteoritic iron, iron ore and nickel-iron alloy. *Geochimica et Cosmochimica Acta*, 40, 915–924.

Nooner, D. W. and Oró, J. (1979). Synthesis of Fatty Acids by a Closed System Fischer-Tropsch Process. In E. L. Kugler and F. W. Steffgen (Eds.), *Hydrocarbon Synthesis from Carbon Monoxide and Hydrogen*, Advances in Chemistry. American Chemical Society, pp. 159–171.

Nuth III, J. A., Johnson, N. M., and Manning, S. (2008). A Self-Perpetuating Catalyst for the Production of Complex Organic Molecules in Protostellar Nebulae. *The Astrophysical Journal Letters*, 673, L225.

Panias, D., Taxiarchou, M., Paspaliaris, I., and Kontopoulos, A. (1996). Mechanisms of dissolution of iron oxides in aqueous oxalic acid solutions. *Hydrometallurgy*, 42, 257–265.

Parenteau, M. N., Jahnke, L. L., Farmer, J. D., and Cady, S. L. (2014). Production and Early Preservation of Lipid Biomarkers in Iron Hot Springs. *Astrobiology*, 14, 502–521.

Pautler, B. G., Austin, J., Otto, A., Stewart, K., Lamoureux, S. F., and Simpson, M. J. (2010). Biomarker assessment of organic matter sources and degradation in Canadian High Arctic littoral sediments. *Biogeochemistry*, 100, 75–87.

Pearson, A., McNichol, A. P., Benitez-Nelson, B. C., Hayes, J. M., and Eglinton, T. I. (2001). Origins of lipid biomarkers in Santa Monica Basin surface sediment: a case study using compound-specific Δ^{14}C analysis. *Geochimica et Cosmochimica Acta*, 65, 3123–3137.

Peters, K. E., Walters, C. C., and Moldowan, J. M. (2005a). *The Biomarker Guide - Part I - Biomarkers and Isotopes in the Environment and Human History*. Cambridge University Press, New York.

Peters, K. E., Walters, C. C., and Moldowan, J. M. (2005b). *The Biomarker Guide - Part II - Biomarkers and Isotopes in Petroleum Exploration and Earth History*. Cambridge University Press, New York.

Proskurowski, G., Lilley, M. D., Seewald, J. S., Früh-Green, G. L., Olson, E. J., Lupton, J. E., Sylva, S. P., and Kelley, D. S. (2008). Abiogenic Hydrocarbon Production at Lost City Hydrothermal Field. *Science*, 319, 604–607.

Riaz, U. and Ashraf, S. M. (2014). Characterization of polymer blends with FTIR spectroscopy. In S. Thomas, Y. Grohens, and P. Jyotishkumar (Eds.), *Characterization of Polymer Blends: Miscibility, Morphology and Interfaces*. Wiley, Weinheim, Germany, pp. 625–678.

Rielley, G., Collier, R. J., Jones, D. M., and Eglinton, G. (1991). The biogeochemistry of Ellesmere Lake, U.K.–I: source correlation of leaf wax inputs to the sedimentary lipid record. *Organic Geochemistry*, 17, 901–912.

Rizzo, W. B. (2014). Fatty aldehyde and fatty alcohol metabolism: Review and importance for epidermal structure and function. *Biochimica et Biophysica Acta (BBA) - Molecular and Cell Biology of Lipids*, 1841, 377–389.

Robinson, N., Cranwell, P. A., Finlay, B. J., and Eglinton, G. (1984). Lipids of aquatic organisms as potential contributors to lacustrine sediments. *Organic Geochemistry*, 6, 143–152.

Robinson, N. and Eglinton, G. (1990). Lipid chemistry of Icelandic hot spring microbial mats. *Organic Geochemistry*, 15, 291–298.

Rushdi, A. I. and Simoneit, B. R. T. (2001). Lipid formation by aqueous Fischer–Tropsch-type synthesis over a temperature range of 100 to 400 °C. *Origins of Life and Evolution of Biospheres*, 31, 103–118.

Rushdi, A. I. and Simoneit, B. R. T. (2006). Abiotic Condensation Synthesis of Glyceride Lipids and Wax Esters Under Simulated Hydrothermal Conditions. *Origins of Life and Evolution of Biospheres*, 36, 93–108.

Sameza, M. L., Bedine Boat, M. A., Nguemezi, S. T., Nguemnang Mabou, L. C., Jazet Dongmo, P. M., Fekam Boyom, F., and Menut, C. (2014). Potential use of *Eucalyptus globulus* essential oil against *Phytophthora colocasiae* the causal agent of taro leaf blight. *European Journal of Plant Pathology*, 140, 243–250.

Sangély, L., Chaussidon, M., Michels, R., Brouand, M., Cuney, M., Huault, V., and Landais, P. (2007). Micrometer scale carbon isotopic study of bitumen associated with Athabasca uranium deposits: Constraints on the genetic relationship with petroleum source-rocks and the abiogenic origin hypothesis. *Earth and Planetary Science Letters*, 258, 378–396.

Schulz, H. (1999). Short history and present trends of Fischer–Tropsch synthesis. *Applied Catalysis A: General*, 186, 3–12.

Sever, J. and Parker, P. L. (1969). Fatty alcohols (normal and isoprenoid) in sediments. *Science*, 164, 1052–1054.

Sharma, A., Cody, G. D., and Hemley, R. J. (2009). In Situ Diamond-Anvil Cell Observations of Methanogenesis at High Pressures and Temperatures. *Energy & fuels*, 23, 5571–5579.

Sherwood Lollar, B., Westgate, T. D., Ward, J. A., Slater, G. F., and Lacrampe-Couloume, G. (2002). Abiogenic formation of alkanes in the Earth's crust as a minor source for global hydrocarbon reservoirs. *Nature*, 416, 522–524.

Shiea, J., Brassell, S. C., and Ward, D. M. (1990). Mid-chain branched mono- and dimethyl alkanes in hot spring cyanobacterial mats: A direct biogenic source for branched alkanes in ancient sediments? *Organic Geochemistry*, 15, 223–231.

Shobier, A. H., Abdel Ghani, S. A., and Barakat, K. M. (2016). GC/MS spectroscopic approach and antifungal potential of bioactive extracts produced by marine macroalgae. *The Egyptian Journal of Aquatic Research*, 42, 289–299.

Simoneit, B. R. T. (1998). Biomarker PAHs in the Environment. In A. H. Neilson (Ed.), *PAHs and Related Compounds*. Springer, Berlin, Heidelberg, pp. 175–221.

Simoneit, B. R. T. (2002). Molecular indicators (biomarkers) of past life. *The Anatomical Record*, 268, 186–195.

Simoneit, B. R. T. (2004). Prebiotic organic synthesis under hydrothermal conditions: an overview. *Advances in Space Research*, 33, 88–94.

Simoneit, B. R. T., Kawka, O. E., and Brault, M. (1988). Origin of gases and condensates in the Guaymas Basin hydrothermal system (Gulf of California). *Chemical Geology*, 71, 169–182.

Simoneit, B. R. T., Rushdi, A. I., and Deamer, D. W. (2007). Abiotic formation of acylglycerols under simulated hydrothermal conditions and self-assembly properties of such lipid products. *Advances in Space Research*, 40, 1649–1656.

Smirnov, A., Hausner, D., Laffers, R., Strongin, D. R., and Schoonen, M. A. A. (2008). Abiotic ammonium formation in the presence of Ni-Fe metals and alloys and its implications for the Hadean nitrogen cycle. *Geochemical Transactions*, 9, 5.

Socrates, G. (2004). *Infrared and Raman characteristic group frequencies: tables and charts*. 3. edition, John Wiley & Sons, Chichester.

Studier, M. H., Hayatsu, R., and Anders, E. (1968). Origin of organic matter in early solar system—I. Hydrocarbons. *Geochimica et Cosmochimica Acta*, 32, 151–173.

Studier, M. H., Hayatsu, R., and Anders, E. (1972). Origin of organic matter in early solar system—V. Further studies of meteoritic hydrocarbons and a discussion of their origin. *Geochimica et Cosmochimica Acta*, 36, 189–215.

Summons, R. E. (1987). Branched alkanes from ancient and modern sediments: Isomer discrimination by GC/MS with multiple reaction monitoring. *Organic Geochemistry*, 11, 281–289.

Summons, R. E. (2014). The exceptional preservation of interesting and informative biomolecules. In M. Laflamme, J. D. Schiffbauer, and S. A. F. Darroch (Eds.), *Reading and Writing of the Fossil Record: Preservational Pathways to Exceptional Fossilization. The Paleontological Society Papers Vol. 20*. The Paleontological Society, pp. 217–236.

Summons, R. E., Albrecht, P., McDonald, G., and Moldowan, J. M. (2008). Molecular Biosignatures. *Space Science Reviews*, 135, 133–159.

Taran, Y. A., Kliger, G. A., and Sevastianov, V. S. (2007). Carbon isotope effects in the open-system Fischer–Tropsch synthesis. *Geochimica et Cosmochimica Acta*, 71, 4474–4487.

Thiel, V., Jenisch, A., Wörheide, G., Löwenberg, A., Reitner, J., and Michaelis, W. (1999). Mid-chain branched alkanoic acids from "living fossil" demosponges: a link to ancient sedimentary lipids? *Organic Geochemistry*, 30, 1–14.

Tian, F., Toon, O. B., Pavlov, A. A., and De Sterck, H. (2005). A Hydrogen-Rich Early Earth Atmosphere. *Science*, 308, 1014–1017.

Treignier, C., Derenne, S., and Saliot, A. (2006). Terrestrial and marine *n*-alcohol inputs and degradation processes relating to a sudden turbidity current in the Zaire canyon. *Organic Geochemistry*, 37, 1170–1184.

Vago, J. L., Westall, F., Pasteur Instrument Teams, L. S. S. W. G., Other, C., Coates, A. J., Jaumann, R., Korablev, O., Ciarletti, V., Mitrofanov, I., Josset, J.-L., De Sanctis, M. C., Bibring, J.-P., Rull, F., Goesmann, F., Steininger, H., Goetz, W., Brinckerhoff, W., Szopa, C., Raulin, F., Edwards, H. G. M., Whyte, L. G., Fairén, A. G., Bridges, J., Hauber, E., Ori, G. G., Werner, S., Loizeau, D., Kuzmin, R. O., Williams, R. M. E., Flahaut, J., Forget, F., Rodionov, D., Svedhem, H., Sefton-Nash, E., Kminek, G., Lorenzoni, L., Joudrier, L., Mikhailov, V., Zashchirinskiy, A., Alexashkin, S., Calantropio, F., Merlo, A., Poulakis, P., Witasse, O., Bayle, O., Bayón, S., Meierhenrich, U., Carter, J., García-Ruiz, J. M., Baglioni, P., Haldemann, A., Ball, A. J., Debus, A., Lindner, R., Haessig, F., Monteiro, D., Trautner, R., Voland, C., Rebeyre, P., Goulty, D., Didot, F., Durrant, S., Zekri, E., Koschny, D., Toni, A., Visentin, G., Zwick, M., van Winnendael, M., Azkarate, M., Carreau, C., and the ExoMars Project Team (2017). Habitability on Early Mars and the Search for Biosignatures with the ExoMars Rover. *Astrobiology*, 17, 471–510.

Van Kranendonk, M. J. (2010). Two types of Archean continental crust: Plume and plate tectonics on early Earth. *American Journal of Science*, 310, 1187–1209.

Van Kranendonk, M. J., Altermann, W., Beard, B. L., Hoffman, P. F., Johnson, C. M., Kasting, J. F., Melezhik, V. A., Nutman, A. P., Papineau, D., and Pirajno, F. (2012). A chronostratigraphic division of the Precambrian: possibilities and challenges. In F. M.

Gradstein, J. G. Ogg, M. D. Schmitz, and G. M. Ogg (Eds.), *The Geologic Time Scale*. Elsevier, Boston, pp. 299–392.

van Zuilen, M. A., Lepland, A., and Arrhenius, G. (2002). Reassessing the evidence for the earliest traces of life. *Nature*, 418, 627–630.

van Zuilen, M. A., Lepland, A., Teranes, J., Finarelli, J., Wahlen, M., and Arrhenius, G. (2003). Graphite and carbonates in the 3.8 Ga old Isua Supracrustal Belt, southern West Greenland. *Precambrian Research*, 126, 331–348.

Volkman, J. K., Barrett, S. M., and Blackburn, S. I. (1999). Eustigmatophyte microalgae are potential sources of C_{29} sterols, $C_{22}-C_{28}$ *n*-alcohols and $C_{28}-C_{32}$ *n*-alkyl diols in freshwater environments. *Organic Geochemistry*, 30, 307–318.

Wakai, C., Yoshida, K., Tsujino, Y., Matubayasi, N., and Nakahara, M. (2004). Effect of Concentration, Acid, Temperature, and Metal on Competitive Reaction Pathways for Decarbonylation and Decarboxylation of Formic Acid in Hot Water. *Chemistry Letters*, 33, 572–573.

Westall, F., Foucher, F., Bost, N., Bertrand, M., Loizeau, D., Vago, J. L., Kminek, G., Gaboyer, F., Campbell, K. A., Bréhéret, J.-G., Gautret, P., and Cockell, C. S. (2015). Biosignatures on Mars: What, Where, and How? Implications for the Search for Martian Life. *Astrobiology*, 15, 998–1029.

Wordsworth, R. and Pierrehumbert, R. (2013). Hydrogen-Nitrogen Greenhouse Warming in Earth's Early Atmosphere. *Science*, 339, 64–67.

Yasaka, Y., Yoshida, K., Wakai, C., Matubayasi, N., and Nakahara, M. (2006). Kinetic and Equilibrium Study on Formic Acid Decomposition in Relation to the Water-Gas-Shift Reaction. *The Journal of Physical Chemistry A*, 110, 11082–11090.

Yoshida, K., Wakai, C., Matubayasi, N., and Nakahara, M. (2004). NMR Spectroscopic Evidence for an Intermediate of Formic Acid in the Water–Gas–Shift Reaction. *The Journal of Physical Chemistry A*, 108, 7479–7482.

Yu, J. and Savage, P. E. (1998). Decomposition of formic acid under hydrothermal conditions. *Industrial & Engineering Chemistry Research*, 37, 2–10.

Zeng, Y. and Liu, J. (2000). Short-chain carboxylates in fluid inclusions in minerals. *Applied Geochemistry*, 15, 13–25.

Ideas and perspectives: Hydrothermally driven redistribution and sequestration of early Archaean biomass—the "hydrothermal pump hypothesis"

Jan-Peter Duda, Volker Thiel, Thorsten Bauersachs, Helge Mißbach, Manuel Reinhardt, Nadine Schäfer, Martin J. Van Kranendonk, Joachim Reitner

Abstract

Archaean hydrothermal chert veins commonly contain abundant organic carbon of uncertain origin (abiotic vs. biotic). In this study, we analysed kerogen contained in a hydrothermal chert vein from the ca. 3.5 Ga Dresser Formation (Pilbara Craton, Western Australia). Catalytic hydropyrolysis (HyPy) of this kerogen yielded n-alkanes up to n-C_{22}, with a sharp decrease in abundance beyond n-C_{18}. This distribution ($\leq n$-C_{18}) is very similar to that observed in HyPy products of recent bacterial biomass, which was used as reference material, whereas it differs markedly from the unimodal distribution of abiotic compounds experimentally formed via Fischer–Tropsch-type synthesis. We therefore propose that the organic matter in the Archaean chert veins has a primarily microbial origin. The microbially derived organic matter may have accumulated in anoxic aquatic (surface and/or subsurface) environments, and was then assimilated, redistributed and sequestered by the hydrothermal fluids ("hydrothermal pump hypothesis").

4.1 Introduction

Extensive hydrothermal chert vein systems containing abundant organic carbon are a unique phenomenon of early Archaean successions worldwide (Lindsay et al., 2005; Van Kranendonk, 2006; Hofmann, 2011). A dense stockwork of several hundred kerogen-rich hydrothermal chert veins that penetrate footwall pillowed komatiitic basalts of the ca. 3.5 Ga Dresser Formation (Pilbara Craton, Western Australia; Fig. 4.1) are up to 2 km deep by 25 m wide (Hickman, 1973, 1983; Nijman et al., 1999; Van Kranendonk and Pirajno, 2004; Lindsay et al., 2005; Van Kranendonk, 2006; Van Kranendonk et al., 2008) (Fig. B.1). Depleted stable carbon isotope signatures (δ^{13}C) of bulk kerogens (-38.1 ‰ to -24.3 ‰) and of organic microstructures (-33.6 ‰ to -25.7 ‰) in these hydrothermal chert veins, as well as remnants of what appear to be microbial remains, are consistent with a biological origin of the organic matter (Ueno et al., 2001, 2004; Glikson et al., 2008; Pinti et al., 2009; Morag et al., 2016). Problematically, however, similarly depleted δ^{13}C values (partly down to ca. -36 ‰ relative to the initial substrate) can also be formed through abiotic processes, for instance via Fischer–Tropsch-type synthesis (McCollom

et al., 1999; McCollom and Seewald, 2006), and putative microbial remains are not always reliable (Schopf, 1993; Brasier et al., 2002, 2005; Schopf et al., 2002; Bower et al., 2016).

Organic biomarkers can help to trace life and biological processes through deep time and add important information on the origin of the organic matter, even in very old sedimentary rocks (Brocks and Summons, 2003; Summons and Hallmann, 2014). In Archaean rocks, however, molecular fingerprints in the conventionally analysed bitumen (i.e., the extractable portion of organic matter) are commonly blurred by thermal maturation and/or ancient or modern contamination (Brocks et al., 2008; Gérard et al., 2009; Brocks, 2011; French et al., 2015). In contrast, the non-extractable portion of organic matter, known as kerogen, tends to be less affected by thermal maturation and contamination and is considered to be syngenetic with the host rock (Love et al., 1995; Brocks et al., 2003b; Marshall et al., 2007; Lockhart et al., 2008). Catalytic hydropyrolysis (HyPy) is a powerful tool for sensitively releasing kerogen-bound hydrocarbon moieties with little structural alteration (Love et al., 1995). HyPy has been successfully applied to Archaean kerogens in rocks from the Pilbara Craton, liberating syngenetic organic compounds consistent with a biogenic origin (Brocks et al., 2003b; Marshall et al., 2007). However, this technique has not yet been used on kerogens contained in hydrothermal chert veins of this age.

Here, we present the results of analyses of kerogen embedded in a freshly exposed hydrothermal chert vein of the ca. 3.5 Ga Dresser Formation. Our analyses include field and petrographic observations, Raman spectroscopy and organic geochemistry ($\delta^{13}C_{TOC}$; kerogen-bound molecules via HyPy followed by gas chromatography–mass spectrometry (GC–MS) and gas chromatography–combustion–isotope ratio mass spectrometry (GC–C–IRMS)). To further constrain potential sources of the Dresser kerogen, we additionally (i) applied HyPy on excessively pre-extracted cyanobacterial biomass and (ii) produced abiotic organic matter via Fischer–Tropsch-type synthesis using a hydrothermal reactor. Results of these investigations suggest that the Dresser kerogen has a primarily microbial origin. We hypothesize that biomass-derived organic compounds accumulated in anoxic aquatic environments and were then redistributed and sequestered by subsurface hydrothermal fluids ("hydrothermal pump hypothesis").

4.2   Material & methods

4.2.1   Sample preparation

A fresh decimetre-sized sample of a Dresser chert vein was obtained from a recent cut wall of the abandoned Dresser Mine in the Pilbara Craton, Western Australia (GPS: 21°09'04.13" S; 119°26'15.21" E; Figs. 4.1, B.1d; for geological maps, see Hickman, 1983; Van Kranendonk, 1999; Hickman and Van Kranendonk, 2012). The external surfaces (ca. $1-2$ cm) of the sample block were removed using an acetone-cleaned rock saw and then used for the preparation of thin sections. The surfaces of the resulting inner block were extensively rinsed with acetone and then removed (ca. $1-2$ cm) with an acetone-cleaned high precision saw (Buehler; Isomet 1000, Germany). The surfaces of the resulting sample were again rinsed with acetone, and then crushed and powdered using a carefully acetone-cleaned pebble mill (Retsch MM 301, Germany).
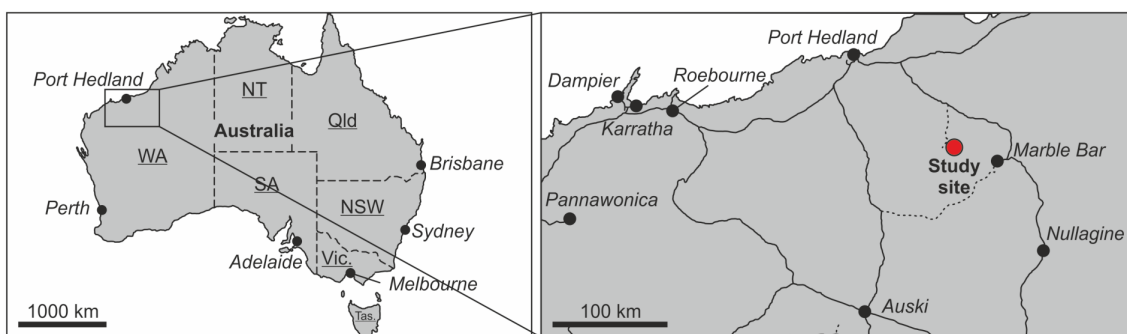
Figure 4.1: Location of the study site in Western Australia. The hydrothermal chert vein analysed occurs in a recent cut wall of the abandoned Dresser Mine close to Marble Bar.

4.2.2   Petrography and Raman spectroscopy

Petrographic analysis was conducted using a Zeiss SteREO Discovery.V8 stereomicroscope (transmitted and reflected light) linked to an AxioCam MRc5 5-megapixel camera.

Raman spectra were recorded using a Horiba Jobin Yvon LabRam-HR 800 UV spectrometer (focal length of 800 mm) attached to an Olympus BX41 microscope. For excitation an Argon ion laser (Melles Griot IMA 106020B0S) with a laser strength of 20 mW was used. The laser beam was focused onto the sample using an Olympus MPlane 100 x objective with a numerical aperture of 0.9 and dispersed by a 600 l/mm grating on a charge-coupled device (CCD) detector with 1024×256 pixels. This yielded a spectral resolution of < 2 cm^{-1} per pixel. Data were acquired over 10 to 30 s for a spectral range of $100 - 4000$ cm^{-1}. The spectrometer was calibrated by using a silicon standard with a major peak at 520.4 cm^{-1}. All spectra were recorded and processed using the LabSpec^{TM} database (version 5.19.17; Jobin-Yvon, Villeneuve d'Ascq, France).

4.2.3   Raman-derived H/C data

H/C values were calculated based on integrated peak intensities of Raman spectra using the formula H/C $= 0.871 \times I_{D5}/(I_{G+D2}) - 0.0508$ (Ferralis et al., 2016). The peaks were fitted in the LabSpec™ software (see 4.2.2) using the Gauss/Lorentz function.

4.2.4   Molecular analysis of the Dresser kerogen

All materials used for preparation were heated to 500 °C for 3h and/or extensively rinsed with acetone prior to sample contact. A laboratory blank was prepared and analysed in parallel to monitor laboratory contaminations.

We applied catalytic hydropyrolysis (HyPy) to release molecules from the Dresser kerogen and pre-extracted biomass of the heterocystous cyanobacterium *Anabaena cylindrica* SAG 1403-2 following previously published protocols (Snape et al., 1989; Love et al., 1995, 2005). HyPy allows the breaking of covalent bonds by progressive heating under high hydrogen pressure (150 bar). The released products are immediately removed from the hot zone by a constant hydrogen flow, and trapped downstream on clean, combusted silica powder cooled with dry ice (Meredith et al., 2004). All hydropyrolysates were eluted from the silica trap with high-purity dichloromethane (DCM), desulfurized

overnight using activated copper and subjected to GC–MS. Before all experiments, the empty HyPy system was heated (ambient temperature to 520 °C, held for 30 min) to remove any residual molecules.

Isolation of the Dresser kerogen followed standard procedures (cf. Brocks et al., 2003b). 57 g of powdered sample was first demineralized with hydrochloric acid (24h) and then hydrofluoric acid (11 days). The purified organic matter was then exhaustively extracted using three excess volumes of DCM and *n*-hexane, respectively (x 3), ultrasonic swelling in pyridine (2 × 20 min at 80 °C), and ultrasonic extraction with methanol, DCM (x 3) and DCM/methanol (1/1; V/V). The kerogen was subsequently extracted with *n*-hexane until no more compounds were detected via GC–MS. The pure kerogen was used for HyPy following an experimental protocol optimized for the analysis of Archaean kerogens (Brocks et al., 2003b; Marshall et al., 2007).

In order to monitor potential contamination, we applied HyPy to blanks before and after the kerogen run. The Dresser kerogen (131.06 mg) and blanks were sequentially heated in the presence of a sulfided molybdenum catalyst (10 wt%) and under a constant hydrogen flow (5 dm^3/min) using a two-step approach (cf. Brocks et al., 2003b; Marshall et al., 2007; Fig. B.2). The low-temperature step included heating from ambient temperature to 250 °C (300 °C/min) and then to 330 °C (8 °C/min) to release any molecules that were strongly adsorbed to the kerogen and not accessible to solvent extraction. The silica powder was subsequently recovered from the product trap, and the trap was refilled with clean, combusted silica powder for the following high-temperature step. This step included heating from ambient temperature to 520 °C (8 °C/min) to release molecules covalently bound to the kerogen.

4.2.5 Molecular analysis of pre-extracted cyanobacterial biomass (*Anabaena cylindrica*)

We used cell material of the heterocystous cyanobacterium *Anabaena cylindrica* strain SAG 1403-2 as it fulfills all criteria for reference material (availability, well characterized, etc.). The material was obtained from the Culture Collection of Algae at the Georg-August-Universität Göttingen (Germany) and grown at the Christian-Albrechts-Universität Kiel (Germany). The axenic batch culture was maintained in 250 ml of BG110 medium free of combined nitrogen sources (Rippka et al., 1979) at 29 °C. A light/dark regime of 14 h/10 h with a photon flux density of 135 μmol photons/(m^{2}s^1) was provided by a white fluorescent light bulb. At the end of the logarithmic growth phase, cells were harvested by centrifugation, and they were lyophilized thereafter. Subsequently, an aliquot of the freeze-dried biomass was exhaustively extracted following the methodology described by Bauersachs et al. (2014).

HyPy was performed following an experimental protocol optimized for biomass applications (Love et al., 2005). Briefly, the material was heated in the presence of a sulfided molybdenum catalyst (1.5 times the weight of the bacterial extraction residue) and under a constant hydrogen flow (6 dm^3/min). The HyPy program included heating from ambient temperature to 260 °C (300 °C/min) and then to 500 °C (8 °C/min).

4.2.6   Fischer–Tropsch-type synthesis of organic matter under hydrothermal conditions

Fischer–Tropsch-type reactions were carried out based on McCollom et al. (1999). A mixture of 2.5 g oxalic acid (dihydrate, suprapur®, Merck KGaA), 1 g montmorillonite (K10, Sigma Aldrich; pre-extracted with DCM; x 4) and ca. 11 ml ultrapure water was heated to 175 °C for 66 to 74 h in a sealed Morey-type stainless steel autoclave. The autoclave was rapidly ($\leq$ 15 min) cooled to room temperature with compressed air.

Fluid and solid phases were collected and extracted with DCM (x4). The montmorillonite was removed by centrifugation and filtration with silica powder and sea sand (combusted, respectively). The obtained extracts were then concentrated by rotary evaporation (40 °C, 670 mbar) and subjected to GC–MS analysis. Analytical blank experiments were carried out with all reactants to keep track of contamination.

4.2.7   Gas chromatography–mass spectrometry (GC–MS)

GC–MS analysis of HyPy products was carried out with a Thermo Scientific Trace 1310 GC coupled to a Thermo Scientific Quantum XLS Ultra MS. The GC instrument was equipped with a capillary column (Phenomenex Zebron ZB-5, 30 m, 0.25 μm film thickness, 0.25 mm inner diameter). Fractions were injected into a splitless injector and transferred to the GC column at 270 °C. He was used as carrier gas with a constant flow rate of 1.5 ml/min. The GC oven temperature was held isothermal at 80 °C for 1 min and then ramped to 310 °C at 5 °C/min, at which it was kept for 20 min. Electron ionization mass spectra were recorded in full scan mode at an electron energy of 70 eV with a mass range of m/z 50 – 600 and scan time of 0.42 s.

4.2.8   Polyaromatic hydrocarbon (PAH) ratios

Polyaromatic hydrocarbons (PAHs) are organic compounds consisting of multiple fused benzene rings. Methylation and isomerization characteristics of various GC-amenable PAH are altered during maturation and thus provide a measure for assessing the thermal maturity of organic matter (Killops and Killops, 2005; Peters et al., 2005). The following PAH maturity parameters were used in this study:

(i) methylnaphthalene ratio (MNR) = 2-MN/1-MN (Radke et al., 1984)

(ii) methylphenanthrene index (MPI-I) = 1.5 × (2-MP + 3-MP)/(P + 1-MP + 9-MP) (Radke and Welte, 1983)

(iii) computed vitrinite reflectance [R_c (MPI-I)] = 0.7 × MPI-1 + 0.22 (according to P/MP > 1; Boreham et al., 1988).

MN stands for methylnaphthalene, P for phenanthrene and MP for methylphenanthrene.

4.2.9   Total organic carbon (TOC) and δ^{13}C analyses (TOC and compound specific)

TOC, δ^{13}C$_{\text{TOC}}$ and compound-specific δ^{13}C analyses were conducted at the Centre for Stable Isotope Research and Analysis (KOSI) at the Georg-August-Universität Göttingen, Germany. Stable carbon isotope data are expressed as delta values relative to the Vienna Pee Dee Belemnite (VPDB) reference standard.

The TOC content and δ^{13}C$_{\text{TOC}}$ values were determined in duplicate using an elemental analyser (NA-2500 CE-Instruments) coupled to an isotope ratio mass spectrometer (Finnigan MAT Delta plus). Ca. 100 mg of powdered and homogenized whole rock material were analysed in each run. For internal calibration an acetanilide standard was used (δ^{13}C = -29.6 ‰; SD = 0.1 ‰). TOC content measurements showed a mean deviation of 0.1 wt%. The average δ^{13}C$_{\text{TOC}}$ value had a standard deviation of 0.3 ‰.

Compound-specific δ^{13}C analyses were conducted with a Trace GC coupled to a Delta Plus isotope-ratio-mass-spectrometer (IRMS) via a combustion interface (all Thermo Scientific). The combustion reactor contained CuO, Ni and Pt and was operated at 940 °C. The GC was equipped with two serially coupled capillary columns (Agilent DB-5 and DB-1; each 30 m, 0.25 μm film thickness, 0.25 mm inner diameter). Fractions were injected into a splitless injector and transferred to the GC column at 290 °C. The carrier gas was He at a flow rate of 1.2 ml/min. The GC oven temperature program was identical to the one used for GC–MS analysis (see above). CO_2 with a known δ^{13}C value was used for internal calibration. Instrument precision was checked using laboratory standards. Standard deviations of duplicate measurements were better than 1.7 ‰.

4.3   Results

The studied hydrothermal chert vein is hosted in komatiitic pillow basalt that has undergone severe hydrothermal acid–sulphate alteration, producing a kaolinite–illite–quartz mineral assemblage (Van Kranendonk and Pirajno, 2004; Van Kranendonk, 2006; Fig. B.1). The sampled vein crops out in a recent cut wall of the abandoned Dresser Mine (Fig. B.1) and consists of a dense chert (microquartz) matrix of deep black colour that contains kerogen and local concentrations of fresh (unweathered) pyrite crystals (Fig. 4.2a, b). There is no field and/or petrographic evidence for fluid-flow events that postdate the initial vein formation (brecciation textures, etc.).

Petrographic analysis and Raman spectroscopy revealed that kerogen (D bands at 1353 cm^{-1}, G bands at 1602 cm^{-1}) is embedded in the chert matrix (SiO_2 band at 464 cm^{-1}; see Fig. 4.2c, for a representative Raman spectrum). The organic matter occurs as small clots (< 50 μm) of variable shape. Raman spectra of the organic matter exhibit relatively wide D and G bands (82 and 55 cm^{-1} width, respectively; Fig. 4.2c). The total organic carbon (TOC) content is 0.2 wt%, and the δ^{13}C$_{\text{TOC}}$ value is -32.8 ± 0.3 ‰ (Table 4.1). Raman-derived H/C ratios range between 0.03 and 0.14.

HyPy was applied to the isolated Dresser kerogen, as well as to preceding and subsequent analytical blanks (combusted sea sand). Hydropyrolysates of the preceding blank contained a series of n-alkanes $\leq n$-C_{24}, with maximum abundances at n-C_{15} (Figs. 4.3, B.2–B.4). Sulfur (only after low-temperature HyPy), traces of siloxanes and a phenol
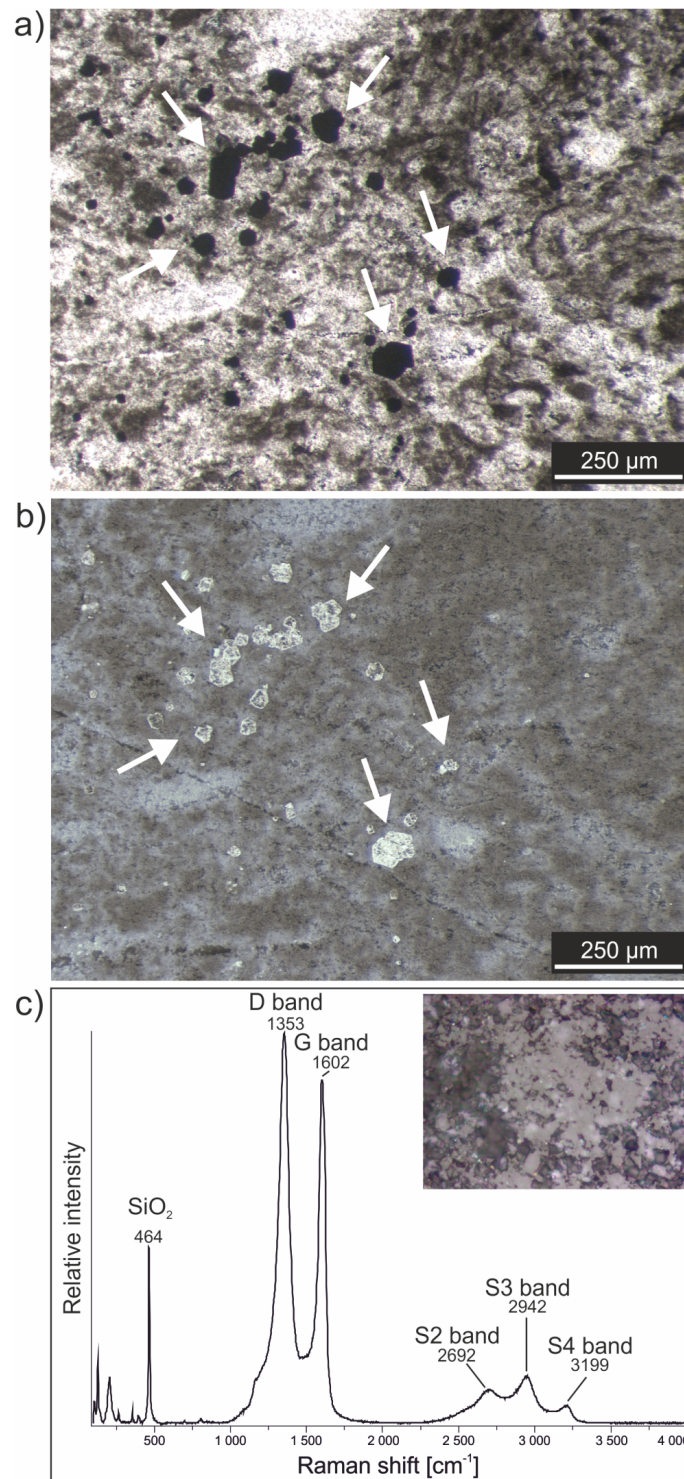
Figure 4.2: Petrographic observations on the hydrothermal chert vein. (**a, b**) Thin section photographs (**a**: transmitted light; **b**: reflected light) showing kerogen (brownish colours) and pyrite (arrows, black colours in **a**, bright colours in **b**) embedded within a fine-grained chert matrix. Note that the pyrite crystals (arrows) are excellently preserved and show no evidence of oxidation. (**c**) Representative Raman spectrum of kerogen (D band at 1353 cm^{-1} and G band at 1602 cm^{-1}) present in the hydrothermal chert vein. Note the wide D and G bands (82 and 55 cm^{-1} width, respectively), pointing to thermally mature and structurally disordered kerogen, and the absence of an S1 band (at 2450 cm^{-1}), consistent with prehnite–pumpellyite to lower greenschist metamorphosis and a temperature of ca. 300 °C (cf. Yui et al., 1996; Delarue et al., 2016).

Table 4.1: Stable carbon isotopic composition (δ^{13}C) of the total organic carbon (TOC) and n-alkanes released from high-temperature HyPy of the Dresser kerogen.

	n-C$_{12}$	n-C$_{13}$	n-C$_{14}$	n-C$_{15}$	n-C$_{16}$	n-C$_{17}$	n-C$_{18}$	n-C$_{12-18}$ (mean)	TOC
δ^{13}C	-30.3	-33.3	-32.7	-31.1	-29.4	-31.2	-31.7	-31.4	-32.8
SD	0.5	1.4	0.2	1.7	0.3	0.8	0.1	1.2	0.3

(Figs. 4.3, B.2, B.4) were also present. The blank runs also contained traces of aromatic hydrocarbons (Fig. B.5).

Low-temperature HyPy of the Dresser kerogen produced traces of C$_{14-18}$ n-alkanes, with a maximum at n-C$_{15}$ (Fig. B.3). However, these compounds were significantly less abundant than those released during high-temperature HyPy (see below). Other compounds observed in the low-temperature step pyrolysate were elemental sulfur, phenols, phthalic acid, siloxanes and traces of aromatic hydrocarbons (Figs. B.2, B.4 – B.5).

High-temperature HyPy of the Dresser kerogen yielded n-alkanes ranging from n-C$_{11}$ to n-C$_{22}$ with a notable decrease ("step") in the abundance of homologues above n-C$_{18}$ (Figs. 4.3b, B.2, B.3), which remained virtually unaffected by blank subtraction (Fig. 4.3c). Apart from that step, no carbon number preference is evident. The n-alkanes have δ^{13}C values ranging from -29.4 ‰ to -33.3 ‰ (mean -31.4 ± 1.2 ‰; Fig. 4.3b; Table 4.1). The hydropyrolysate also contained isomeric mixtures of C$_{12-18}$ monomethylalkanes (Fig. B.3) and a variety of aromatic hydrocarbons, including (dimethyl-, methyl-) naphthalene(s), (methyl-) biphenyl(s), (methyl-) acenaphthene(s), dibenzofuran and (methyl-) phenanthrene(s) (Figs. 4.3b, c, B.4 – B.6). Biologically diagnostic hydrocarbons such as hopanoids or steroids were absent.

HyPy treatment of excessively pre-extracted biomass of the heterocystous cyanobacterium *Anabaena cylindrica* SAG 1403-2 yielded a variety of organic compounds, but also included n-alkanes with a clear restriction in carbon number to homologues $\leq n$-C$_{18}$ (Fig. 4.3d). In contrast, our experimental synthesis of abiotic n-alkanes through Fischer–Tropsch-type reactions under hydrothermal conditions produced a unimodal distribution of homologues ranging from n-C$_{12}$ to n-C$_{41}$ without any carbon number preference (Fig. 4.3e).

4.4 Discussion

4.4.1 Maturity of the Dresser kerogen

The organic record of Archaean rocks is commonly affected by thermal maturation (Brocks et al., 2008; Brocks, 2011; French et al., 2015). The kerogen within the analysed Dresser sample is thermally mature and structurally disordered, as evidenced by relatively wide D and G bands in the Raman spectra (see Fig. 4.2c for a representative Raman spectrum). This is also supported by the absence of S1 bands at 2450 cm^{-1}, high R1 ratios (0.98 – 1.05) and low FWHM-D1 values (68.64 – 76.12), consistent with prehnite–pumpellyite to lower greenschist metamorphism at a temperature of ca. 300 °C (cf. Yui et al., 1996; Delarue et al., 2016). All of these observations are well in line with published Raman spectra of Archaean organic matter from the same region (Ueno et al.,
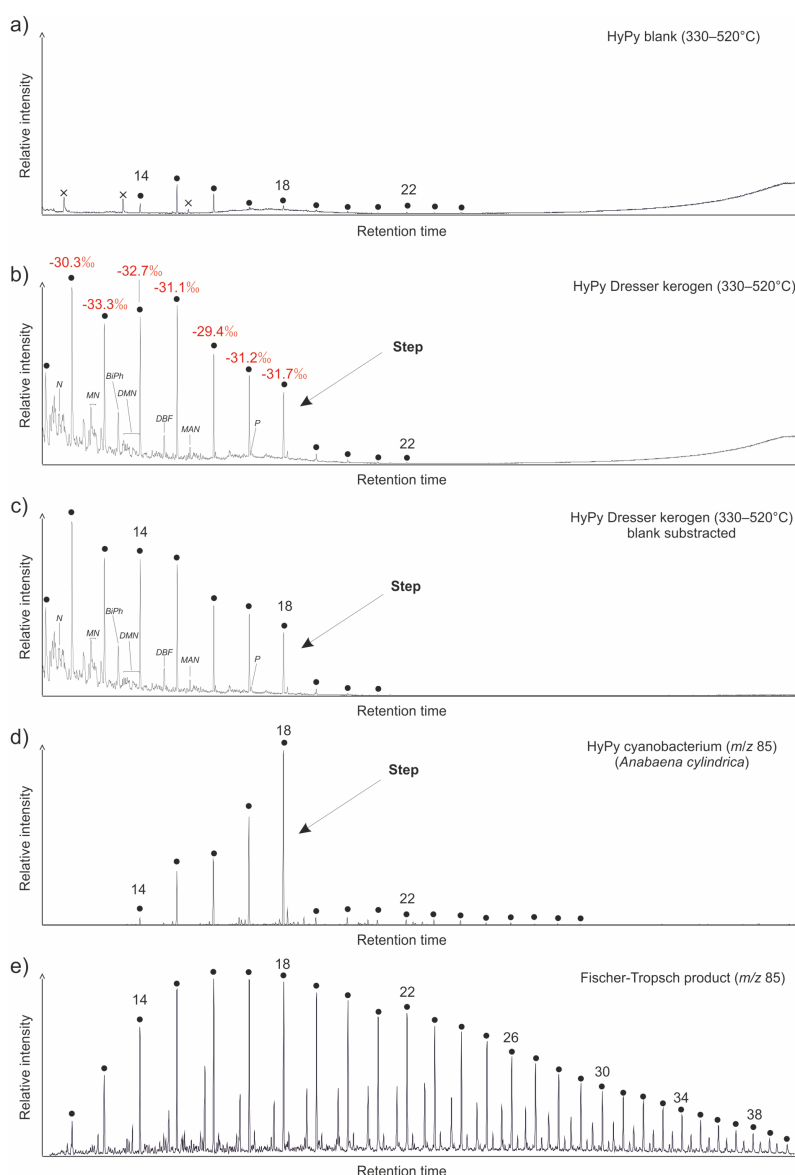
Figure 4.3: Total ion current ($\mathbf{a}$–$\mathbf{c}$; on the same scale) and ion chromatograms selective for alkanes ($\mathbf{d}$–$\mathbf{e}$; m/z 85). ($\mathbf{a}$) High-temperature HyPy (330–520 °C) product of analytical blank (combusted sea sand) obtained prior to HyPy of the Dresser kerogen. n-Alkanes in the range of n-C_{14} to n-C_{24} (maxima at n-C_{15}) represent HyPy background contamination. ($\mathbf{b}$) High-temperature HyPy (330–520 °C) product of the Dresser kerogen. Note the sharp decrease in abundance of n-alkanes beyond n-C_{18} (see arrows). $\delta^{13}C$ values of n-C_{12} to n-C_{28} show a high similarity to the $\delta^{13}C_{TOC}$ value (-32.8 ± 0.3 ‰), further confirming syngeneity. ($\mathbf{c}$) Blank subtraction ($\mathbf{b}$ minus $\mathbf{a}$) showing that contaminants have no major impact on the n-alkane pattern yielded during the high-temperature HyPy step of the Dresser kerogen ($\mathbf{b}$). ($\mathbf{d}$) HyPy products of cell material of the heterocystous cyanobacterium *Anabaena cylindrica*. Note the sharp decrease in abundance of n-alkanes beyond n-C_{18} (see arrows), similar to the n-alkane distribution of the Dresser kerogen ($\mathbf{b}$). ($\mathbf{e}$) Products of experimental Fischer–Tropsch-type synthesis under hydrothermal conditions; abiogenic n-alkanes show a unimodal distribution that is distinctly different from the Dresser kerogen. Black dots: n-alkanes (numbers refer to carbon chain lengths); N: naphthalene; MN: methylnaphthalenes; BiPh: 1,1'-biphenyl; DMN: dimethylnaphthalenes; DBF: dibenzofuran; MAN: methylacenaphthene; P: phenanthrene; crosses: siloxanes (GC column or septum bleeding).

89

2001; Marshall et al., 2007; Delarue et al., 2016) and the general thermal history of the host rock (regional prehnite–pumpellyite to lower greenschist metamorphism; Hickman, 1975, 1983, 2012; Terabayashi et al., 2003).

Fitting of D5 peaks can be difficult for Raman spectra of highly mature organic matter (Ferralis et al., 2016). Therefore, the H/C ratios calculated herein (0.03 – 0.14) should be treated with caution. However, the Raman-based H/C ratios and the methylphenanthrene/phenanthrene value (MP/P = 0.33; Table 4.2) of the Dresser kerogen are in good accordance with data reported from more mature kerogens from the same region (ca. 3.4 Ga Strelley Pool Formation: 0.08 – 0.14 and 0.37 – 0.24, respectively; Marshall et al., 2007). The low methylphenanthrene index (MPI-I = 0.23) and high phenanthrene/methylphenanthrene index (P/MP = 3.01) result in a computed vitrinite reflectance (R_c (MPI-I)) of 2.87 (Table 4.2), indicating a thermal maturity far beyond the oil-generative stage (Radke and Welte, 1983; Boreham et al., 1988). However, it has to be considered that the MPI-I is potentially affected by (de-)methylation reactions (Brocks et al., 2003a). The calculated methylnaphthalene ratio (MNR = 2.52; Table 4.2) corresponds to a somewhat lower mean vitrinite reflectance of ca. 1.5, which is again in line with a post-oil window maturity (cf. Radke et al., 1984). The mismatches between single aromatic maturity parameters are negligible, as these indices have limited application for highly mature Archaean organic matter (Brocks et al., 2003a). The putative offset between the indices and the metamorphic overprint indicated by Raman data is most likely due to the protection of kerogen-bound moieties even under elevated thermal stress (Love et al., 1995; Lockhart et al., 2008). Furthermore, it has been shown that kerogen isolated from the Strelley Pool Formation also contains larger PAH clusters which are not GC-amenable (> 10 – 15 rings; Marshall et al., 2007). Consequently, it can be anticipated that the compounds detected in the HyPy pyrolysate of the Dresser kerogen represent only a small fraction of the bulk macromolecular organic matter.

Table 4.2: Maturity indices (based on aromatic hydrocarbons) of the Dresser kerogen.

MP/P	MPI-I	P/MP	R_c (MPI-I)	MNR
0.33	0.23	3.01	2.87	2.52

MP/P: methylphenanthrene/phenanthrene ratio.
MPI-I: methylphenanthrene index ($1.5 \times (2\text{-MP} + 3\text{-MP})/(\text{P} + 1\text{-MP} + 9\text{-MP})$; Radke and Welte, 1983).
P/MP: phenanthrene/methylphenanthrene ratio.
R_c (MPI-I): computed vitrinite reflectance ($0.7 \times \text{MPI-}1 + 0.22$, according to P/MP > 1; Boreham et al., 1988).
MNR: methylnaphthalene ratio (2-MN/1-MN; Radke et al., 1984).

The distribution of monomethylalkanes $\leq n\text{-}C_{18}$ (Figs. B.3, B.4) released from the Dresser kerogen resembles high-temperature HyPy products from the Strelley Pool kerogen (Marshall et al., 2007; their Fig. 15). Such isomeric mixtures are typically formed during thermal cracking of alkyl moieties (Kissin, 1987) and are in good agreement with the estimated maturity range. Methylated aromatics such as methylnaphthalenes and methylphenanthrenes have also been observed in other hydropyrolysates from Archaean kerogens that experienced low-grade metamorphism (Brocks et al., 2003b; Marshall et al.,

2007; French et al., 2015). In all of these cases, the degree of alkylation varied with the exact thermal alteration of the respective kerogens (Marshall et al., 2007; French et al., 2015).

4.4.2   Syngeneity of the Dresser kerogen-derived compounds

The kerogen of the Dresser Formation exclusively occurs in the form of fluffy aggregates and clots embedded within a very dense chert matrix that is, once solidified, highly impermeable to fluids. The depositional age of the formation is constrained to 3481 ± 3.6 Ma (Van Kranendonk et al., 2008), and the investigated chert vein shows no evidence for disruption by post-depositional hydrothermal fluids. This has also been described for other hydrothermal chert veins of the Dresser Formation, where the kerogen has been interpreted as being syngenetic (i.e., formed prior to host rock lithification; Ueno et al., 2001, 2004; Morag et al., 2016). Furthermore, the maturity of the embedded kerogen is in good accordance with the thermal history of the host rock. An introduction of solid macromolecular organic matter from stratigraphically younger units in this region during later fluid-flow phases, as proposed for the younger Apex chert (Olcott Marshall et al., 2014), can therefore be excluded.

As the bitumen fractions of Precambrian rocks are easily biased by the incorporation of contaminants during later stages of rock history (Brocks et al., 2008; Brocks, 2011; French et al., 2015), studies have increasingly focussed on kerogen-bound compounds that are more likely to be syngenetic to the host rock (Love et al., 1995; Brocks et al., 2003b; Marshall et al., 2007; French et al., 2015). Potential volatile organic contaminants adhering to the kerogen are removed through excessive extraction and a thermal desorption step (350 °C) prior to high-temperature HyPy (550 °C; cf. Brocks et al., 2003b; Marshall et al., 2007). The recurrence of few n-alkanes in the range of n-C_{14} to n-C_{24} (maximum at n-C_{15}) in high-temperature HyPy blank runs obtained immediately before and after the actual sample run (Figs. 4.3a, B.2, B.3) indicates minor background contamination during pyrolysis, with a source most likely within the HyPy system. However, these contaminants do not significantly affect the n-alkane pattern yielded by high-temperature HyPy of the Dresser kerogen, as evidenced by blank subtraction (Fig. 4.3c).

Contamination of the sample can be further deciphered by the presence of polar additives or hydrocarbons that are not consistent with the thermal history of the host rock. Plastic-derived branched alkanes with quaternary carbon centres (BAQCs), a common contaminant in Precambrian rock samples (Brocks et al., 2008), have not been detected (Fig. B.7). Traces of functionalized plasticizers (phenols and phthalic acid; Figs. B.2, B.6, B.8) are unlikely to survive (or result from) HyPy treatment. These compounds are therefore considered as background contamination introduced during sample preparation and analysis after HyPy. The observed siloxanes (Fig. 4.3, B.2) probably originate from the GC column or septum bleeding and are unlikely to be contained in the sample. All of these compounds occur only in low or trace abundances and can be clearly distinguished from the ancient aliphatic and aromatic hydrocarbons contained in the Dresser kerogen.

Contamination by (sub-)recent endoliths can be excluded as sample surfaces have been carefully removed and there is no petrographic indication for borings or fissures containing recent organic material (Fig. 4.2). HyPy of untreated or extracted biomass would yield a variety of acyclic and cyclic biomarkers (cf. Love et al., 2005). However,

high-temperature HyPy of the Dresser kerogen almost exclusively yielded *n*-alkanes, minor amounts of monomethylalkanes, and various aromatic hydrocarbons (Figs. 4.3b, c, B.2–B.6), while hopanoids or steroids were absent (Figs. B.8, B.9). This is in good agreement with the maturity of the Dresser kerogen and previous HyPy studies of Archaean rocks (Brocks et al., 2003b; Marshall et al., 2007; French et al., 2015).

Accidental contamination of the kerogen by mono-, di- and triglycerides (e.g., dust, skin surface lipids) can also be ruled out as HyPy treatment of these compounds typically results in *n*-alkane distributions with a distinct predominance of *n*-C_{16} and *n*-C_{18} homologues, corresponding to the *n*-C_{16} and *n*-C_{18} fatty acid precursors (Craig et al., 2004; Love et al., 2005; unpublished data from our own observations). At the same time, the observed distribution of kerogen-derived *n*-alkanes, with a distinct decrease beyond *n*-C_{18} (Fig. 4.3b, c) is notably similar to high-temperature HyPy products of kerogens isolated from the ca. 3.4 Ga Strelley Pool Formation of the Pilbara Craton (Marshall et al., 2007; their Fig. 14). Marshall and co-workers considered these *n*-alkanes unlikely to be contaminants as they were released only in the high-temperature HyPy step. Furthermore, the stable carbon isotopic composition of *n*-alkanes in the Dresser high-temperature pyrolysate (−29.4 ‰ to −33.3 ‰; mean −31.4 ± 1.2 ‰) is very similar to the $\delta^{13}C_{TOC}$ signature of the sample (−32.8 ± 0.3 ‰; Figs. 4.3, B.10; Table 4.1), indicating that these compounds were generated from the kerogen. Hence, we consider the compounds released from the Dresser kerogen during high-temperature HyPy (Fig. 4.3b, c) as syngenetic.

High-temperature HyPy of the Dresser kerogen yielded a variety of aromatic hydrocarbons, which are orders of magnitudes lower or absent in all other pyrolysates (Figs. 4.3, B.2, B.4 – B.6). It also produced significantly higher amounts of *n*-alkanes than the low-temperature step, and these further showed a distinct distribution pattern (i.e., a step ≤ *n*-C_{18}; Figs. 4.3, B.2, B.3). The lack of even low quantities of *n*-alkenes that typically accompany bond cleavage in kerogen pyrolysis was also observed by Marshall et al. (2007) in their HyPy analysis of cherts from the Strelley Pool Formation. As a possible explanation for the lack of *n*-alkenes, these authors suggested that the *n*-alkanes were not cracked from the kerogen but were rather trapped in closed micropores until the organic host matrix was pyrolytically disrupted. Alternatively, however, unsaturated cleavage products may have been immediately reduced during HyPy by the steadily available hydrogen and catalysts. Indeed, it has been demonstrated that double bonds in linear alkyl chains are efficiently hydrogenated during HyPy, even in the case of pre-extracted microbial biomass (e.g., Love et al., 2005; our Fig. 4.3d). We consider both as plausible scenarios to explain the absence of *n*-alkenes in the Dresser chert hydropyrolysate.

4.4.3 Origin of the Dresser kerogen: Hydrothermal vs. biological origin

The $\delta^{13}C_{TOC}$ value of −32.8 ± 0.3 ‰ is consistent with carbon fixation by photo- or chemoautotrophs (cf. Schidlowski, 2001). However, organic compounds exhibiting similar ^{13}C depletions (partly down to ca. −36 ‰ relative to the initial substrate) could also be formed abiotically during the serpentinization of ultramafic rocks (Fischer–Tropsch-type synthesis; McCollom et al., 1999; McCollom and Seewald, 2006; Proskurowski et al., 2008). A further constraint on the origin of the Dresser kerogen is provided by the distinct decrease in *n*-alkane abundance beyond *n*-C_{18} observed in the high-temperature HyPy py-

rolysate (Fig. 4.3b, c). This distribution resembles HyPy products of pre-extracted recent cyanobacterial biomass, which also shows a very pronounced restriction in carbon number to homologues $\leq n\text{-}C_{18}$ (Fig. 4.3d).

The pre-extracted cyanobacterial cell material and the abiotically produced n-alkanes studied as reference samples experienced no thermal maturation. It can nevertheless be expected that burial, and thus heating, of *Anabaena* biomass (Fig. 4.3d) would initially liberate lower n-alkane homologues from their predominant n-alkyl moieties while, up to a certain point, retaining the distinct step at $n\text{-}C_{18}$. Experimental maturation of an immature kerogen revealed the preservation of distinct alkyl-chain length preferences even after 100 days at 300 °C (Mißbach et al., 2016; e.g., a step beyond $n\text{-}C_{31}$ in their Fig. 2). Further maturation would ultimately lead to a unimodal distribution of short-chain n-alkanes and erase the biologically inherited pattern (cf. Mißbach et al., 2016). In contrast, abiotically synthesized extractable organic compounds show a unimodal homologue distribution from the beginning (Fig. 4.3e) and will retain it, while thermal maturation would gradually shift the n-alkane pattern towards shorter homologues. It can therefore be expected that organic compounds cleaved from an abiotic "Fischer–Tropsch-kerogen" – whose existence has not been proven yet – would also exhibit a unimodal distribution. Consequently, the distinctive distribution of n-alkanes released from the Dresser kerogen (i.e., the step $\leq n\text{-}C_{18}$; Figs. 4.3b, c) can be regarded as a molecular fingerprint relating to a biosynthetic origin of the organic matter.

Highly ^{13}C-depleted methane in primary fluid inclusions in hydrothermal chert veins of the Dresser Formation ($\delta^{13}C < 56\ ‰$) was taken as evidence for biological methanogenesis and thus the presence of Archaea (Ueno et al., 2006). Our $\delta^{13}C_{TOC}$ value ($-32.8 \pm 0.3\ ‰$; Table 4.1; Fig. B.10) would generally be consistent with both bacterial and archaeal sources (cf. Schidlowski, 2001). Archaea only synthesize isoprene-based compounds (Koga and Morii, 2007; Matsumi et al., 2011). Straight-chain (acetyl-based) hydrocarbon moieties such as fatty acids – the potential precursors of the kerogen-derived n-alkanes – are to current knowledge being formed only by Bacteria and Eukarya, where they typically function as constituents of membranes or storage lipids (cf. Erwin, 1973; Kaneda, 1991). The formation of these lipids is tightly controlled by different biosynthetic pathways resulting in characteristic chain-length distributions. In bacterial lipids, carbon chain lengths typically do not extend above $n\text{-}C_{18}$ (cf. Kaneda, 1991). Consequently, given the lack of convincing evidence for the presence of Eukarya as early as 3.5 Ga (cf. Parfrey et al., 2011; Knoll, 2014; French et al., 2015), the most plausible source of kerogen-occluded n-alkanes in the Dresser hydrothermal chert is Bacteria. Strongly reducing conditions during the deposition of the Dresser Formation are indicated by widespread pyrite, Fe-rich carbonates, and trace element signatures (Van Kranendonk et al., 2003, 2008). Potential microbial sources for the Dresser kerogen therefore may have included anoxygenic photoautotrophic, chemoautotrophic, and heterotrophic microorganisms.

4.4.4   The "hydrothermal pump hypothesis"

Our results strongly support a biological origin of the kerogen found in the early Archaean hydrothermal chert veins of the Dresser Formation. We explain this finding by the redistribution and sequestration of microbial organic matter that may have formed in a variety of Dresser environments through hydrothermal circulation (proposed herein as the "hy-

drothermal pump hypothesis"; Fig. 4.4). Higher geothermal gradients prior to the onset of modern-type plate tectonics at ca 3.2 – 3.0 Ga (Smithies et al., 2005; Shirey and Richardson, 2011) were possibly important drivers of early Archaean hydrothermal systems. In fact, the Dresser Formation was formed in a volcanic caldera environment affected by strong hydrothermal circulation, where voluminous fluid circulation locally caused intense acid–sulphate alteration of basalts and the formation of a dense hydrothermal vein swarm (Nijman et al., 1999; Van Kranendonk and Pirajno, 2004; Van Kranendonk, 2006; Van Kranendonk et al., 2008; Harris et al., 2009). In addition to the high crustal heat flow, the absence of thick sedimentary cover may have facilitated the intrusion of seawater into the hydrothermal system. The associated large-scale assimilation of particulate and dissolved organic matter and its transport and alteration by hydrothermal fluids (Fig. 4.4) therefore appears to be a plausible mechanism that may, at least partly, explain the high amounts of kerogen in early Archaean hydrothermal veins.
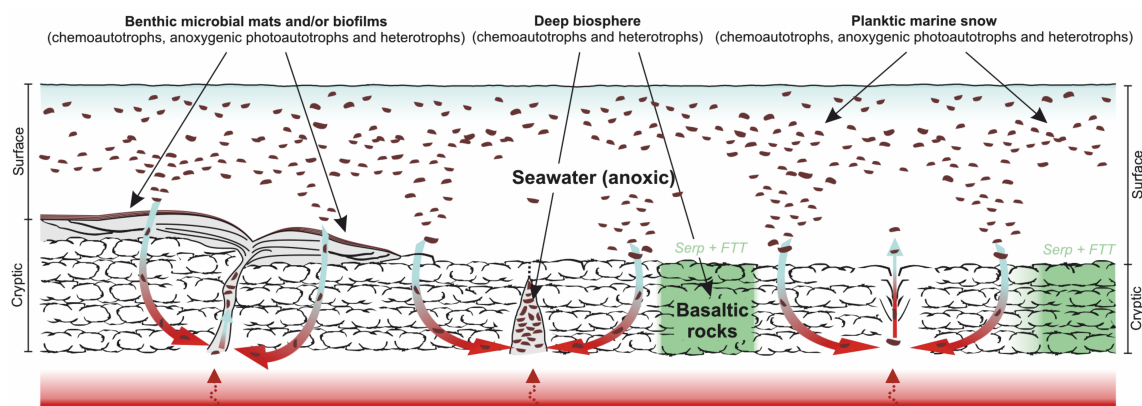

Figure 4.4: The "hydrothermal pump hypothesis". Organic matter was predominantly biologically produced and heterotrophically processed by Bacteria and, possibly, Archaea. Additionally, Fischer–Tropsch-type synthesis of organic matter linked to the serpentinization of ultramafic rocks (McCollom et al., 1999; McCollom and Seewald, 2006) may have occurred locally. Primary producers (chemoautotrophs, anoxygenic photoautotrophs) and heterotrophs may have flourished in surface waters (planktic "marine snow"), at the water-rock interface (microbial mats and/or biofilms), and in cryptic environments (e.g., within basalts and hydrothermal vent systems). After accumulating in different Dresser environments, the organic matter was redistributed and sequestered in veins by hydrothermal fluids.

The "hydrothermal pump hypothesis" requires a source of organic matter during the deposition of the Dresser Formation (Fig. 4.4). Whereas contributions from extraterrestrial sources, as well as from Fischer–Tropsch-type synthesis linked to the serpentinization of ultramafic rocks, cannot be excluded, our results indicate a primarily biological origin for the kerogen contained in the chert veins (Fig. 4.4). The inferred biogenicity is also in line with the consistent δ^{13}C offset between bulk kerogens (ca. -20 to -30 ‰) and carbonate (ca. ± 2 ‰) in Archaean rocks (Hayes, 1983; Schidlowski, 2001). Prokaryotic primary producers and heterotrophs may have flourished in microbial mats (Dresser stromatolites; Walter et al., 1980; Van Kranendonk, 2006, 2011; Philippot et al., 2007; Van Kranendonk et al., 2008), the water column (planktic "marine snow", Brasier et al., 2006; Blake et al., 2010) and even hot springs on land (Djokic et al., 2017). Another biological source for the ancient organic matter could have been chemoautotrophs and heterotrophs

thriving in subsurface environments, such as basalts (Banerjee et al., 2007; Furnes et al., 2008) and hydrothermal vent systems (Shen et al., 2001; Ueno et al., 2001, 2004, 2006; Pinti et al., 2009; Morag et al., 2016) (Fig. 4.4). All of these systems are not mutually exclusive and the largely anoxic conditions would have encouraged a high steady-state abundance of organic matter in the aquatic environment (Fig. 4.4).

Dissolved organic matter (DOM) in modern seawater may resist decomposition over millennial timescales (Druffel and Griffin, 2015). In recent hydrothermal fields, however, organic matter becomes thermally altered and redistributed (Simoneit, 1993; Delacour et al., 2008; Konn et al., 2009). Laboratory experiments using marine DOM indicate that thermal alteration already occurs at temperatures $> 68 - 100$ °C, and efficient removal of organic molecules at $212 - 401$ °C (Hawkes et al., 2015, 2016). It has been argued, however, that such DOM removal may also be due to transformation into immiscible material through, for example, condensation (Castello et al., 2014) and/or defunctionalization reactions (Hawkes et al., 2016). These processes, however, are as yet poorly understood. In the Dresser Formation, hydrothermal temperatures ranged from ca. 300 °C at depth to 120 °C near the palaeosurface, causing propylitic (ca. $250 - 350$ °C) and argillic (including advanced argillic: ca. $100 - 200$ °C) alteration of the host rocks (Van Kranendonk and Pirajno, 2004; Van Kranendonk et al., 2008; Harris et al., 2009). Given this variety of thermal regimes, and the generally anoxic nature of early Archaean seawater (e.g. Van Kranendonk et al., 2003, 2008; Li et al., 2013), it is likely that some of the organic substances underwent in situ alteration, but not complete oxidation, during hydrothermal circulation. The entrained organics would have been trapped in the chert that instantaneously precipitated from the ascending hydrothermal fluids due to subsurface cooling (cf. Van Kranendonk, 2006).

In summary, the "hydrothermal pump hypothesis" proposed here (Fig. 4.4) includes (i) a net build-up of organic matter in different Dresser environments under largely anoxic conditions, (ii) a large-scale assimilation of particulate and dissolved organic matter from various biological sources and its subsurface transport and alteration by hydrothermal fluids, and (iii) its sequestration within hydrothermal chert veins as kerogen. This model explains the presence of abundant organic carbon in early Archaean hydrothermal veins, as well as its morphological, structural and isotopic variability observed in the Dresser hydrothermal chert veins (Ueno et al., 2001, 2004; Pinti et al., 2009; Morag et al., 2016). It does not, however, help to pinpoint the formation pathways of distinct carbonaceous structures, as for instance those preserved in the Dresser Formation (Glikson et al., 2008) or the younger Apex chert (e.g. Schopf, 1993; Brasier et al., 2002, 2005; Schopf et al., 2002; Bower et al., 2016). Further work is necessary to test whether consistent molecular and compound-specific isotopic patterns can be generated from a larger set of Archaean kerogens.

4.5   Conclusions

Kerogen embedded in a hydrothermal chert vein from the ca. 3.5 Ga Dresser Formation (Pilbara Craton, Western Australia) is syngenetic. A biological origin is inferred from the presence of short-chain n-alkanes in high-temperature HyPy pyrolysates, showing a sharp decrease in homologue abundance beyond n-C_{18}. HyPy products of pre-extracted recent

bacterial biomass exhibited a similar restriction to carbon chain lengths $\leq n\text{-}C_{18}$, whereas abiotic compounds experimentally formed via Fischer–Tropsch-type synthesis exhibited a unimodal distribution. A biological interpretation for Dresser organics is further consistent with the $\delta^{13}C_{TOC}$ value ($-32.8 \pm 0.3\ ‰$) and the stable carbon isotopic composition of n-alkanes in the Dresser high-temperature pyrolysate ($-29.4\ ‰$ to $-33.3\ ‰$; mean $-31.4 \pm 1.2\ ‰$). Based on these observations, we propose that the original organic matter was primarily biologically synthesized. We hypothesize that microbially derived organic matter accumulating in anoxic aquatic (surface and/or subsurface) environments was assimilated, redistributed and sequestered by hydrothermal fluids ("hydrothermal pump hypothesis").

Author contributions

JPD, JR and MVK conducted the field work and designed the study. JR conducted petrographic analyses. NS performed Raman spectroscopic analyses. MR and JPD conducted pyrolysis experiments. HM conducted Fischer–Tropsch-type synthesis. TB prepared cyanobacterial cell material. JPD, HM, MR and VT performed biomarker analyses. JPD wrote the manuscript. All authors discussed the results and provided input to the manuscript.

Acknowledgments

References

Banerjee, N. R., Simonetti, A., Furnes, H., Muehlenbachs, K., Staudigel, H., Heaman, L., and Van Kranendonk, M. J. (2007). Direct dating of Archean microbial ichnofossils. *Geology*, 35, 487–490.

Bauersachs, T., Mudimu, O., Schulz, R., and Schwark, L. (2014). Distribution of long chain heterocyst glycolipids in N_2-fixing cyanobacteria of the order Stigonematales. *Phytochemistry*, 98, 145–150.

Blake, R. E., Chang, S. J., and Lepland, A. (2010). Phosphate oxygen isotopic evidence for a temperate and biologically active Archaean ocean. *Nature*, 464, 1029–1032.

Boreham, C. J., Crick, I. H., and Powell, T. G. (1988). Alternative calibration of the Methylphenanthrene Index against vitrinite reflectance: Application to maturity measurements on oils and sediments. *Organic Geochemistry*, 12, 289–294.

Bower, D. M., Steele, A., Fries, M. D., Green, O. R., and Lindsay, J. F. (2016). Raman Imaging Spectroscopy of a Putative Microfossil from the ~3.46 Ga Apex Chert: Insights from Quartz Grain Orientation. *Astrobiology*, 16, 169–180.

Brasier, M., McLoughlin, N., Green, O., and Wacey, D. (2006). A fresh look at the fossil evidence for early Archaean cellular life. *Philosophical Transactions of the Royal Society of London B: Biological Sciences*, 361, 887–902.

Brasier, M. D., Green, O. R., Jephcoat, A. P., Kleppe, A. K., Van Kranendonk, M. J., Lindsay, J. F., Steele, A., and Grassineau, N. V. (2002). Questioning the evidence for Earth's oldest fossils. *Nature*, 416, 76–81.

Brasier, M. D., Green, O. R., Lindsay, J. F., McLoughlin, N., Steele, A., and Stoakes, C. (2005). Critical testing of Earth's oldest putative fossil assemblage from the ~3.5 Ga Apex chert, Chinaman Creek, Western Australia. *Precambrian Research*, 140, 55–102.

Brocks, J. J. (2011). Millimeter-scale concentration gradients of hydrocarbons in Archean shales: Live-oil escape or fingerprint of contamination? *Geochimica et Cosmochimica Acta*, 75, 3196–3213.

Brocks, J. J., Buick, R., Logan, G. A., and Summons, R. E. (2003a). Composition and syngeneity of molecular fossils from the 2.78 to 2.45 billion-year-old Mount Bruce Supergroup, Pilbara Craton, Western Australia. *Geochimica et Cosmochimica Acta*, 67, 4289–4319.

Brocks, J. J., Grosjean, E., and Logan, G. A. (2008). Assessing biomarker syngeneity using branched alkanes with quaternary carbon (BAQCs) and other plastic contaminants. *Geochimica et Cosmochimica Acta*, 72, 871–888.

Brocks, J. J., Love, G. D., Snape, C. E., Logan, G. A., Summons, R. E., and Buick, R. (2003b). Release of bound aromatic hydrocarbons from late Archean and Mesoproterozoic kerogens via hydropyrolysis. *Geochimica et Cosmochimica Acta*, 67, 1521–1530.

References

Brocks, J. J. and Summons, R. E. (2003). Biomarkers for Early Life. In W. H. Schlesinger (Ed.), *Biogeochemistry*. Elsevier, Oxford, pp. 63–115.

Castello, D., Kruse, A., and Fiori, L. (2014). Supercritical water gasification of hydrochar. *Chemical Engineering Research and Design*, 92, 1864–1875.

Craig, O. E., Love, G. D., Isaksson, S., Taylor, G., and Snape, C. E. (2004). Stable carbon isotopic characterisation of free and bound lipid constituents of archaeological ceramic vessels released by solvent extraction, alkaline hydrolysis and catalytic hydropyrolysis. *Journal of Analytical and Applied Pyrolysis*, 71, 613–634.

Delacour, A., Früh-Green, G. L., Bernasconi, S. M., Schaeffer, P., and Kelley, D. S. (2008). Carbon geochemistry of serpentinites in the Lost City Hydrothermal System (30°N, MAR). *Geochimica et Cosmochimica Acta*, 72, 3681–3702.

Delarue, F., Rouzaud, J.-N., Derenne, S., Bourbin, M., Westall, F., Kremer, B., Sugitani, K., Deldicque, D., and Robert, F. (2016). The Raman-Derived Carbonization Continuum: A Tool to Select the Best Preserved Molecular Structures in Archean Kerogens. *Astrobiology*, 16, 407–417.

Djokic, T., Van Kranendonk, M. J., Campbell, K. A., Walter, M. R., and Ward, C. R. (2017). Earliest signs of life on land preserved in ca. 3.5 Ga hot spring deposits. *Nature Communications*, 8, 15263.

Druffel, E. R. M. and Griffin, S. (2015). Radiocarbon in dissolved organic carbon of the South Pacific Ocean. *Geophysical Research Letters*, 42, 4096–4101.

Erwin, J. (1973). *Lipids and Biomembranes of Eukaryotic Microorganisms*. Academic Press, New York.

Ferralis, N., Matys, E. D., Knoll, A. H., Hallmann, C., and Summons, R. E. (2016). Rapid, direct and non-destructive assessment of fossil organic matter via microRaman spectroscopy. *Carbon*, 108, 440–449.

French, K. L., Hallmann, C., Hope, J. M., Schoon, P. L., Zumberge, J. A., Hoshino, Y., Peters, C. A., George, S. C., Love, G. D., and Brocks, J. J. (2015). Reappraisal of hydrocarbon biomarkers in Archean rocks. *Proceedings of the National Academy of Sciences of the United States of America*, 112, 5915–5920.

Furnes, H., McLoughlin, N., Muehlenbachs, K., Banerjee, N., Staudigel, H., Dilek, Y., de Wit, M., Van Kranendonk, M., and Schiffman, P. (2008). Oceanic pillow lavas and hyaloclastites as habitats for microbial life through time–a review. In Y. Dilek, H. Furnes, and K. Muehlenbachs (Eds.), *Links Between Geological Processes, Microbial Activities & Evolution of Life*. Springer Netherlands, Amsterdam, pp. 1–68.

Gérard, E., Moreira, D., Philippot, P., Van Kranendonk, M. J., and López-García, P. (2009). Modern subsurface bacteria in pristine 2.7 Ga-old fossil stromatolite drillcore samples from the Fortescue Group, Western Australia. *PLoS One*, 4, e5298.

Glikson, M., Duck, L. J., Golding, S. D., Hofmann, A., Bolhar, R., Webb, R., Baiano, J. C. F., and Sly, L. I. (2008). Microbial remains in some earliest Earth rocks: Comparison with a potential modern analogue. *Precambrian Research*, 164, 187–200.

Harris, A. C., White, N. C., McPhie, J., Bull, S. W., Line, M. A., Skrzeczynski, R., Mernagh, T. P., and Tosdal, R. M. (2009). Early Archean Hot Springs above Epithermal Veins, North Pole, Western Australia: New Insights from Fluid Inclusion Microanalysis. *Economic Geology*, 104, 793–814.

Hawkes, J. A., Hansen, C. T., Goldhammer, T., Bach, W., and Dittmar, T. (2016). Molecular alteration of marine dissolved organic matter under experimental hydrothermal conditions. *Geochimica et Cosmochimica Acta*, 175, 68–85.

Hawkes, J. A., Rossel, P. E., Stubbins, A., Butterfield, D., Connelly, D. P., Achterberg, E. P., Koschinsky, A., Chavagnac, V., Hansen, C. T., Bach, W., and Dittmar, T. (2015). Efficient removal of recalcitrant deep–ocean dissolved organic matter during hydrothermal circulation. *Nature Geoscience*, 8, 856.

Hayes, J. M. (1983). Geochemical evidence bearing on the origin of aerobiosis, a speculative hypothesis. In J. W. Schopf (Ed.), *The Earth's Earliest Biosphere: Its Origin and Evolution*. Princeton University Press, New York, pp. 291–301.

Hickman, A. H. (1973). The North Pole barite deposits, Pilbara Goldfield. *Geol. Survey of Western Australia Annual Report*, 1972, 57–60.

Hickman, A. H. (1975). Precambrian structural geology of part of the Pilbara region. *Geol. Survey of Western Australia Annual Report*, 1974, 68–73.

Hickman, A. H. (1983). Geology of the Pilbara Block and its environs. *Western Australian Geological Survey Bulletin*, 127, 1–268.

Hickman, A. H. (2012). Review of the Pilbara Craton and Fortescue Basin, Western Australia: Crustal evolution providing environments for early life. *Island Arc*, 21, 1–31.

Hickman, A. H. and Van Kranendonk, M. J. (2012). *A Billion Years of Earth History: A Geological Transect Through the Pilbara Craton and the Mount Bruce Supergroup–a Field Guide to Accompany 34th IGC Excursion WA-2*. Geological Survey of Western Australia, Perth.

Hofmann, A. (2011). Archaean hydrothermal systems in the Barberton greenstone belt and their significance as a habitat for early life. In S. D. Golding and M. Glikson (Eds.), *Earliest Life on Earth: Habitats, Environments and Methods of Detection*. Springer, Dordrecht, pp. 51–78.

Kaneda, T. (1991). *Iso-* and *anteiso*-fatty acids in bacteria: biosynthesis, function, and taxonomic significance. *Microbiological Reviews*, 55, 288–302.

Killops, S. D. and Killops, V. J. (2005). *Introduction to organic geochemistry*. 2. edition, Blackwell Publishing Ltd, Oxford.

Kissin, Y. V. (1987). Catagenesis and composition of petroleum: Origin of *n*-alkanes and isoalkanes in petroleum crudes. *Geochimica et Cosmochimica Acta*, 51, 2445–2457.

Knoll, A. H. (2014). Paleobiological Perspectives on Early Eukaryotic Evolution. *Cold Spring Harbor Perspectives in Biology*, 6, a016121.

Koga, Y. and Morii, H. (2007). Biosynthesis of Ether-Type Polar Lipids in Archaea and Evolutionary Considerations. *Microbiology and Molecular Biology Reviews*, 71, 97–120.

Konn, C., Charlou, J. L., Donval, J. P., Holm, N. G., Dehairs, F., and Bouillon, S. (2009). Hydrocarbons and oxidized organic compounds in hydrothermal fluids from Rainbow and Lost City ultramafic-hosted vents. *Chemical Geology*, 258, 299–314.

Li, W., Czaja, A. D., Van Kranendonk, M. J., Beard, B. L., Roden, E. E., and Johnson, C. M. (2013). An anoxic, Fe(II)-rich, U-poor ocean 3.46 billion years ago. *Geochimica et Cosmochimica Acta*, 120, 65–79.

Lindsay, J. F., Brasier, M. D., McLoughlin, N., Green, O. R., Fogel, M., Steele, A., and Mertzman, S. A. (2005). The problem of deep carbon—An Archean paradox. *Precambrian Research*, 143, 1–22.

Lockhart, R. S., Meredith, W., Love, G. D., and Snape, C. E. (2008). Release of bound aliphatic biomarkers via hydropyrolysis from Type II kerogen at high maturity. *Organic Geochemistry*, 39, 1119–1124.

Love, G. D., Bowden, S. A., Jahnke, L. L., Snape, C. E., Campbell, C. N., Day, J. G., and Summons, R. E. (2005). A catalytic hydropyrolysis method for the rapid screening of microbial cultures for lipid biomarkers. *Organic Geochemistry*, 36, 63–82.

Love, G. D., Snape, C. E., Carr, A. D., and Houghton, R. C. (1995). Release of covalently-bound alkane biomarkers in high yields from kerogen via catalytic hydropyrolysis. *Organic Geochemistry*, 23, 981–986.

Marshall, C. P., Love, G. D., Snape, C. E., Hill, A. C., Allwood, A. C., Walter, M. R., Van Kranendonk, M. J., Bowden, S. A., Sylva, S. P., and Summons, R. E. (2007). Structural characterization of kerogen in 3.4 Ga Archaean cherts from the Pilbara Craton, Western Australia. *Precambrian Research*, 155, 1–23.

Matsumi, R., Atomi, H., Driessen, A. J. M., and van der Oost, J. (2011). Isoprenoid biosynthesis in Archaea—Biochemical and evolutionary implications. *Research in Microbiology*, 162, 39–52.

McCollom, T. M., Ritter, G., and Simoneit, B. R. T. (1999). Lipid Synthesis Under Hydrothermal Conditions by Fischer–Tropsch-Type Reactions. *Origins of Life and Evolution of Biospheres*, 29, 153–166.

McCollom, T. M. and Seewald, J. S. (2006). Carbon isotope composition of organic compounds produced by abiotic synthesis under hydrothermal conditions. *Earth and Planetary Science Letters*, 243, 74–84.

Meredith, W., Russell, C. A., Cooper, M., E. Snape, C., Love, G. D., Fabbri, D., and Vane, C. H. (2004). Trapping hydropyrolysates on silica and their subsequent thermal desorption to facilitate rapid fingerprinting by GC–MS. *Organic Geochemistry*, 35, 73–89.

Mißbach, H., Duda, J.-P., Lünsdorf, N. K., Schmidt, B. C., and Thiel, V. (2016). Testing the preservation of biomarkers during experimental maturation of an immature kerogen. *International Journal of Astrobiology*, 15, 165–175.

Morag, N., Williford, K. H., Kitajima, K., Philippot, P., Van Kranendonk, M. J., Lepot, K., Thomazo, C., and Valley, J. W. (2016). Microstructure-specific carbon isotopic signatures of organic matter from ~3.5 Ga cherts of the Pilbara Craton support a biologic origin. *Precambrian Research*, 275, 429–449.

Nijman, W., de Bruijne, K. C. H., and Valkering, M. E. (1999). Growth fault control of Early Archaean cherts, barite mounds and chert–barite veins, North Pole Dome, Eastern Pilbara, Western Australia. *Precambrian Research*, 95, 247–274.

Olcott Marshall, A., Jehlička, J., Rouzaud, J.-N., and Marshall, C. P. (2014). Multiple generations of carbonaceous material deposited in Apex chert by basin-scale pervasive hydrothermal fluid flow. *Gondwana Research*, 25, 284–289.

Parfrey, L. W., Lahr, D. J. G., Knoll, A. H., and Katz, L. A. (2011). Estimating the timing of early eukaryotic diversification with multigene molecular clocks. *Proceedings of the National Academy of Sciences of the United States of America*, 108, 13624–13629.

Peters, K. E., Walters, C. C., and Moldowan, J. M. (2005). *The Biomarker Guide - Part II - Biomarkers and Isotopes in Petroleum Exploration and Earth History*. Cambridge University Press, New York.

Philippot, P., Van Zuilen, M., Lepot, K., Thomazo, C., Farquhar, J., and Van Kranendonk, M. J. (2007). Early Archaean Microorganisms Preferred Elemental Sulfur, Not Sulfate. *Science*, 317, 1534–1537.

Pinti, D. L., Hashizume, K., Sugihara, A., Massault, M., and Philippot, P. (2009). Isotopic fractionation of nitrogen and carbon in Paleoarchean cherts from Pilbara craton, Western Australia: Origin of ^{15}N-depleted nitrogen. *Geochimica et Cosmochimica Acta*, 73, 3819–3848.

Proskurowski, G., Lilley, M. D., Seewald, J. S., Früh-Green, G. L., Olson, E. J., Lupton, J. E., Sylva, S. P., and Kelley, D. S. (2008). Abiogenic Hydrocarbon Production at Lost City Hydrothermal Field. *Science*, 319, 604–607.

Radke, M., Leythaeuser, D., and Teichmüller, M. (1984). Relationship between rank and composition of aromatic hydrocarbons for coals of different origins. *Organic Geochemistry*, 6, 423–430.

Radke, M. and Welte, D. (1983). The Methylphenanthrene Index (MPI): a maturity parameter based on aromatic hydrocarbons. In M. Bjoroy and EAOG (Eds.), *10th International Meeting on Organic Geochemistry, Bergen, Sept. 1981*. John Wiley and Sons, Chichester, pp. 504–512.

Rippka, R., Deruelles, J., Waterbury, J. B., Herdman, M., and Stanier, R. Y. (1979). Generic Assignments, Strain Histories and Properties of Pure Cultures of Cyanobacteria. *Microbiology*, 111, 1–61.

Schidlowski, M. (2001). Carbon isotopes as biogeochemical recorders of life over 3.8 Ga of Earth history: evolution of a concept. *Precambrian Research*, 106, 117–134.

Schopf, J. W. (1993). Microfossils of the Early Archean Apex Chert: New Evidence of the Antiquity of Life. *Science*, 260, 640 – 646.

Schopf, J. W., Kudryavtsev, A. B., Agresti, D. G., Wdowiak, T. J., and Czaja, A. D. (2002). Laser–Raman imagery of Earth's earliest fossils. *Nature*, 416, 73–76.

Shen, Y., Buick, R., and Canfield, D. E. (2001). Isotopic evidence for microbial sulphate reduction in the early Archaean era. *Nature*, 410, 77–81.

Shirey, S. B. and Richardson, S. H. (2011). Start of the Wilson Cycle at 3 Ga Shown by Diamonds from Subcontinental Mantle. *Science*, 333, 434 – 436.

Simoneit, B. R. T. (1993). Aqueous high-temperature and high-pressure organic geochemistry of hydrothermal vent systems. *Geochimica et Cosmochimica Acta*, 57, 3231–3243.

Smithies, R. H., Champion, D. C., Van Kranendonk, M. J., Howard, H. M., and Hickman, A. H. (2005). Modern-style subduction processes in the Mesoarchaean: Geochemical evidence from the 3.12 Ga Whundo intra-oceanic arc. *Earth and Planetary Science Letters*, 231, 221–237.

Snape, C. E., Bolton, C., Dosch, R. G., and Stephens, H. P. (1989). High liquid yields from bituminous coal via hydropyrolysis with dispersed catalysts. *Energy & Fuels*, 3, 421–425.

Summons, R. E. and Hallmann, C. (2014). Organic geochemical signatures of early life on Earth. In P. Falkowski and K. Freeman (Eds.), *Treatise on geochemistry, 2nd Edition*. Elsevier Netherlands, Amsterdam, pp. 33–46.

Terabayashi, M., Masada, Y., and Ozawa, H. (2003). Archean ocean-floor metamorphism in the North Pole area, Pilbara Craton, Western Australia. *Precambrian Research*, 127, 167–180.

Ueno, Y., Isozaki, Y., Yurimoto, H., and Maruyama, S. (2001). Carbon Isotopic Signatures of Individual Archean Microfossils(?) from Western Australia. *International Geology Review*, 43, 196–212.

Ueno, Y., Yamada, K., Yoshida, N., Maruyama, S., and Isozaki, Y. (2006). Evidence from fluid inclusions for microbial methanogenesis in the early Archaean era. *Nature*, 440, 516–519.

Ueno, Y., Yoshioka, H., Maruyama, S., and Isozaki, Y. (2004). Carbon isotopes and petrography of kerogens in ~3.5-Ga hydrothermal silica dikes in the North Pole area, Western Australia. *Geochimica et Cosmochimica Acta*, 68, 573–589.

Van Kranendonk, M. J. (1999). *North Shaw, W.A. Sheet 2755: Geolocial Survey of Western Australia 1:100000 Geol. Series*. Technical report.

Van Kranendonk, M. J. (2006). Volcanic degassing, hydrothermal circulation and the flourishing of early life on Earth: A review of the evidence from c. 3490–3240 Ma rocks of the Pilbara Supergroup, Pilbara Craton, Western Australia. *Earth-Science Reviews*, 74, 197–240.

Van Kranendonk, M. J. (2011). Morphology as an Indictor of Biogenicity for 3.5–3.2 Ga Fossil Stromatolites from the Pilbara Craton, Western Australia. In J. Reitner, N.-V. Quéric, and G. Arp (Eds.), *Advances in Stromatolite Geobiology*. Springer, Berlin, Heidelberg, pp. 537–554.

Van Kranendonk, M. J., Philippot, P., Lepot, K., Bodorkos, S., and Pirajno, F. (2008). Geological setting of Earth's oldest fossils in the ca. 3.5 Ga Dresser Formation, Pilbara Craton, Western Australia. *Precambrian Research*, 167, 93–124.

Van Kranendonk, M. J. and Pirajno, F. (2004). Geochemistry of metabasalts and hydrothermal alteration zones associated with c. 3.45 Ga chert and barite deposits: implications for the geological setting of the Warrawoona Group, Pilbara Craton, Australia. *Geochemistry: Exploration, Environment, Analysis*, 4, 253–278.

Van Kranendonk, M. J., Webb, G. E., and Kamber, B. S. (2003). Geological and trace element evidence for a marine sedimentary environment of deposition and biogenicity of 3.45 Ga stromatolitic carbonates in the Pilbara Craton, and support for a reducing Archaean ocean. *Geobiology*, 1, 91–108.

Walter, M. R., Buick, R., and Dunlop, J. S. R. (1980). Stromatolites 3,400–3,500 Myr old from the North Pole area, Western Australia. *Nature*, 284, 443–445.

Yui, T.-F., Huang, E., and Xu, J. (1996). Raman spectrum of carbonaceous material: a possible metamorphic grade indicator for low-grade metamorphic rocks. *Journal of Metamorphic Geology*, 14, 115–124.

The Mars Organic Molecule Analyzer (MOMA) instrument: Characterization of organic material in martian sediments

(published in *Astrobiology*)

Fred Goesmann, William B. Brinckerhoff, François Raulin, Walter Goetz, Ryan M. Danell, Stephanie A. Getty, Sandra Siljeström, Helge Mißbach, Harald Steininger, Ricardo D. Jr. Arevalo, Arnaud Buch, Caroline Freissinet, Andrej Grubisic, Uwe J. Meierhenrich, Veronica T. Pinnick, Fabien Stalport, Cyril Szopa, Jorge L. Vago, Robert Lindner, Mitchell D. Schulte, John Robert Brucato, Daniel P. Glavin, Noel Grand, Xiang Li, Friso H. W. van Amerom, and the MOMA Science Team

Abstract

The Mars Organic Molecule Analyzer (MOMA) instrument onboard the ESA/Roscosmos ExoMars rover (to launch in July, 2020) will analyze volatile and refractory organic compounds in martian surface and subsurface sediments. In this study, we describe the design, current status of development, and analytical capabilities of the instrument. Data acquired on preliminary MOMA flight-like hardware and experimental setups are also presented, illustrating their contribution to the overall science return of the mission.

Keywords: Mars, Mass spectrometry, Life detection, Planetary instrumentation.

5.1 Introduction: The Mars Organic Molecule Analyzer (MOMA) investigation

The Mars Organic Molecule Analyzer (MOMA) investigation directly addresses the Exo-Mars scientific objective (Vago et al., 2017) to search for signs of past or present life on Mars. It achieves this by analyzing a wide range of organic compounds that may be found in drill samples acquired up to 2 m below the martian surface. MOMA must first volatilize organic compounds so that they can be detected by a mass spectrometer (MS). Volatilization of organic material is achieved by either one of its two operational modes: (1) heating of the sample to induce evaporation and/or thermochemical decomposition (pyrolysis) and liberate species into the gas phase, possibly also being preceded by a chemical derivatization step to aid in this gas-phase transition, and (2) direct interrogation of the sample by intense ultraviolet (UV) laser pulses inducing prompt desorption into the gas phase. In the case of operational mode (1), the organic compounds will be separated by gas chromatographic columns before they reach the MS, while in the case of operational mode (2), the laser-desorbed species are sent directly to the MS without

further separation. Either mode enables direct detection of indigenous martian organic molecules (in some cases, as unfragmented parent ions) and will thus be of high diagnostic and scientific value. MOMA can also detect some thermally released inorganic molecules (e.g., SO_2) or laser-desorbed fragments of inorganic minerals (e.g., iron oxide or silicate fragments). By characterizing the types, distributions, and molecular structures of detected organics, MOMA can provide powerful insights into the origin and processing of potential molecular biosignatures.

While the existence of a singular, unambiguous martian biosignature may be endlessly debated, a common pragmatic position—that taken by ExoMars—is that a martian biosphere would be reflected to some degree in the distribution and structures of organic compounds associated with past or present organisms (Summons et al., 2008; Westall et al., 2015). For example, certain lipids may be produced by the chemical and thermal degradation of biomolecules forming cell membranes and can be preserved over geological timescales (Brocks and Summons, 2003). The aliphatic groups of these and other organics may also exhibit biogenic features, such as a strong even-over-odd bias in fatty acid carbon chain lengths, which are not present in abiogenic organic material (e.g., McCollom et al., 1999; Peters et al., 2005). If biogenic, such compounds may be found at high concentrations only over a discrete range of molecular weights (such as the $C_{14}-C_{20}$ fatty acids). This is in contrast to that observed in carbonaceous meteorites where these compounds are detected over a broader range of molecular weights (typically hundreds of atomic mass units) and with decreasing abundance as molecular weight increases (Sephton, 2002; Summons et al., 2008). Molecular chirality (handedness) is another important property of some organic compounds (e.g., amino acids and sugars) that can be used to discriminate between biological and nonbiological sources if there is shown to be a strong enantiomeric excess (ee; Meierhenrich, 2008). Particular isomers of high-molecular-weight organics (10^2-10^3 u), specifically those with identifiable biochemical functionality such as terpenoids and peptides, can be potential biosignatures when identified in concert with other supporting evidence.

MOMA has been designed to enable an investigation of such molecular signs of life—extinct or extant—through a combination of *detection and characterization* of key complex organic compounds and *contextual measurements* of organic and inorganic inventories. Understanding these broader inventories, by using combined data from MOMA and other ExoMars instruments, can provide a more complete understanding of active processes, such as organic delivery, degradation, and cycling, as well as the preservation potential of the local environment.

Several regions on Mars have been advocated as appropriate exploration areas for the ExoMars rover mission. These regions either show fine-grained sedimentary deposits (e.g., clay minerals) that may adsorb and trap organic material due to their high specific surface area or the deposits have been rapidly buried (e.g., by lava) and later exposed by slow and still ongoing Amazonian erosion. The latter process would have shielded organic compounds against destructive cosmic particle radiation (Goetz et al., 2016b, and references therein). As of April 2017, two candidate landing sites are being considered: Oxia Planum and Mawrth Vallis (Vago et al., 2017). Both areas are located in western Arabia Terra ($15°-25°$N, $15°-25°$W, less than 500 km from each other), off the dusty terrain, and at altitudes (-3 to -2 km) compatible with EDL (Entry, Descent, and Landing) constraints (Vago et al., 2017). Both locations lie in a clay rich late-Noachian/early-

Hesperian region that was covered by an Amazonian lava flow (c. 2.6 Ga). Since then, denudation and scarp retreat have been ongoing, providing access to old sediments that may have preserved pristine Noachian organic compounds (Carter et al., 2016; Quantin et al., 2016).

5.2 Science goals

The overarching goal of MOMA is to seek the signs of past or present life on Mars through analysis of the molecular, primarily organic, composition of acquired samples on the ExoMars rover. This overarching goal is divided into three subgoals, here updated for clarity from the work by Debus et al. (2012), as follows:

G1. Search for molecular biosignatures: A molecular biosignature is a pattern or distribution of molecules or molecular structures that results from biological processes, past or present. Molecular, primarily organic, biosignatures may represent or derive from parts of the organisms themselves, such as cell wall lipids, or reflect the products of life processes, such as biogenic methane. On Earth, such biosignatures are ubiquitous and recognizable. On Mars, molecular structures, let alone those associated with viable organisms, face what appear to be severe conditions likely rendering them more obscure. Degradational processes, such as radiolysis and oxidation that dominate near the surface, may leave only ambiguous remnants of a potential biosignature. However, under favorable taphonomic conditions (e.g., rapid burial), certain biosignatures such as isomeric and abundance biases might be preserved on Mars, even over geologic timescales. As such, the search for evidence of molecular biosignatures by MOMA must be broad, able to detect the widest range of molecular structures, and must be interpreted in the context of both preservation potential and an expected background of abiotic chemistry.

The focus of ExoMars is on signs of ancient life. Under appropriate geological conditions, such as rapid sedimentary burial and limited oxidation potential, martian molecular biosignatures could be detectable through their diagenetic products, distinct from an abiotic (e.g., exogenous) organic background. Certain classes of molecular fossils such as acetogenic and isoprenoidal lipids, carotenoids (such as β-carotene), and key biomarker species, such as pristane, phytane, and hopanes, have been studied for their specificity to terrestrial microorganisms and their ability to be preserved over long timescales (Summons, 2014). Both modes of MOMA, separately and in concert, may contribute critical data toward their identification. The Laser Desorption Mass Spectrometry (LDMS) mode may provide initial indication of higher-molecular-weight (hundreds of atomic mass units) nonvolatile organics, consistent with such compounds, which can be structurally analyzed through subsequent tandem mass spectrometry as well as derivatization- or thermochemolysis based Gas Chromatography–Mass Spectrometry (GC–MS). Moreover, when coupled with the mission's ability to analyze depth profiles, the molecular weight distribution of a wide variety of organics, from amino and carboxylic acids, to polycyclic aromatic hydrocarbons (PAHs) and their alkylated homologs, to larger moieties such as porphyrin-based species and macromolecular carbon, covered by MOMA's broad based detection approach, may help resolve the provenance of any detected organics.

One of the more important signatures in terrestrial biochemistry involves the use of only one enantiomer of amino acids as monomers for peptide synthesis, referred to

as homochirality. A significant left or right imbalance or ee (defined as ($[L] - [R]) \times 100\%/([L] + [R])$) where [L] and [R] refer to the abundance levels of, respectively, left and right enantiomers), detected with the appropriate chemical derivatization tag and a chiral-selective GC column, represents a *potential* molecular biosignature. Abiotic processes such as UV polarized radiation and surface catalysis on specific crystals are generally only known to produce tiny ee of any sign and up to 1% (Modica et al., 2014). However, significant ee (up to $+60\%$) has been observed for certain amino acids in carbonaceous chondrites, implying the existence of prebiotic mechanisms to amplify tiny initial ee (Glavin and Dworkin, 2009; Glavin et al., 2012, and references therein; Tarasevych et al., 2015); any positive ee detection by MOMA would thus require additional correlative evidence from a suite of measurements. In particular, a significant (say, greater than 20%) L-excess in a suite of martian amino acids, although potentially a compelling observation, would require further corroborating chemical evidence. Similarly, a very significant D-excess would be a remarkable finding as this could indicate a biochemistry entirely independent from that of Earth.

Molecular biosignatures caused by extant or very recent (dormant or extinct) biology on Mars would be more pronounced and thus more easily detectable than those caused by ancient biology. However, the ExoMars rover mission (as opposed to the Viking landers, Goetz et al., 2016b, and references therein) is not designed to distinguish between signs of current and past life. Absent a parallel direct search for metabolism or cells and organisms, it will be difficult to distinguish extant versus extinct potential molecular biosignatures in isolation without a full understanding of the taphonomic conditions of any particular structure or pattern, which is not well constrained for the martian near-subsurface.

Nevertheless, due to the predicted degradation rates for certain signatures, based on terrestrial biology and laboratory observations, detection of certain classes of complex organics, in the context of other measurements, could provide some evidence of potential extant or recent biology. Assuming martian life would be carbon-based and cellular as on Earth, one would expect common or analogous biomolecular building blocks such as chains of amino acids (peptides and proteins or their analogs) and oligomers of nucleobases (RNA, DNA, or their analogs such as PNA—peptide nucleic acid; Nelson et al., 2000; Zimmer, 2009). Such larger, more fragile polymeric biomolecules are less likely to survive environmental processes and could indicate recent biosynthesis. Similarly, phospholipids would be prevalent in the cell membranes of any viable community of bacteria or archaea, and the internal lipid structure could be used to distinguish among these (e.g., isoprenoid side chains in archaea). Individual compound classes targeted for detection would thus include fatty acids, sterols, and hopanoids. Strong evidence of ee in amino acids within such a population may also be an indicator of current or recent biological activity due to the tendency for racemization over geologic time (Bada and McDonald, 1995; Bada et al., 1999).

G2. Search for evidence of active processes (geochemical, biologic, or exogenous): The astrobiological interpretation of the martian organic inventory, as it varies over spatial and temporal dimensions, requires a broad understanding of its carbon and other chemical processes and cycles. Such an understanding is only now beginning to emerge with a synthesis of results from multiple missions, including MER, MEX, MSL (Curiosity rover), and MAVEN (see the Abbreviations Used section for expansion of mission acronyms).

The ExoMars rover, with MOMA, has the opportunity to achieve a new view of Mars, with its combination of depth sampling, likely late Noachian terrain, and MOMA's sensitivity to a variety of molecules over a range of volatilities and molecular weights. Detection of compounds with relatively weak bonds, such as $C-O-C$ or $C-N-C$, in the harsh near-surface environment implies replenishment over a given depth-dependent timescale or high erosion rates/recent exposure. Abundance levels of such species significantly exceeding those expected from exogenous infall (Steininger et al., 2012, and references therein; in particular Flynn and McKay, 1990), correlated with any higher-molecular-weight organics containing such bonds, may comprise a potential biomarker. Lighter, volatile, and semivolatile compounds (with enthalpies of vaporization below ~ 50 kJ/mol), including *n*-alkanes, some amino acids, benzene, and even naphthalene and benzoic acid, detectable by the GC–MS mode, may provide insights into active processes (e.g., recent exposure due to sublimation of surface ice or eolian denudation) that broadly determine the organic inventory. Additionally, the surface of Mars should have accumulated significant quantities of larger more refractory organics based on the abundance levels found in interplanetary dust particles and carbonaceous meteorites. MOMA's characterization of this fraction, primarily by LDMS, may determine not only the abundance of this potential background for trace biomarker detection but also the degree of processing of this matter by radiation (Moores and Schuerger, 2012; Pavlov et al., 2012; Poch et al., 2014, 2015) and oxidation (Benner et al., 2000) as a function of depth. Some refractory material can also be volatized by thermochemolysis or derivatization and thereby analyzed with GC–MS.

G3. Understand the geologic context: MOMA is primarily focused on organic compounds. Important ExoMars objectives related to determining geological and geochemical context through inorganic composition are well handled by other highly capable instruments. Nevertheless, MOMA does possess some capabilities for inorganic elemental and mineralogical analysis that complement those instruments. The presence or absence of certain elements (including S, Ca, and some transition metals) and of general mineral classes (e.g., carbonates, sulfates, sulfides, iron oxides) provides important contextual information about the processing and chemical complexity of the material, as well as correlation with any detection of organic compounds in the same sample. In the LDMS mode, diagnostic laser-desorbed metal ions, metal clusters, or metal oxide molecules (with characteristic isotope patterns) are produced during the standard analysis. While not part of the baseline investigation, MOMA does additionally have the capability to perform both evolved gas analysis (EGA), by monitoring the release of small molecules (e.g., SO_2, OCS, CS_2) as a function of temperature, and differential thermal analysis (DTA; Goetz et al., 2011; Archer Jr. et al., 2013) by comparing EGA temperature ramp data from two successive runs of a common sample at exactly the same oven power profile. EGA has been conducted very successfully by the SAM instrument (sample analysis at Mars) onboard the Curiosity rover (McAdam et al., 2014, 2016; Sutter et al., 2016). Differential scanning calorimetry (DSC) experiments were successfully conducted by TEGA (thermal and evolved gas analyzer) onboard the Phoenix Mars lander (Boynton et al., 2009; Sutter et al., 2012). The latter technique (DSC) consists of measuring the differential energy needed to increase the sample temperature by a small amount (denoted as $\Delta E/\Delta T$) at any time while the sample is heated. All thermal analysis techniques described so far (EGA, DTA, DSC) are not part of MOMA instrument requirements (Section 5.3) and

would therefore be performed on a best effort basis based on the rover's science operation team decision process. Overall, MOMA's constraints on the chemical and mineralogical composition of samples must be combined with data from the RLS (Raman Laser Spectrometer) and MicrOmega (Micro Observatoire pour la Mineralogie, l'Eau, les Glaces et l'Activité, i.e., NIR imaging spectrometer) instruments. The fine focus of the MOMA laser enables qualitative association of any organic compounds with the mineral matrix.

5.3   Objectives and requirements

To achieve these goals, MOMA is tasked by ExoMars with four analytical objectives as follows:

O1. Detect and characterize organic molecular species in solid samples with high (ppb) sensitivity.

O2. Analyze patterns of, and interrelationships among, a variety of organic molecules over a wide range of molecular weights and volatilities.

O3. Analyze for the presence and degree of ee in detected chiral organics.

O4. Characterize the inorganic geochemical context of the organic analyses.

These objectives translate into a set of performance requirements (Debus et al., 2012) that have dictated MOMA design and development:

R1. MOMA shall be able to detect organic molecules in the collected samples at concentrations as low as 10 parts-per-billion by weight (ppbw) or ng/g.

R2. MOMA shall be able to identify organics with chain-based or ring-based structures, which could indicate potential biosignatures, at concentrations as low as 10 ppmw.

R3. MOMA shall be able to characterize molecular weight distribution patterns in organic molecules (e.g., odd vs. even chained hydrocarbons, heteroatom, or methyl substitution in aromatics) over mass-to-charge (m/z) ratio as high as 1000 u at concentrations as low as 10 ppmw.

R4. MOMA shall be able to detect compounds of low stability (e.g., formaldehyde) at concentrations as low as 1 ppmv.

R5. MOMA shall investigate the biotic or abiotic origin of organic chiral molecules (e.g., amino acids, carboxylic acids, and amines) by analyzing their enantiomers at molecular concentrations as low as 1 ppmw.

R6. MOMA shall be able to detect light volatile organics (e.g., benzene, alkanes, and amines) at concentrations as low as 1 ppmw.

R7. MOMA shall be able to detect refractory organics (e.g., heavy PAHs, kerogen-like material) with molecular weights up to 1000 u at concentrations as low as 10 ppmw.

R8. MOMA shall be able to provide diagnostic presence/absence information on contextual elemental composition (e.g., inorganic breakdown products produced upon pyrolytic heating or laser desorption).

R9. MOMA shall be able to provide diagnostic presence/absence information on contextual mineralogical composition (e.g., inorganic breakdown products produced upon pyrolytic heating or laser desorption) at a threshold of 1 wt%.

5.4   Instrument top-level description

The task of the MOMA instrument is the detection and identification of various molecular species and classes at low concentrations with high analytic specificity. One mode of MOMA is the use of GC–MS for volatile molecule characterization. Volatile compounds thermally evolved from solid samples in a pyrolysis oven are separated by the GC and then analyzed individually with the MS. For nonvolatile molecules, MOMA provides a method (LDMS) to produce gas phase ions by high-intensity laser pulses applied directly to a crushed sample surface. These ions are transferred into the MS and analyzed. Both modes of operation use a common linear ion trap MS (ITMS) for detection and identification of molecular ions. Table 5.1 summarizes the basic characteristics of the MOMA instrument. Figure 5.1 shows a three-dimensional (3D) view of the MOMA instrument in its flight configuration, and Figure 5.2 outlines a decision tree and the flow of events for a notional sample analysis.

Table 5.1: Main characteristics of the Mars Organic Molecule Analyzer instrument.

Mass	11.5 kg *w/o* margin
Average power	65 W (LDMS) 82 W (GC–MS)
Maximum power	133 W (LDMS) 154 W (GC–MS)
Operational temperature range	$(-40 + 20)$ °C (upper value limited by laser)

GC–MS = Gas Chromatography–Mass Spectrometry; LDMS = Laser Desorption Mass Spectrometry.

Samples to be investigated will be powdered (crushed) drill cores of sedimentary rocks obtained from the uppermost 2 m of the martian surface. For LDMS, samples are dispensed into a refillable container (Figs. 5.1, 5.2) and leveled, providing a flat sample focal plane for the MOMA laser as well as other optical instruments. The LDMS mode may be used to determine the presence and chemical makeup of nonvolatile compounds in the sample and the results used in subsequent science operation decisions. Second, in GC–MS, samples are dispensed into one of the MOMA ovens. There, samples may be directly heated (pyrolyzed) or subjected to a derivatization procedure. The evolved species are transferred to a GC where the compounds are separated into a time sequence and then, after detection by a TCD (thermal conductivity detector), fed into the MS to be separated by mass. The combination of methods covers a wide range of molecules from the light- (e.g., chloromethane) to medium-sized ones (e.g., naphthalene) by GC–MS and up to more complicated molecules (e.g., peptides, large PAHs) by LDMS at rather low detection limits (as low as 10 ppbw for GC–MS and in the sub-pmol/mm^2 range for LDMS). In this study, it should be noted that limits of detection are generally given as bulk abundance levels (ppmw, Section 5.3), while MS testing in the laboratory often requires the use of samples with a known density of these molecules on some substrate (pmol/mm^2). This discrepancy is unavoidable for technical and practical reasons. However, both quantities
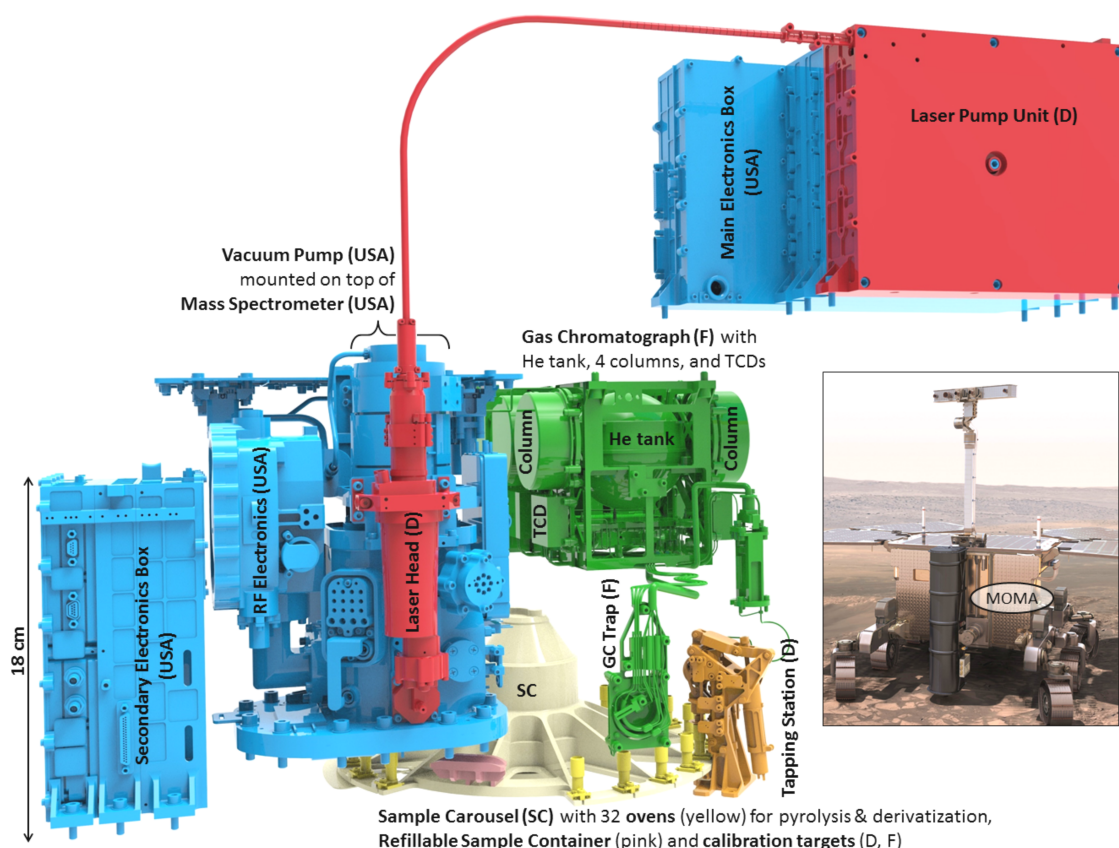
Figure 5.1: The different parts of MOMA and their contributors (France (F), Germany (D), United States) are displayed in the figure above. The LPU that controls the LH is mounted as a slice on the MEB (top right). Sample carousel (SC) and refillable sample container are not part of MOMA. LH, Laser Head; LPU, Laser Pump Unit; MEB, Main Electronic Box; MOMA, Mars Organic Molecule Analyzer.
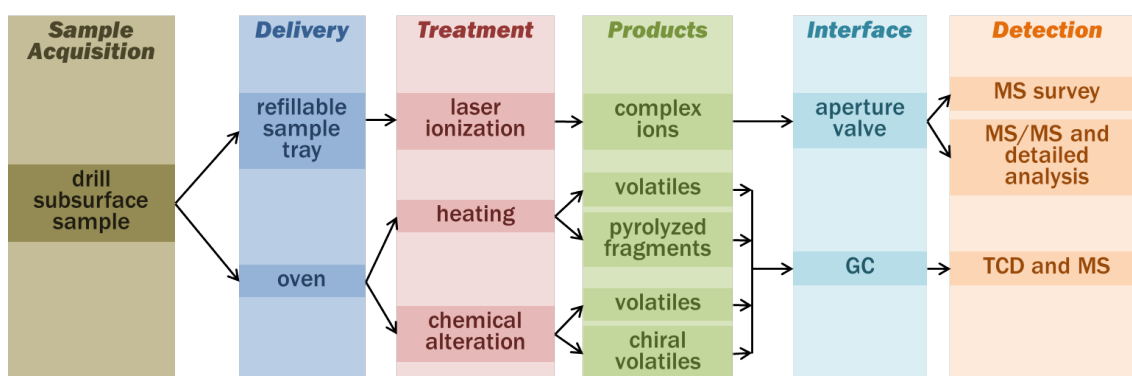
Figure 5.2: Chain of sample processing and analysis. The subsurface sample is received from drill and crushing station. Important decisional points are the MOMA operational mode, in particular, choose delivery to refillable sample tray/laser ionization versus pyrolysis oven and select chemical alteration (derivatization agent) and GC column. In the latter case, the signal is generally detected by both MS and TCD (Section 5.6.2.2). GC, Gas Chromatography; MS, Mass Spectrometer; TCD, Thermal Conductivity Detector.

(bulk abundance and surface density) can be related to each other through basic assumptions on the accessibility of organic molecules in an inorganic matrix allowing testable quantities to be used in the verification of MOMA's performance as outlined below.

The components of MOMA related to GC–MS have strong space heritage dating back to the days of Viking. Most recent developments include the COSAC experiment (COmetary SAmpling and Composition) onboard the comet lander Philae (Goesmann et al., 2007) and SAM onboard Curiosity (Mahaffy et al., 2012) on which several members of the MOMA team were also involved. The LDMS method is of more recent design and the first such implementation developed for Mars exploration. The concept of joining the GC–MS and LDMS functions through a common MS and pumping system, identified at the first Pasteur payload meeting in 2004, led to the present tightly integrated MOMA system.

5.5   Instrument development

5.5.1   Team organization

The MOMA instrument is assembled from modules produced and tested at several institutions. The Rosetta heritage ovens and tapping station (TS) are developed at the Max Planck Institute for Solar System Research (MPS) in Germany. The gas chromatograph (GC) is built at Laboratoire Interuniversitaire des Systèmes Atmosphériques (LISA) and Laboratoire ATmosphères, Milieux, Observations Spatiales (LATMOS) in France with some German participation in the electronics by MPS. Pyrolysis GC testing campaigns have been managed in a partnership between the German and French teams. The MS and its drive electronics, as well as the main electronics of MOMA, are developed by NASA's Goddard Space Flight Center (GSFC) and its partners at the Space Physics Research Laboratory (SPRL) at the University of Michigan in conjunction with Battel Engineering. The laser drive electronics are built at MPS, while the laser head (LH) is designed and built at Laser Zentrum Hannover (LZH).

The integration of MOMA hardware in the rover is distributed as well: MOMA does not form a single compact unit, but remains modular with numerous mechanical and thermal interfaces with the rover's Analytical Laboratory Drawer (ALD). As such, the integration activities are highly collaborative between rover and instrument teams. The sample drilling and distribution system, which needs to retrieve, grind, portion, and deliver the samples to either a refillable container for LDMS or the ovens for GC–MS, is not part of MOMA. The carousel element of this system, a critical functional part of the MOMA analytical sequence, but not part of MOMA, is included in Figure 5.1.

5.5.2   Instrument integration flow

Upon delivery, the MOMA instrument will be integrated into the analytical drawer of the rover (Vago et al., 2017). The integration will happen at Thales Alenia Space in Torino, Italy (TAS-I). The steps to arrive at an integrated instrument are as follows: The ovens and the TS are directly delivered from MPS to TAS-I. They need to be among the cleanest parts of MOMA since they will be in direct contact with the samples and

will be situated in the Ultra-Clean Zone (UCZ) (Vago et al., 2017). Hence, they will be delivered in specially designed transport containers that are pressurized to prevent exposure to ambient conditions. The laser electronics are delivered from MPS to LZH to complete the laser. The laser is delivered to GSFC so that the LH can be integrated to the MS while the laser electronics become part of the larger electronic unit built at GSFC. This constitutes the LDMS subsystem of MOMA. The total LDMS is then delivered to TAS-I. The MS itself forms a part of the closeout of the UCZ: the bottom plate and inlet valve system for LDMS are therefore subject to the same extreme contamination controls as the ovens and TS. After necessary interface testing, the GC is also directly delivered from LISA/LATMOS to TAS-I.

5.5.3 Instrument verification

The modularity requires multiple coupling tests between instrument subsystems to verify instrument performance. To date, several GC–MS campaigns have been conducted at GSFC (Section 5.6.2.2) where a series of models of the GC were coupled to breadboards and an engineering model of the MS. The sample chain from oven to TS to GC was verified during campaigns at LISA/LATMOS. The LDMS performance was tested with lasers and mass spectrometers at different stages of development as well. Final instrument-level flight testing and calibration under Mars environmental conditions will occur as each subsystem achieves performance verification and acceptance at the component level.

5.5.4 Achieved milestones and deliveries

The Preliminary and Critical Design Reviews (referred to as PDR and CDR) of the MOMA instrument are conducted by ESA. The MOMA PDR was completed in 2016, whereas the MOMA CDR will occur late in 2017. The NASA CDR of the MS subsystem was already completed in September 2014. The structural and thermal model of the instrument was delivered in early 2016. The Qualification Simulator Model (QSM) has been delivered in stages over 2015–2016. This will be followed by the Flight Model (FM) when ready and all delivery reviews have been passed.

5.6 Instrument subsystems

5.6.1 Oven and tapping station subsystems

Pyrolysis and derivatization implemented in an array of ovens was already developed for the COSAC GC–MS onboard Philae (Goesmann et al., 2007). With this heritage, the path of development for specific science requirements and anticipated sample compositions for MOMA was started. For the ovens, a larger diameter was chosen to pyrolyze larger amounts of sample to account for the lower organic concentrations expected in Mars samples. The development ended with ovens of a diameter of 6 mm and an inner volume of slightly more than 200 mm^3. One aliquot of powderized martian drill sample from the jaw crusher and dosing station (both are part of the SPDS, i.e., the sample processing and distribution system) is expected to have a volume of ~ 100 mm^3 and may correspond to an approximate mass of 100 mg (assuming a bulk density of 1 g/cm^3). Given the

uncertainty on that volume, the oven can only receive a single aliquot from the SPDS. All ovens are designed for *single use*, that is, they shall receive one aliquot of a given sample that may then be subjected to one or several processing steps, for example, two heating cycles in DTA mode (Section 5.2) or stepwise pyrolysis (Section 5.7). Pyrolysis and derivatization ovens will be heated to a maximum temperature of 850 °C and 600 °C (thermochemolysis), respectively (Table 5.2). The ovens are made from high-temperature steel. Their inner temperature is measured by a Pt100 sensor in the bottom of the oven. The heating is conducted by a platinum filament incorporated in a ceramic cylinder. To minimize thermal losses during heating, the oven is mounted on a thin-walled stand and the oven with the heater is wrapped in platinum foil to decrease radiative losses during heating. The TS ensures the electrical and pneumatic contact with each oven: (1) spring pins in connectors at the oven's base engage to achieve the necessary electrical contact between oven and TS and (2) a TS zirconia sphere is pressed onto the oven top's knife edge for gas sealing. The power lines to the oven heater and the lines to the temperature sensor are contacted by a small bridge that engages with the oven when the oven is closed by the zirconia sphere. The latter provides connection to two gas lines: one delivers helium, while the other line conducts the pyrolysis products entrained in the helium flow to the GC for separation and analysis.

Table 5.2: Characteristics of Mars Organic Molecule Analyzer ovens (for GC–MS) and the rover's Refillable Sample Container (for LDMS).

Thirty-two GC ovens	Twenty for pyrolysis/EGA, 12 for derivatization
Maximum temperature of GC oven	850 °C for pyrolysis/EGA, 600 °C for derivatization
Desired sample quantity	$100 - 200$ mm^3 for GC oven ~ 600 mm^3 for refillable sample container

A GC oven can receive any (powdered) sample whose bulk volume (including pore space) is in the range $100 - 200$ mm^3 (200 mm^3 is the critical upper limit, especially for pyrolysis ovens); EGA = Evolved Gas Analysis.

The TS was modified from the Philae design to provide for larger ovens and the difference in electrical contacts. As a result of the redesign, an increase in force of 200 N was necessary to close the oven and resulted in a design optimization effort, thus increasing the number of structural and mechanical parts of the TS considerably. The greatest changes were necessary in the spring system to ensure that the required force could be applied over a short stroke. Given the need to minimize any potential organic contamination within the UCZ (Vago et al., 2017) to meet the strict ExoMars contamination control requirements, several materials were replaced by metallic or ceramic parts. The concern that a blocked TS would represent a single-point failure for all rover ALD science operations (MOMA-LDMS, MicrOmega, RLS) led to the design of an emergency release mechanism for the oven TS. Several possible emergency releases were evaluated resulting in implementation of a motorized knee leverage release.

5.6.1.1   Derivatization

To allow analysis by GC, analytes have to be extracted from the mineral matrix into the gas phase. MOMA will accomplish this through thermal desorption (Buch et al., 2009) instead of solvent extraction, which is generally used in laboratory experiments, but requires excessive resources (Buch et al., 2006, 2009). Once released, the volatile, nonreactive, and thermally stable fraction of the sample can be analyzed with GC–MS. Some of the compounds targeted by MOMA contain a labile polar functional group (e.g., $-OH$, $-COOH$, $-NH$, $-SH$, or $-PH$). We anticipate that these compounds could form intramolecular bonding that (under the MOMA GC conditions) would result in poor separation or a degraded peak shape, limiting selectivity and/or sensitivity of GC–MS for certain compounds. Polar compounds, in particular, tend to be adsorbed on the active surface of the column and on the tubing walls (e.g., transfer lines), which can lead to a peak tailing and poor specificity. Given the importance of polar compounds in the characterization of biosignatures on Mars, these difficulties drive MOMA's requirements on heated line temperatures and onboard derivatization chemistry.

In practice, a derivatization agent produces a controlled reaction to protect the reactive group, thus decreasing the polarity of the molecule and thermally stabilizing it (Knapp, 1979). Several derivatization agents were considered and reagents were selected based on chemistry of the targeted labile group and on the required yield of the derivatization reaction. In addition, the nature of the detector used for the analysis is a key parameter to be considered. Two derivatization reagents have been chosen for implementation in MOMA: *N,N*-methyltert-butyl-dimethylsilyltrifluoroacetamide (MTBSTFA) and *N,N*-dimethylformamide dimethyl acetal (DMF-DMA).

MTBSTFA. MTBSTFA is a silyl reagent that readily reacts with a wide range of labile groups by replacing labile hydrogen by a tert-butyl-dimethylsilyl group (TBDMS; $Si(CH_3)_2C(CH_3)_3$), and the yield of this reaction is close to 96% (Mawhinney and Madson, 1982). The resulting derivatized compound is sufficiently stable to enable GC separation and sensitive detection by mass spectrometry. Moreover, when using mass spectrometry as the detection technique, the ions produced from silylated species generate very characteristic ions, making their identification easier, and the MS response is enhanced due to the presence of fluorine in the ions. Usually, *N,N*-dimethylformamide (DMF) is added to MTBSTFA not only to play the role of a solvent but it can also promote the derivatization reaction as a proton acceptor. A disadvantage of MTBSTFA is its preferential reaction with water to produce both mono- and bisilylated water compounds that can produce sizable background signals and compete with derivatization of the compounds of interest, as shown with measurements currently done with the SAM experiment on Mars (Leshin et al., 2013). Moreover, no separation of enantiomers derivatized when using this technique has ever been obtained by our team, nor has it ever been reported in the literature. While the reason for this lack of chromatographic separation is unclear, MTBSTFA cannot be used for enantiomer analysis. MTBSTFA reactions are typically conducted in the laboratory (a typical example is shown in Fig. 5.3a) at a temperature of $\sim 75\,°C$, but for in situ analysis on Mars, we anticipate thermal desorption of organic matter to occur at a higher temperature, in the vicinity of 250 °C, and silyl derivatization with MTBSTFA is therefore implemented on MOMA at 250 °C (the sample shall be held at that temperature

for about 10 min). At this temperature and in the absence of oxygen, MTBSTFA has been shown to be stable for more than 2 h.
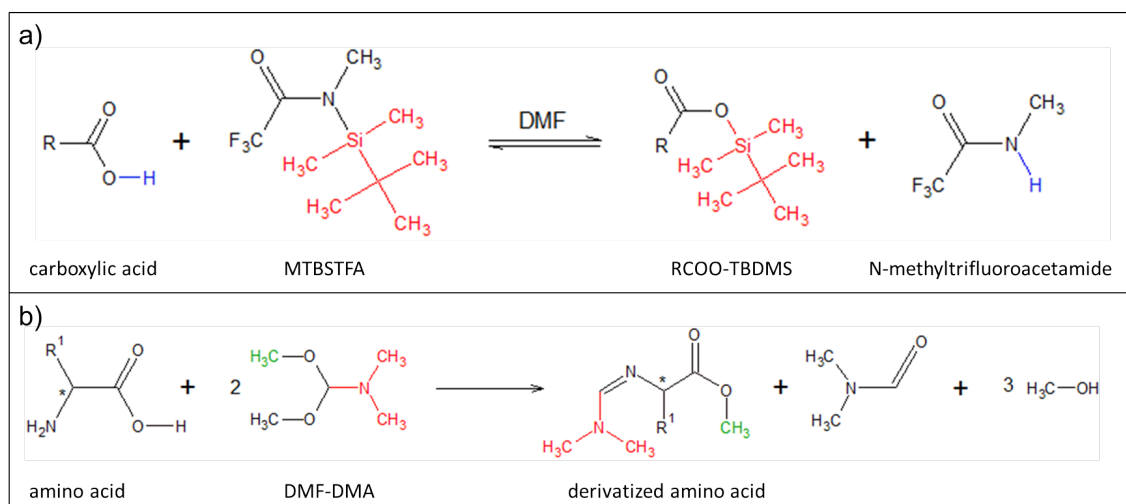

Figure 5.3: (**a**) MTBSTFA/DMF derivatization reaction with a carboxylic acid. (**b**) DMF-DMA derivatization reaction with an amino acid. The asymmetric center (*) is conserved.

DMF-DMA. DMF-DMA is a methylation reagent developed for use by COSAC that reacts solely with fatty acids, primary amines, and amino acids, replacing a labile hydrogen atom by a methyl group (Meierhenrich et al., 2001). Although it is less efficient than MTBSTFA (detection limit of 1.3 ppm rather than 80 ppb for amino acids), it is still compatible with the concentration of organic compounds found in micrometeorites due to a better MS response. The most important property of DMF-DMA is its capability to enable separation of amino acid enantiomers when used with an enantioselective GC column (Freissinet et al., 2010). With MOMA's enantioselective column (Table 5.3), DMF-DMA derivatization GC–MS will allow us to quantify robustly and sensitively the presence of an ee. To avoid racemization, the DMF-DMA methylation reaction (typical example in Fig. 5.3b) is programmed to occur at 145 °C (temperature of the capsule eutectic) for 3 min (Freissinet et al., 2010). In this way, we perform a single-step extraction and derivatization of labile (chiral and nonchiral) compounds.

5.6.1.2   Thermochemolysis

While GC of many nonvolatile compounds in space is enabled by derivatization (MTBSTFA and DMF-DMA), the moderate reaction temperature range of $75 - 300$ °C does limit access to refractory and/or insoluble organic material, including macromolecular organics such as kerogen-like compounds. Pyrolysis of such organic matter occurs at much higher temperatures ($800 - 1000$ °C) and results in typically unacceptable fragmentation of the parent molecule due to thermal stress, limiting important identifications. That is the reason why several workers (Challinor, 1989, 2001; Rodier et al., 2005) have introduced thermochemolysis, which is a thermally assisted hydrolysis/methylation technique. It allows the analysis of refractory and/or insoluble matter in complex matrices containing low

amounts of organic material with minimal destruction of the organic material (Geffroy-Rodier et al., 2009). Thermochemolysis is a technique that combines the advantage of derivatization (methylation) without the drawbacks of pyrolysis. Indeed, thermochemolysis with tetramethylammonium hydroxide (TMAH) improves the pyrolysis technique by mild thermal decomposition (hold sample at 600 °C for 40 s) and a selective cleavage of ester and ether bonds rather than random and non-controlled thermal decomposition and fragmentation of the organic material. TMAH thermochemolysis is also included in a small number of sample cups available in the SAM investigation (Mahaffy et al., 2012).

Figure 5.4 demonstrates the complementarity of thermochemolysis with desorption/derivatization (MTBSTFA and DMF-DMA) and pyrolysis at, respectively, lower and higher temperatures. However, this experimental strategy is jeopardized by the competing combustion of organic compounds by oxygen that is released during decomposition of oxychlorine species (up to ~ 1 wt%, Hecht et al., 2009) in the sample. SAM onboard the Curiosity rover uses oxygen detected during EGA experiments as a proxy for the presence of oxychlorine species in soils and sediments (Glavin et al., 2013; Archer Jr. et al., 2016). Based on SAM–EGA data, the oxygen is generally released in a $100-150$ °C-wide temperature window that can move up and down within ~ 200 °C and ~ 600 °C, as indicated in Figure 5.4. Moreover, these data indicate that the abundance levels of oxychlorines in Gale surface samples vary by at least one order of magnitude (Archer Jr. et al., 2016). Thus, clues from different instruments (including MOMA itself) must be used to assess the potential presence and abundance of oxychlorine species in drill samples (Section 5.7.3).

Table 5.3: List of GC columns selected for Mars Organic Molecule Analyzer GC and their main characteristics.

Name (supplier)	Stationary phase	Dimensions L/ID/d_f [m/mm/µm]	Compounds targeted
MXT-Q-BOND (Restek)	Divinylbenzene	25/0.25/8	Inorganic volatile molecules C_1-C_5 organic molecules
MXT CLP (Restek)	Not available from the supplier	25/0.25/0.25	C_4-C_{25} organic molecules
MXT-5 (Restek)	95% dimethylsiloxane 5% diphenylsiloxane	25/0.25/0.25	C_4-C_{25} organic molecules
CP-Chirasil-Dex CB (Agilent)	enantioselective, B-cyclodextrin bonded to dimethylpolysiloxane	25/0.25/0.25	Organic enantiomers

5.6.1.3   Wet chemistry: Storage and release of chemical agents

To be adapted for use in space, each chemical reagent must be stored under a robust hermetic seal to avoid any potential background contamination of the chromatograms. Moreover, as described in Figure 5.4, each wet chemistry technique occurs at different temperatures, from 140 °C for the chiral derivatization up to a maximum of 600 °C for thermochemolysis. To accommodate this range, each reagent has been sealed into a stainless steel capsule. The stainless steel surface has been treated with a Silcosteel® passivating layer to avoid any oxidative attack by the corrosive reagents (MTBSTFA, DMF-DMA,

and TMAH). The Silcosteel® coating is thermally resistant up to 400 °C. The capsule has the following dimensions: external $\varphi = 3.2$ mm, h = 4.3 mm, with an internal volume of about 25 µL. Because each reagent has to be released at a specific temperature, three different eutectic alloys have been implemented to seal the capsule up to a minimal temperature reached by the oven (Fig. 5.5). Thus, MOMA capsules will release DMF-DMA at 145 °C, MTBSTFA/DMF at 221 °C, and TMAH at 309 °C. The reagent is initially loaded into capsules through fine tubing, which is hermetically closed by using a seal welding technique. About 15 µL of each reagent is stored in each capsule.
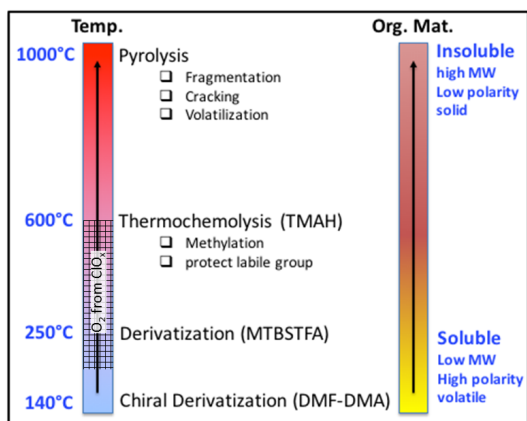

Figure 5.4: Overview of the space-compatible sample treatment for in situ GC–MS analysis. Release of oxygen and chlorine from oxychlorine species in the temperature range 200 – 600 °C (Archer Jr. et al., 2016) competes with MTBSTFA derivatization and thermochemolysis. GC–MS, Gas Chromatography–Mass Spectrometry.
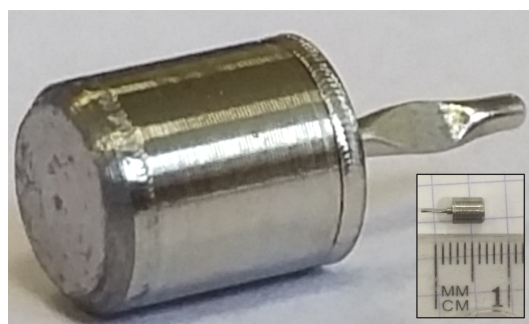
Figure 5.5: Picture of a MOMA derivatization capsule. The inset shows the same capsule next to a metric length scale (the smallest subdivision is 1 mm). The cylindrical container is 4.3 mm high and 3.2 mm in diameter (external dimensions). The 4-mm-long shaft (in the right part of the image) is the remaining part of the filling port.

5.6.2   Gas chromatograph subsystem

Considering the number of organic and inorganic volatile compounds, including isomers, which potentially could be released from a martian sample, mass spectrometry alone is not sufficient to discriminate and identify all molecules. Moreover, mass spectral techniques do not offer the possibility to separate and quantify the relative amounts of enantiomers. For MOMA, a GC was chosen to achieve the requisite additional separation, following the approach used on the Viking landers/GC–MS (Biemann et al., 1977) and on MSL/SAM (Mahaffy et al., 2012). A description of the GC instrument, the basic way it operates, and its current performance is provided here.

5.6.2.1   Design requirements

To meet the MOMA science objectives (Section 5.3), the GC must be able to separate a wide range of organic compounds. The main classes of chemical species to be separated are (i) regular volatile organic molecules consisting of 1 to about 25 carbon atoms;

(ii) organic enantiomers; (iii) species produced from derivatization with the three chemical reactants to be used in MOMA (Section 5.6.1); and (iv) inorganic volatiles. The GC therefore contains four individual column modules, each targeting a specific class of chemical compounds, packaged into a highly constrained instrument volume.

5.6.2.2   Design overview

General architecture.   The MOMA GC (Fig. 5.6) is packaged into a volume of $14 \times 12 \times 20$ cm and a mass of 1.6 kg. It provides all necessary functionality for GC, including injection, separation, detection, carrier gas delivery and flow regulation, fluidic plumbing, and control electronics.
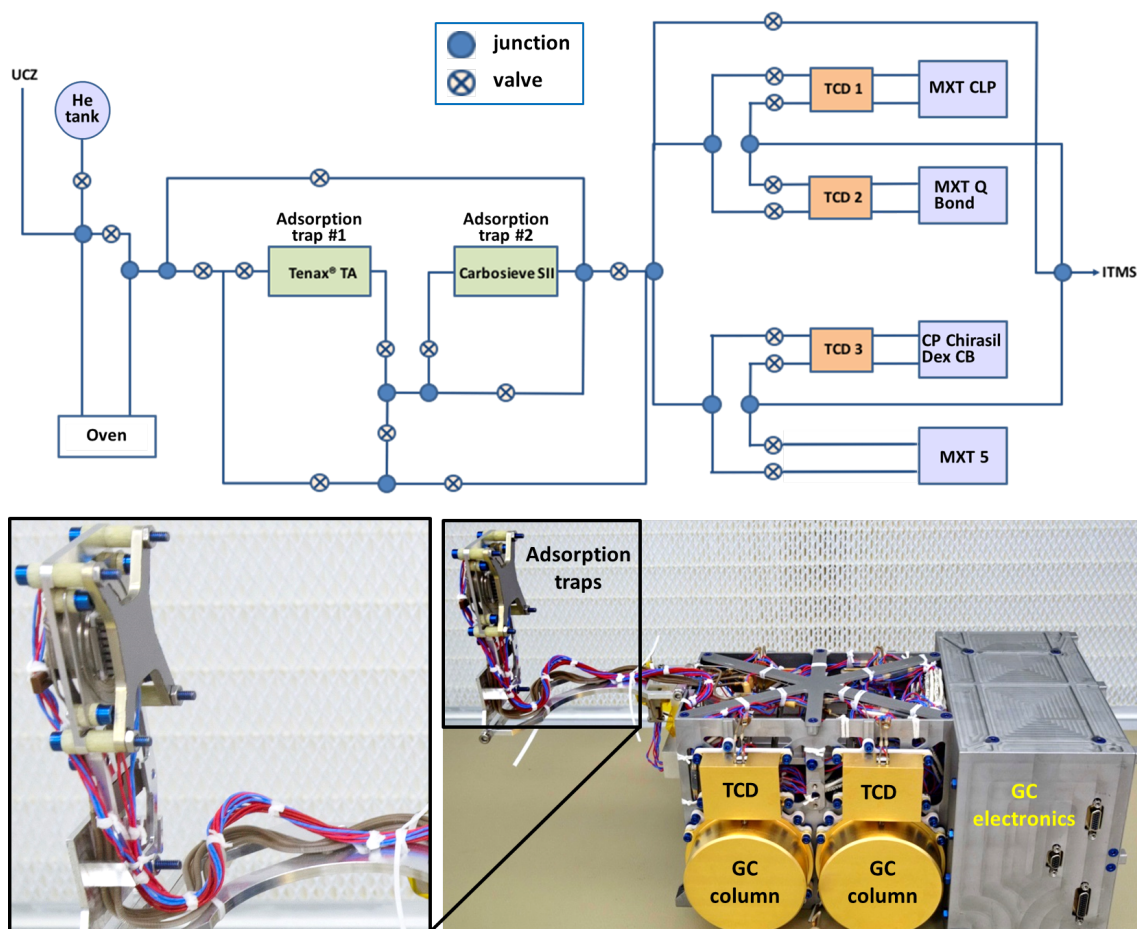

Figure 5.6: Top: Simplified gas flow diagram of MOMA GC. Volatiles derived from the sample are carried by a steady helium flow, trapped, and concentrated in one of the adsorption traps and thermally released in backflush mode. Finally, the volatiles are separated by one of the GC columns (MXT CLP, MXT-Q-Bond, CP-Chirasil-Dex CB, or MXT-5) and detected by both TCD and ITMS, except in the case of MXT-5, where the separated compounds are detected by ITMS only. Bottom: GC QSM as of March 2016 with zoom of the adsorption traps. ITMS, Ion Trap Mass Spectrometer; QSM, Qualification Simulator Model.

Injection system.   To get the best separation of the analyzed compounds, their injection into the separation system (chromatographic columns) should be as brief as possible, generally a couple of seconds in laboratory applications. Direct transfer to a column for the low pyrolysis heating rates of the MOMA ovens (~ 200 °C/min) would result in poor chromatographic resolution and would compromise the analytical capabilities of the GC. For this reason, adsorption/ thermal desorption traps are used on MOMA.

The MOMA design uses two separate complementary traps, each devoted to concentration and injection of a specific range of compounds. Taking into account the chemical species to be analyzed with MOMA, Tenax® GR adsorbent is used to trap most of the organic compounds consisting of more than three carbon atoms, whereas Carbosieve SIII is used for the lightest organic molecules and inorganic volatiles. For each trap, a few tens of milligrams of adsorbent are packed into a 3-cm-long stainless steel tubing with an internal diameter of 1.6 mm.

Temperature control of the traps is provided by a Peltier cooler, holding the traps at ~ 30 °C below the experiment ambient temperature. Targeted volatiles are trapped from the gas evolved from the oven while the trap is cooled to enhance adsorption. Once trapping is done, a dedicated heater brazed to the tubing rapidly raises trap temperatures to 300 °C in less than 15 s. This near-flash heating quickly releases the trapped chemical species to the chromatographic columns to enable a sufficiently short injection time. To further improve the recovery efficiency from the trap, a backflush procedure is used by reversing the helium flow during the desorption step. The gas flow pathway was designed to allow maximum flexibility for injecting the trapped species. While only one trap may be used at a time, each trap can be coupled to any of the four GC columns (eight available analytical combinations).

Separation of volatiles.   MOMA includes four columns (Table 5.3) allowing complementary separation of different compound classes. The 25-m-long × 0.25 mm internal diameter columns are of high chromatographic efficiency (more than 25,000 theoretical plates) while meeting overall resource constraints. Stainless steel column tubing was selected for its robustness and ease of integration with gas plumbing. Each column is integrated into a module (Fig. 5.6), coiled around a cylinder with a dedicated heater to control the column temperature from ambient to 250 °C (for CP-Chirasil-Dex CB (Table 5.3), the temperature may not exceed 220 °C). Both column and heater are imbedded in ceramic glue to ensure robustness and temperature homogeneity of a whole column. A gold-coated cap covers each module for mechanical packaging and thermal control reasons.

Detection of volatiles.   The MS (Section 5.6.4) is used to record the retention time of each compound eluting from the column over a period of 30 min following the injection (see above, "Injection system"). Three of the four chromatographic columns include a TCD that can also measure the retention time of the eluted compounds (Fig. 5.6 and Table 5.3). MXT-5, the most versatile of these four chromatographic columns, is not configured with a TCD for risk mitigation in the event of TCD failure. These TCDs are based on compact micro-electromechanical systems technology with picomole sensitivity. The power requirements of the TCDs are low and their use allows acquisition of a signal with sufficiently fast temporal sampling for peak resolution. In spite of a lower

sensitivity compared with the MS, the linearity of the TCD response will complement the MS measurement to quantify the most abundant compounds released by the samples.

The TCDs are accommodated on a dedicated plate, which is mounted to ensure thermal decoupling between the chromatographic column and the TCD and to provide the 110 °C required by the detectors. However, this operating temperature may present a cold trap for compounds eluting from the columns. For this reason, no TCD is coupled to the MXT-5 column to limit the presence of cold spots in this channel and enable the analysis of more complex organic species that could condense when analyzed with the other modules.

Gas handling system.   The fluidic system of the GC comprises a Gas Tank (GT), one pressure control valve (PCV), 19 on/off valves allowing the selection of different fluidic pathways by a series of valve configurations, and stainless steel tubing (with external/internal diameter of 0.8/0.5 mm) used as plumbing between components (see Fig. 5.6 for a simplified diagram).

The GT contains the carrier gas required for chromatographic analyses. The carrier gas selected is ultrapure helium (99.9999%) as it is the most efficient carrier gas for chromatography (after H_2) and is safe to handle. The GT is spherical (8 cm in diameter) and made of titanium. It contains ~ 150 mL of helium, initially at a pressure of 80 bars.

The PCV allows regulation of carrier gas column inlet pressure, and subsequently the carrier gas flow rate through the column. The pressure can be set from the ambient to about four bars absolute pressure and is controlled by physical measurement of the inlet pressure with a micropressure sensor mounted just after the PCV. A control pressure sensor is also mounted just before the column to get the exact column inlet pressure, which is a key parameter to achieve good separation and to help when analyzing the GC data.

Except for the GT, all components of the GC fluidic system are heated up to ≥ 135 °C (the maximum temperature is controlled by convection and available power) by different heaters of various shapes, depending on the component. The upper mass limit of detectable organic compounds depends critically on the type of the chromatographic column and its temperature ramp (see above, "Detection of volatiles"), as well as the heating of the gas transfer tubing. Overall, the upper mass limit is expected to lie around 300 and 500 u for, respectively, pyrolysis and derivatization runs.

GC–MS coupling campaigns.   To demonstrate the functionality of the GC–MS experiment, the two independent instruments need to be coupled and their performance characterized as a single unit. The coupling campaigns are international efforts and therefore finite-time opportunities to test the interface of hardware, electronics, and software controls at a given point in time for each development effort.

The GC used for the campaign was the QM (qualification model), comprising a hydrocarbon trap as the injector, an MXT-5 column (25 m, 0.25 mm, 0.25 μm, Restek), and a TCD. The GC was coupled with ETU (engineering test unit) of the ITMS. The TCD and analytical column can be heated and their maximum temperature is, respectively, 100 °C and 200 °C. Ultrahigh-purity helium (99.9999%) is used as the carrier gas at a mean 1.1 mL/min flow rate.

In this experiment, volatile compounds contained in a gas mixture (butane, pentane, hexane, and benzene, 1000 ppm each) were used as calibrant standards. A sampling loop of 10 µL allowed for the injection (via an atmospheric inlet) of a known quantity of analyte onto the Tenax® GR trap. The gas mixture was trapped by the Tenax® trap and released at 156 °C. The column temperature was kept constant at 30 °C.

A second liquid calibration mixture was used for injection into the MOMA oven and comprised 5 µL of phenylethanol, 1-butanol, methyl-acetate, hexane, benzene, toluene, dodecane, heptanol, pentanol, fluoronaphthalene, and DMF diluted in 100 µL of pure methanol. For the liquid mixture, a volume varying from 0.05 to 0.1 µL was injected in the MOMA oven at ambient temperature. The oven was sealed and heated to 350 °C under helium flow and volatiles were trapped by the Tenax® GR adsorbent. Finally, the Tenax trap was rapidly heated up to 300 °C and the volatilized sample was injected in the GC column. The column temperature was ramped from 30 °C to 200 °C with a ramp rate of 15 °C/min. Figures 5.7 and 5.8 show the signals acquired during both experiments.
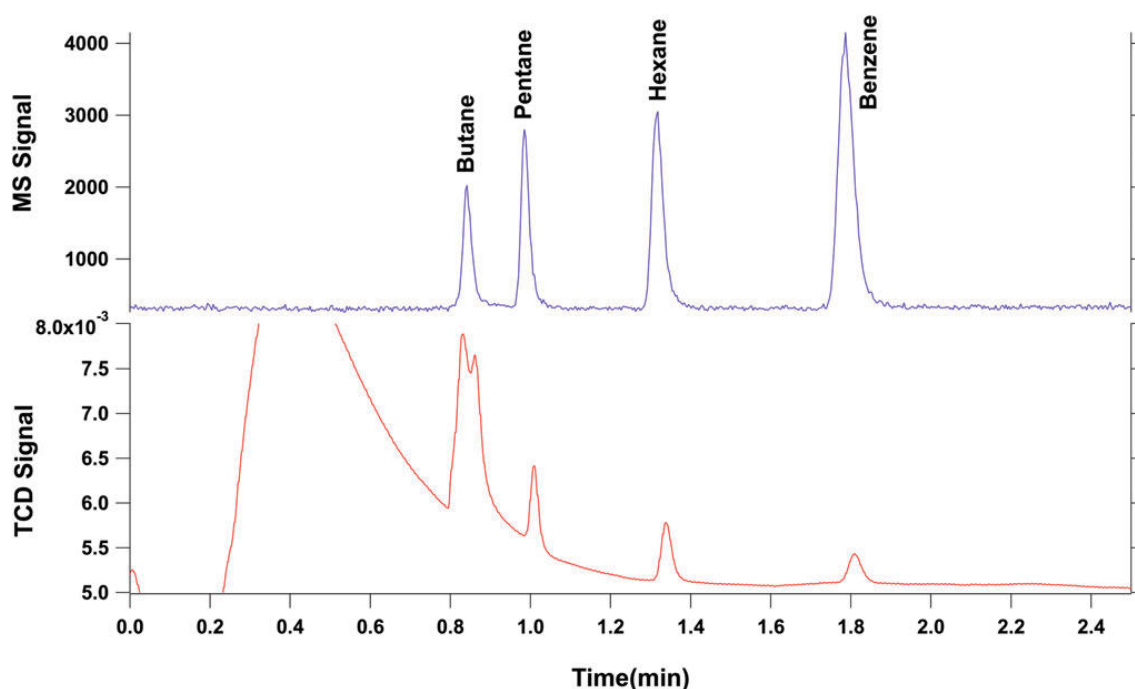

Figure 5.7: Separation of volatile compounds (butane, pentane, hexane, and benzene). The chromatogram obtained shows good separation of the four compounds injected in both the MS (above) and TCD (below) signals. The double peak observed on the TCD signal at a retention time of 0.85 min is due to the presence of air, which is not observed by the MS as it is below its mass range. MS, Mass Spectrometer.

In conclusion, we successfully demonstrated the first end-to-end GC–MS coupling tests with a QM GC (including high-fidelity oven) and ETU MS. Gaseous and volatile calibration compounds were successfully separated and detected in GC–TCD mode and in GC–MS mode as well. Limits of detection have been determined and a value under the pmol/mm^2 level has been obtained for each analyzed compound, as required for MOMA.
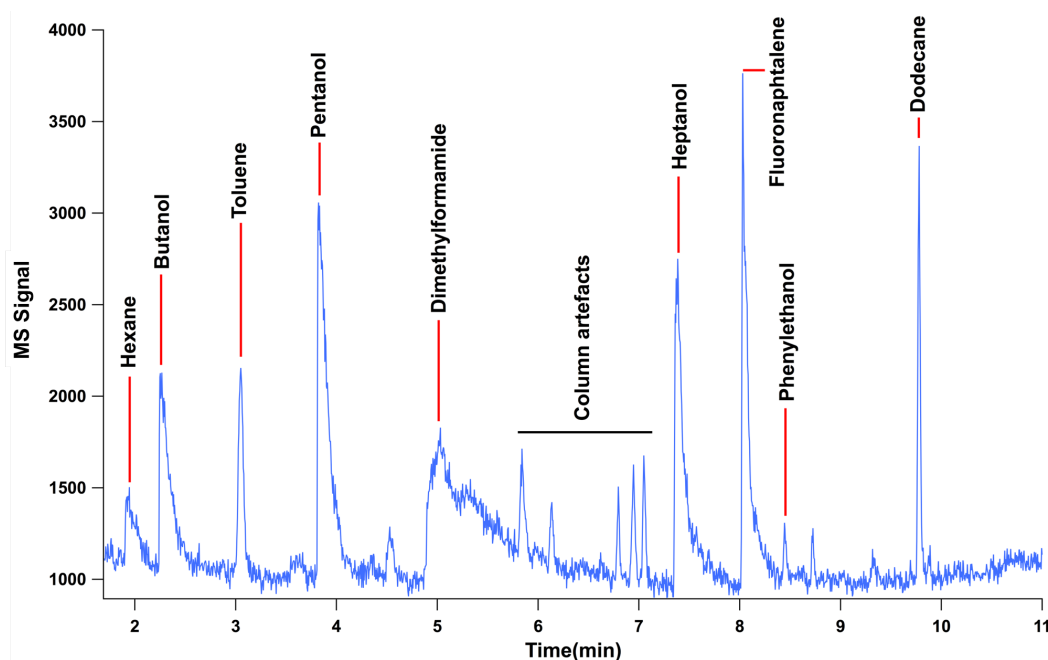
Figure 5.8: MS chromatogram for separation of the mixture of phenylethanol, 1-butanol, methyl-acetate, hexane, benzene, toluene, dodecane, heptanol, pentanol, fluoronaphthalene, and dimethyl-formamide diluted in methanol. Methyl acetate and methanol were not detected by the MS since these molecules (or their heaviest fragments) have masses below its mass cutoff set to $m/z \sim 40$.

5.6.3 Laser subsystem

The laser subsystem serves as the ionization source in the LDMS mode of operation. It has been designed to efficiently desorb and ionize primarily nonvolatile, high-molecular-weight organic molecules in the crushed rock samples delivered by the SPDS, while minimizing thermal and photochemical alteration/degradation effects on the sample.

5.6.3.1 Design requirements

MS subsystem (LDMS mode) requirements (Section 5.6.4.1) are the primary drivers for the design of the laser subsystem. Specifically, a short pulse width ($\tau_P \approx 1$ ns) UV ($\lambda = 266$ nm) laser was selected due to its efficiency in desorbing and ionizing organic molecules and thus enabling their sensitive mass spectrometric detection. Aromatic compounds, in particular, are readily ionized by the laser as they exhibit strong absorption near 266 nm wavelength. The laser is incident onto the sample at 44° relative to surface normal and is focused to ≈ 400-μm-diameter (slightly elliptical) spot on the sample surface. The laser pulse energy on the FM laser is expected to be adjustable from 13 to 130 μJ, which approximately translates into peak beam irradiance of 35 to 250 MW/cm². The laser is capable of emitting bursts of up to 50 laser pulses at a 100 Hz repetition rate, within a thermally limited average repetition rate of 2 Hz. The tunability of both the average pulse energy and the number of laser pulses within a burst is critical in ensuring that an appropriate amount of ions is injected into the ion trap, preserving optimal mass spectral performance of the MS subsystem (see LDMS mode automatic gain control description in Section 5.7.4). A detailed list of laser subsystem requirements is given in Table 5.4.

Table 5.4: Performance requirements for the laser subsystem.

Specification	MOMA Laser
Output wavelength	266 nm
Pulse energy	$13 - 130\ \mu J$
Pulse duration (FWHM)	< 2.5 ns
Beam quality	$M^2 < 4$
Burst repetition rate	100 Hz
Burst laser shots	≤ 50
Avg. repetition rate	2 Hz
Spot size (on sample)	$\approx 400\ \mu m$
Peak irradiance (on sample)	> 30 MW/cm2
Peak fluence (on sample)	> 60 mJ/cm^2
Lifetime	10 Mshot
Operational T	$- 50\ °C$ to $+ 25\ °C$

MOMA = Mars Organic Molecule Analyzer.

5.6.3.2   Laser architecture

The laser subsystem comprises the Laser Pump Unit (LPU) and the LH. The LPU is mounted on the main electronic box (MEB; Section 5.6.4.4) and contains all laser electronics as well as the pump diode outputting 70 W peak optical power for $\sim 140 - 200$ ms at the center wavelength of $\lambda = 806$ nm. The pump diode output is fiber-optically coupled into the LH mounted on the side of the MS housing (Fig. 5.1). It pumps an Nd:Cr:YAG crystal within a compact passively Q-switched oscillator cavity in the LH that emits ≈ 1.5 mJ of $\lambda = 1064$ nm laser pulses with a pulse duration of $\tau_P \approx 1 - 2$ ns. The output pulses are frequency quadrupled to $\lambda = 266$ nm by two frequency conversion stages, spectrally filtered by dichroic mirrors, and a small fraction of the UV output sampled by a calibrated internal photodiode, thus enabling energy monitoring on a pulse-bypulse basis during LDMS operations. The balance of the UV beam is sent onto the sample located in the UCZ through an external beam steering unit and a Brewster-angled laser window, which hermetically seals the rover's UCZ, yet provides optical access. A slow-focusing optic in the LH ensures the projected beam spot size of $\approx 400\ \mu m$ on the sample and sufficiently large focal depth to accommodate a crushed and leveled sample surface expected to exhibit a typical surface roughness of $< 200\ \mu m$. The output pulse energy is adjustable down to 10% of the maximum output energy and is achieved through thermal tuning of the frequency conversion crystals. More detailed information on the MOMA laser optical layout and design can be found elsewhere (Kolleck et al., 2010). Overall, laser/optomechanical design is capable of withstanding mission's shock and vibration requirements as well as maintaining laser to MS ion inlet tube axis alignment (Section 5.6.4.2) within ~ 0.5 mm, driven by the tolerance of the ion sampling off the MS inlet axis.

5.6.3.3 Verification data

A flight-like ETU laser subsystem (Fig. 5.9) has undergone extensive characterization and verification process in both a stand-alone configuration and mounted to the MS FM. Temperature tuning of the frequency conversion crystals has been demonstrated to vary the UV output energy of the ETU laser from 21 to 260 μJ, yielding peak irradiance at the sample location ranging from 50 to 450 MW/cm^2. A representative beam profile projected 44° onto the sample location for the *highest* output pulse energy is shown in Figure 5.9 and indicates a full-width tenth-maximum spot size of $\approx 400 \times 200$ μm at the sample.
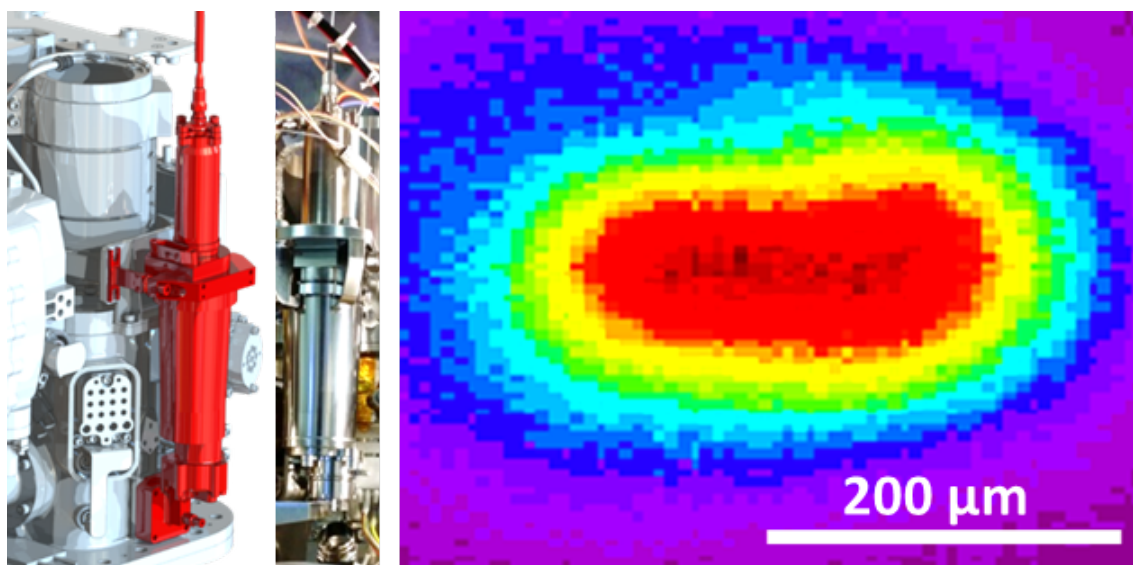

Figure 5.9: Left: MOMA laser subsystem highlighted in red: LH mounted to the side of the MOMA-MS housing (Fig. 5.1). Middle: Photograph of the ETU LH and (right) UV beam profile at the sample location for high-energy output of the ETU laser. ETU, Engineering Test Unit.

The FM laser is expected to inherit most performance characteristics of the ETU laser, with the largest difference being the output derating to $35 - 250$ MW/cm^2 due to intense ion generation from most realistic samples when laser intensities exceed ≈ 250 MW/cm^2.

5.6.4 Mass spectrometer subsystem

The MS subsystem of the MOMA instrument serves to collect, manipulate, and detect ionized particles based on their respective mass-to-charge (*m/z*) ratios. As described above, the MOMA-MS subsystem supports two independent, but highly complementary, modes of operation: (i) GC–MS of gases derived from the pyrolysis of crushed rock powder and (ii) LDMS of sample fines deposited into a refillable tray. Multiple copies of the MS subsystem have been designed, built, and tested with progressive technical maturity, beginning with proof-of-concept prototypes, advancing to the ETU, and culminating in the actual FM and viable Flight Spare (FS). A brief introduction to the driving requirements and basic design of this subsystem is described here; more details can be found in the work by Arevalo et al. (2015).

5.6.4.1   Design requirements

Derived from the original Level 1 Science Objectives of the ExoMars rover mission, a number of specific functional requirements were flowed down to the MS subsystem. Of these requirements, which define key characteristics of the instrument such as acceptable/unacceptable vibration resonances, shock responses, and thermal limitations, the driving requirements for both modes of operation are provided in Table 5.5. Because each mode of operation targets a specific category of biosignature (although with some overlap), each mode carries distinct performance requirements, such as mass range, sensitivity (limit of detection), and mass resolution. These metrics must be verified experimentally through testing of the FM (and FS) across a range of pressures and temperatures representative of those likely to be encountered on the martian surface.

Table 5.5: Performance requirements of MOMA-MS subsystem.

Specification	Pyr-GC–MS Mode	LDMS Mode
Targeted biosignatures	Volatile organics (e.g., alkanes, amines, alcohols, carboxylic acids)	Nonvolatile organics (e.g., macromolecular carbon, proteins), inorganic species
Mass range	50 – 500 u	50 – 1000 u
Limit of detection	$\leq$ nmol analyte[1] (SNR^3 > 10)	$\leq$ pmol/mm^2 analyte[2] ($SNR^3 \geq 3$)
Resolution (FWHM[4])	$\leq$ 1 u	$\leq$ 2 u
Single scan dynamic range	$\geq$ 100 over 50 – 1000 u	
Mass isolation	$\pm$ 5 u precision over 50 – 1000 u	
Accuracy	Observed mass $\pm$ 0.4 u actual mass	
Instrument drift	< 0.4 u over 30 min	
Operational P	4 to 8 torr of Mars atmosphere	
Operational T	$-$ 40 °C to $+$ 20 °C	
Non-op T	$-$ 50 °C to $+$ 60 °C	
Survival T	Up to $+$ 145 °C	

[1] pyr-GC–MS analyte: PFTBA.
[2] LDMS analytes: Rhodamine 6G and Angiotensin II.
[3] SNR of mass peak.
[4] FWHM of mass peak.
  FWHM = Full-Width Half Maximum; PFTBA = perfluorotributylamine; SNR = Signal-to-Noise Ratio.

5.6.4.2   Analyzer architecture

To realize the science objectives of the mission, particularly the characterization of martian (near-)surface materials through LDMS, the MOMA instrument centers around an ion trap mass analyzer. Quadrupole Mass Spectrometers (QMSs), such as those flown to the Moon (via LADEE), Mars (via Curiosity rover and MAVEN), and Saturn (via Cassini–Huygens), require high vacuum to achieve performance ($< 10^{-6}$ torr). In contrast, ion traps thrive at higher operating pressures ($\sim 10^{-3}$ torr); thus, this class of analyzer more easily accommodates LDMS operations at Mars ambient pressures. In addition, the MOMA ion trap is 5x smaller in volume than the QMS onboard Curiosity and more than 2.5x smaller in volume than the miniaturized QMS onboard LADEE, MAVEN, and Cassini–Huygens. Because ion traps inherently serve as ion storage devices, the MOMA MS is also capable of conducting advanced ion manipulation experiments, such as SWIFT

(Stored Waveform Inverse Fourier Transform) ion excitation and tandem Mass Spectrometry (MS/MS), both techniques are described further below.

Linear Ion Trap assembly. In contrast to a traditional Paul ion trap (or 3D type), a Linear Ion Trap (LIT, or two-dimensional type) offers two symmetrical ion injection pathways along the long axis of the rod assembly, thus reducing space-charge effects and enhancing trapping efficiency. As a consequence, the MOMA MS employs an LIT analyzer to directly support both GC–MS and LDMS modes of operation. The MOMA-MS LIT comprises four hyperbolic rods situated in parallel with one another, two solid and two with slits down the lengths of their vertices, and two end plates. Defined by an $r_0 = 3$ mm (the distance between the solid rods and the central axis of the rod assembly), the MOMA-MS dual-source LIT is a miniaturized (1:4 scale by volume) version of the Thermo Fisher LTQ design. Compared with a Paul trap with a similar physical volume, the LIT leveraged by MOMA offers the following analytical advantages: i) increased ion storage volume and, by extension, reduced space-charge effects; ii) higher trapping efficiency (increased sensitivity); and iii) redundant detection sub-assemblies as ions are ejected radially through two slit rods. Moreover, the mechanical design and implementation of the MOMA LIT draw strongly from heritage QMS rod assemblies, which are bound by comparable engineering requirements, machining tolerance levels, and assembly logistics.

Detection channels. As outlined above, the MOMA LIT ejects ions radially during mass scanning, allowing two detection channels to be situated around the analyzer; these channels may be activated simultaneously to maximize sensitivity or individually as fully redundant elements (thereby doubling the operational lifetime of the instrument). Each detection assembly consists of a stainless steel conversion dynode, which converts ions ejected from the LIT into electrons, and a Channel Electron Multiplier (CEM, Photonis Spiraltron 4219) that collects the electrons generated by the dynode and amplifies them into a detectable current pulse. Both detection chains are shielded from stray electrons and ions to establish low noise floor and improve limits of detection.

The potential of each CEM may be varied from -1.8 to -3.0 kV to maximize electron gain over the life of the device, but the dynode potential is held constant at -5 kV. The high-voltage stability of each detection channel was verified at the operational pressures of the LIT ($\sim 10^{-3}$ torr). The detection system has been shown to have a maximum count rate of $10^6 - 10^7$ counts per second.

Electron Ionization Source. When neutral effluent derived from the GC is introduced into the MOMA MS, the gas is ionized by an Electron Ionization Source (EI) with redundant electron gun assemblies. This source is a near-replica of the closed EI sources flown on LADEE/MSL/ MAVEN. Each fully operational electron gun relies on a 0.003 inches diameter W:Re (97:3) filament to generate $10 - 100$ µA of emission with an average electron energy of 70 eV. Each filament is accompanied by a series of ion lenses that serve to focus and direct the beam of electrons toward the neutral gas. An independent stack of lenses accelerates the ion products into the LIT for mass analysis. During mass scanning, the electron beam is gated off by switching the applied voltage on two of the electron gun lenses.

Fast-actuating aperture valve. A pull-type aperture valve, inspired by the discontinuous atmospheric pressure inlet valve design pioneered by researchers at the University of Purdue, was developed specifically for the MOMA instrument (Gao et al., 2008). Coupled with the high-pressure operation of the LIT, fast actuation (< 20 ms to open or close) of this solenoid-driven valve enables LDMS operations at Mars ambient pressures (i.e., 4 to 8 torr, primarily CO_2). Specifically, ions enter the instrument and are trapped at an elevated pressure in the 10 s of mtorr. This pressure serves to help cool the ions and promotes very efficient ion trapping. After the aperture valve closes, the Wide-Range Pump (WRP; see below, Paragraph "*Wide-Range Pump*") evacuates the extra gas in the MS housing down to a total pressure < 0.5 mtorr. This low-pressure environment is both safe to turn on the CEM and dynode high voltages and ideal for collecting a high-quality mass spectrum. As a result of this experimental sequence, the MOMA instrument circumvents the need to hold the sample at vacuum, saving considerable mass, volume, and power that would have been required to implement a vacuum seal.

The aperture valve supports vacuum during clean-up mode bakes, ensures constant pressure during pyr-GC–MS testing, and facilitates the dynamics of ion transport (from the irradiated sample surface into the LIT) and rapid pump down during LDMS operations. A sliding ball creates a vacuum-tight seal when compressed against a stationary seat in the valve, which is designed to fail in the closed position as an operational safety. The ETU version of the MOMA aperture valve demonstrated an operational lifetime well in excess of 30,000 actuations while ensuring a leak rate of $\leq 10^{-6}$ mbar L/s of helium.

Micropirani pressure sensor. Because the MOMA MS operates at fundamentally higher pressures than heritage QMS instruments, a micropirani pressure gauge (based on a commercial Heimann transducer) was qualified for the ExoMars mission. This device, defined by two temperature- and pressure-sensitive resistors contained within shared silicon housing, operates at pressures ranging from 10^0 to 10^{-6} torr and consumes on the order of ~ 0.5 mW (Völklein et al., 2013). Although the response time of the gauge is limited by its heat capacity, which dictates the time required for the resistors to reach equilibrium, a physics-based algorithm enables the sensor to accurately predict pressures under dynamic conditions associated with LDMS operation at Mars ambient pressures. Pressure changes with time constants of ≤ 0.25 s have been tracked down to 0.5 mtorr with a relative error of $\leq 3.4\%$ (2σ; Southard et al., 2014).

Wide-Range Pump. The MOMA WRP employs the same core design as the two 100 krpm WRPs now operating successfully on Mars aboard the SAM suite on MSL. The WRP consists of a molecular drag pump in series with a turbomolecular pump designed to exhaust to ambient Mars pressures (qualified for the range 4 to 8 torr). MOMA utilizes a single WRP with a pumping speed of ~ 4 L/s and a compression ratio of 10^8 for N_2 to provide (1) consistent pumping efficiency against a constant helium flow for GC–MS mode and (2) a dynamic pump down environment for LDMS mode.

5.6.4.3 Temperature control

The MOMA instrument resides within a protective cavity held at Mars ambient pressures in the rover's ALD, thus heat transfer is dominated by thermal conduction rather than

forced convection. As a result, the instrument relies on mechanical contact with the upper and lower decks of the ALD for thermal control. With an array of heaters and thermal straps, the MS subsystem employs four thermal zones to control the temperatures of the sample path and critical hardware elements, including the manifolds (Zone 1); ion trap and mechanical housing (Zone 2); WRP (Zone 3); and plumbing lines (Zone 4).

To enable science operations, the WRP (Zone 3) must first be heated to $+ 25\,°C$ before the rotors can begin to spin; this heating step initiates both GC–MS and LDMS experiments. During GC–MS operations, Zones 1 and 4 are also activated to achieve $\geq 135\,°C$ along the sample path, extending from the GC column to the ion trap analyzer. In contrast, during LDMS operations, no hardware is heated actively other than the WRP. In between science experiments, Zone 2 may be engaged opportunistically for clean-up operations to bake out accumulated volatile contamination within the sensor. The temperatures of optical components within the LH are managed by a separate service; thermal manipulation of this cavity serves to control the output energy of the laser.

5.6.4.4   Driving electronics

The driving and control electronics for MOMA are generally broken up into two electronic boxes to allow optimal accommodation in the ExoMars rover and to provide efficient delivery of relevant signals to the sensor. These electronic boxes were built and developed through collaboration between GSFC, Space Physics Research Laboratory at the University of Michigan, and Battel Engineering.

The MEB houses the primary power supply (PS), command and data handling board (CDH), motor and analog interface (MAIF), and LPU. The PS takes in the bus power from the rover and distributes it to various components of the instrument. The CDH houses the main computer that controls all of the MOMA subsystem operations and sends the acquired data and telemetry back to the rover. The MAIF controls the WRP, the various valves that are part of the MS, GC and LDI (Laser Desorption and Ionization) inlet, the micropirani pressure gauge, and the heaters that are part of the MS and its GC inlet. Finally, the LPU provides the diode pump pulse and control and monitoring of the physical LH that is mounted to the MS housing.

The secondary electronic box (SEB) houses the control board (CTL), power and high-voltage (PH) board, and filament bias (FB) board. The CTL contains all of the low-level MS control electronics that handle the sequencing, monitoring, and signal counting necessary to perform the ion trap MS experiment. The PH and FB boards together provide all of the lens voltages that are necessary to generate, trap, and detect ions from the MS.

There are a few other smaller distributed pieces of electronics necessary to complete the operation of MOMA. Specifically, the GC contains its own set of control electronics that interface to the CDH to receive instruction and provide data and telemetry back to the central control computer. There is also a separate RF (Radio Frequency) PS to provide RF voltages to the rods necessary to trap and eject ions in the ion trap. The RF supply is physically mounted to the MS housing to minimize power losses and optimize efficiency. Finally, there is a dedicated set of detection electronics with two duplicate circuits (one for each detection channel) that amplify and discriminate the pulses generated by the CEMs and feed counters in the CTL. The detection electronics are also physically mounted to the MS housing to reduce the signal-out cable length and minimize noise and signal loss in these very low-level signals.

5.7   Operation of MOMA on the surface of Mars

5.7.1   Expected measurement scenarios

The ExoMars rover will physically and chemically characterize the martian terrain encountered during a nominal 218 sol Reference Surface Mission (RSM). The RSM comprises two types of scientific and engineering sequences: experiment cycles and vertical surveys. During an experiment cycle, anticipated to last $13-18$ sols, the rover will (1) traverse to a pre-identified location of interest based on orbital and rover data, (2) perform a full measurement cycle, and (3) transmit all of the scientific, housekeeping, and navigation data to Earth. Within a measurement cycle, crushed powder is produced from a drill sample and delivered to the refillable sample tray (a.k.a. refillable container) inside the UCZ. Before sample analysis by MOMA, the MicrOmega and RLS instruments will conduct contextual measurements of mineralogy and organic functional groups that may be present (Vago et al., 2017). In cases where uplink and downlink schedules permit a tactical response during the science operations cycle, quicklook snapshots of these data may be used to select or tune the MOMA analytical approach.

Following special, high-priority experiment cycles, the mission may elect to perform a vertical survey to obtain deep samples. A minimum of two vertical surveys are allocated in the RSM. The purpose of the vertical survey is to fully characterize the martian soil's geochemical and organic distribution as a function of depth, particularly to characterize the ratio between organic and oxidant molecules. This vertical survey obtains crushed regolith samples from depths of 0 (i.e., surface-bounded), 50, 100, 150, and 200 cm and delivers these samples to each of the analytical laboratory instruments. MOMA will provide information on organic content through LDMS and GC–MS modes described below.

5.7.2   Sequenced operational modes

The MOMA instrument can perform complementary experiments, independently or sequentially, to analyze the martian soil (Fig. 5.10). The two modes are LDMS and GC–MS. GC–MS offers two types of sample analyses (pyrolysis and wet chemistry) that allow MOMA to target specific molecules such as volatile compounds, polar compounds, or macromolecules. MOMA examines solid crushed sample exclusively; it does not include atmospheric analyses. LDMS desorbs and analyzes only the outer surface (μm scales) of sample grains. In GC–MS mode, the ovens (pyrolysis or wet chemistry) receive $\sim 100\,\text{mm}^3$ of loosely packed sample. By design, MOMA's analytical capabilities are not applied to the very same sample, but only to different aliquots of a given crushed drill core. The extent of MOMA analysis of a sample depends on tactical science decisions in concert with the mission team. Nominally, LDMS is the first MOMA mode to be applied to a given sample (referred to as subsample #1). This will give us information about the sample's potential organic content. In particular, LDMS targets heavier nonvolatile compounds that may be present in the martian sediment. LDMS additionally provides information about the presence or absence of labile hydrogen and polar compounds. LDMS results will thus drive the decision of performing GC–MS analysis.

If pyrolysis GC–MS is to be performed (subsample #2), several GC parameters have to be chosen, including column and trap type, temperature ramp profile, and carrier gas
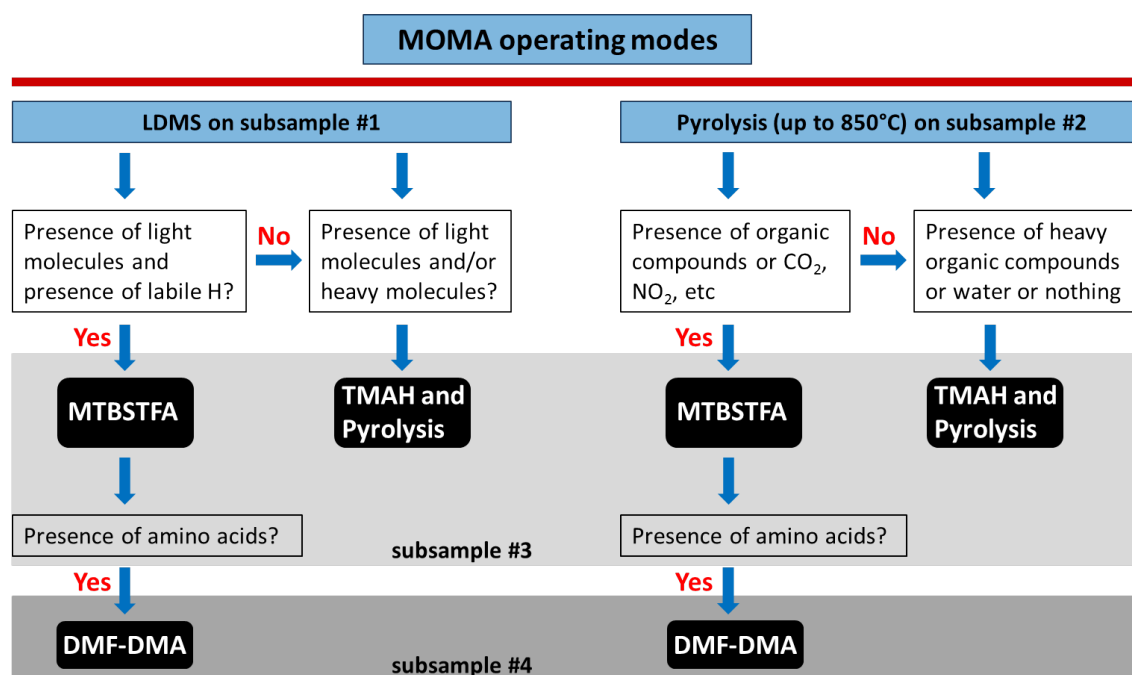
Figure 5.10: Flow diagram for MOMA operating modes. Quick survey analyses will only use subsample #1. Experiment cycles and vertical surveys will use subsamples #1 and #2 and, depending on quick assessment of the data, also subsamples #3 and #4. Direct detection of CO_2 and NO_2 (mentioned in the flow diagram) may or may not be possible, depending on the mass cutoff of the MS.

pressure. The column and trap choices will depend on the kind of molecules present (low-mass volatile, chiral, or refractory compounds). These options will depend, in part, on initial results from the LDMS analysis.

If labile and/or polar compounds are found in the subsample, then an additional subsample (#3) may be analyzed by using a derivatization or thermochemolysis reagent. Such a decision would be discovery driven and made in the context of all mission science data and operational reviews. A sample sufficiently rich in bound water (e.g., clay minerals) could inhibit the MTBSTFA or DMF-DMA reaction if release temperatures were comparable. In this case, TMAH, which is relatively immune to water, could be chosen. Otherwise, MTBSTFA would be used. If the MTBSTFA reaction leads to detection of amino acids in the sample, an additional subsample (#4) could be used with the DMF-DMA reagent to allow a chiral separation in conjunction with the enantioselective GC column (CP-Chirasil-Dex CB).

If heavier compounds such as macromolecules are detected, then thermochemolysis and pyrolysis would likely be used to reach the most refractory compounds of the sample (Fig. 5.10).

5.7.3 Synergy with other instruments

The samples most likely to contain undegraded organic molecules, as they have been protected from cosmic and UV radiation, will be deep drill samples. Therefore, the decision to drill as taken from WISDOM radar data (Water Ice Subsurface Deposit Observation on Mars; Vago et al., 2017) will affect overall operational decisions made by MOMA. The most extensive MOMA investigations will probably be performed on these samples.

The presence of water and hydrated minerals as detected by the various instruments on the rover (Vago et al., 2017), ISEM (infrared spectrometer for ExoMars), Ma_MISS (Mars Multispectral Imager for Subsurface Studies), MicrOmega, ADRON (Active Detector for gamma Rays and Neutrons), and RLS, will affect the experimental strategy in different ways. Most surface samples analyzed to date do contain oxychlorine species (including perchlorates and chlorates) at various abundance levels (probably ranging from almost zero to a few wt%). If the NIR reflectance as measured by MicrOmega is indeed consistent with concentrated perchlorate (Morris et al., 2009; Cull et al., 2010), then only LDMS experiments may be performed, possibly followed by low-temperature GC–MS experiments. However, if no traces of hydrated oxychlorines can be detected and if most water is apparently held by other hydrated compounds (such as smectites or sulfates), default MOMA experiments will be conducted. In any case, excess water from the sample is generally unsafe for the instrument; as such, preheating of the sample will be necessary, with the disadvantage of some volatile organic molecules potentially being lost. Preheating to remove water might also be necessary when operating MOMA in the derivatization mode (MTBSTFA, DMF-DMA) if the water is not removed during the default temperature rise to the melting point of the capsule.

5.7.3.1 Data interpretation

Information on minerals as provided by the above listed instruments will affect the interpretation of LDMS data. Raw LDMS data comprise a mix of peaks originating from both organic and inorganic molecules. Any information on the sample's mineral content will help more completely identify which peaks in the spectra originate from minerals and zero in on organic signals. Spatially precise mineralogical data obtained by MicrOmega and RLS will support MOMA LDMS point-bypoint analyses (typically $5-10$ adjacent RLS spots and $10-20$ MicrOmega pixels will span the ellipse probed by MOMA LDMS). In addition to any inorganic signal, MicrOmega and RLS are expected to provide information on organic molecules.

In case of the detection of indigenous martian organic molecules by MOMA, the overall geological context such as the depositional environment, including mineralogy from outcrop to grain scale, will be of great importance (Siljeström et al., 2014). This will provide further constraints on the abiotic versus biological origin of these molecules. Although some specific organic molecules might act as biosignatures on their own, for example, amino acids in ee or hopanes, many organic molecules, for example, PAHs or macromolecular carbon (known to occur on Mars and in martian meteorites, Steele et al., 2012; Freissinet et al., 2015), might be part of meteoritic infall or may have formed by abiotic processes on Mars or even by diagenetic breakdown of biological molecules. Therefore, any information provided by other instruments on the rover will be key to the interpretation of the origin of the organic matter. For example, PanCam (panoramic cam-

era system) together with ISEM, ADRON, and CLUPI (CLose-Up Imager) will provide the overall geological context of the sample location on Mars (Vago et al., 2017), and although MOMA might provide some information regarding mineralogy, other instruments on the rover are better equipped to do so, such as ISEM on the outcrop scale, Ma_MISS from the drill hole, and MicrOmega and RLS on the single-grain scale. All three ALD instruments will probe the same delivered subsample, providing in situ correlation between data from these instruments.

Even in the case of detection of a clear biosignature, such as a hopane, the direct connection of this signature with a morphological feature as spotted by either CLUPI or MicrOmega will strengthen the case for biology. In addition to the mineralogical context, RLS will also help MOMA in detection and characterization of any organic matter in samples (Edwards et al., 2012, 2013). In particular, it can help assess crystallinity and thermal maturity of any macromolecular organic matter. Any information on the organic content from MOMA will be important to decide if the rover should stay at the current location or move on to another area.

5.7.4 LDMS operations on Mars and test experiments on LDMS prototype system

MOMA's LDMS mode (Li et al., 2017) provides a rapid and essentially nondestructive method to analyze the higher-molecular-weight (up to 1000 u) organic content of a crushed sample before detailed analysis by pyrolysis GC–MS. The LDMS experiment consists of the following major steps: (1) LDMS analysis of the MOMA calibration target at a fixed laser energy, (2) rotation of the carousel to a designated sample location in the refillable container, (3) LDMS analysis under an autonomous ramp of increasing laser shot count and pulse energy, and (4) repetition of (2) and (3) for at least two addition sample locations. Alternatively, the number of sample locations could be increased to 10, providing more coverage and/or finer analysis at the cost of fewer spectra obtained per location. The autonomous ramp is a type of automatic gain control (AGC) for LDMS. Laser desorption/ionization typically exhibits threshold behavior: signal levels increase exponentially immediately above a sample-dependent threshold laser fluence. Sample factors that impact the threshold fluence include chemical composition (matrix), morphology, and microstructure, with mixed-phase samples exhibiting more diffuse threshold behavior than simple and homogeneous samples. Optimal performance of MOMA when ion signals exceed the background sufficiently for detection, but do not overfill the trap capacity, is realized slightly above the LDI threshold. The laser AGC algorithm includes a data-dependent feedback loop that adjusts the laser energy as well as the number of pulses per spectrum based on the appropriate ion count. No human intervention or operational delay is needed.

LDMS data are acquired autonomously during a sample run comprising several hundred individual mass spectra produced from a few thousand laser pulses. After data collected during the most recent sol are downlinked to the ExoMars science operations center, the MOMA science team will have an opportunity to provide a preliminary processing step to generate quicklook products suitable for rapid decision-making. Aside from basic health and quality checks, LDMS data will be reviewed for general features of interest, and a consensus decision will be made to recommend one of three potential next

steps: (1) pursue a detailed follow-up LDMS investigation of a set of individual peaks or mass-to-charge ranges of interest by SWIFT isolation and MS/MS fragment analysis (Li et al., 2017), (2) investigate the organic composition further by delivering sample from the crusher to a pyrolysis oven for the MOMA GC mode, or (3) defer or end the investigation of the current sample in favor of further analyses by other ALD instruments and/or continued rover operations in pursuit of a new sample. Option (1) would likely be invoked for a rich mass spectrum that exhibited one or several high-intensity peaks at mid- or high-molecular-weight matching patterns consistent with organic composition. Option (2) would most likely be implemented as a subsequent experiment following SWIFT and MS/MS or for a sample that exhibited a broadly rich sequence of peaks across the LDI mass range. Option (3) would most likely be pursued in the case that few features were observed in LDI mode and it was deemed in the mission's interests to conserve consumable MOMA resources, such as ovens or carrier gas. In the case where the Raman or MicrOmega spectrometers subsequently identified additional points of interest on the sample that were also within the MOMA laser field of view, Option (3) could also result in a return to LDMS runs on the same sample.

During development of the relatively new application of Mars ambient LDI of mineralogic samples using the MOMA LIT, a library of test data acquired by using natural and synthetic analog samples has been started. This process is based upon empirical comparisons of spectra of mineral matrices with and without organic spikes, built up from simple combinations using pure phases. Previous work has demonstrated that LDI enables detection of trace amounts (ppmw levels) of complex organics at fine scales in mineral matrices, even in the presence of 1 wt% of perchlorate salt (Li et al., 2015).

Figure 5.11 shows LDI mass spectra for another example: a chlorite mineral spiked with 0.01 wt% coronene. Chlorite clays are of high interest for potential detection on Mars and in particular could be a pointer to burial, and organic preservation, processes if found in a bedding relationship with smectite clays, already identified at Oxia Planum (Section 5.1). Coronene is readily detected at this concentration level at low-to-moderate laser pulse energies relative to the MOMA laser range (see also Li et al., 2017). The mass spectrum of the spiked sample showed a dominant base peak associated with the molecular ion of coronene at m/z 300. Data from the pure chlorite powder under the same laser conditions confirm that the mass signature at m/z 300 arises solely from organic parent ions without significant interference.

Other types of mineral phases can yield a host of inorganic molecular ions, primarily cation oxide clusters, under moderate fluence laser desorption, for example, Fe_x and Fe_xO_y from magnetite or Mg_xO_y and $Mg_xSi_yO_z$ from forsterite with x, y, and z being small integers (Goetz et al., 2016a, 2017). These clusters serve to probe the sample's mineral composition and can be used to identify minor phases as well as provide a localized association with any detected organics. When a putative organic compound is identified in such an LDMS matrix background, techniques such as SWIFT and MS/MS may be employed to isolate it to minimize any potential interference and resolve the structure of the organic species. With the recent downselection of candidate landing sites for the rover (Section 5.1), the MOMA team is focusing testing efforts on appropriate analogs of the materials identified from orbit. Through measurement of the mineral matrix- and laser-induced effects on organic sensitivities, procedures for systematically reducing data from these more complex real-world samples are being established.
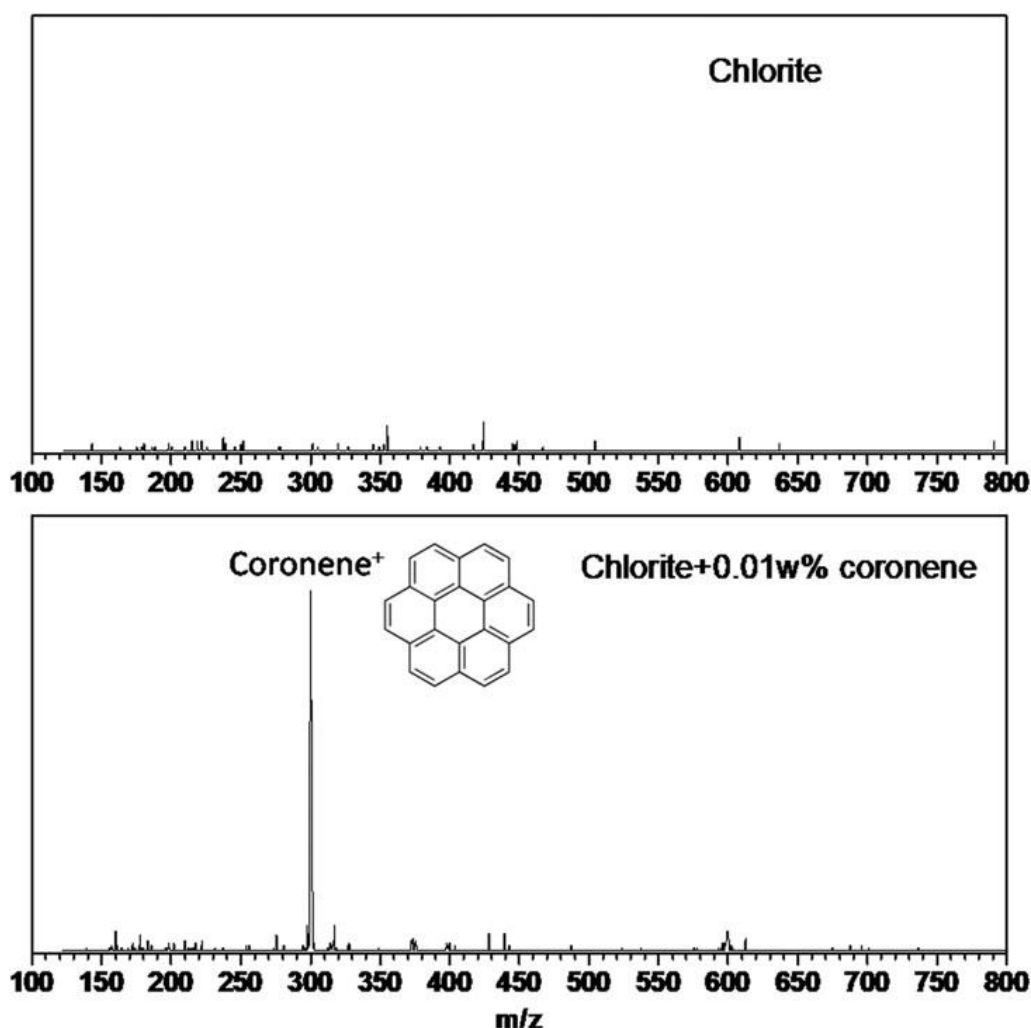
Figure 5.11: Positive ion LDMS spectrum of chlorite alone (top) and chlorite doped 0.01 wt% with example PAH coronene. In this example case, the coronene molecular ion is readily detectable above the very low background contributed by the mineral analog. LDMS, laser desorption mass spectrometry.

5.7.5   Test experiments on GC–MS prototype system: A case study

Here we present a case study to illustrate MOMA GC–MS capabilities on a specific type of sedimentary rock. The goal of this study was threefold: first, to demonstrate how the analytical methods work independently; second, to compare different MOMA GC–MS methods (pyrolysis and derivatization) by using only one sample; and last, to learn about advantages and disadvantages of these methods. The study was carried out in a laboratory configuration that mimics the MOMA flight instrument and was designed to gain qualitative information only.

5.7.5.1   Sample and setup

The case study was carried out on a silica-dominated black radiolarian chert from the Holy Cross Mountains in central Poland near the village of Zalesie Nowe (for details, see

Kremer, 2005; Kremer and Kazmierczak, 2005; Bauersachs et al., 2009). The sample has a total organic carbon content of 0.49 wt% (determined by thermal decomposition and combustion; Activation Laboratories Ltd., Canada). Despite its biogenic origin, the sample can serve as a Mars analog sample as the original biogenic chert has been completely recrystallized since its deposition and diagenesis in Silurian time. Opaline silica deposits are known to exist on Mars and have been detected both from orbit (Milliken et al., 2008) and in situ by the Mars Exploration Rover Spirit (Squyres et al., 2008). The relatively high total organic carbon content (in comparison with Mars) is beneficial for analysis under common laboratory conditions to reach a better signal/noise or sample/contamination ratio. Before the analyses, the sample was manually powdered (< 50 μm) with a mortar and pestle that were pre-cleaned with isopropanol to prevent any contamination by organics.

The measurements were performed with a flight analog system (FAS; only MOMA pyrolysis/derivatization oven, adsorption trap, and TS) connected to a Varian CP-3800 GC coupled to a Varian 240-MS/4000 MS. The GC column was a Varian Factor Four™ VF-5ms (30 m in length, inner diameter 0.25 mm, 0.25 μm film thickness) that is similar to the MOMA Restek MXT-5 column (Table 5.3). Helium was used as the carrier gas. The gas flow could be switched between internal (GC–MS only) and external (FAS and GC–MS). The FAS consists of a flight-like reusable MOMA oven and MOMA TS, including the adsorption trap (filled with Tenax® GR adsorbent; see also Section 5.6.2). Closing and reopening the oven were possible by hand with a flight-like zirconium ball sealing. The trap was cooled down by a Peltier element and heated to ~ 150 °C by an external heating element (heating rate 200 °C/min). The major differences between the FAS and the flight system are (1) the wet chemistry reagent is already added to the sample at room temperature (instead of being released by the MOMA flight capsule at temperatures above ~ 140 °C, Section 5.6.1.3 and Fig. 5.4), (2) the volatiles need to pass through the whole trap to get into the GC (instead of being subjected to flow inversion that is referred to as backflush, Section 5.6.2.2), (3) the trap can only be heated to ~ 150 °C (instead of 300 °C, as planned during Mars surface operations), and (4) the capillary transfer lines from oven to trap and trap to GC in the FAS can only be heated to 110 °C (instead of ≥ 135 °C when operated on Mars).

5.7.5.2 Methods

Stepwise pyrolysis. Three measurement cycles were performed on the same sample material with successive pyrolysis temperatures (300 °C/500 °C/700 °C), without opening the system in between. A pyrolysis step at 300 °C is useful for removing volatile components and any contaminants from the sample (e.g., Brocks et al., 2003). The oven was filled with 3 to 3.5 mg of the sample and sealed. The oven could have received ~ 20 x more sample (Section 5.6.1). Smaller sample masses compensated somewhat for the high abundance (~ 5000 ppm C_{tot}) of carbonaceous material in the sample. External helium flow was then activated and the trap was cooled down. When the trap reached 0 °C, pyrolysis of the sample with a heating rate of 300 °C/min was activated and held at the relevant temperature for 10 s. Then, flash heating of the trap was synchronized with the start of GC–MS data acquisition. After 45 s into the GC run, the helium flow was switched to internal to guarantee optimal helium flow for the entire measurement.

Derivatization/thermochemolysis. The following wet chemistry reagents were used:

- MTBSTFA (> 97%, Sigma-Aldrich) with DMF (> 99.5%, Thermo Scientific™ in a 3:1 (V:V) mixture

- DMF-DMA (Sigma-Aldrich)

- TMAH (25 wt% in methanol, Sigma-Aldrich)

Three to 3.5 mg of sample was filled into the oven and pre-dried at 80 °C for 10 min with the oven disconnected from the TS; 3.5 μL of liquid chemical reagent was added to the sample and the oven was sealed. Hence, we used the same amount of sample as for the pyrolysis experiments (see above) and about five times less reagent than released by the MOMA flight capsules (∼ 15 μL, Section 5.6.1.3). These experimental parameters follow expected conditions during MOMA surface operations as closely as possible given (i) the real differences between FAS and MOMA flight system (Section 5.7.5.1), (ii) the differences between our test sample (Silurian radiolarite) and expected martian subsurface samples, and (iii) practical constraints in the laboratory (less than ∼ 3 μL could not be handled in a reproducible way, even with microliter syringes). External helium flow was activated, the trap was cooled down to 0 °C, and derivatization was initiated by heating the oven/sample to the desired temperature. The following reaction times and temperatures were chosen for these experiments: 10 min at 250 °C for MTBSTFA/DMF; 4 min at 140 °C for DMF-DMA; 40 s at 600 °C for TMAH with a general heating rate of 300 °C/min for the oven, again following expected MOMA protocols (Sections 5.6.1.1 and 5.6.1.2). After the reaction, flash heating of the trap and GC–MS data acquisition started simultaneously. After 1 min into the GC run, the helium flow was switched back to internal.

GC–MS parameters. The carrier gas flow rate was set to 2 mL/min (for all measurements) with a split ratio of 30; the injector temperature was 250 °C; and the GC column was heated from 30 °C to 250 °C with a 10 °C/min ramp, holding at the maximum temperature for 5 min. Starting points for ionization (MS filament switched on) were 1 min for pyrolysis, 8 min for MTBSTFA/DMF and DMF-DMA, and 7 min for TMAH (solvent delay). Full-scan mass spectra were recorded with ionization fast-scan mode and a scan time of 0.58 s over a mass range of m/z 35 to 1000.

Before each analysis, a cleaning run and a system blank run (GC–MS and FAS) were performed to check for contamination. Additional blank runs were performed for every derivatization analysis (GC–MS, FAS with wet chemistry reagents).

5.7.5.3 Results and discussion

Pyrolysis. The stepwise pyrolysis displayed a huge inventory of aliphatic and aromatic hydrocarbons. A selection of the most abundant and important ones are presented in Figure 5.12. Additionally, a significant amount of contamination signals were identified. Especially in the 300 °C step, abundant acetone and phthalate peaks were present that are probably contamination from sample collection and preparation (i.e., plastic boxes, tool cleaning; Fig. 5.12). Other contamination (mostly siloxanes and DMF) is visible in each
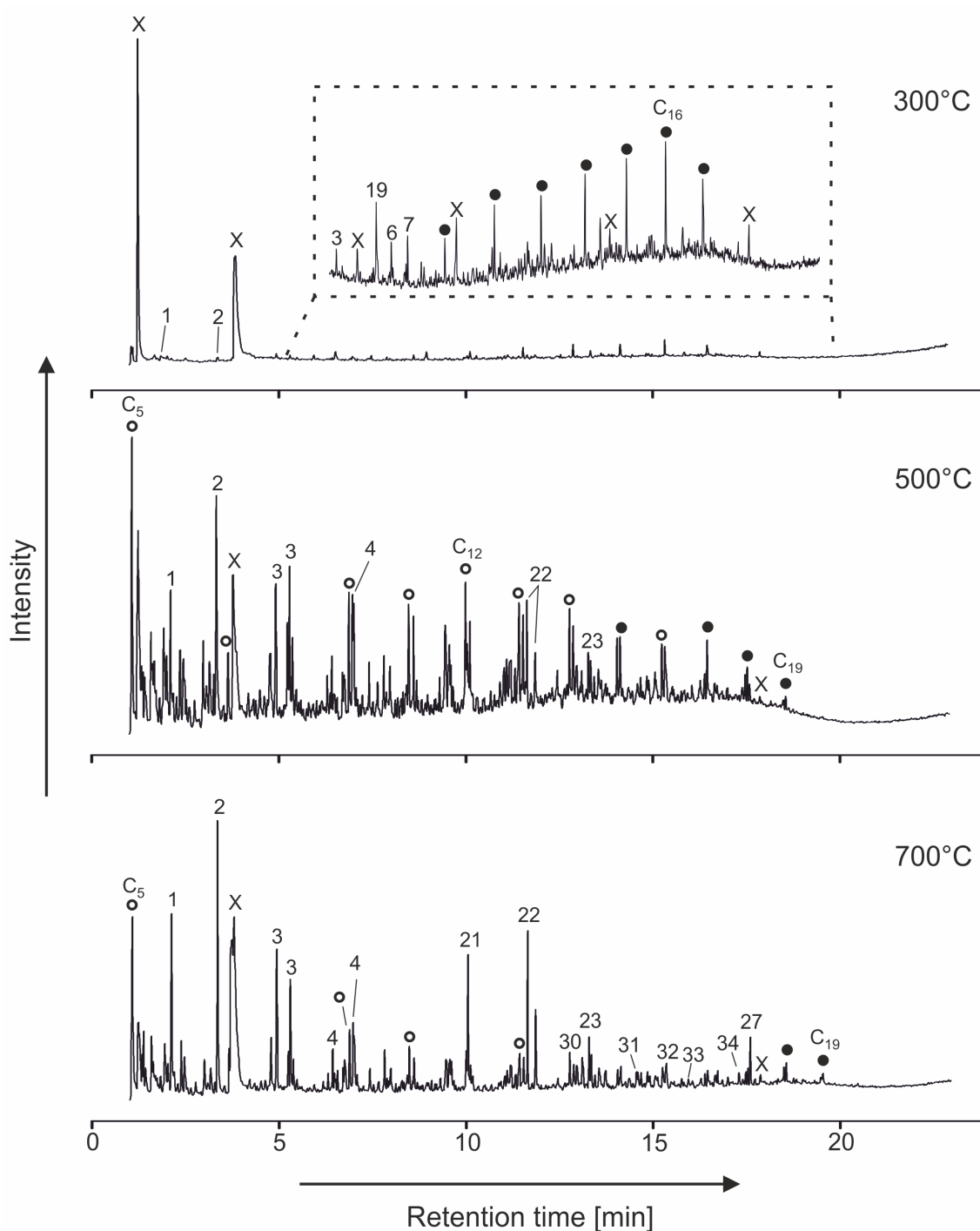
Figure 5.12: GC–MS chromatograms (total ion current) of stepwise pyrolysis (300 °C, 500 °C, 700 °C). Open and filled circles indicate *n*-alkenes and *n*-alkanes, respectively; X indicates contaminants; and numbers indicate aromatic compounds (Table 5.6). Note that in the 500 °C and 700 °C chromatograms, only a small selection of peaks are marked; for further details, see Figure 5.13.

Note: Numbers 31 and 33 were missing in the original figure (Figure 12 in Goesmann et al., 2017) due to a mistake during manuscript processing.

heating step. Siloxane is a typical signal from column degradation, whereas the DMF signal is caused by a carryover effect from the trap and derives from prior measurements with MTBSTFA/DMF.

Aliphatic hydrocarbons from the sample are mainly represented by n-alkanes/n-alkenes (Figs. 5.12, 5.13a). It should be noted that the n-alkenes in this case are by-products of cracking hydrocarbon compounds (e.g., n-alkanes) from kerogen (i.e., refractory material not extractable by organic solvent; Durand, 1980) by open-system pyrolysis and are therefore not indicative of the original hydrocarbon inventory of the sample (e.g., Burnham et al., 1982; Huizinga et al., 1988). This bias is intrinsic to the pyrolysis technique. Whereas the 300 °C step only shows n-alkanes in the range of C_{11} to C_{17} with low abundance (Fig. 5.12, 300 °C), higher-temperature pyrolysis yields much higher abundance levels of n-alkane/n-alkene doublets in the range between C_5 and C_{19}. Particularly, the 500 °C pyrolysis run is dominated by n-alkanes/n-alkenes with a predominance of n-alkenes in the range of C_{10} to C_{14} (Figs. 5.12, 5.13a). n-Alkanes are not detectable in at least the first 5 min of each pyrolysis run.

The abundance of aromatic hydrocarbons released from the sample increases with increasing temperature of the single steps. Only traces of benzene (1) and toluene (2) are found in the 300 °C step, whereas aromatic hydrocarbons are the dominant compounds in the 700 °C run (Fig. 5.12). The predominance of aromatic compounds at 700 °C is probably (at least partly) an artifact from pyrolysis due to cyclization and aromatization of unsaturated hydrocarbons during heating (e.g., Saiz-Jimenez, 1994; Hartgers et al., 1994, 1995). In particular, very high amounts of toluene, benzene, and methylnaphthalene could be seen (Fig. 5.12, 700 °C). Besides these compounds, a variety of benzene/alkylbenzenes (Fig. 5.13b), naphthalene/alkylnaphthalenes (Fig. 5.13c), and phenanthrene/ methylphenanthrenes/anthracene (Fig. 5.13d) were observed. For an overview of the most abundant aromatic hydrocarbons detected, see Table 5.6.

The results found from the FAS pyrolysis experiments are comparable with data from analysis performed on a similar type of sample (mudstones and black shales from the Ordovician–Silurian boundary, Holy Cross Mountains, Poland) with standard pyrolysis instruments (Mustafa et al., 2015). The authors found a similar inventory of aliphatic and aromatic hydrocarbon compounds. Few differences could be seen in the range of organic compounds (e.g., n-alkanes, alkylbenzenes) detected where the FAS analysis showed distribution over a wider range of chain lengths. Overall, stepwise pyrolysis experiments have confirmed that this method is capable of giving clear insight into and a good overview of the hydrocarbon inventory of an unknown sample. However, a distinction whether hydrocarbons (or possible biomarkers) derive from the bitumen or kerogen fraction cannot be done. For this purpose, a pre-extraction of samples would be necessary to remove the bitumen fraction (i.e., solvent-extractable organics; Durand, 1980), which of course is not possible for MOMA. Nonetheless, it would be useful to investigate the kerogen separately as it is assumed to be more resistant against maturation, to be immobile, and therefore syngenetic to the host rock and less affected by contamination compared with the bitumen (Brocks et al., 2003; Love et al., 2005; Marshall et al., 2007). These important points clearly highlight an inherent weakness of the MOMA instrument that is like any other remotely operated space instrument, a trade-off between low complexity and science return.
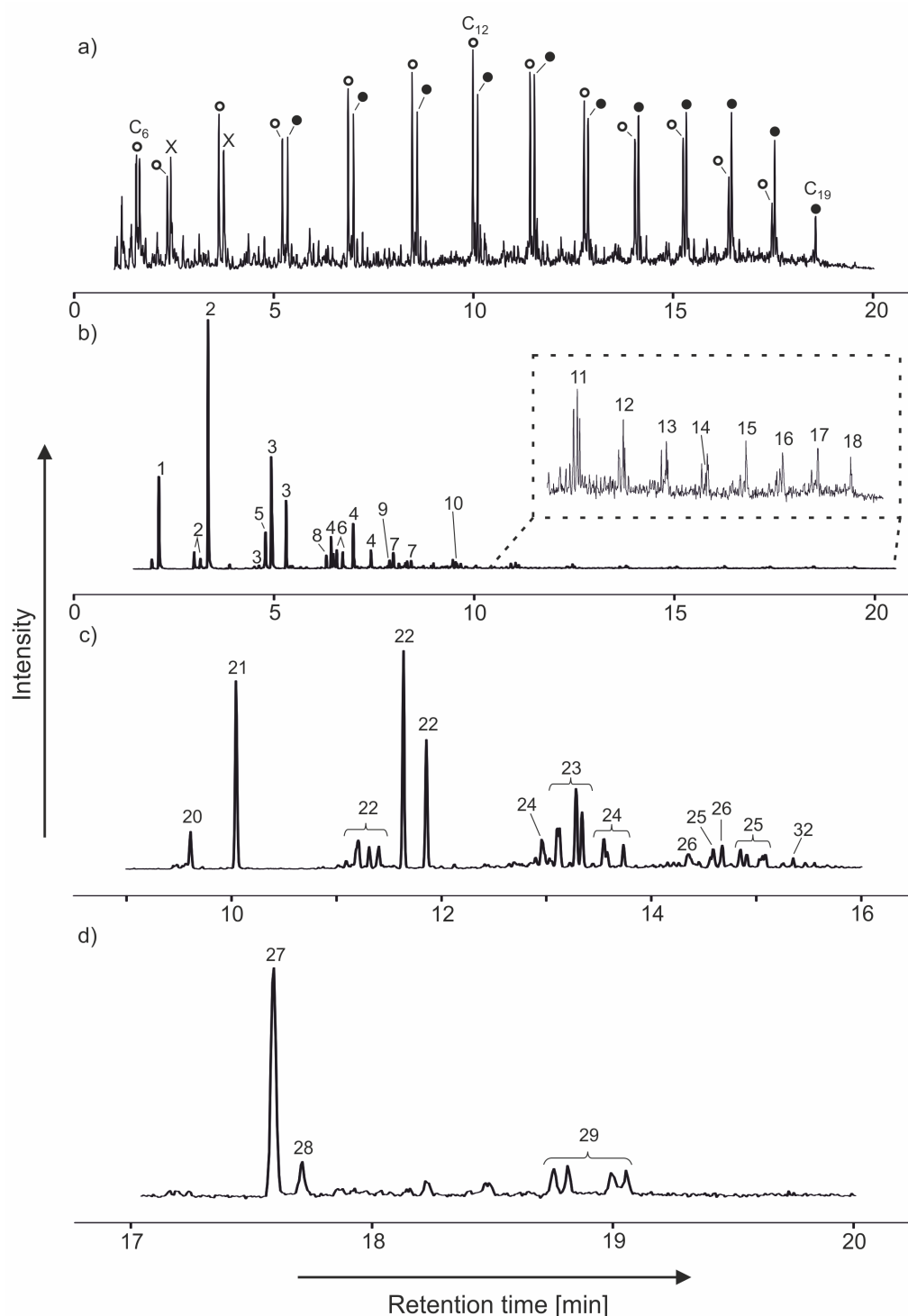
Figure 5.13: GC–MS chromatograms of stepwise pyrolysis filtered for certain compounds. (**a**) *n*-Alkenes and *n*-alkanes (500 °C, *m/z* 69, 71, 83, 85), (**b**) benzene and alkylbenzenes (700 °C, *m/z* 78, 91, 92, 105, 106, 119, 120), (**c**) naphthalene and alkylnaphthalenes (700 °C, *m/z* 128, 141, 142, 155, 156, 170), and (**d**) phenanthrene, anthracene, and methylphenanthrenes (700 °C, *m/z* 178, 191, 192). Open and filled circles indicate *n*-alkenes and *n*-alkanes, respectively; X indicates contaminants; numbers indicate aromatic compounds (Table 5.6).

Note: Positions of numbers 4 and 6 were changed (compared to original Figure 13 in Goesmann et al., 2017), based on new results.

Table 5.6: Peak labels and compound names of aromatic hydrocarbons.

Peak label	Compound	Peak label	Compound
1	Benzene	18	Tridecylbenzene
2	Toluene	19	Benzaldehyde
3	Xylene	20	Naphthalene
4	Trimethylbenzene	21	Naphthalene
5	Ethylbenzene	22	Methylnaphthalene
6	Ethyl-methylbenzene	23	Dimethylnaphthalene
7	methyl-(1-methylethyl)benzene	24	Ethylnaphthalene
8	Propylbenzene	25	Trimethylnaphthalene
9	Butylbenzene	26	(1-Methylethyl)-naphthalene
10	Pentylbenzene	27	Phenantrene
11	Hexylbenzene	28	Anthracene
12	Heptylbenzene	29	Methylphenantrene
13	Octylbenzene	30	Biphenyl
14	Nonylbenzene	31	Dibenzofuran
15	Decylbenzene	32	Fluorene
16	Undecylbenzene	33	Methyldibenzofuran
17	Dodecylbenzene	34	Dibenzothiophene

Two peaks (20 & 21) have been labeled confidently as naphthalene, although the appearance of two peaks for this compound is poorly understood.

It can only be speculated here that compounds (including alkanes and aromatics) released in the 300 °C run were contamination or probably released from the free bitumen fraction (not chemically bound) and therefore less thermal energy is needed for release. Additional compounds released at 500 °C can possibly be organics from the bitumen fraction (also with higher molecular weight) or derive from the kerogen and/or mineral-bound bitumen, whereas the compounds found in the 700 °C run may only derive from kerogen.

Derivatization and thermochemolysis.   The analysis with MTBSTFA/DMF derivatization does not show any usable results. Only a low abundance of sulfuric acid, few fatty acids, and alcohols, which are most likely contamination from sample processing, could be detected. Most peaks were also present in the blanks (Fig. 5.14a,b). The same goes for the analysis with DMF-DMA. A possible explanation for this negative result is that the sample did not contain compounds detectable with derivatization (no compounds with functional groups) as the sample has been too weathered and diagenetically altered to contain any compounds with functional groups. Alternatively, the low temperature of the derivatization procedure (250 °C for MTBSTFA/DMF, 140 °C for DMF-DMA) did not allow the molecules to be extracted from the sample and thus functional groups of the molecules were not available to the derivatization reagent. An additional step of preheating the sample to higher temperature may be necessary to thermodesorb the molecules before derivatization. Further investigations are needed to optimize the method. However, some fatty acids (most likely contaminants) were identified, which confirms the efficiency of the derivatization method.
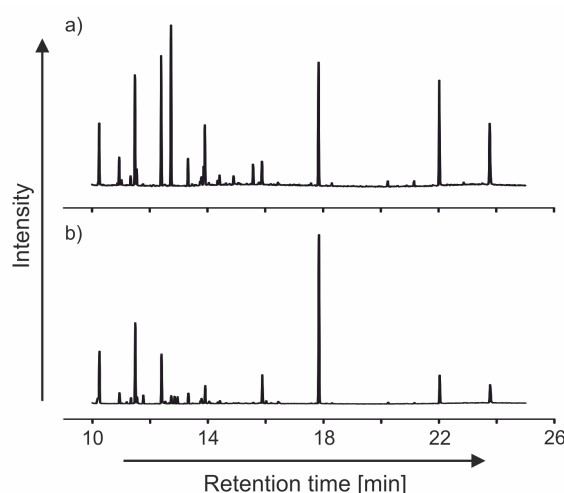
Figure 5.14: GC–MS chromatograms (total ion current) of the MTBSTFA/DMF derivatization. (**a**) Blank run with MTBSTFA/DMF, (**b**) derivatization of the sample with MTBSTFA/DMF. No major differences are noted.

The case study showed that some issues persist and need to be considered before in situ derivatization. The samples need to be dried out carefully (not too much blowoff from the sample) before derivatization to avoid total consumption of the reagent by water. Additionally, carryover effects need to be considered when using a surplus of derivatization reagents (Fig. 5.14a) as this will also derivatize residual material from prior analysis out of the trap, the GC column, and all low-temperature areas (e.g., transfer lines), leading to cross-contamination of samples.

Thermochemolysis of samples analyzed with TMAH showed mostly the same compounds as the stepwise pyrolysis (Fig. 5.15, see also above, Paragraph "Pyrolysis" at the begin of this section). However, one crucial difference is that two fatty acid methyl esters could be identified (Fig. 5.15), but they only show low abundance. An exact classification of these was not possible because of co-elution with aromatic compounds. It is likely that these two fatty acids are contamination from sample preparation as the sample is otherwise free from functionalized compounds. Nonetheless, we were able to analyze and identify these fatty acids by in situ thermochemolysis.

5.8   Discussion

MOMA is a mass spectrometer-based instrument onboard the ExoMars rover designed for in situ analysis of martian samples. This article describes the scope and development of MOMA from its science requirements to the complete instrument as currently expected (about 1 year before completion of the integrated MOMA FM). We have described MOMA's major subsystems (ovens, TS, GC, laser, and MS) and test experiments conducted on subsystem test modules, as well as coupling campaigns between selected subsystem modules. However, tests of the fully integrated instrument are yet to come. The overarching goal of MOMA is to characterize the inventory of organic material in martian sediments. According to the ExoMars mission goals (Vago et al., 2017), such
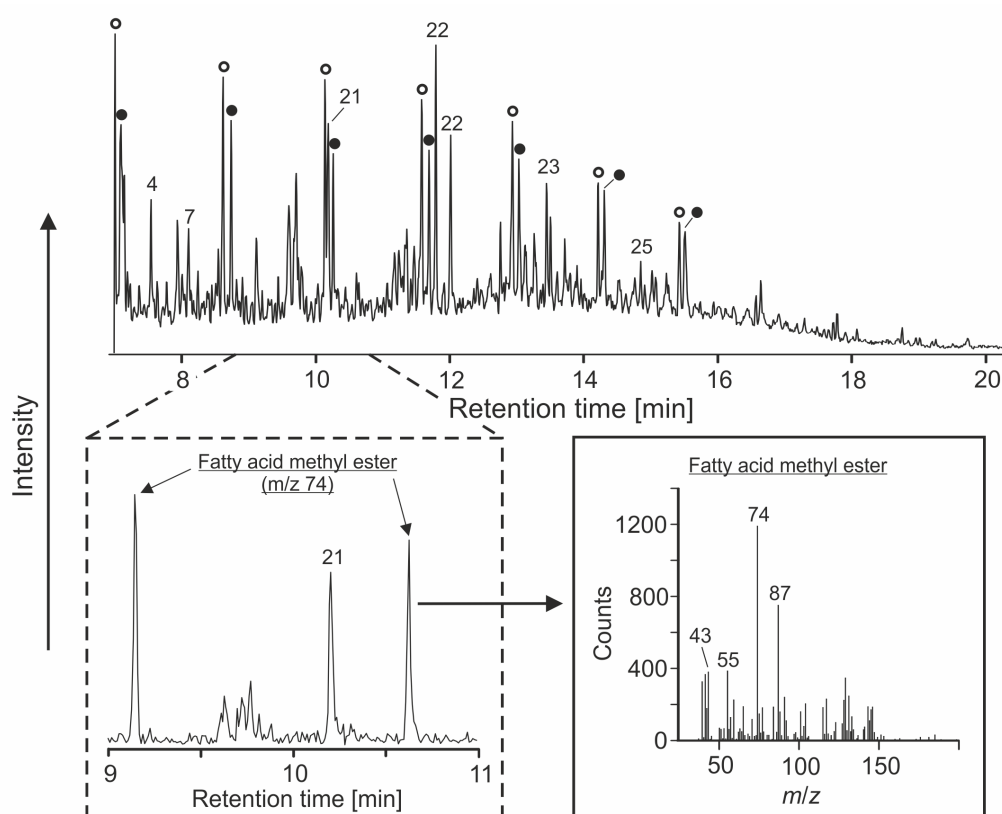
Figure 5.15: GC–MS chromatograms of TMAH thermochemolysis. Top: total ion current, similar to pyrolysis. Bottom left: part of the chromatogram (*m/z* 74) with identified fatty acid methyl esters. Bottom right: corresponding mass spectrum of fatty acid methyl esters. Open and filled circles indicate *n*-alkenes and *n*-alkanes, respectively; numbers indicate aromatic compounds (Table 5.6). TMAH, tetramethylammonium hydroxide.

characterization shall be detailed enough to address and constrain the sources (biotic or abiotic) of that material and, in particular, to address the question of whether or not that material is formed from biologic activity. The task is complex as up to now, only little organic material ($\sim$ 150 ppbw of chlorobenzene and tens of ppbw of $C_2 - C_4$ chlorohydrocarbons) has been identified in situ in martian sediments that has clearly been recognized to belong to the indigenous organic part of these sediments (Freissinet et al., 2015). The organic molecules detected so far have been thermally released from its sedimentary environment. We still do not know if these molecules occur as discrete molecules in the rock or if they are part of a macromolecular organic compound, although the latter seems to be more likely. Hence, we do not know the nature of the organic material contained in the martian sediment. The methods applied to date (especially pyrolysis-GC–MS onboard the Viking landers and the Curiosity rover) are fairly destructive, and consequently important information on the potential sources of this organic material is lost. In this respect, MOMA will represent a clear advance as it combines destructive methods such as classical pyrolysis (Viking landers, MSL-SAM) and pyrolysis–derivatization (MSL-SAM) with a less destructive method, that is, LDMS, which allows laser-ablated, fairly large, and intact molecular fragments to be detected and characterized by the MS. Tandem

mass spectrometry can then be used to further characterize these molecules. This method has never been applied to martian material by any previous landed mission.

Classical pyrolysis-GC–MS-based techniques have two major drawbacks: (1) only volatile molecules can be detected and, moreover, only nonpolar molecules can get through the GC columns to the detector and (2) heating of samples to temperatures beyond $\sim 200 - 300\,°C$ causes oxidative destruction (chlorination and combustion) of organic compounds by (per)chlorates. These salts have been detected (directly and indirectly) by previous missions (especially Phoenix and Curiosity) and are believed to occur at all latitudes and in sediments of any age (Glavin et al., 2013; Archer Jr. et al., 2016).

The LDMS technique is not affected by these drawbacks as this technique is insensitive to the presence of (per)chlorates (Li et al., 2015) and to the polarity of laser-desorbed molecules. Additionally, MOMA tackles the above drawbacks by offering a broader set of derivatization agents than currently available on SAM: (ad 1) different derivatization agents target different types of molecules, including molecules of different polarity; and (ad 2) MOMA offers two derivatization techniques that both occur at rather low temperature: MTBSTFA/DMF ($\sim 250\,°C$) and DMF-DMA ($\sim 140\,°C$). Based on SAM data (acquired on 10 samples, Archer Jr. et al., 2016), both temperatures are below the temperature where most samples start to decompose their (per)chlorates and release O_2 that leads to combustion of organic molecules.

In addition to the mass range and polarity of any martian organic compounds, we do not know if the organic material detected so far represents a homogeneously distributed discrete phase (such as a mineraloid per se) or if it is preferentially associated with specific (primary magmatic or secondary) minerals. MOMA LDMS can also help constrain the host mineral phase as the MOMA UV laser ablates both organic and inorganic fragments to be analyzed by the MS. Further constraints will come from MicrOmega and RLS. Both techniques are particularly diagnostic not only for inorganic minerals but can also detect some organic compounds. Therefore, the synergy of MOMA with these instruments is considerable in view of the overall goal of the mission (Vago et al., 2017).

Finally, one of the most significant improvements of the ExoMars rover mission compared with previous missions is its capability to acquire samples from the subsurface down to a depth of about 2 m. This capability enables the mission to acquire and analyze samples that have been potentially shielded from solar and galactic radiation (mostly high-energy gamma radiation) over geologic timescales (Pavlov et al., 2012) and that may contain highly pristine martian organic material, perhaps at much higher abundance than at the top surface.

5.9   Summary

The access to samples from up 2 m below the martian surface and the wide range of analytical capabilities will enable MOMA to play a major role in constraining potential sources of organic material in martian sediments and in constraining processes (be they of abiotic or biogenic nature) that might have altered this material. This new insight will inform the next step of Mars exploration: Mars Sample Return.

Acknowledgments

References

Archer Jr., P. D., Ming, D. W., and Sutter, B. (2013). The effects of instrument parameters and sample properties on thermal decomposition: interpreting thermal analysis data from Mars. *Planetary Science*, 2, 2.

Archer Jr., P. D., Ming, D. W., Sutter, B., Morris, R. V., Clark, B. C., Mahaffy, P. R., Wray, J. J., Fairen, A. G., Gellert, R., and Yen, A. S. (2016). Oxychlorine species on Mars: implications from Gale Crater samples. In *47th Lunar and Planetary Science Conference, #2947*.

Arevalo, R., Brinckerhoff, W., van Amerom, F., Danell, R., Pinnick, V., Li, X., Getty, S., Hovmand, L., Grubisic, A., Mahaffy, P., Goesmann, F., and Steininger, H. (2015). Design and demonstration of the Mars Organic Molecule Analyzer (MOMA) on the ExoMars 2018 rover. In *Aerospace Conference, 2015 IEEE*.

Bada, J. L. and McDonald, G. D. (1995). Amino Acid Racemization on Mars: Implications for the Preservation of Biomolecules from an Extinct Martian Biota. *Icarus*, 114, 139–143.

Bada, J. L., Wang, X. S., and Hamilton, H. (1999). Preservation of key biomolecules in the fossil record: current knowledge and future challenges. *Philosophical Transactions of the Royal Society of London. Series B: Biological Sciences*, 354, 77–87.

Bauersachs, T., Kremer, B., Schouten, S., and Sinninghe Damsté, J. S. (2009). A biomarker and δ^{15}N study of thermally altered Silurian cyanobacterial mats. *Organic Geochemistry*, 40, 149–157.

Benner, S. A., Devine, K. G., Matveeva, L. N., and Powell, D. H. (2000). The missing organic molecules on Mars. *Proceedings of the National Academy of Sciences of the United States of America*, 97, 2425–2430.

Biemann, K., Oró, J., Toulmin, P., Orgel, L. E., Nier, A. O., Anderson, D. M., Simmonds, P. G., Flory, D., Diaz, A. V., Rushneck, D. R., Biller, J. E., and Lafleur, A. L. (1977).

The search for organic substances and inorganic volatile compounds in the surface of Mars. *Journal of Geophysical Research*, 82, 4641–4658.

Boynton, W. V., Ming, D. W., Kounaves, S. P., Young, S. M. M., Arvidson, R. E., Hecht, M. H., Hoffman, J., Niles, P. B., Hamara, D. K., Quinn, R. C., Smith, P. H., Sutter, B., Catling, D. C., and Morris, R. V. (2009). Evidence for Calcium Carbonate at the Mars Phoenix Landing Site. *Science*, 325, 61–64.

Brocks, J. J., Love, G. D., Snape, C. E., Logan, G. A., Summons, R. E., and Buick, R. (2003). Release of bound aromatic hydrocarbons from late Archean and Mesoproterozoic kerogens via hydropyrolysis. *Geochimica et Cosmochimica Acta*, 67, 1521–1530.

Brocks, J. J. and Summons, R. E. (2003). Biomarkers for Early Life. In W. H. Schlesinger (Ed.), *Biogeochemistry*. Elsevier, Oxford, pp. 63–115.

Buch, A., Glavin, D. P., Sternberg, R., Szopa, C., Rodier, C., Navarro-González, R., Raulin, F., Cabane, M., and Mahaffy, P. R. (2006). A new extraction technique for in situ analyses of amino and carboxylic acids on Mars by gas chromatography mass spectrometry. *Planetary and Space Science*, 54, 1592–1599.

Buch, A., Sternberg, R., Szopa, C., Freissinet, C., Garnier, C., Bekri, E. J., Rodier, C., Navarro-González, R., Raulin, F., Cabane, M., Stambouli, M., Glavin, D. P., and Mahaffy, P. R. (2009). Development of a gas chromatography compatible Sample Processing System (SPS) for the in-situ analysis of refractory organic matter in martian soil: preliminary results. *Advances in Space Research*, 43, 143–151.

Burnham, A. K., Clarkson, J. E., Singleton, M. F., Wong, C. M., and Crawford, R. W. (1982). Biological markers from Green River kerogen decomposition. *Geochimica et Cosmochimica Acta*, 46, 1243–1251.

Carter, J., Quantin, C., Thollot, P., Loizeau, D., Ody, A., and Lozach, L. (2016). Oxia planum: A clay-laden landing site proposed for the ExoMars rover mission: Aqueous mineralogy and alteration scenarios. In *47th Lunar and Planetary Science Conference, #2064*.

Challinor, J. M. (1989). A pyrolysis-derivatisation-gas chromatography technique for the structural elucidation of some synthetic polymers. *Journal of Analytical and Applied Pyrolysis*, 16, 323–333.

Challinor, J. M. (2001). Review: the development and applications of thermally assisted hydrolysis and methylation reactions. *Journal of Analytical and Applied Pyrolysis*, 61, 3–34.

Cull, S. C., Arvidson, R. E., Catalano, J. G., Ming, D. W., Morris, R. V., Mellon, M. T., and Lemmon, M. (2010). Concentrated perchlorate at the Mars Phoenix landing site: Evidence for thin film liquid water on Mars. *Geophysical Research Letters*, 37, L22203.

Debus, A., Haldemann, A., Vago, J. L., and McCoy, D. (2012). *ExoMars Rover Scientific Payload Requirements Document (SPRD) EXM-PL-RS-ESA-00001, Issue 3, Rev. 5*. Technical report.

References

Durand, B. (1980). Sedimentary organic matter and kerogen. Definition and quantitative importance of kerogen. In B. Durand (Ed.), *Kerogen*. Éditions Technip, Paris, pp. 13–34.

Edwards, H. G. M., Hutchinson, I., and Ingley, R. (2012). The ExoMars Raman spectrometer and the identification of biogeological spectroscopic signatures using a flight-like prototype. *Analytical and Bioanalytical Chemistry*, 404, 1723–1731.

Edwards, H. G. M., Hutchinson, I. B., Ingley, R., Parnell, J., Vítek, P., and Jehlička, J. (2013). Raman Spectroscopic Analysis of Geological and Biogeological Specimens of Relevance to the ExoMars Mission. *Astrobiology*, 13, 543–549.

Flynn, G. J. and McKay, D. S. (1990). An assessment of the meteoritic contribution to the Martian soil. *Journal of Geophysical Research: Solid Earth*, 95, 14497–14509.

Freissinet, C., Buch, A., Sternberg, R., Szopa, C., Geffroy-Rodier, C., Jelinek, C., and Stambouli, M. (2010). Search for evidence of life in space: Analysis of enantiomeric organic molecules by *N,N*-dimethylformamide dimethylacetal derivative dependant Gas Chromatography–Mass Spectrometry. *Journal of Chromatography A*, 1217, 731–740.

Freissinet, C., Glavin, D. P., Mahaffy, P. R., Miller, K. E., Eigenbrode, J. L., Summons, R. E., Brunner, A. E., Buch, A., Szopa, C., Archer, P. D., Franz, H. B., Atreya, S. K., Brinckerhoff, W. B., Cabane, M., Coll, P., Conrad, P. G., Des Marais, D. J., Dworkin, J. P., Fairén, A. G., François, P., Grotzinger, J. P., Kashyap, S., ten Kate, I. L., Leshin, L. A., Malespin, C. A., Martin, M. G., Martin-Torres, F. J., McAdam, A. C., Ming, D. W., Navarro-González, R., Pavlov, A. A., Prats, B. D., Squyres, S. W., Steele, A., Stern, J. C., Sumner, D. Y., Sutter, B., Zorzano, M. P., and the MSL Science Team (2015). Organic molecules in the Sheepbed Mudstone, Gale Crater, Mars. *Journal of Geophysical Research: Planets*, 120, 495–514.

Gao, L., Cooks, R. G., and Ouyang, Z. (2008). Breaking the Pumping Speed Barrier in Mass Spectrometry: Discontinuous Atmospheric Pressure Interface. *Analytical Chemistry*, 80, 4026–4032.

Geffroy-Rodier, C., Grasset, L., Sternberg, R., Buch, A., and Amblès, A. (2009). Thermochemolysis in search for organics in extraterrestrial environments. *Journal of Analytical and Applied Pyrolysis*, 85, 454–459.

Glavin, D. P. and Dworkin, J. P. (2009). Enrichment of the amino acid L-isovaline by aqueous alteration on CI and CM meteorite parent bodies. *Proceedings of the National Academy of Sciences of the United States of America*, 106, 5487–5492.

Glavin, D. P., Elsila, J. E., Burton, A. S., Callahan, M. P., Dworkin, J. P., Hilts, R. W., and Herd, C. D. K. (2012). Unusual nonterrestrial l-proteinogenic amino acid excesses in the Tagish Lake meteorite. *Meteoritics & Planetary Science*, 47, 1347–1364.

Glavin, D. P., Freissinet, C., Miller, K. E., Eigenbrode, J. L., Brunner, A. E., Buch, A., Sutter, B., Archer, P. D., Atreya, S. K., Brinckerhoff, W. B., Cabane, M., Coll, P.,

Conrad, P. G., Coscia, D., Dworkin, J. P., Franz, H. B., Grotzinger, J. P., Leshin, L. A., Martin, M. G., McKay, C., Ming, D. W., Navarro-González, R., Pavlov, A., Steele, A., Summons, R. E., Szopa, C., Teinturier, S., and Mahaffy, P. R. (2013). Evidence for perchlorates and the origin of chlorinated hydrocarbons detected by SAM at the Rocknest aeolian deposit in Gale Crater. *Journal of Geophysical Research: Planets*, 118, 1955–1973.

Goesmann, F., Brinckerhoff, W. B., Raulin, F., Goetz, W., Danell, R. M., Getty, S. A., Siljeström, S., Mißbach, H., Steininger, H., Arevalo, R. D., Buch, A., Freissinet, C., Grubisic, A., Meierhenrich, U. J., Pinnick, V. T., Stalport, F., Szopa, C., Vago, J. L., Lindner, R., Schulte, M. D., Brucato, J. R., Glavin, D. P., Grand, N., Li, X., van Amerom, F. H. W., and the Moma Science Team (2017). The Mars Organic Molecule Analyzer (MOMA) Instrument: Characterization of Organic Material in Martian Sediments. *Astrobiology*, 17, 655–685.

Goesmann, F., Rosenbauer, H., Roll, R., Szopa, C., Raulin, F., Sternberg, R., Israel, G., Meierhenrich, U., Thiemann, W., and Munoz-Caro, G. (2007). Cosac, The Cometary Sampling and Composition Experiment on Philae. *Space Science Reviews*, 128, 257–280.

Goetz, W., Arevalo, R., Pinnick, V., Danell, R., Getty, S., Oehlke, M., John, H., Li, X., Grubisic, A., and Brinckerhoff, W. (2016a). Characterization of Mineral Targets by Laser Desorption and Ionization in Preparation of the MOMA Investigation Onboard the ExoMars-2018 Rover. In *47th Lunar and Planetary Science Conference, #2614*.

Goetz, W., Arevalo, R. D., Oehlke, M., Danell, R., Siljeström, S., Kronz, A., John, H., Pinnick, V., Brinckerhoff, W. B., and Steininger, H. (2017). Characterization of Minerals by Laser Desorption/Ablation and Ionization in Preparation of the MOMA Investigation Onboard the Exomars Rover. In *48th Lunar and Planetary Science Conference, #2536*.

Goetz, W., Brinckerhoff, W. B., Arevalo, R., Freissinet, C., Getty, S., Glavin, D. P., Siljeström, S., Buch, A., Stalport, F., Grubisic, A., Li, X., Pinnick, V., Danell, R., van Amerom, F. H. W., Goesmann, F., Steininger, H., Grand, N., Raulin, F., Szopa, C., Meierhenrich, U., and Brucato, J. R. (2016b). MOMA: the challenge to search for organics and biosignatures on Mars. *International Journal of Astrobiology*, 15, 239–250.

Goetz, W., Steininger, H., Steinmetz, E., Bierwirth, M., Goesmann, F., Philippon, C., Lustrement, B., Szopa, C., Buch, A., and Amundsen, H. (2011). Mars Organic Molecule Analyzer (Moma) Field Test as Part of the AMASE 2010 Svalbard Expedition. In *42th Lunar and Planetary Science Conference, #2460*.

Hartgers, W. A., Damsté, J. S. S., and de Leeuw, J. W. (1994). Geochemical significance of alkylbenzene distributions in flash pyrolysates of kerogens, coals, and asphaltenes. *Geochimica et Cosmochimica Acta*, 58, 1759–1775.

Hartgers, W. A., Sinninghe Damsté, J. S., and de Leeuw, J. W. (1995). Curie-point pyrolysis of sodium salts of functionalized fatty acids. *Journal of Analytical and Applied Pyrolysis*, 34, 191–217.

Hecht, M. H., Kounaves, S. P., Quinn, R. C., West, S. J., Young, S. M. M., Ming, D. W., Catling, D. C., Clark, B. C., Boynton, W. V., Hoffman, J., DeFlores, L. P., Gospodinova, K., Kapit, J., and Smith, P. H. (2009). Detection of Perchlorate and the Soluble Chemistry of Martian Soil at the Phoenix Lander Site. *Science*, 325, 64–67.

Huizinga, B. J., Aizenshtat, Z. A., and Peters, K. E. (1988). Programmed pyrolysis-gas chromatography of artificially matured Green River kerogen. *Energy & Fuels*, 2, 74–81.

Knapp, D. R. (1979). *Handbook of analytical derivatization reactions*. John Wiley & Sons, New York.

Kolleck, C., Büttner, A., Ernst, M., Hülsenbusch, T., Lang, T., Marwah, R., Mebben, S., Priehs, M., Kracht, D., and Neumann, J. (2010). Development of a pulsed UV laser system for laser-desorption mass spectrometry on Mars. In *International Conference on Space Optics (ICOS), 4–8 October 2010, Greece*.

Kremer, B. (2005). Mazuelloids: Product of Post-Mortem Phosphatization of Acanthomorphic Acritarchs. *PALAIOS*, 20, 27–36.

Kremer, B. and Kazmierczak, J. (2005). Cyanobacterial Mats from Silurian Black Radiolarian Cherts: Phototrophic Life at the Edge of Darkness? *Journal of Sedimentary Research*, 75, 897–906.

Leshin, L. A., Mahaffy, P. R., Webster, C. R., Cabane, M., Coll, P., Conrad, P. G., Archer, P. D., Atreya, S. K., Brunner, A. E., Buch, A., Eigenbrode, J. L., Flesch, G. J., Franz, H. B., Freissinet, C., Glavin, D. P., McAdam, A. C., Miller, K. E., Ming, D. W., Morris, R. V., Navarro-González, R., Niles, P. B., Owen, T., Pepin, R. O., Squyres, S., Steele, A., Stern, J. C., Summons, R. E., Sumner, D. Y., Sutter, B., Szopa, C., Teinturier, S., Trainer, M. G., Wray, J. J., and Grotzinger, J. P. (2013). Volatile, Isotope, and Organic Analysis of Martian Fines with the Mars Curiosity Rover. *Science*, 341, 1238937.

Li, X., Danell, R. M., Brinckerhoff, W. B., Pinnick, V. T., van Amerom, F., Arevalo, R. D., Getty, S. A., Mahaffy, P. R., Steininger, H., and Goesmann, F. (2015). Detection of Trace Organics in Mars Analog Samples Containing Perchlorate by Laser Desorption/Ionization Mass Spectrometry. *Astrobiology*, 15, 104–110.

Li, X., Danell, R. M., Pinnick, V. T., Grubisic, A., van Amerom, F., Arevalo, R. D., Getty, S. A., Brinckerhoff, W. B., Southard, A. E., Gonnsen, Z. D., and Adachi, T. (2017). Mars Organic Molecule Analyzer (MOMA) laser desorption/ionization source design and performance characterization. *International Journal of Mass Spectrometry*, 422, 177–187.

Love, G. D., Bowden, S. A., Jahnke, L. L., Snape, C. E., Campbell, C. N., Day, J. G., and Summons, R. E. (2005). A catalytic hydropyrolysis method for the rapid screening of microbial cultures for lipid biomarkers. *Organic Geochemistry*, 36, 63–82.

Mahaffy, P. R., Webster, C. R., Cabane, M., Conrad, P. G., Coll, P., Atreya, S. K., Arvey, R., Barciniak, M., Benna, M., Bleacher, L., Brinckerhoff, W. B., Eigenbrode, J. L.,

Carignan, D., Cascia, M., Chalmers, R. A., Dworkin, J. P., Errigo, T., Everson, P., Franz, H., Farley, R., Feng, S., Frazier, G., Freissinet, C., Glavin, D. P., Harpold, D. N., Hawk, D., Holmes, V., Johnson, C. S., Jones, A., Jordan, P., Kellogg, J., Lewis, J., Lyness, E., Malespin, C. A., Martin, D. K., Maurer, J., McAdam, A. C., McLennan, D., Nolan, T. J., Noriega, M., Pavlov, A. A., Prats, B., Raaen, E., Sheinman, O., Sheppard, D., Smith, J., Stern, J. C., Tan, F., Trainer, M., Ming, D. W., Morris, R. V., Jones, J., Gundersen, C., Steele, A., Wray, J., Botta, O., Leshin, L. A., Owen, T., Battel, S., Jakosky, B. M., Manning, H., Squyres, S., Navarro-González, R., McKay, C. P., Raulin, F., Sternberg, R., Buch, A., Sorensen, P., Kline-Schoder, R., Coscia, D., Szopa, C., Teinturier, S., Baffes, C., Feldman, J., Flesch, G., Forouhar, S., Garcia, R., Keymeulen, D., Woodward, S., Block, B. P., Arnett, K., Miller, R., Edmonson, C., Gorevan, S., and Mumm, E. (2012). The Sample Analysis at Mars Investigation and Instrument Suite. *Space Science Reviews*, 170, 401–478.

Marshall, C. P., Love, G. D., Snape, C. E., Hill, A. C., Allwood, A. C., Walter, M. R., Van Kranendonk, M. J., Bowden, S. A., Sylva, S. P., and Summons, R. E. (2007). Structural characterization of kerogen in 3.4 Ga Archaean cherts from the Pilbara Craton, Western Australia. *Precambrian Research*, 155, 1–23.

Mawhinney, T. P. and Madson, M. A. (1982). *N*-Methyl-*N*-(tert-butyldimethylsilyl)trifluoroacetamide and related *N*-tert-butyldimethylsilyl amides as protective silyl donors. *The Journal of Organic Chemistry*, 47, 3336–3339.

McAdam, A. C., Franz, H. B., Sutter, B., Archer, P. D., Freissinet, C., Eigenbrode, J. L., Ming, D. W., Atreya, S. K., Bish, D. L., Blake, D. F., Bower, H. E., Brunner, A., Buch, A., Glavin, D. P., Grotzinger, J. P., Mahaffy, P. R., McLennan, S. M., Morris, R. V., Navarro-González, R., Rampe, E. B., Squyres, S. W., Steele, A., Stern, J. C., Sumner, D. Y., and Wray, J. J. (2014). Sulfur-bearing phases detected by evolved gas analysis of the Rocknest aeolian deposit, Gale Crater, Mars. *Journal of Geophysical Research: Planets*, 119, 373–393.

McAdam, A. C., Knudson, C. A., Sutter, B., Franz, H. B., Archer Jr, P. D., Eigenbrode, J. L., Ming, D. W., Morris, R. V., Hurowitz, J. A., and Mahaffy, P. R. (2016). Reactions involving calcium and magnesium sulfates as potential sources of sulfur dioxide during MSL SAM evolved gas analyses. *47th Lunar and Planetary Science Conference, #2277*.

McCollom, T. M., Ritter, G., and Simoneit, B. R. T. (1999). Lipid Synthesis Under Hydrothermal Conditions by Fischer–Tropsch-Type Reactions. *Origins of Life and Evolution of Biospheres*, 29, 153–166.

Meierhenrich, U. (2008). *Amino acids and the asymmetry of life: caught in the act of formation*. Springer Science & Business Media, Berlin, Heidelberg.

Meierhenrich, U., Thiemann, W. H. P., and Rosenbauer, H. (2001). Pyrolytic methylation assisted enantioseparation of chiral hydroxycarboxylic acids. *Journal of Analytical and Applied Pyrolysis*, 60, 13–26.

Milliken, R. E., Swayze, G. A., Arvidson, R. E., Bishop, J. L., Clark, R. N., Ehlmann, B. L., Green, R. O., Grotzinger, J. P., Morris, R. V., Murchie, S. L., Mustard, J. F., and Weitz, C. (2008). Opaline silica in young deposits on Mars. *Geology*, 36, 847–850.

Modica, P., Meinert, C., de Marcellus, P., Nahon, L., Meierhenrich, U. J., and D'Hendecourt, L. L. S. (2014). Enantiomeric Excesses Induced in Amino Acids by Ultraviolet Circularly Polarized Light Irradiation of Extraterrestrial Ice Analogs: A Possible Source of Asymmetry for Prebiotic Chemistry. *The Astrophysical Journal*, 788, 79.

Moores, J. E. and Schuerger, A. C. (2012). UV degradation of accreted organics on Mars: IDP longevity, surface reservoir of organics, and relevance to the detection of methane in the atmosphere. *Journal of Geophysical Research: Planets*, 117, E08008.

Morris, R. V., Ming, W., Golden, D. C., Arvidson, R. E., Wiseman, S. M., Lichtenberg, K. A., Cull, S., and Graff, T. G. (2009). Visible and near-IR reflectance spectra for smectite, sulfate and perchlorate under dry conditions for interpretation of martian surface mineralogy. In *40th Lunar and Planetary Science Conference, #2317*.

Mustafa, K. A., Sephton, M. A., Watson, J. S., Spathopoulos, F., and Krzywiec, P. (2015). Organic geochemical characteristics of black shales across the Ordovician–Silurian boundary in the Holy Cross Mountains, central Poland. *Marine and Petroleum Geology*, 66, 1042–1055.

Nelson, K. E., Levy, M., and Miller, S. L. (2000). Peptide nucleic acids rather than RNA may have been the first genetic molecule. *Proceedings of the National Academy of Sciences of the United States of America*, 97, 3868–3871.

Pavlov, A. A., Vasilyev, G., Ostryakov, V. M., Pavlov, A. K., and Mahaffy, P. (2012). Degradation of the organic molecules in the shallow subsurface of Mars due to irradiation by cosmic rays. *Geophysical Research Letters*, 39, L13202.

Peters, K. E., Walters, C. C., and Moldowan, J. M. (2005). *The Biomarker Guide*. Cambridge University Press, New York.

Poch, O., Jaber, M., Stalport, F., Nowak, S., Georgelin, T., Lambert, J.-F., Szopa, C., and Coll, P. (2015). Effect of Nontronite Smectite Clay on the Chemical Evolution of Several Organic Molecules under Simulated Martian Surface Ultraviolet Radiation Conditions. *Astrobiology*, 15, 221–237.

Poch, O., Kaci, S., Stalport, F., Szopa, C., and Coll, P. (2014). Laboratory insights into the chemical and kinetic evolution of several organic molecules under simulated Mars surface UV radiation conditions. *Icarus*, 242, 50–63.

Quantin, C., Carter, J., Thollot, P., Broyer, J., Lozach, L., Davis, J., Grindrod, P., Pajola, M., Baratti, E., and Rossato, S. (2016). Oxia Planum, the landing site for ExoMars 2018. In *47th Lunar and Planetary Science Conference Abstracts, #2863*.

Rodier, C., Sternberg, R., Szopa, C., Buch, A., Cabane, M., and Raulin, F. (2005). Search for organics in extraterrestrial environments by in situ gas chromatography analysis. *Advances in Space Research*, 36, 195–200.

Saiz-Jimenez, C. (1994). Production of alkylbenzenes and alkylnaphthalenes upon pyrolysis of unsaturated fatty acids. *Naturwissenschaften*, 81, 451–453.

Sephton, M. A. (2002). Organic compounds in carbonaceous meteorites. *Natural Product Reports*, 19, 292–311.

Siljeström, S., Freissinet, C., Goesmann, F., Steininger, H., Goetz, W., Steele, A., and Amundsen, H. (2014). Comparison of Prototype and Laboratory Experiments on MOMA GCMS: Results from the AMASE11 Campaign. *Astrobiology*, 14, 780–797.

Southard, A., Adachi, T., Arevalo, R., Brown, G., Johnson, C., Gonnsen, Z., Meyer, S., Brinckerhoff, W., and Mahaffy, P. (2014). High speed and accurate pressure measurement with a micropirani pressure gauge for pressures from 100 mTorr to sub 1mTorr. In *62nd ASMS, TP711*.

Squyres, S. W., Arvidson, R. E., Ruff, S., Gellert, R., Morris, R. V., Ming, D. W., Crumpler, L., Farmer, J. D., Marais, D. J. D., Yen, A., McLennan, S. M., Calvin, W., Bell, J. F., Clark, B. C., Wang, A., McCoy, T. J., Schmidt, M. E., and de Souza, P. A. (2008). Detection of Silica-Rich Deposits on Mars. *Science*, 320, 1063–1067.

Steele, A., McCubbin, F. M., Fries, M., Kater, L., Boctor, N. Z., Fogel, M. L., Conrad, P. G., Glamoclija, M., Spencer, M., Morrow, A. L., Hammond, M. R., Zare, R. N., Vicenzi, E. P., Siljeström, S., Bowden, R., Herd, C. D. K., Mysen, B. O., Shirey, S. B., Amundsen, H. E. F., Treiman, A. H., Bullock, E. S., and Jull, A. J. T. (2012). A Reduced Organic Carbon Component in Martian Basalts. *Science*, 337, 212–215.

Steininger, H., Goesmann, F., and Goetz, W. (2012). Influence of magnesium perchlorate on the pyrolysis of organic compounds in Mars analogue soils. *Planetary and Space Science*, 71, 9–17.

Summons, R. E. (2014). The exceptional preservation of interesting and informative biomolecules. In M. Laflamme, J. D. Schiffbauer, and S. A. F. Darroch (Eds.), *Reading and Writing of the Fossil Record: Preservational Pathways to Exceptional Fossilization. The Paleontological Society Papers Vol. 20*. The Paleontological Society, pp. 217–236.

Summons, R. E., Albrecht, P., McDonald, G., and Moldowan, J. M. (2008). Molecular Biosignatures. *Space Science Reviews*, 135, 133–159.

Sutter, B., Boynton, W. V., Ming, D. W., Niles, P. B., Morris, R. V., Golden, D. C., Lauer, H. V., Fellows, C., Hamara, D. K., and Mertzman, S. A. (2012). The detection of carbonate in the martian soil at the Phoenix Landing site: A laboratory investigation and comparison with the Thermal and Evolved Gas Analyzer (TEGA) data. *Icarus*, 218, 290–296.

Sutter, B., McAdam, A. C., Rampe, E. B., Ming, D. W., Mahaffy, P. R., Navarro-González, R., Stern, J. C., Eigenbrode, J. L., and Archer, P. D. (2016). Evolved gas analyses of sedimentary materials in Gale Crater, Mars: Results of the curiosity Rover's Sample Analysis at Mars (SAM) instrument from Yellowknife Bay to the Stimson formation. In *47th Lunar and Planetary Science Conference, #2048*.

Tarasevych, A. V., Sorochinsky, A. E., Kukhar, V. P., and Guillemin, J.-C. (2015). High temperature sublimation of α-amino acids: a realistic prebiotic process leading to large enantiomeric excess. *Chemical Communications*, 51, 7054–7057.

Vago, J. L., Westall, F., Pasteur Instrument Teams, L. S. S. W. G., Other, C., Coates, A. J., Jaumann, R., Korablev, O., Ciarletti, V., Mitrofanov, I., Josset, J.-L., De Sanctis, M. C., Bibring, J.-P., Rull, F., Goesmann, F., Steininger, H., Goetz, W., Brinckerhoff, W., Szopa, C., Raulin, F., Edwards, H. G. M., Whyte, L. G., Fairén, A. G., Bridges, J., Hauber, E., Ori, G. G., Werner, S., Loizeau, D., Kuzmin, R. O., Williams, R. M. E., Flahaut, J., Forget, F., Rodionov, D., Svedhem, H., Sefton-Nash, E., Kminek, G., Lorenzoni, L., Joudrier, L., Mikhailov, V., Zashchirinskiy, A., Alexashkin, S., Calantropio, F., Merlo, A., Poulakis, P., Witasse, O., Bayle, O., Bayón, S., Meierhenrich, U., Carter, J., García-Ruiz, J. M., Baglioni, P., Haldemann, A., Ball, A. J., Debus, A., Lindner, R., Haessig, F., Monteiro, D., Trautner, R., Voland, C., Rebeyre, P., Goulty, D., Didot, F., Durrant, S., Zekri, E., Koschny, D., Toni, A., Visentin, G., Zwick, M., van Winnendael, M., Azkarate, M., Carreau, C., and the ExoMars Project Team (2017). Habitability on Early Mars and the Search for Biosignatures with the ExoMars Rover. *Astrobiology*, 17, 471–510.

Völklein, F., Grau, M., Meier, A., Hemer, G., Breuer, L., and Woias, P. (2013). Optimized MEMS Pirani sensor with increased pressure measurement sensitivity in the fine and high vacuum regime. *Journal of Vacuum Science & Technology A: Vacuum, Surfaces, and Films*, 31, 61604.

Westall, F., Foucher, F., Bost, N., Bertrand, M., Loizeau, D., Vago, J. L., Kminek, G., Gaboyer, F., Campbell, K. A., Bréhéret, J.-G., Gautret, P., and Cockell, C. S. (2015). Biosignatures on Mars: What, Where, and How? Implications for the Search for Martian Life. *Astrobiology*, 15, 998–1029.

Zimmer, C. (2009). On the Origin of Life on Earth. *Science*, 323, 198–199.

Abbreviations

ADRON	Active Detector for gamma Rays and Neutrons
AGC	Automatic Gain Control (for laser output control)
ALD	Analytical Laboratory Drawer (containing the analytical instruments (MicroOmega, RLS, MOMA) and UCZ)
CDH	Command and Data Handling board (part of MEB)
CEM	Channel Electron Multiplier (part of MS detector)
CLUPI	CLose-UP Imager
COSAC	COmetary SAmpling and Composition (GC–MS instrument onboard Philae Lander that is part of the Rosetta mission to comet 67P)
CTL	Control board (part of SEB)
DMF	*N*,*N*-dimethylformamide (solvent for MTBSTFA and GC calibrant)
DMF-DMA	*N*,*N*-dimethylformamide-dimethylacetal (MOMA derivatization agent)
DSC	Differential Scanning Calorimetry
DTA	Differential Thermal Analysis
EDL	Entry Descent Landing
ee	enantiomeric excess (of chiral organic molecules)
EGA	Evolved Gas Analysis
EI	Electron Ionization Source (part of MS)
ETU	Engineering Test Unit (flight-like test unit for LDMS)
FAS	Flight Analog System (setup at MPS, replicating some aspects of GC–MS)
FB	Filament Bias board (part of SEB)
FM	Flight Model
FS	Flight Spare
FWHM	Full-Width Half-Maximum
GC	Gas Chromatograph or Gas Chromatography
GC–MS	Gas Chromatography–Mass Spectrometry
GSFC	Goddard Space Flight Center, Greenbelt (NASA center developing MS and electronics)
GT	Gas Tank (of GC system)
ISEM	Infrared Spectrometer for ExoMars
ITMS	Ion Trap Mass Spectrometry
LADEE	Lunar Atmosphere and Dust Environment Explorer (orbiter, September 2013 to April 2014)
LATMOS	Laboratoire ATmosphéres, Milieux, Observations Spatiales, Guyancourt (developing GC–MS and electronics)
LD	Laser Desorption
LDI	Laser Desorption and Ionization

LDMS	Laser Desorption Mass Spectrometry
LH	Laser Head
LISA	Laboratoire Interuniversitaire des Systémes Atmosphériques, Créteil (developing GC–MS and electronics)
LIT	Linear Ion Trap (part of MS)
LPU	Laser Power Unit (part of MEB)
LZH	Laser-Zentrum Hannover (developing UV laser for LDMS, MPS subcontractor)
MAIF	Motor and Analog Interface (part of MEB)
Ma_MISS	Mars Multispectral Imager for Subsurface Studies
MAVEN	Mars Atmosphere and Volatile EvolutioN (orbiter, since 2014)
MEB	Main Electronic Box
MER	Mars Exploration Rovers (since 2004)
MEX	Mars EXpress (orbiter since 2004)
MicrOmega	"Micro version" of OMEGA (ALD instrument)
MOMA	Mars Organic Molecule Analyzer (ALD instrument)
MPS	Max Planck Institute for Solar System Research, Göttingen (developing MOMA subsystems (oven, TP, laser) and electronics)
MS	Mass Spectrometer or Mass Spectrometry
MS/MS	tandem MS (MS operational mode)
MSL	Mars Science Laboratory (Curiosity rover, since 2012)
MTBSTFA	*N,N*-methyl-tert.-butyl-dimethylsilyltrifluoroacetamide (MOMA derivatization agent)
OMEGA	Observatoire pour la Minéralogie, l'Eau, les Glaces et l'Activité (VIS/NIR mineralogical mapping spectrometer on-board MEX)
PAH	Polyaromatic Hydrocarbon
PanCam	Panoramic Camera System
PCV	Pressure Control Valve (controlling GC gas flow)
PFTBA	pertrifluorotributylamine
PH	Power and High-Voltage (part of SEB)
PS	Power Supply
QM	Qualification Model
QMS	Quadrupole Mass Spectrometer
QSM	Qualification Simulator Model
RF	Radio Frequency (power supply for LIT control)
RLS	Raman Laser Spectrometer (ALD instrument)
RSM	Reference Surface Mission (preliminary rover mission plan, feasibility study in terms of time, power, and data resources)

SAM	Sample Analysis at Mars (organic molecule and volatile analyzer onboard MSL)
SEB	Secondary Electronics Box
SNR	Signal-to-Noise Ratio
SPDS	Sample Processing and Distribution System (composed of sample inlet, sample path, and oven carousel, not part of MOMA)
SPRL	Space Physics Research Laboratory
SWIFT	Stored Waveform Inverse Fourier Transform (MS operational mode)
TAS-I	Thales Alenia Space in Torino, Italy
TCD	Thermal Conductivity Detector (GC detector)
TEGA	Thermal and Evolved Gas Analyzer (onboard the Phoenix Mars Lander, May to October 2008)
TMAH	tetramethylammonium hydroxide (MOMA derivatization agent)
TS	Tapping Station (sealing the oven for GC–MS)
UCZ	Ultra-Clean Zone (part of SPDS that is in direct contact with martian samples)
UV	Ultraviolet
WISDOM	Water Ice Subsurface Deposit Observation on Mars (radar for shallow subsurface)
WRP	Wide-Range Pump

- Chapter 6 -

Investigating the effect of perchlorate on flight-like gas chromatography–mass spectrometry as performed by MOMA onboard the ExoMars 2020 rover

(in preparation, to be submitted to *Icarus*)

Helge Mißbach, Harald Steininger, Volker Thiel, Walter Goetz

Abstract

The Mars Organic Molecule Analyzer (MOMA) instrument will be the key instrument onboard ESA's ExoMars 2020 rover (launch in July 2020) and will be essential in the search for organic matter and molecular biosignatures. One analytical approach for the investigation of potential martian organics will be gas chromatography–mass spectrometry (GC–MS). All MOMA GC–MS techniques rely on thermal volatilization of organic compounds. Problematically, perchlorates and chlorates in martian soils become highly reactive during heating and can lead to oxidation and chlorination of organic compounds, potentially rendering them unidentifiable. In this study we analyzed a synthetic and a natural sample with and without Mg-perchlorate (0 wt%, 1 wt%, 10 wt%) aiming at evaluating the applicability of MOMA-like GC–MS techniques to different sample types and assessing the impact of perchlorate on the analysis. We used a MOMA flight analog system coupled to a commercial GC–MS to perform MOMA-like pyrolysis (700 °C, 10 s), in situ derivatization with *N/N*-methyl-tert-butyl-dimethylsilyltrifluoroacetamide/*N/N*-dimethylformamide (MTBSTFA/DMF; 250 °C, 10 min) and *N/N*-dimethylformamide dimethyl acetal (DMF-DMA; 140 °C, 4 min) as well as in situ thermochemolysis with tetramethylammonium hydroxide (TMAH; 600 °C, 40 s). We showed that pyrolysis can provide a sufficient overview of the organic inventory but is largely affected by the presence of perchlorates. In situ derivatization with MTBSTFA/DMF facilitates the identification of functionalized organics but has a low efficiency for *n*-alkanoic acids. Meanwhile, no results could be obtained with DMF-DMA on the types of organics studied here. Thermochemolysis has been shown to be an effective technique for the identification of both refractory and functional compounds, although analytical by-products were observed. Most importantly, this technique was not affected by perchlorates. Therefore, we demonstrated that perchlorates in martian soils do not necessarily hinder MOMA-like GC–MS analysis. Furthermore, we illustrate the complementarity of different MOMA GC–MS techniques in order to characterize the full organic inventory of a given sample. Hence, the results of our study will serve current and future missions to Mars and provide a reference for the interpretation of upcoming MOMA data.

Keywords: Mars, Mars Organic Molecule Analyzer, ExoMars, gas chromatography-mass spectrometry, pyrolysis, thermochemolysis, perchlorate, organics.

6.1   Introduction

After four decades of Mars exploration, beginning with the first investigation by the Viking Landers in 1976 (Biemann et al., 1977; ten Kate, 2010; Goetz et al., 2016; Levin and Straat, 2016), the search for biosignatures and therefore indications for past or present life is still one of the key objectives for future robotic missions to the martian surface (Westall et al., 2015; Vago et al., 2017). One of the next missions is ESA's ExoMars rover that shall be launched in 2020. The instruments onboard include a variety of optical and analytical instruments that allow to perform a broad search for morphological and chemical biosignatures as well as geological context information on the surface and in the near subsurface of Mars (2 m depth, with help of a drilling device; Vago et al., 2017). The Mars Organic Molecule Analyzer (MOMA; Goesmann et al., 2017) is the largest instrument on the rover and the key instrument to detect molecular biosignatures. Together with an infrared spectrometer (MicrOmega; Bibring et al., 2017) and the Raman Laser Spectrometer (RLS; Rull et al., 2017) it makes up the rover's analytical laboratory which is meant to perform detailed analysis of martian sediments (Vago et al., 2017).

MOMA will examine martian samples by laser desorption/ionization mass spectrometry (LDMS) or gas chromatography–mass spectrometry (GC–MS) techniques (Goesmann et al., 2017; Li et al., 2017). GC–MS provides the opportunity to separate and identify organics with high sensitivity and is therefore well suited to search for molecular biosignatures in extraterrestrial samples (Summons et al., 2008). Lately, the SAM instrument (Sample Analysis at Mars) onboard the Curiosity rover demonstrated that GC–MS is a powerful tool to detect low molecular weight organics in martian surface sediments (Mahaffy et al., 2012; Freissinet et al., 2015). MOMA GC–MS has 3 different operational modes, including pyrolysis (thermal volatilization), in situ derivatization and in situ thermochemolysis (on-line methylation). In situ derivatization and in situ thermochemolysis onboard MOMA are complemented by thermal desorption of the (derivatized) organics from crushed sample material. These techniques are meant to facilitate the analysis of polar compounds (e.g., alkanols, fatty acids, amino acids) via GC–MS and, in the case of thermochemolysis, to limit destruction of refractory organics at higher desorption temperatures (Challinor, 2001; Rodier et al., 2005; Buch et al., 2006; Geffroy-Rodier et al., 2009; Zaikin and Halket, 2009). A detailed description of the MOMA GC–MS and the operational modes is given in Goesmann et al. (2017).

Organic signatures in martian sediments can potentially derive from biological sources (i.e., past or present life) or from abiotic sources, as for example meteorites or in situ abiotic synthesis (Flynn, 1996; Shock and Schulte, 1998; Botta and Bada, 2002; McCollom and Seewald, 2007; Summons et al., 2011; Konn et al., 2015; Westall et al., 2015). Therefore, it is crucial to determine whether potential organic molecules found on Mars derive from abiotic or biological sources, for example by looking for specific distribution patterns of organic compounds, stable isotope patterns or enantiomeric excess (Meierhenrich, 2008; Summons et al., 2008; Cady and Noffke, 2009; Westall et al., 2015; Vago et al., 2017). Especially lipid biomarkers have the potential to be preserved over geological timescales (Brocks and Summons, 2003; Summons, 2014). However, discrimination between abiotic and biologically derived organics can be hampered by degradation of organic molecules, for example, via thermal alteration or radiation (Oró and Holzer, 1979; Brocks and Summons, 2003; Peters et al., 2005a,b; Kminek and Bada, 2006; Pavlov

et al., 2012; Mißbach et al., 2016). On the martian surface and in the near subsurface, organics are probably largely degraded by primary (i.e., impact fragmentation of organic compounds) or secondary (oxidation of organic compounds by e.g., O$^{\bullet}$ or HO$^{\bullet}$ radicals generated from particle impacts with the mineral matrix) effects from solar and/or galactic cosmic rays (Pavlov et al., 2012).

The ExoMars rover's capability to collect samples from 2 m depth allows obtaining martian sediments that were protected from radiation and thus, potentially, inhabit preserved organic matter (Westall et al., 2015; Goetz et al., 2016; Vago et al., 2017). However, analysis of these potential organics can be further complicated by the presence of oxychlorine compounds (Ca- and Mg-perchlorates and chlorates, hereafter for the sake of simplicity referred to as "perchlorates") in martian sediments whose presence was revealed by Phoenix and MSL (Hecht et al., 2009; Kounaves et al., 2010, 2014; Glavin et al., 2013; Sutter et al., 2017). Reevaluation of Viking results (Biemann et al., 1976, 1977) suggested that perchlorates were also present at Viking landing sites, although these results were questioned and intensively discussed (Navarro-González et al., 2010, 2011; Biemann and Bada, 2011; Navarro-González and McKay, 2011). The interference of perchlorates in pyrolysis measurements of martian sediments is known from SAM analysis (Glavin et al., 2013; Freissinet et al., 2015). Perchlorates itself are relatively inactive and thus remain in soils unless they are washed away by water flows (Brown and Gu, 2006; Catling et al., 2010). However, they become reactive during heating, as the perchlorate molecule decomposes in the temperature range 200 – 600 °C, and can lead to oxidation and chlorination of organic compounds (Navarro-González et al., 2010, 2011; Steininger et al., 2012; Sephton et al., 2014). Potential biosignatures may therefore being rendered unidentifiable in the presence of perchlorates (i.e., transformation in CO_2; Steininger et al., 2012).

Analog studies are necessary to determine analytical limits and pitfalls and hence, they are an essential prerequisite to support data interpretation for upcoming space missions. In this study we analyzed two different samples (synthetic and natural) with addition of different amounts of perchlorate using a flight analog system coupled to a commercial GC–MS and MOMA-like pyrolysis and in situ derivatization/thermochemolysis techniques. The study aims at (i) evaluating the applicability of MOMA-like GC–MS techniques to different sample types, (ii) assessing the impact of Mg-perchlorates (martian soil constituents) on organics during heating and (iii) providing reference data for interpretation of potential MOMA results. It is not meant to give a detailed quantitative evaluation of the two samples. Our results demonstrate that especially thermochemolysis with TMAH is a powerful technique to determine different organics in perchlorate rich samples.

6.2   Materials and methods

6.2.1   Samples

Two different samples were used in this study. A standard mix consisting of primary and secondary alkanols (n-C_{11} – n-C_{13} alkan-1-ols; n-C_{11} and n-C_{12} alkan-2-ols, respectively) and n-alkanoic acids (C_{11} – C_{13}) with the following general molar abundances:

n-alkan-1-ols $> n$-alkanoic acids $> n$-alkan-2-ols. The mixture was deposited on SiO_2 (silica gel; pre cleaned at 550 °C for > 3 h). These compounds are some of the main compound classes resulting from abiotic synthesis (McCollom et al., 1999; Rushdi and Simoneit, 2001; Mißbach et al., 2018), and are also important biotic organic lipids that will be targeted by ExoMars and MOMA (Summons et al., 2008; Goesmann et al., 2017; Vago et al., 2017). The second sample was a silica-rich Silurian black chert from the Holy Cross Mountains in central Poland (for details see Kremer, 2005; Kremer and Kazmier-czak, 2005), containing ~ 0.5 wt% total organic carbon. This sample was also used in an earlier study (Goesmann et al., 2017; their Chapter 7.5) and is meant as a natural ref-erence in this study. It has been manually powdered using a mortar that was intensively rinsed with isopropanol and dried prior to use. Higher organic content of the samples compared to martian sediments is helpful in the laboratory environment to guarantee a clear distinction between signals from the samples and background/contamination.

For this study, magnesium perchlorate (Mg-perchlorate) was used to test the effects of perchlorates on MOMA-like GC–MS techniques. Two different Mg-perchlorate con-centrations were used: ~ 1 wt% and ~ 10 wt%, meaning to represent concentrations close to those detected on Mars (Hecht et al., 2009; Glavin et al., 2013; Sutter et al., 2017) and a worst-case scenario, respectively. Perchlorates are highly mobile in water (Brown and Gu, 2006). Therefore, local enrichment of perchlorates via formation of salt brines in subsurface areas is possible (Cull et al., 2010; Martín-Torres et al., 2015). Depending on the desired concentration, perchlorate was added to the sample in different ways. For samples with 1 wt% perchlorate content, the perchlorate was first mixed with pre-cleaned (550 °C for > 3 h) and powdered (pebble mill) sea sand and afterwards mixed with the sample in the right ratio. This step was necessary for an easier and more exact handling of small amounts of perchlorate. Pure Mg-perchlorate was mixed with the samples to reach 10 wt% perchlorate content.

6.2.2 MOMA flight analog system and experimental procedure

The experiments were performed with a MOMA flight analog system (FAS) connected to a commercial GC–MS (see also Section 6.2.3). This setup was described for earlier ex-periments in Goesmann et al. (2017). The FAS consists of a MOMA oven, an adsorption trap (filled with Tenax® GR; see Goesmann et al., 2017 for details) and a tapping station including all the tubing to connect the different parts with the GC–MS (Fig. 6.1). All transfer lines were heated to circa 110 °C.

The analyses in this study were performed as close as possible to MOMA conditions. However, there are differences to the MOMA flight GC–MS instrument and the basic pro-cedures as they had to be transferred to a laboratory configuration. The major differences are: (i) The maximum temperatures of the transfer lines and the adsorption trap are lower in the FAS light compared to those planned for the MOMA flight instrument (transfer lines: 110 °C vs. 135 °C, trap: 160 °C vs. 300 °C, respectively); (ii) the adsorption trap in the FAS does not support flow inversion so that volatiles have to pass through the whole trap on their way to the GC. This increases the chance of cross contamination; (iii) less derivatization agent was used (3.5 μL vs. 15 μL in MOMA) and it was added to the cold sample, instead of being released from derivatization capsules at elevated temperatures. A detailed discussion on this matter and the exact MOMA GC–MS conditions are given
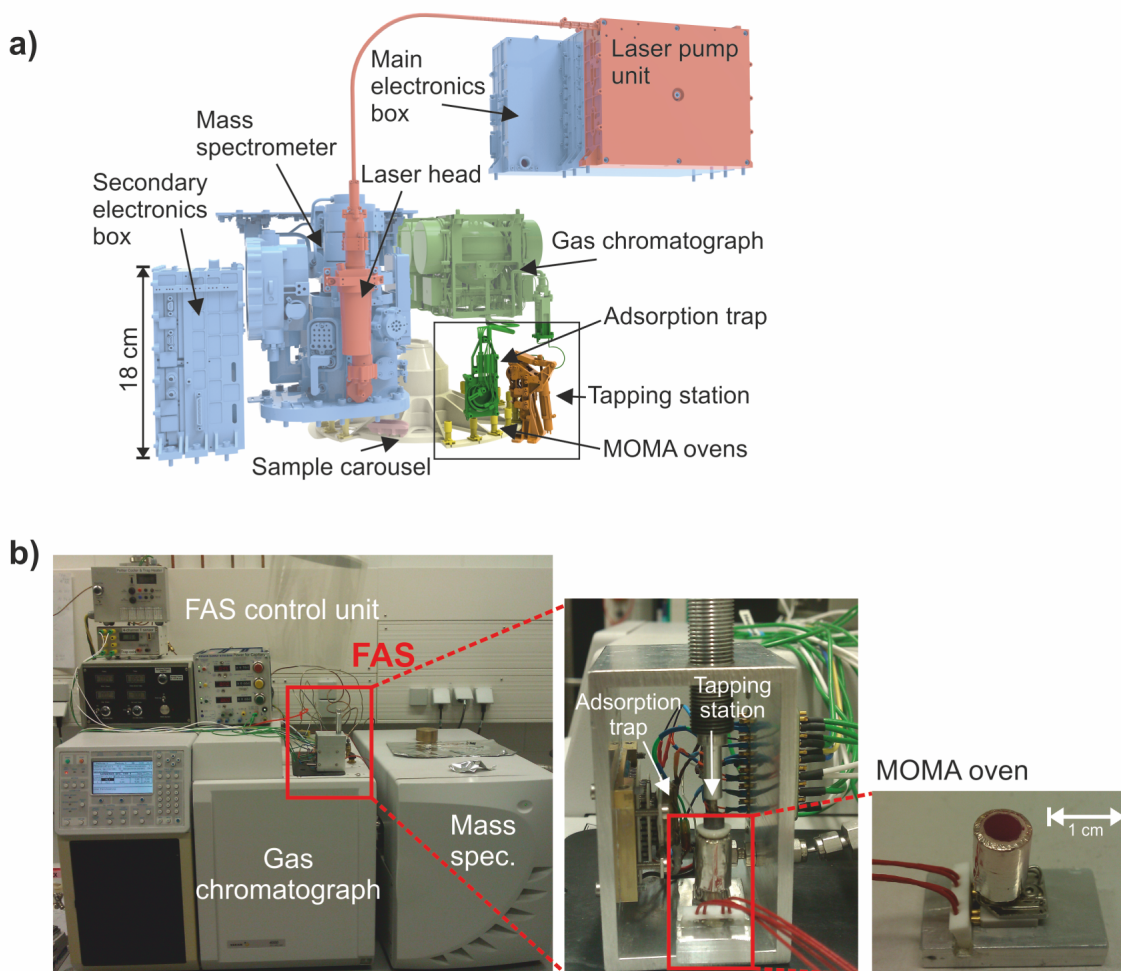
Figure 6.1: (**a**) The MOMA instrument and (**b**) the flight analog system (FAS). Parts highlighted in box of (**a**) are part of the FAS. (**b**) FAS mounted on GC (left), view inside the FAS with adsorption trap and tapping station that seals the oven (middle) and the oven when separated from the tapping station (right).

in Goesmann et al. (2017).

For every analysis, between 3.5 and 4 mg of sample was used. If applicable, the sample was mixed with ∼ 1 mg perchlorate mix or ∼ 0.5 mg pure perchlorate (aiming for 1 wt% or 10 wt% Mg- perchlorate, respectively). After transferring the sample to the oven, it was pre-dried at 80 °C for 10 min, leaving the oven unconnected to the tapping station. For in situ derivatization and thermochemolysis, 3.5 µL of the particular wet chemistry reagent were added to the dried sample. The following reagents were used:

- *N,N*-methyl-tert-butyl-dimethylsilyltrifluoroacetamide (MTBSTFA; > 97%, Sigma-Aldrich) with *N,N*-dimethylformamide (DMF; > 99.5%, Thermo Scientific™) in a 3:1 (V:V) mixture, while DMF is added to gain derivatization efficiency (Buch et al., 2006)

- *N,N*-dimethylformamide dimethyl acetal (DMF-DMA; Sigma-Aldrich)

- Tetramethylammonium hydroxide (TMAH, 25 wt% in methanol; Sigma-Aldrich)

163

MTBSTFA/DMF and DMF-DMA were used for in situ derivatization, TMAH for in situ thermochemolysis. MTBSTFA and TMAH are available in the SAM instrument onboard the Curiosity rover (Mahaffy et al., 2012). All three reagents will be available in the MOMA instrument.

After connecting the oven to the tapping station, the adsorption trap was cooled to 0 °C by a Peltier element. Pyrolysis was performed directly as a single heating step to 700 °C for 10 s. The heating rate of the oven is circa 300 °C/min. Reaction temperatures and times for in situ derivatization/thermochemolysis with MTBSTFA/DMF, DMF-DMA and TMAH were the following: 250 °C for 10 min, 140 °C for 4 min and 600 °C for 40 s, respectively. Flash heating of the adsorption trap to 160 °C (circa 200 °C/min) was initiated right afterwards to release volatiles into the GC–MS, which was started in parallel. Slight fluctuations of the heating rate of the adsorption trap and temperature of transfer lines can occur. Thus, the release of compounds from the adsorption trap is not steady and can eventually lead to variations in the retention times of compounds of 0.1 – 0.3 min.

Multiple cleaning runs and system blank analyses were carried out between the sample runs to control cross contamination. Furthermore, blank analyses of Mg-perchlorate and all wet chemistry reagents were conducted. All blanks were carried out in pyrolysis mode.

6.2.3 GC–MS parameters

A Varian 3800 GC coupled to a Varian 240-MS was used for this study. The GC was equipped with a capillary column (Varian Factor Four VF-5ms; 30 m length, 0.25 mm inner diameter, 0.25 μm film thickness). This column has similar properties as the Restek MXT-5 used in the MOMA instrument (Goesmann et al., 2017). The carrier gas (helium) flow was set to 2 mL/min. The injector temperature was 250 °C and the split ratio was set to 30. The GC oven was heated from 30 (isotherm for 1 min) to 250 °C (isotherm for 5 min) with 10 °C/min. The solvent delay was 1 min for pyrolysis, 10 min for MTBSTFA/DMF, 8 min for DMF-DMA and 7 min for TMAH. Recording of full scan mass spectra proceeded in fast scan mode with a scan time of 0.58 s and a mass range from m/z 35 to 1000. Compounds were determined by comparison to reference spectra (NIST mass spectral library). n-Alkenes were also identified by elution order (Nierop and van Bergen, 2002).

6.3   Results

6.3.1   Blanks

Blanks showed traces of contamination, mostly in the form of siloxanes (e.g., column degradation), phthalates (e.g., from plasticizers from transport boxes, vial caps), silanes and DMF (carryover from previous runs with derivatization agents, Fig. C.1a). Additionally, minor amounts of cross contamination in varying composition from earlier analyses with different samples were detected. The most prominent were for example chloroalkanes and sulfur (from black chert) in some of the runs.

The perchlorate blank showed a variety of chlorinated organics, including chloroethene,

carbon tetrachloride, pentachlorobenzene and hexachlorobenzene (Fig. C.1b). Furthermore, compounds bearing both nitrogen and chlorine were detected. Formation of these compounds might be explained by the reaction of chlorine with N-bearing compounds (e.g., DMF carryover, see above and Fig. C.1a).

6.3.2 Pyrolysis

Pyrolysis of standard mix yielded n-alkenes (including n-alk-1-enes, n-alk-2-enes and mid-chain alkenes; in the following summarized as n-alkenes), n-alkanals and n-alkanones and benzene, whereby three of the n-alkenes ($C_{11}-C_{13}$) were dominant compounds (Fig. 6.2a). Only low amounts of n-alkanones and benzene were detected, relative to the abundance of n-alkenes. None of functionalized compounds initially present in the standard mix were observed. Addition of 1 wt% of Mg-perchlorate to standard mix basically led to the same range of compounds during pyrolysis (Fig. 6.2b), although lower amounts of n-alkenes were detected (note different y-axis ranges in Figs. 6.2a−c). Furthermore, low amounts of chloroalkanes were observed. The analysis of standard mix with 10 wt% Mg-perchlorate again shows the same compounds. n-Alkenes further lost in abundance, whereas n-alkanals only minorly changed. Additionally, n-alkynes were observed. A major difference is the dominant appearance of chlorinated compounds, including for example chloroalkanes, dichloroalkanes, dichloromethane and chlorobenzene (Fig. 6.2c).

Pyrolysis of the black chert revealed n-alkenes (C_5-C_{20}), n-alkanes (C_7-C_{21}) and a variety of aromatic hydrocarbons (e.g., benzene, toluene, xylenes, naphthalene, phenanthrene; Fig. C.2a). Analysis of the sample with 1 wt% of Mg-perchlorate resulted in the same variety of compounds. Nevertheless, the relative abundances of some compounds to each other are shifted (e.g., benzene vs. toluene; naphthalene vs neighboring n-alkene/n-alkane; Fig. C.2b). Also an overall lower abundance of aliphatic hydrocarbons and shorter range of n-alkenes (C_5-C_{16}) was observed (Fig. C.2b). The pyrolysis experiment of the black chert with 10 wt% Mg-perchlorate mostly led to chlorinated compounds (e.g., carbon tetrachloride, chloral hydrate, chlorobenzenes; Fig. C.2c). The only aromatic hydrocarbon observed was toluene. No aliphatic hydrocarbons were detected. Some of the chlorinated compounds seen in this run were also detected in the perchlorate blank, but in much lower amounts (Fig. C.1b).

6.3.3 Derivatization with MTBSTFA/DMF and DMF-DMA

In situ derivatization of n-alkanols and n-alkanoic acids from the standard mix with MTBSTFA/DMF resulted in their tert-butyldimethylsilyl ethers and esters, respectively (Fig. 6.3a). n-Alkanoic acids showed lower abundances in comparison to n-alkan-2-ols and only traces of n-tridecanoic acid were observed (not shown in Fig. 6.3a). Beside the standard mix compounds, major contamination from the derivatization agent was present. The analysis with 1 wt% of Mg-perchlorate yielded the same compounds with almost the same response (Fig. 6.3b). Analyses with high amounts of perchlorate were not carried out with that sample (discussed in Section 6.4.2.2).

After in situ derivatization with DMF-DMA, only contamination from the derivatization agent and the system were identified. None of the expected derivatized compounds (e.g., alkanoic acid methyl esters) have been detected.
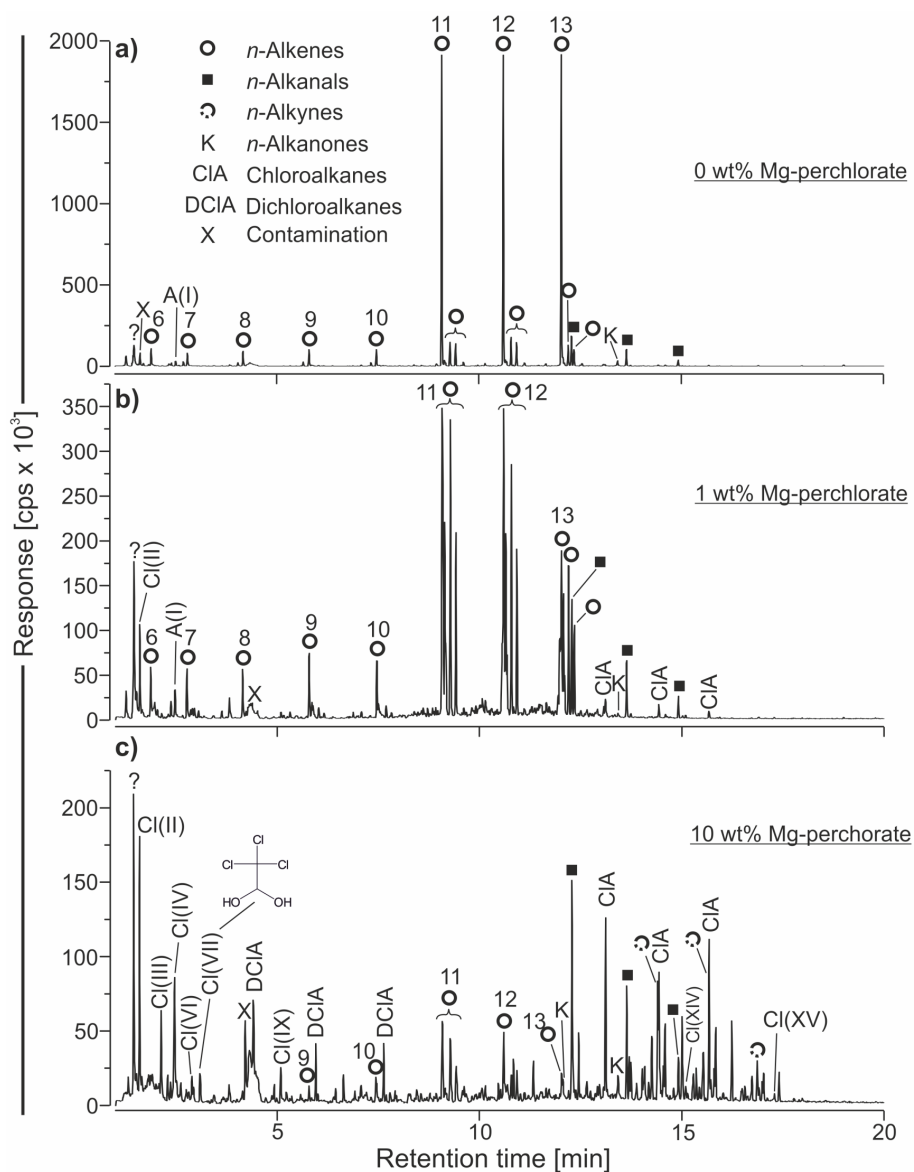
Figure 6.2: GC–MS chromatograms (total ion current) of the pyrolysis analysis of the standard mix with (**a**) 0 wt% Mg-perchlorate, (**b**) 1 wt% Mg-perchlorate and (**c**) 10 wt% Mg-perchlorate. Numbers indicate the carbon chain lengths of corresponding *n*-alkenes. Signatures with roman numerals denote aromatic and chlorinated compounds: A(I) benzene, Cl(II) dichloromethane, Cl(III) trichloromethane, Cl(IV) carbon tetrachloride, Cl(VI) trichloroethylene, Cl(VII) chloral hydrate, Cl(IX) chlorobenzene, Cl(XIV) pentachlorobenzene, Cl(XV) hexachlorobenzene; see also table C.1. Note that none of the functionalized compounds from the standard mix (i.e., *n*-alkanols or *n*-alkanoic acids) can be identified. Degradation (especially of *n*-alkenes) and formation of chlorinated compounds increases (**a**–**c**). A lot of compounds in the pyrolysis run of the standard mix with 10 wt% Mg-perchlorate could not be identified, as mass spectra were very similar (unmarked peaks in **c**). cps, counts per second.
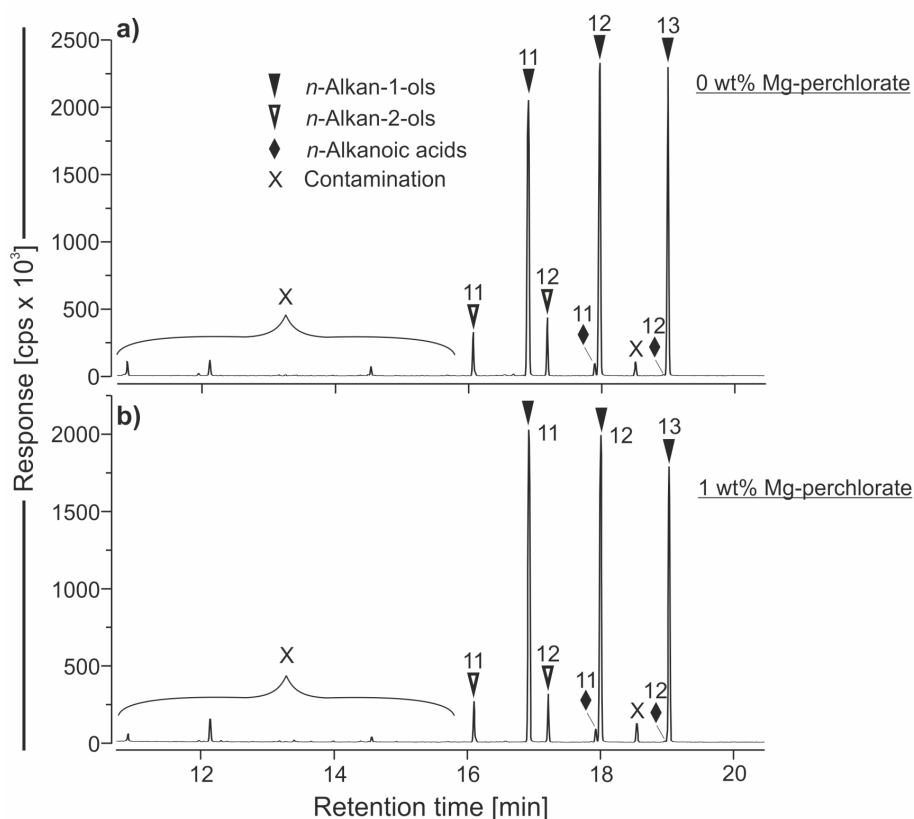
Figure 6.3: GC–MS chromatograms (total ion current) of the in situ derivatization with MTBSTFA/DMF of the standard mix with (**a**) 0 wt% Mg-perchlorate and (**b**) 1 wt% Mg-perchlorate. *n*-Alkanols and *n*-alkanoic acids were analyzed as their tert-butyldimethylsilyl ethers and esters, respectively. Numbers indicate the carbon chain lengths of corresponding *n*-alkan-1-ols, *n*-alkan-2-ols and *n*-alkanoic acids. Note that (**a**) and (**b**) look similar. Furthermore, *n*-alkanoic acids show generally low abundances and only traces of *n*-tridecanoic acid are present (not shown). cps, counts per second.

6.3.4 Thermochemolysis with TMAH

All 8 compounds from standard mix were observed in the expected abundances after in situ thermochemolysis (as their corresponding methyl ethers and methyl esters, Fig. 6.4a). Additionally, high abundances of *n*-C_{11} to *n*-C_{13} alkenes as well as lower amounts of shorter *n*-alkenes, *n*-alk-2-enes, mid chain alkenes and *n*-alkanals were observed. The same compounds were visible with 1 wt% Mg-perchlorate (Fig. 6.4b). *n*-Alkan-1-ols show the same abundance, whereas most *n*-alkanoic acids, *n*-alkenes and *n*-alkanals have lower intensities compared to the perchlorate-free analysis (see Figs. 6.4a, b). Furthermore, chloroalkanes were observed (also present in lower amounts in previous blanks). Thermochemolysis of the standard mix with 10 wt% Mg-perchlorate revealed the same compounds as for the measurements with 1 wt% Mg-perchlorate, also with similar abundances. Additionally, a variety of nitrogen-bearing compounds was detected in this run, including high amounts of 1,5-dicyano-2,4-dimethyl-2,4-diazapentane (Fig. 6.4c; Morisson, 2017; NIST mass spectral library).

The analysis of the black chert by in situ thermochemolysis is comparable to the
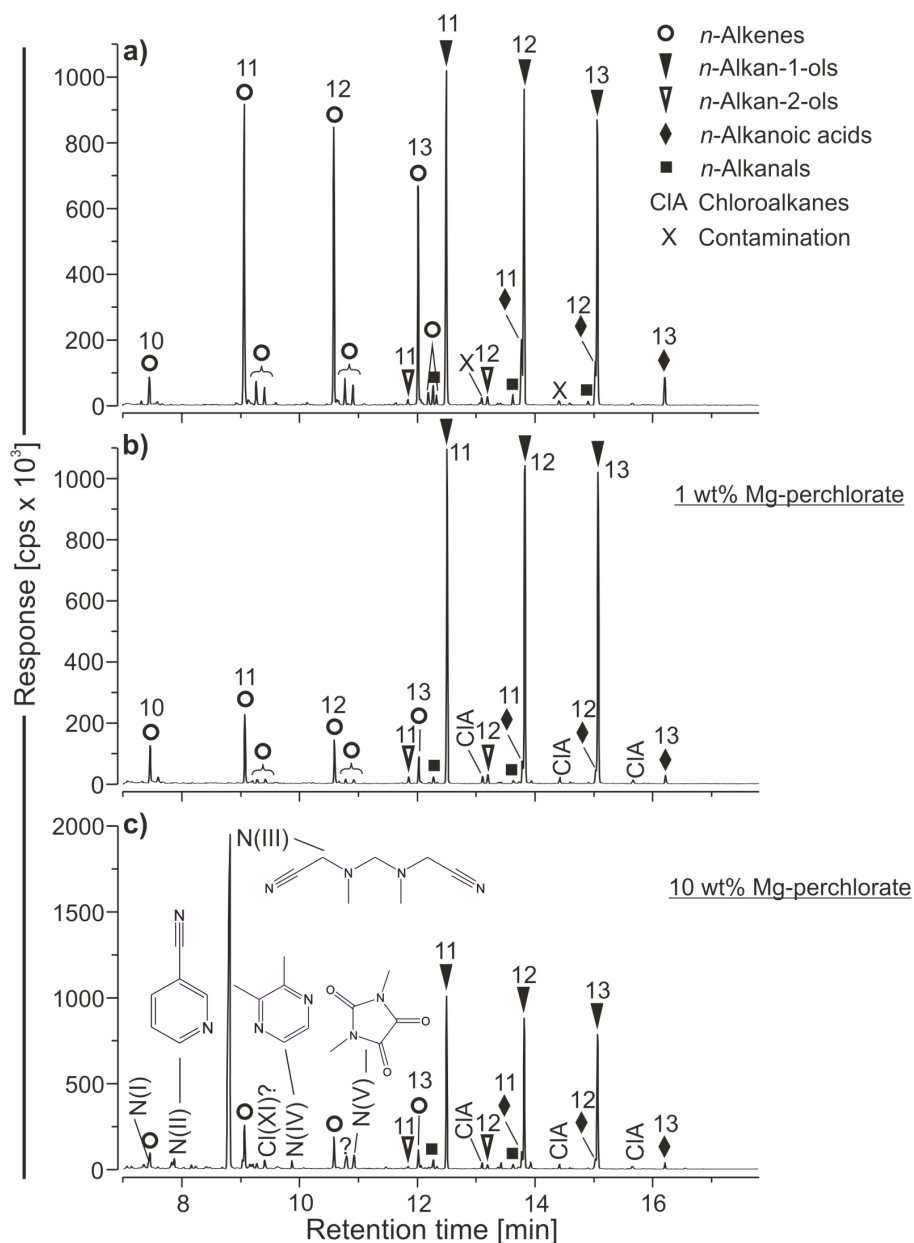
Figure 6.4: GC–MS chromatograms (total ion current) of the in situ thermochemolysis with TMAH of the standard mix with (**a**) 0 wt% Mg-perchlorate, (**b**) 1 wt% Mg-perchlorate and (**c**) 10 wt% Mg-perchlorate. *n*-Alkanols and *n*-alkanoic acids were analyzed as their methyl ethers and esters, respectively. Numbers indicate the carbon chain lengths of corresponding *n*-alkan-1-ols, *n*-alkan-2-ols, *n*-alkanoic acids and *n*-alkenes. Signatures with roman numerals denote chlorinated and nitrogen-bearing compounds: Cl(XI) chloroniconitrile, N(I) benzonitrile, N(II) pyridinecarbonitrile, N(III) 1,5-dicyano-2,4-dimethyl-2,4-diazapentane, N(IV) dimethylpyrazine, N(V) 1,3-dimethyl-2,4,5-trioxoimidazolidine; see also table C.1. Note that all compounds from the standard mix are clearly identifiable in (**a**–**c**). Thus, Mg-perchlorate does not have a large effect on these analyses. Note furthermore the dominant appearance of nitrogen-bearing compounds in (**c**). cps, counts per second.

pyrolysis run. The same compounds were detected, with a lower abundance of some aromatics relative to aliphatic hydrocarbons. Additionally, n-C$_8$ to n-C$_{14}$ alkanoic acids were detected as their methyl esters (Fig. C.3a). Thermochemolysis of the black chert with 10 wt% Mg-perchlorate led to the same array of aliphatic and aromatic hydrocarbons, compared to the analysis without perchlorate (Fig. C.3b). However, some aromatic compounds show higher abundance relative to neighboring aliphatic hydrocarbons as for example, 1-ethynyl-4-methyl-benzene and naphthalene. Acenaphtylene was identified as a dominant compound that has not been observed in other runs. Furthermore, dominant nitrogen-bearing compounds (e.g., benzonitrile, 1,5-Dicyano-2,4-dimethyl-2,4-diazapentane) were detected by thermochemolysis of both standard mix and black chert with 10 wt% Mg-perchlorate, although at very different relative abundances (Fig. C.3b; see also Fig. 6.4c).

6.4   Discussion

6.4.1   Thermal decomposition and possible by-products

Pyrolysis can transform organic compounds into other moieties via cracking of chemical bonds. The products depend on the structure of the initial organic compounds but are further controlled by temperature, ambient atmosphere, presence or absence of catalysts and reaction time (Moldoveanu, 2010).

The virtual absence of the (initially present) functionalized compounds (n-alkan-1-ols, n-alkan-2-ols, n-alkanoic acids) among the pyrolysis products of the standard mix (Fig. 6.2a) are results of thermal decomposition. Pyrolysis of an n-alkan-1-ol usually leads to the formation of the corresponding n-alkenes (n-alk-1-ene, n-alk-2-ene and mid chain varieties) and n-alkanal via dehydration and dehydrogenation, respectively, although shorter n-alkene moieties are also common products resulting from further fragmentation (Boss and Hazlett, 1976; Nierop and van Bergen, 2002; Moldoveanu, 2010). Secondary alkanols (e.g., alkan-2-ols) principally undergo the same main reactions during pyrolysis, generating n-alkenes and n-alkanones (Boss and Hazlett, 1976; Moldoveanu, 2010). Pyrolysis products of n-alkanoic acids can include n-alkanes and n-alkanones, mainly due to decarboxylation reactions (Nierop and van Bergen, 2002; Moldoveanu, 2010). n-Alkenes and n-alkanals observed after in situ thermochemolysis of the standard mix are also products of the reactions described above (Fig. 6.4a).

Dominant aromatic hydrocarbons and n-alkene/n-alkane doublets were observed after pyrolysis of the black chert (Fig. C.2a). Thermal decomposition can lead to cyclization and aromatization reactions of hydrocarbons and functionalized compounds, for example via formation of radicals or unsaturated molecules (Lockhart et al., 1981; Hartgers et al., 1994, 1995; Moldoveanu, 2010). Hereby, higher pyrolysis temperatures can cause a greater variety of aromatic compounds and thus, potentially, hamper the identification of parent compounds (Moldoveanu, 2010; Goesmann et al., 2017, their Figure 12). Furthermore, n-alkenes are frequently observed as pyrolysis products from kerogens, leading to typical n-alkene/n-alkane doublets (Lewan et al., 1979; Burnham et al., 1982; Huizinga et al., 1988). Thus, some of the compounds observed in the pyrolysis and thermochemolysis runs of the black chert might be by-products from high temperature thermal decom-

position (e.g., benzene, toluene, naphthalene, fluorine; Figs. C.2a, C.3a). In comparison, only one aromatic compound was observed in the pyrolysis of standard mix (i.e., benzene; Fig. 6.2a).

By-products from decomposition of the Tenax trap are also a potential source for hydrocarbon contamination, for example, benzene, toluene, xylene and naphthalene, as detected in the SAM instrument (Freissinet et al., 2015). A clear distinction between pyrolysis products of the black chert and these contaminants is barely possible. However, blank runs never showed these by-products (Fig. C.1) and also runs with standard mix only revealed traces of these compounds. Hence, probably most of the aromatic hydrocarbons stem from thermal decomposition of parent organics in the black chert.

6.4.2 Applicability of different techniques and impact of perchlorate

6.4.2.1 Pyrolysis

This technique is a simple way to search for organics in soils and surface rocks and has been applied during previous landed missions to Mars (Biemann et al., 1976, 1977; Sutter et al., 2012; Glavin et al., 2013; Freissinet et al., 2015). Furthermore, it is widely applied to study refractory organics that are bound to kerogen (Vandenbroucke and Largeau, 2007; Hallmann et al., 2011). An identification of (intact) functional compounds through pyrolysis with the given setup and parameters was not possible, as demonstrated by the standard mix (Fig. 6.2a). Thus, this approach is not ideally suited for this sample.

Pyrolysis of the black chert without Mg-perchlorate seems to give a sufficient overview of the organic inventory of the sample. However, high-temperature pyrolysis of the black chert leads to detection of aromatic and unsaturated hydrocarbons that do not necessarily reflect the true inventory of organic compounds in the sample (see discussion in Section 6.4.1). Here, overall lower pyrolysis temperatures or a stepwise approach (presented in Goesmann et al., 2017) might be possibilities to minimize analytical by-products.

While after the addition of 1 wt% Mg-perchlorate to the pyrolysis of both samples all compounds were still clearly identifiable, the addition of 10 wt% Mg-perchlorate led to degradation of existing organics and major amounts of chlorinated hydrocarbons (Figs. 6.2b, c, C.2b, c). This is well in line with earlier observations (Steininger et al., 2012). Decomposition of Mg-perchlorate leads to formation of MgO and $MgCl_2$ as well as O_2 and Cl_2, or their associated radicals (Manelis et al., 2003; Navarro-González et al., 2010, 2011; Steininger et al., 2012). $O^\bullet$ and $Cl^\bullet$ radicals further lead to the formation of CO_2 and chlorinated compounds via oxidation and chlorination of organic compounds, respectively (Sephton et al., 2014). A determination of exact parent molecules of chlorinated compounds in our study is difficult, if not impossible. Nevertheless, most of the chlorinated organics probably derived from the sample organics (not from background, e.g., cross contamination), as a clear increase in abundance compared to blank signal was observed. Our results further illustrate that the ratio of organic content to perchlorate controls the degree of degradation that can be observed. In particular, more perchlorate relative to organics has a stronger observable effect (e.g., Figs. 6.2b, c).

6.4.2.2 In situ derivatization

Derivatization with MTBSTFA/DMF (i.e., silylation) can be used for a variety of functional molecules (e.g., acids, alcohols, amines) and is usually producing high analytical responses (Schummer et al., 2009). Indeed, most functional compounds in the standard mix were successfully silylated via in situ derivatization with MTBSTFA/DMF leading to a good GC–MS response. Characteristic key ions (m/z 73, 75, M − 57 , where M denotes the mass of the molecular ion; Schummer et al., 2009) simplified the identification of specific molecules. The lower response of n-alkanoic acids (especially n-tridecanoic acid) compared to n-alkan-2-ols (Fig. 6.3a) is due to a lower reactivity of n-alkanoic acids towards silylation compared to n-alkanols (Villas-Bôas et al., 2005, 2007).

In situ DMF-DMA derivatization was developed for use in the COSAC instrument onboard the Rosetta lander Philae and it is exclusively meant for the derivatization of alkanoic acids, primary amines and amino acids via methylation (Meierhenrich et al., 2001). However, this technique was unsuccessful for derivatization of n-alkanoic acids in the standard mix. This might be explained by a lower derivatization efficiency of DMF-DMA compared to MTBSTFA/DMF (Rodier et al., 2001; Meunier et al., 2007; Goesmann et al., 2017) with the latter already giving low responses for n-alkanoic acids. However, the strength of DMF-DMA lies in the identification of chiral molecules (e.g., amino acids), by using it together with an enantioselective column (Freissinet et al., 2010), which was not part of this study.

Earlier analyses revealed that both derivatization techniques are not suited for a sufficient specification of the black chert's organic inventory. This matter is discussed in Goesmann et al. (2017, their Chapter 7.5).

Both techniques (MTBSTFA/DMF and DMF-DMA; 250 °C and 140 °C, respectively) were not affected by addition of 1 wt% Mg-perchlorates (e.g., Fig. 6.3b). Earlier test experiments (not shown) revealed that even high amounts of Mg-perchlorate do not have a large effect on these analyses. This might be explained by the fact that reaction temperatures of these techniques are below the main decomposition temperature of Mg-perchlorate (i.e., release of high amounts of oxygen and chlorine > 300 °C; Navarro-González et al., 2010, 2011; Sephton et al., 2014). Still, this might not account for other perchlorates on Mars (Kounaves et al., 2014; Sutter et al., 2017) which possibly differ in decomposition temperatures.

6.4.2.3 Thermochemolysis with TMAH: A perchlorate resistant technique?

Thermochemolysis with TMAH combines derivatization and pyrolysis. It can be used for an extraction of organic compounds from mineral matrices and selective cracking of ester and ether bonds from macromolecular organic networks (i.e., kerogen) at elevated temperatures while simultaneously limiting thermal decomposition of organic compounds (Challinor, 2001; Geffroy-Rodier et al., 2009). Compounds from the standard mix were successfully derivatized using thermochemolysis (Fig. 6.4a). The technique revealed higher sensibility for n-alkanoic acids in the standard mix compared to in situ derivatization with MTBSTFA/DMF (Fig. 6.4a; see also Fig. 6.3a). However, high abundances of thermal decomposition products (e.g., n-alkenes; Fig. 6.4a) suggest that not all compounds were protected by methylation. One reason for this might be insufficient mixing of the TMAH and the sample, so that functional compounds were decomposed at high tem-

peratures before the protecting methylation took place. Additionally, this could have been enhanced by partial evaporation of reagent at elevated temperatures. A possible solution might be the use of more TMAH. Indeed, this will be the case for MOMA (Goesmann et al., 2017).

For the black chert, thermochemolysis enabled the detection of *n*-alkanoic acids in addition to the products that were obtained during pyrolysis (Fig. C.3a). However, it could not be clarified whether these *n*-alkanoic acids were cleaved from the kerogen or were introduced as contaminants (not observed in pre- and post-analysis blanks).

While most organics were largely degraded during pyrolysis with up to 10 wt% Mg-perchlorate (Figs. 6.2c, C.2c), they stayed widely unaffected by perchlorate during thermochemolysis with TMAH (Figs. 6.4c, C.3b). However, the observed lower abundance of *n*-alkenes and *n*-alkanals in the standard mix (compared to analysis without perchlorate; Fig. 6.4a) might be caused by perchlorate-induced degradation or by variations in the thermal decomposition behavior of parent molecules (see Section 6.4.1). Meanwhile, the lower abundance of *n*-alkanoic acids as methyl esters can be explained by slight variations in the efficiency of the methylation reaction. Larger variety and higher abundance of (specific) aromatic hydrocarbons observed in the black chert are probably an effect of perchlorate addition (Fig. C.3b).

Our results suggest that TMAH buffers the oxidation and chlorination reactions triggered by perchlorate decomposition and thus protect the organics contained in the samples. We hypothesize that the methyl groups of the tetramethylammonium ion react with the $O^{\bullet}$ and $Cl^{\bullet}$ radicals (radical-substitution) and potentially form, for example, CO_2, HCl and low molecular weight chlorinated organics. As a by-product, this reaction might lead to the formation of dimethylamine, methylamine or nitrogen radicals which have the potential to form the nitrogen-bearing organics that were observed in high abundances (e.g., 1,5-Dicyano-2,4-dimethyl-2,4-diazapentane, benzonitrile; Figs. 6.4c, C.3b). More systematic studies are necessary to determine the exact mechanisms of this reaction. However, this lies beyond the scope of this study.

6.4.3   Implications for current/future missions

Given the advantages and limits of the single methods, a complementary use of different techniques seems necessary to obtain a full picture of the organics contained in a given sample. In this study, especially in situ derivatization with MTBSTFA/DMF and thermochemolysis with TMAH of the standard mix demonstrate the advantage of a complementary analysis. While the former allowed a clear-cut identification of specific compounds (via key ions) without production of by-products, the latter revealed the full range of functionalized compounds in the proper relative abundances. Additionally, TMAH not only widely preserves the derivatives of *n*-alkanols and *n*-alkanoic acids from thermal decompositions, but also from the destructive influence of Mg-perchlorates at high temperatures (TMAH buffer). Further systematic studies with different perchlorates (Mars-like mixtures) and flight-like derivatization capsules carried out under Mars-like conditions will be necessary to fully validate these results. In any case, the TMAH buffer appears to support the search and detection of organic compounds in perchlorate-bearing martian surface material and will therefore be of great use to the ongoing MSL-Curiosity as well as the future ExoMars rover mission.

6.5   Conclusions

MOMA-like pyrolysis, in situ derivatization and thermochemolysis GC–MS techniques were successfully applied on a synthetic sample (standard mix; *n*-alkan-1-ols, *n*-alkan-2-ols, *n*-alkanoic acids) and a natural sample (Silurian black chert). However, not every technique is equally suitable for different types of organic compounds.

- Pyrolysis of synthetic *n*-alkanols and *n*-alkanoic acids at 700 °C only yielded their respective thermal decomposition products (e.g., *n*-alkenes, *n*-alkanals, *n*-alkanones). Meanwhile, pyrolysis of the black chert provided a sufficient overview of its entire organic inventory. However, high temperatures led to the production of analytical by-products, for example, aromatic and unsaturated compounds. Furthermore, the impact of perchlorate (up to 10 wt%) on pyrolysis was high so that organics in the black chert were completely degraded.

- In situ derivatization with MTBSTFA/DMF resulted in tert-butyldimethylsilyl ethers and esters of corresponding *n*-alkanols and *n*-alkanoic acids, respectively, and facilitated their identification due to specific key ions. On the other hand, this technique only revealed low abundances of *n*-alkanoic acids (when analyzing the standard mix) and only contamination signal for the black chert (see also Goesmann et al., 2017). No impact of perchlorate on the analyses has been observed under given test conditions.

- The DMF-DMA derivatization technique is not applicable to the types of organic compounds present in our samples.

- In situ thermochemolysis with TMAH of the standard mix generated methyl ethers and esters of *n*-alkanols and *n*-alkanoic acids, respectively, in their expected abundance ratios (*n*-alkan-1-ols > *n*-alkanoic acids > *n*-alkan-2-ols). It also revealed the full organic inventory of the black chert. Nevertheless, thermal decomposition products for *n*-alkanols and *n*-alkanoic acids were observed suggesting an incomplete reaction of TMAH with the organics. Up to 10 wt% perchlorate content did not affect the analysis of organics using thermochemolysis with TMAH. We infer that methyl groups from TMAH reacted with $O^{\bullet}$ and $Cl^{\bullet}$ radicals from perchlorate decomposition and therefore buffered the oxidation and chlorination of other organic compounds.

Summarizing, we demonstrated that perchlorates in martian soils do not necessarily hinder MOMA-like GC–MS analysis. Furthermore, we underlined that the complementary use of different MOMA-like GC–MS techniques is advantageous to the detection of the full organic inventory of a given sample.

Acknowledgements

References

Bibring, J.-P., Hamm, V., Pilorget, C., Vago, J. L., and the MicrOmega, T. (2017). The MicrOmega Investigation Onboard ExoMars. *Astrobiology*, 17, 621–626.

Biemann, K. and Bada, J. L. (2011). Comment on "Reanalysis of the Viking results suggests perchlorate and organics at midlatitudes on Mars" by Rafael Navarro-González et al. *Journal of Geophysical Research: Planets*, 116, E12001.

Biemann, K., Oró, J., Toulmin, P., Orgel, L. E., Nier, A. O., Anderson, D. M., Simmonds, P. G., Flory, D., Diaz, A. V., Rushneck, D. R., and Biller, J. A. (1976). Search for Organic and Volatile Inorganic Compounds in Two Surface Samples from the Chryse Planitia Region of Mars. *Science*, 194, 72–76.

Biemann, K., Oró, J., Toulmin, P., Orgel, L. E., Nier, A. O., Anderson, D. M., Simmonds, P. G., Flory, D., Diaz, A. V., Rushneck, D. R., Biller, J. E., and Lafleur, A. L. (1977). The search for organic substances and inorganic volatile compounds in the surface of Mars. *Journal of Geophysical Research*, 82, 4641–4658.

Boss, B. D. and Hazlett, R. N. (1976). Application of pyrolysis, gas chromatography, and mass spectrometry for identification of alcohol and carbonyl isomers. *Analytical Chemistry*, 48, 417–420.

Botta, O. and Bada, J. L. (2002). Extraterrestrial Organic Compounds in Meteorites. *Surveys in Geophysics*, 23, 411–467.

Brocks, J. J. and Summons, R. E. (2003). Biomarkers for Early Life. In W. H. Schlesinger (Ed.), *Biogeochemistry*. Elsevier, Oxford, pp. 63–115.

Brown, G. M. and Gu, B. (2006). The Chemistry of Perchlorate in the Environment. In B. Gu and J. D. Coates (Eds.), *Perchlorate: Environmental Occurrence, Interactions and Treatment*. Springer US, Boston, MA, pp. 17–47.

Buch, A., Glavin, D. P., Sternberg, R., Szopa, C., Rodier, C., Navarro-González, R., Raulin, F., Cabane, M., and Mahaffy, P. R. (2006). A new extraction technique for in situ analyses of amino and carboxylic acids on Mars by gas chromatography mass spectrometry. *Planetary and Space Science*, 54, 1592–1599.

Burnham, A. K., Clarkson, J. E., Singleton, M. F., Wong, C. M., and Crawford, R. W. (1982). Biological markers from Green River kerogen decomposition. *Geochimica et Cosmochimica Acta*, 46, 1243–1251.

Cady, S. L. and Noffke, N. (2009). Geobiology: evidence for early life on Earth and the search for life on other planets. *GSA Today*, 19, 4–10.

Catling, D. C., Claire, M. W., Zahnle, K. J., Quinn, R. C., Clark, B. C., Hecht, M. H., and Kounaves, S. (2010). Atmospheric origins of perchlorate on Mars and in the Atacama. *Journal of Geophysical Research: Planets*, 115, E00E11.

Challinor, J. M. (2001). Review: the development and applications of thermally assisted hydrolysis and methylation reactions. *Journal of Analytical and Applied Pyrolysis*, 61, 3–34.

Cull, S. C., Arvidson, R. E., Catalano, J. G., Ming, D. W., Morris, R. V., Mellon, M. T., and Lemmon, M. (2010). Concentrated perchlorate at the Mars Phoenix landing site: Evidence for thin film liquid water on Mars. *Geophysical Research Letters*, 37, L22203.

Flynn, G. J. (1996). The delivery of organic matter from asteroids and comets to the early surface of Mars. *Earth, Moon, and Planets*, 72, 469–474.

Freissinet, C., Buch, A., Sternberg, R., Szopa, C., Geffroy-Rodier, C., Jelinek, C., and Stambouli, M. (2010). Search for evidence of life in space: Analysis of enantiomeric organic molecules by *N,N*-dimethylformamide dimethylacetal derivative dependant Gas Chromatography–Mass Spectrometry. *Journal of Chromatography A*, 1217, 731–740.

Freissinet, C., Glavin, D. P., Mahaffy, P. R., Miller, K. E., Eigenbrode, J. L., Summons, R. E., Brunner, A. E., Buch, A., Szopa, C., Archer, P. D., Franz, H. B., Atreya, S. K., Brinckerhoff, W. B., Cabane, M., Coll, P., Conrad, P. G., Des Marais, D. J., Dworkin, J. P., Fairén, A. G., François, P., Grotzinger, J. P., Kashyap, S., ten Kate, I. L., Leshin, L. A., Malespin, C. A., Martin, M. G., Martin-Torres, F. J., McAdam, A. C., Ming, D. W., Navarro-González, R., Pavlov, A. A., Prats, B. D., Squyres, S. W., Steele, A., Stern, J. C., Sumner, D. Y., Sutter, B., Zorzano, M. P., and the MSL Science Team (2015). Organic molecules in the Sheepbed Mudstone, Gale Crater, Mars. *Journal of Geophysical Research: Planets*, 120, 495–514.

Geffroy-Rodier, C., Grasset, L., Sternberg, R., Buch, A., and Amblès, A. (2009). Thermochemolysis in search for organics in extraterrestrial environments. *Journal of Analytical and Applied Pyrolysis*, 85, 454–459.

Glavin, D. P., Freissinet, C., Miller, K. E., Eigenbrode, J. L., Brunner, A. E., Buch, A., Sutter, B., Archer, P. D., Atreya, S. K., Brinckerhoff, W. B., Cabane, M., Coll, P., Conrad, P. G., Coscia, D., Dworkin, J. P., Franz, H. B., Grotzinger, J. P., Leshin, L. A., Martin, M. G., McKay, C., Ming, D. W., Navarro-González, R., Pavlov, A., Steele, A., Summons, R. E., Szopa, C., Teinturier, S., and Mahaffy, P. R. (2013). Evidence for perchlorates and the origin of chlorinated hydrocarbons detected by SAM at the Rocknest aeolian deposit in Gale Crater. *Journal of Geophysical Research: Planets*, 118, 1955–1973.

Goesmann, F., Brinckerhoff, W. B., Raulin, F., Goetz, W., Danell, R. M., Getty, S. A., Siljeström, S., Mißbach, H., Steininger, H., Arevalo, R. D., Buch, A., Freissinet, C., Grubisic, A., Meierhenrich, U. J., Pinnick, V. T., Stalport, F., Szopa, C., Vago, J. L., Lindner, R., Schulte, M. D., Brucato, J. R., Glavin, D. P., Grand, N., Li, X., van Amerom, F. H. W., and the Moma Science Team (2017). The Mars Organic Molecule Analyzer (MOMA) Instrument: Characterization of Organic Material in Martian Sediments. *Astrobiology*, 17, 655–685.

Goetz, W., Brinckerhoff, W. B., Arevalo, R., Freissinet, C., Getty, S., Glavin, D. P., Siljeström, S., Buch, A., Stalport, F., Grubisic, A., Li, X., Pinnick, V., Danell, R., van Amerom, F. H. W., Goesmann, F., Steininger, H., Grand, N., Raulin, F., Szopa, C., Meierhenrich, U., and Brucato, J. R. (2016). MOMA: the challenge to search for organics and biosignatures on Mars. *International Journal of Astrobiology*, 15, 239–250.

Hallmann, C., Kelly, A. E., Gupta, S. N., and Summons, R. E. (2011). Reconstructing deep-time biology with molecular fossils. In M. Laflamme, D. J. Schiffbauer, and Q. S. Dornbos (Eds.), *Quantifying the Evolution of Early Life: Numerical Approaches to the Evaluation of Fossils and Ancient Ecosystems*. Springer Netherlands, Dordrecht, pp. 355–401.

Hartgers, W. A., Damsté, J. S. S., and de Leeuw, J. W. (1994). Geochemical significance of alkylbenzene distributions in flash pyrolysates of kerogens, coals, and asphaltenes. *Geochimica et Cosmochimica Acta*, 58, 1759–1775.

Hartgers, W. A., Sinninghe Damsté, J. S., and de Leeuw, J. W. (1995). Curie-point pyrolysis of sodium salts of functionalized fatty acids. *Journal of Analytical and Applied Pyrolysis*, 34, 191–217.

Hecht, M. H., Kounaves, S. P., Quinn, R. C., West, S. J., Young, S. M. M., Ming, D. W., Catling, D. C., Clark, B. C., Boynton, W. V., Hoffman, J., DeFlores, L. P., Gospodinova, K., Kapit, J., and Smith, P. H. (2009). Detection of Perchlorate and the Soluble Chemistry of Martian Soil at the Phoenix Lander Site. *Science*, 325, 64–67.

Huizinga, B. J., Aizenshtat, Z. A., and Peters, K. E. (1988). Programmed pyrolysis-gas chromatography of artificially matured Green River kerogen. *Energy & Fuels*, 2, 74–81.

Kminek, G. and Bada, J. L. (2006). The effect of ionizing radiation on the preservation of amino acids on Mars. *Earth and Planetary Science Letters*, 245, 1–5.

Konn, C., Charlou, J. L., Holm, N. G., and Mousis, O. (2015). The Production of Methane, Hydrogen, and Organic Compounds in Ultramafic-Hosted Hydrothermal Vents of the Mid-Atlantic Ridge. *Astrobiology*, 15, 381–399.

Kounaves, S. P., Chaniotakis, N. A., Chevrier, V. F., Carrier, B. L., Folds, K. E., Hansen, V. M., McElhoney, K. M., O'Neil, G. D., and Weber, A. W. (2014). Identification of the perchlorate parent salts at the Phoenix Mars landing site and possible implications. *Icarus*, 232, 226–231.

Kounaves, S. P., Hecht, M. H., Kapit, J., Gospodinova, K., DeFlores, L., Quinn, R. C., Boynton, W. V., Clark, B. C., Catling, D. C., Hredzak, P., Ming, D. W., Moore, Q., Shusterman, J., Stroble, S., West, S. J., and Young, S. M. M. (2010). Wet Chemistry experiments on the 2007 Phoenix Mars Scout Lander mission: Data analysis and results. *Journal of Geophysical Research: Planets*, 115, E00E10.

Kremer, B. (2005). Mazuelloids: Product of Post-Mortem Phosphatization of Acanthomorphic Acritarchs. *PALAIOS*, 20, 27–36.

176

Kremer, B. and Kazmierczak, J. (2005). Cyanobacterial Mats from Silurian Black Radiolarian Cherts: Phototrophic Life at the Edge of Darkness? *Journal of Sedimentary Research*, 75, 897–906.

Levin, G. V. and Straat, P. A. (2016). The Case for Extant Life on Mars and Its Possible Detection by the Viking Labeled Release Experiment. *Astrobiology*, 16, 798–810.

Lewan, M. D., Winters, J. C., and McDonald, J. H. (1979). Generation of Oil-Like Pyrolyzates from Organic-Rich Shales. *Science*, 203, 897–899.

Li, X., Danell, R. M., Pinnick, V. T., Grubisic, A., van Amerom, F., Arevalo, R. D., Getty, S. A., Brinckerhoff, W. B., Southard, A. E., Gonnsen, Z. D., and Adachi, T. (2017). Mars Organic Molecule Analyzer (MOMA) laser desorption/ionization source design and performance characterization. *International Journal of Mass Spectrometry*, 422, 177–187.

Lockhart, T. P., Comita, P. B., and Bergman, R. G. (1981). Kinetic evidence for the formation of discrete 1, 4-dehydrobenzene intermediates. Trapping by inter-and intramolecular hydrogen atom transfer and observation of high-temperature CIDNP. *Journal of the American Chemical Society*, 103, 4082–4090.

Mahaffy, P. R., Webster, C. R., Cabane, M., Conrad, P. G., Coll, P., Atreya, S. K., Arvey, R., Barciniak, M., Benna, M., Bleacher, L., Brinckerhoff, W. B., Eigenbrode, J. L., Carignan, D., Cascia, M., Chalmers, R. A., Dworkin, J. P., Errigo, T., Everson, P., Franz, H., Farley, R., Feng, S., Frazier, G., Freissinet, C., Glavin, D. P., Harpold, D. N., Hawk, D., Holmes, V., Johnson, C. S., Jones, A., Jordan, P., Kellogg, J., Lewis, J., Lyness, E., Malespin, C. A., Martin, D. K., Maurer, J., McAdam, A. C., McLennan, D., Nolan, T. J., Noriega, M., Pavlov, A. A., Prats, B., Raaen, E., Sheinman, O., Sheppard, D., Smith, J., Stern, J. C., Tan, F., Trainer, M., Ming, D. W., Morris, R. V., Jones, J., Gundersen, C., Steele, A., Wray, J., Botta, O., Leshin, L. A., Owen, T., Battel, S., Jakosky, B. M., Manning, H., Squyres, S., Navarro-González, R., McKay, C. P., Raulin, F., Sternberg, R., Buch, A., Sorensen, P., Kline-Schoder, R., Coscia, D., Szopa, C., Teinturier, S., Baffes, C., Feldman, J., Flesch, G., Forouhar, S., Garcia, R., Keymeulen, D., Woodward, S., Block, B. P., Arnett, K., Miller, R., Edmonson, C., Gorevan, S., and Mumm, E. (2012). The Sample Analysis at Mars Investigation and Instrument Suite. *Space Science Reviews*, 170, 401–478.

Manelis, G. B., Nazin, G. M., Rubtsov, Y. I., and Strunin, V. A. (2003). *Thermal decomposition and combustion of explosives and propellants*. Taylor & Francis, London.

Martín-Torres, F. J., Zorzano, M.-P., Valentín-Serrano, P., Harri, A.-M., Genzer, M., Kemppinen, O., Rivera-Valentin, E. G., Jun, I., Wray, J., Bo Madsen, M., Goetz, W., McEwen, A. S., Hardgrove, C., Renno, N., Chevrier, V. F., Mischna, M., Navarro-González, R., Martínez-Frías, J., Conrad, P., McConnochie, T., Cockell, C. S., Berger, G., R. Vasavada, A., Sumner, D., and Vaniman, D. (2015). Transient liquid water and water activity at Gale crater on Mars. *Nature Geoscience*, 8, 357.

McCollom, T. M., Ritter, G., and Simoneit, B. R. T. (1999). Lipid Synthesis Under Hydrothermal Conditions by Fischer–Tropsch-Type Reactions. *Origins of Life and Evolution of Biospheres*, 29, 153–166.

McCollom, T. M. and Seewald, J. S. (2007). Abiotic Synthesis of Organic Compounds in Deep-Sea Hydrothermal Environments. *Chemical Reviews*, 107, 382–401.

Meierhenrich, U. (2008). *Amino acids and the asymmetry of life: caught in the act of formation*. Springer Science & Business Media, Berlin, Heidelberg.

Meierhenrich, U., Thiemann, W. H. P., and Rosenbauer, H. (2001). Pyrolytic methylation assisted enantioseparation of chiral hydroxycarboxylic acids. *Journal of Analytical and Applied Pyrolysis*, 60, 13–26.

Meunier, D., Sternberg, R., Mettetal, F., Buch, A., Coscia, D., Szopa, C., Rodier, C., Coll, P., Cabanec, M., and Raulin, F. (2007). A laboratory pilot for in situ analysis of refractory organic matter in Martian soil by gas chromatography–mass spectrometry. *Advances in Space Research*, 39, 337–344.

Mißbach, H., Duda, J.-P., Lünsdorf, N. K., Schmidt, B. C., and Thiel, V. (2016). Testing the preservation of biomarkers during experimental maturation of an immature kerogen. *International Journal of Astrobiology*, 15, 165–175.

Mißbach, H., Schmidt, B. C., Duda, J.-P., Lünsdorf, N. K., Goetz, W., and Thiel, V. (2018). Assessing the diversity of lipids formed via Fischer-Tropsch-type reactions. *Organic Geochemistry*, 119, 110–121.

Moldoveanu, S. C. (2010). *Pyrolysis of Organic Molecules with Applications to Health and Environmental Issues*. Elsevier Science, Amsterdam.

Morisson, M. (2017). *Optimisation des techniques de pyrolyse et de thermochimiolyse pour la recherche de matière organique d'origine extraterrestre : application aux cas de Titan et Mars*. PhD thesis, Université Paris-Saclay.

Navarro-González, R. and McKay, C. P. (2011). Reply to comment by Biemann and Bada on "Reanalysis of the Viking results suggests perchlorate and organics at midlatitudes on Mars". *Journal of Geophysical Research: Planets*, 116, E12002.

Navarro-González, R., Vargas, E., de la Rosa, J., Raga, A. C., and McKay, C. P. (2010). Reanalysis of the Viking results suggests perchlorate and organics at midlatitudes on Mars. *Journal of Geophysical Research: Planets*, 115, E12010.

Navarro-González, R., Vargas, E., de la Rosa, J., Raga, A. C., and McKay, C. P. (2011). Correction to "Reanalysis of the Viking results suggests perchlorate and organics at midlatitudes on Mars". *Journal of Geophysical Research: Planets*, 116, E08011.

Nierop, K. G. J. and van Bergen, P. F. (2002). Clay and ammonium catalyzed reactions of alkanols, alkanoic acids and esters under flash pyrolytic conditions. *Journal of Analytical and Applied Pyrolysis*, 63, 197–208.

Oró, J. and Holzer, G. (1979). The photolytic degradation and oxidation of organic compounds under simulated Martian conditions. *Journal of Molecular Evolution*, 14, 153–160.

Pavlov, A. A., Vasilyev, G., Ostryakov, V. M., Pavlov, A. K., and Mahaffy, P. (2012). Degradation of the organic molecules in the shallow subsurface of Mars due to irradiation by cosmic rays. *Geophysical Research Letters*, 39, L13202.

Peters, K. E., Walters, C. C., and Moldowan, J. M. (2005a). *The Biomarker Guide - Part I - Biomarkers and Isotopes in the Environment and Human History*. Cambridge University Press, New York.

Peters, K. E., Walters, C. C., and Moldowan, J. M. (2005b). *The Biomarker Guide - Part II - Biomarkers and Isotopes in Petroleum Exploration and Earth History*. Cambridge University Press, New York.

Rodier, C., Sternberg, R., Raulin, F., and Vidal-Madjar, C. (2001). Chemical derivatization of amino acids for in situ analysis of Martian samples by gas chromatography. *Journal of Chromatography A*, 915, 199–207.

Rodier, C., Sternberg, R., Szopa, C., Buch, A., Cabane, M., and Raulin, F. (2005). Search for organics in extraterrestrial environments by in situ gas chromatography analysis. *Advances in Space Research*, 36, 195–200.

Rull, F., Maurice, S., Hutchinson, I., Moral, A., Perez, C., Diaz, C., Colombo, M., Belenguer, T., Lopez-Reyes, G., Sansano, A., Forni, O., Parot, Y., Striebig, N., Woodward, S., Howe, C., Tarcea, N., Rodriguez, P., Seoane, L., Santiago, A., Rodriguez-Prieto, J. A., Medina, J., Gallego, P., Canchal, R., Santamaría, P., Ramos, G., Vago, J. L., and On behalf of the, R. L. S. T. (2017). The Raman Laser Spectrometer for the ExoMars Rover Mission to Mars. *Astrobiology*, 17, 627–654.

Rushdi, A. I. and Simoneit, B. R. T. (2001). Lipid formation by aqueous Fischer–Tropsch-type synthesis over a temperature range of 100 to 400 °C. *Origins of Life and Evolution of Biospheres*, 31, 103–118.

Schummer, C., Delhomme, O., Appenzeller, B. M. R., Wennig, R., and Millet, M. (2009). Comparison of MTBSTFA and BSTFA in derivatization reactions of polar compounds prior to GC/MS analysis. *Talanta*, 77, 1473–1482.

Sephton, M. A., Lewis, J. M. T., Watson, J. S., Montgomery, W., and Garnier, C. (2014). Perchlorate-induced combustion of organic matter with variable molecular weights: Implications for Mars missions. *Geophysical Research Letters*, 41, 7453–7460.

Shock, E. L. and Schulte, M. D. (1998). Organic synthesis during fluid mixing in hydrothermal systems. *Journal of Geophysical Research: Planets*, 103, 28513–28527.

Steininger, H., Goesmann, F., and Goetz, W. (2012). Influence of magnesium perchlorate on the pyrolysis of organic compounds in Mars analogue soils. *Planetary and Space Science*, 71, 9–17.

Summons, R. E. (2014). The exceptional preservation of interesting and informative biomolecules. In M. Laflamme, J. D. Schiffbauer, and S. A. F. Darroch (Eds.), *Reading and Writing of the Fossil Record: Preservational Pathways to Exceptional Fossilization. The Paleontological Society Papers Vol. 20*. The Paleontological Society, pp. 217–236.

Summons, R. E., Albrecht, P., McDonald, G., and Moldowan, J. M. (2008). Molecular Biosignatures. *Space Science Reviews*, 135, 133–159.

Summons, R. E., Amend, J. P., Bish, D., Buick, R., Cody, G. D., Des Marais, D. J., Dromart, G., Eigenbrode, J. L., Knoll, A. H., and Sumner, D. Y. (2011). Preservation of Martian Organic and Environmental Records: Final Report of the Mars Biosignature Working Group. *Astrobiology*, 11, 157–181.

Sutter, B., Boynton, W. V., Ming, D. W., Niles, P. B., Morris, R. V., Golden, D. C., Lauer, H. V., Fellows, C., Hamara, D. K., and Mertzman, S. A. (2012). The detection of carbonate in the martian soil at the Phoenix Landing site: A laboratory investigation and comparison with the Thermal and Evolved Gas Analyzer (TEGA) data. *Icarus*, 218, 290–296.

Sutter, B., McAdam, A. C., Mahaffy, P. R., Ming, D. W., Edgett, K. S., Rampe, E. B., Eigenbrode, J. L., Franz, H. B., Freissinet, C., Grotzinger, J. P., Steele, A., House, C. H., Archer, P. D., Malespin, C. A., Navarro-González, R., Stern, J. C., Bell, J. F., Calef, F. J., Gellert, R., Glavin, D. P., Thompson, L. M., and Yen, A. S. (2017). Evolved gas analyses of sedimentary rocks and eolian sediment in Gale Crater, Mars: Results of the Curiosity rover's sample analysis at Mars instrument from Yellowknife Bay to the Namib Dune. *Journal of Geophysical Research: Planets*, 122, 2574–2609.

ten Kate, I. L. (2010). Organics on Mars? *Astrobiology*, 10, 589–603.

Vago, J. L., Westall, F., Pasteur Instrument Teams, L. S. S. W. G., Other, C., Coates, A. J., Jaumann, R., Korablev, O., Ciarletti, V., Mitrofanov, I., Josset, J.-L., De Sanctis, M. C., Bibring, J.-P., Rull, F., Goesmann, F., Steininger, H., Goetz, W., Brinckerhoff, W., Szopa, C., Raulin, F., Edwards, H. G. M., Whyte, L. G., Fairén, A. G., Bridges, J., Hauber, E., Ori, G. G., Werner, S., Loizeau, D., Kuzmin, R. O., Williams, R. M. E., Flahaut, J., Forget, F., Rodionov, D., Svedhem, H., Sefton-Nash, E., Kminek, G., Lorenzoni, L., Joudrier, L., Mikhailov, V., Zashchirinskiy, A., Alexashkin, S., Calantropio, F., Merlo, A., Poulakis, P., Witasse, O., Bayle, O., Bayón, S., Meierhenrich, U., Carter, J., García-Ruiz, J. M., Baglioni, P., Haldemann, A., Ball, A. J., Debus, A., Lindner, R., Haessig, F., Monteiro, D., Trautner, R., Voland, C., Rebeyre, P., Goulty, D., Didot, F., Durrant, S., Zekri, E., Koschny, D., Toni, A., Visentin, G., Zwick, M., van Winnendael, M., Azkarate, M., Carreau, C., and the ExoMars Project Team (2017). Habitability on Early Mars and the Search for Biosignatures with the ExoMars Rover. *Astrobiology*, 17, 471–510.

Vandenbroucke, M. and Largeau, C. (2007). Kerogen origin, evolution and structure. *Organic Geochemistry*, 38, 719–833.

Villas-Bôas, S. G., Koulman, A., and Lane, G. A. (2007). Analytical methods from the perspective of method standardization. In J. Nielsen and M. Jewett (Eds.), *Metabolomics*. Springer, Berlin, Heidelberg, pp. 11–52.

Villas-Bôas, S. G., Mas, S., Åkesson, M., Smedsgaard, J., and Nielsen, J. (2005). Mass spectrometry in metabolome analysis. *Mass Spectrometry Reviews*, 24, 613–646.

Westall, F., Foucher, F., Bost, N., Bertrand, M., Loizeau, D., Vago, J. L., Kminek, G., Gaboyer, F., Campbell, K. A., Bréhéret, J.-G., Gautret, P., and Cockell, C. S. (2015). Biosignatures on Mars: What, Where, and How? Implications for the Search for Martian Life. *Astrobiology*, 15, 998–1029.

Zaikin, V. and Halket, J. M. (2009). *A handbook of derivatives for mass spectrometry*. IM publications.

Implications for the ExoMars rover mission and MOMA analysis

Two landing sites were selected for the ExoMars rover mission, Oxia Planum and Mawrth Vallis (Bridges et al., 2016; Vago et al., 2017). They were chosen based on engineering constraints (e.g., elevation, relief, obstacles), scientific criteria (e.g., age, preservation, water activity) and planetary protection restrictions (Vago et al., 2015, 2017). The landing sites are located in the same region of Mars, southeast of Chryse Planitia, roughly at the border of the southern highland terrain to the northern lowlands (Fig. 1.3). Both areas show deposits that are probably of Noachian to early Hesperian age (and also younger; Vago et al., 2017); the time, when chances for the potential emergence of life were the highest (see Section 1.4).

Channel features and high abundances of clay minerals at these landing sites indicate the former presence of liquid surface water (Bridges et al., 2016; Vago et al., 2017). In particular, clay mineral deposits on Mars are of high interest for astrobiological research, as it is generally assumed that these minerals have a high potential for adsorbing and protecting organic compounds (Kennedy et al., 2002; Ehlmann et al., 2008; Summons et al., 2011). Oxia Planum possibly provides relatively fresh clay deposit exposures (< 100 Ma) in places where material has been removed by aeolian erosion (Quantin et al., 2016). Mawrth Vallis shows a large accumulation of phyllosilicates with high mineralogical variety. These deposits are potentially well preserved because they are locally covered by volcanic layers which are probably more weathering resistant (Poulet et al., 2005; Loizeau et al., 2007; Bishop et al., 2008; Ehlmann et al., 2011; Vago et al., 2017). This increases their value as targets for the ExoMars mission.

The preservation potential of organic matter on the martian surface is primarily limited by radiation and oxidation. UV and particle radiation (i.e., galactic or solar cosmic rays) can lead to a direct degradation of organic compounds on the surface and the close subsurface (Oró and Holzer, 1979; Kminek and Bada, 2006; Stalport et al., 2009; Pavlov et al., 2012; Poch et al., 2014). Furthermore, interaction of UV radiation or energetic particles with H_2O and/or the mineral matrix (e.g., SiO_2) can for example produce $O^\bullet$, $H^\bullet$, $HO^\bullet$ or superoxide radicals. These radicals can readily react with nearby organic molecules, potentially leading to their decomposition (secondary oxidation; Benner et al., 2000; Yen et al., 2000; Shkrob et al., 2010; Pavlov et al., 2012). Some organic molecules (e.g., mellitic acid, adenine) have been shown to be more photostable than others (Stalport et al., 2009; Poch et al., 2014). Additionally, clay minerals potentially hamper direct photodecomposition of at least certain organic molecules by UV radiation at the surface (Poch et al., 2015; Ertem et al., 2017). In any case, rapid burial would have been important for long term preservation of organic matter (Oehler and Allen, 2012; Westall et al., 2015). To obtain sample material that is less likely degraded by radiation effects, the ExoMars rover has the ability to take samples from 2 m depth (Vago et al., 2017).

Buried organic matter could have still experienced thermal maturation. However, without plate tectonics and generally low tectonic activity after ~ 3.8 Ga (van Thienen et al., 2004; Golombek and Phillips, 2010), thermal alteration via deep burial and high

tectonic stress (e.g., during subduction or orogenesis) was probably not abundant on Mars. There is local evidence for diagenetic processes on Mars (Grotzinger and Milliken, 2012), but whether burial progressed far enough to possibly thermally degrade organic matter (e.g., during catagenesis, 50–150 °C; Tissot and Welte, 1984) remains unclear. Nevertheless, episodic and locally restricted thermal alteration could have occurred due to impact or volcanic activity (Westall et al., 2015). Especially Noachian units in Oxia Planum and Mawrth Vallis could have been affected by these scenarios, as Mars was more active in its early history (see Section 1.4). Generally, carbon compounds can survive high pressures and temperatures upon impacts (Parnell and Lindgren, 2006; Montgomery et al., 2016). However, impact events potentially lead to degradation of organic biomarkers and/or biological distribution patterns.

Preservation of organic biomarkers upon thermal stress strongly depends on the maximum temperature. Additionally, the heating rate and, up to a certain degree, the heating duration can influence the preservation potential (Price, 1983, 1993; Waples, 2000; Brocks and Summons, 2003). The study presented in Chapter 2 demonstrates that classical lipid biomarkers (e.g., pristane, phytane, steranes, hopanes) can survive heat pulses of 300 °C over short durations (2400 h). Under same conditions, the biological n-alkane odd-over-even predominance was decreasing but still recognizable after 2400 h (Figs. 2.2, A.5) and abiotic unimodal distribution patterns remain largely unchanged (Fig. D.1). Further results demonstrate that short chain n-alkanols ($< C_{16}$) quickly degraded at 300 °C, while short chain n-alkanoic acids ($\leq C_{13}$) were preserved for 2400 h (Figs. D.2 and D.3). At 400 °C, classical lipid biomarkers and also biological distribution patterns of n-alkanes quickly vanished (< 48 h; Chapter 2; see also Fig. A.5), suggesting that preservation above these temperatures is unlikely. Nonetheless, these results imply that lipid biomarkers do not necessarily vanish as a result of locally restricted thermal alteration.

Chapter 4 presents an example for preservation of biologically derived organic matter under extreme conditions. Enclosure in a dense mineral matrix and incorporation into kerogen probably have, at least partially, enhanced its preservation potential. Fine-grained mineral matrices with low permeability (e.g., chert or clay minerals) are favorable for the preservation of organic compounds as they prevent fluid alteration (Summons et al., 2011). Additionally, organic compounds bound to kerogen have a higher preservation potential as these macromolecular structures have an enhanced stability in the sedimentary environment compared to single compounds (Brocks and Summons, 2003; Killops and Killops, 2005; Hallmann et al., 2011). Whether or not kerogen could be formed on Mars is unclear. Abiotic FTT synthesis potentially produces organic polymers, but not kerogen-like macromolecules (Chapter 3). Nevertheless, abiotically derived kerogens are known from carbonaceous chondrites and were probably delivered to Mars (Kerridge et al., 1987; Chyba, 1990; Botta and Bada, 2002; Kissin, 2003). If potential biologically derived organic compounds on Mars were not incorporated into kerogen, and considering (impact related) thermal alteration, this could have led to a preservation bias between biologically and abiotically derived organic matter. (Montgomery et al., 2016).

The studies presented in Section 5.7.5 and Chapter 6 underline that MOMA-like GC–MS is capable of analyzing a variety of polar and nonpolar organic compounds with in situ techniques, also as part of complex bulk samples. It was shown that even an analysis of organics in perchlorate rich sediments is possible, not only by MOMA LDMS (Chapter 5), but also by using in situ thermochemolysis with TMAH in MOMA GC–MS

mode (Chapter 6). Thus, possible problems in the detection of organic molecules due to perchlorates (Navarro-González et al., 2010, 2011; Steininger et al., 2012; Freissinet et al., 2015) can be overcome. Moreover, Figure 7.1 demonstrates that the discrimination of biologically from abiotically derived organic material is principally possible with MOMA-like GC–MS techniques, even with limited capabilities compared to conventional bench-top techniques. However, not every MOMA-like GC–MS technique is applicable to each sample type or organic compound class. Hence, advantages and disadvantages of each technique must be carefully weighed up and complementary analyses of a given sample using different techniques should be considered (Chapter 6). Nonetheless, these studies emphasize that MOMA can principally detect organic molecules in martian sediments, and if sufficiently preserved, constrain the source of these compounds.
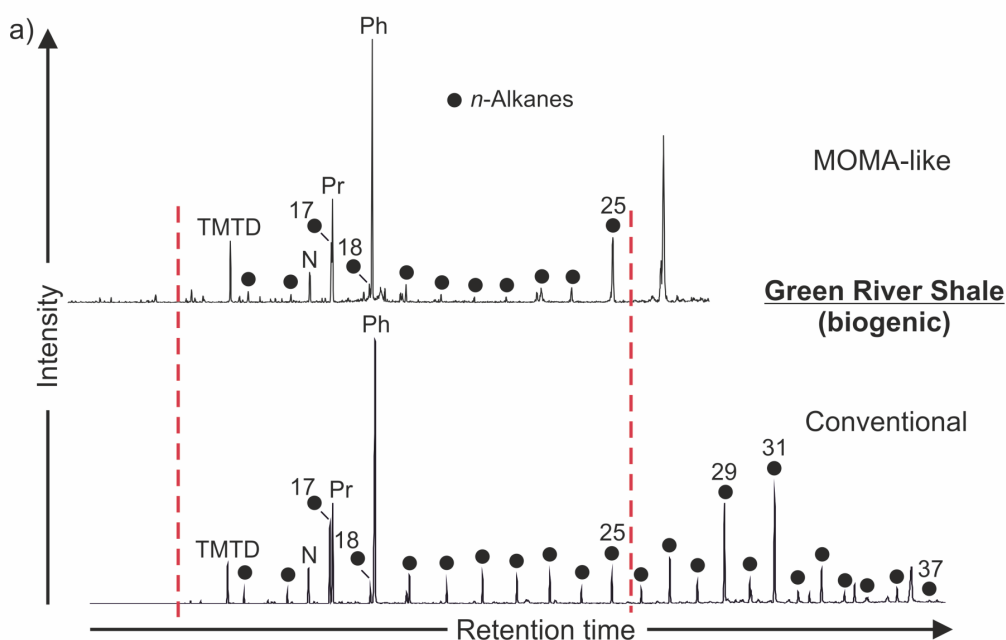
Figure 7.1: Discrimination of biologically and abiotically derived organics via MOMA-like and conventional bench-top GC–MS analyses. (a) Partial mass chromatograms (m/z 85) of the biogenic Green River Shale and (b) partial total ion current chromatograms of abiogenic organics derived from Fischer–Tropsch-type (FTT) reactions (see next page). Numbers indicate the carbon chain lengths of corresponding n-alkanes and n-alkan-1-ols. MOMA-like analyses were conducted using the flight analog system and the in situ derivatization method with MTBSTFA/DMF at 250 °C for 10 min (see Sections 5.7.5 and 6.2 for a detailed description). For these analyses, raw Green River Shale (only crushed) and solvent extracted organics from FTT reactions (deposited on SiO_2) were used. Conventional bench-top analysis was conducted as described in Sections 2.2 and 3.2. n-Alkan-1-ols were analyzed as their tert-butyldimethylsilyl or trimethylsilyl ethers. Note that the detected range of compounds is smaller for the MOMA-like analyses, due to low transfer line temperatures (110 °C) and lower maximum GC oven temperatures compared to the conventional bench-top method (250 °C vs. 310 °C, respectively). However, distinct homolog preferences in (a) and the unimodal distribution pattern in (b) are clearly detectable with both methods.
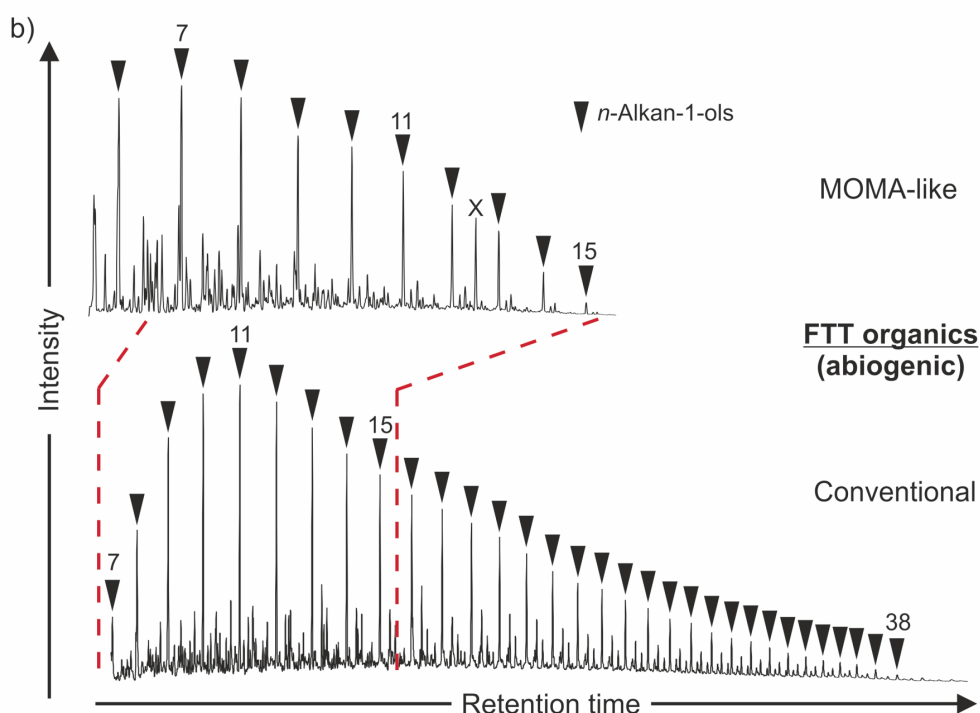
Figure 7.1: Continued.

References

Benner, S. A., Devine, K. G., Matveeva, L. N., and Powell, D. H. (2000). The missing organic molecules on Mars. *Proceedings of the National Academy of Sciences of the United States of America*, 97, 2425–2430.

Bishop, J. L., Dobrea, E. Z. N., McKeown, N. K., Parente, M., Ehlmann, B. L., Michalski, J. R., Milliken, R. E., Poulet, F., Swayze, G. A., Mustard, J. F., Murchie, S. L., and Bibring, J.-P. (2008). Phyllosilicate Diversity and Past Aqueous Activity Revealed at Mawrth Vallis, Mars. *Science*, 321, 830–833.

Botta, O. and Bada, J. L. (2002). Extraterrestrial Organic Compounds in Meteorites. *Surveys in Geophysics*, 23, 411–467.

Bridges, J., Henson, R., Vago, J., Loizeau, D., Williams, R. M. E., Hauber, E., and Sephton-Nash, E. (2016). ExoMars Landing Site Characterisation and Selection. In *47th Lunar and Planetary Science Conference, #2170*.

Brocks, J. J. and Summons, R. E. (2003). Biomarkers for Early Life. In W. H. Schlesinger (Ed.), *Biogeochemistry*. Elsevier, Oxford, pp. 63–115.

Chyba, C. F. (1990). Impact delivery and erosion of planetary oceans in the early inner Solar System. *Nature*, 343, 129–133.

Ehlmann, B. L., Mustard, J. F., Fassett, C. I., Schon, S. C., Head III, J. W., Des Marais,

D. J., Grant, J. A., and Murchie, S. L. (2008). Clay minerals in delta deposits and organic preservation potential on Mars. *Nature Geoscience*, 1, 355–358.

Ehlmann, B. L., Mustard, J. F., Murchie, S. L., Bibring, J.-P., Meunier, A., Fraeman, A. A., and Langevin, Y. (2011). Subsurface water and clay mineral formation during the early history of Mars. *Nature*, 479, 53–60.

Ertem, G., Ertem, M. C., McKay, C. P., and Hazen, R. M. (2017). Shielding biomolecules from effects of radiation by Mars analogue minerals and soils. *International Journal of Astrobiology*, 16, 280–285.

Freissinet, C., Glavin, D. P., Mahaffy, P. R., Miller, K. E., Eigenbrode, J. L., Summons, R. E., Brunner, A. E., Buch, A., Szopa, C., Archer, P. D., Franz, H. B., Atreya, S. K., Brinckerhoff, W. B., Cabane, M., Coll, P., Conrad, P. G., Des Marais, D. J., Dworkin, J. P., Fairén, A. G., François, P., Grotzinger, J. P., Kashyap, S., ten Kate, I. L., Leshin, L. A., Malespin, C. A., Martin, M. G., Martin-Torres, F. J., McAdam, A. C., Ming, D. W., Navarro-González, R., Pavlov, A. A., Prats, B. D., Squyres, S. W., Steele, A., Stern, J. C., Sumner, D. Y., Sutter, B., Zorzano, M. P., and the MSL Science Team (2015). Organic molecules in the Sheepbed Mudstone, Gale Crater, Mars. *Journal of Geophysical Research: Planets*, 120, 495–514.

Golombek, M. P. and Phillips, R. J. (2010). Mars tectonics. In T. R. Watters and R. A. Schultz (Eds.), *Planetary Tectonics*. Cambridge University Press, New York, pp. 183–232.

Grotzinger, J. P. and Milliken, R. E. (2012). The Sedimentary Rock Record of Mars: Distribution, Origins, and Global Stratigraphy. In J. P. Grotzinger and R. E. Milliken (Eds.), *Sedimentary Geology of Mars, SEPM Special Publication 102*. Society for Sedimentary Geology, Tulsa, Oklahoma, pp. 1–48.

Hallmann, C., Kelly, A. E., Gupta, S. N., and Summons, R. E. (2011). Reconstructing deep-time biology with molecular fossils. In M. Laflamme, D. J. Schiffbauer, and Q. S. Dornbos (Eds.), *Quantifying the Evolution of Early Life: Numerical Approaches to the Evaluation of Fossils and Ancient Ecosystems*. Springer Netherlands, Dordrecht, pp. 355–401.

Kennedy, M. J., Pevear, D. R., and Hill, R. J. (2002). Mineral Surface Control of Organic Carbon in Black Shale. *Science*, 295, 657–660.

Kerridge, J. F., Chang, S., and Shipp, R. (1987). Isotopic characterisation of kerogen-like material in the Murchison carbonaceous chondrite. *Geochimica et Cosmochimica Acta*, 51, 2527–2540.

Killops, S. D. and Killops, V. J. (2005). *Introduction to organic geochemistry*. 2. edition, Blackwell Publishing Ltd, Oxford.

Kissin, Y. V. (2003). Hydrocarbon components in carbonaceous meteorites. *Geochimica et Cosmochimica Acta*, 67, 1723–1735.

Kminek, G. and Bada, J. L. (2006). The effect of ionizing radiation on the preservation of amino acids on Mars. *Earth and Planetary Science Letters*, 245, 1–5.

Loizeau, D., Mangold, N., Poulet, F., Bibring, J., Gendrin, A., Ansan, V., Gomez, C., Gondet, B., Langevin, Y., Masson, P., and Neukum, G. (2007). Phyllosilicates in the Mawrth Vallis region of Mars. *Journal of Geophysical Research: Planets*, 112, E08S08.

Montgomery, W., Bromiley, G. D., and Sephton, M. A. (2016). The nature of organic records in impact excavated rocks on Mars. *Scientific Reports*, 6, 30947.

Navarro-González, R., Vargas, E., de la Rosa, J., Raga, A. C., and McKay, C. P. (2010). Reanalysis of the Viking results suggests perchlorate and organics at midlatitudes on Mars. *Journal of Geophysical Research: Planets*, 115, E12010.

Navarro-González, R., Vargas, E., de la Rosa, J., Raga, A. C., and McKay, C. P. (2011). Correction to "Reanalysis of the Viking results suggests perchlorate and organics at midlatitudes on Mars". *Journal of Geophysical Research: Planets*, 116, E08011.

Oehler, D. Z. and Allen, C. C. (2012). Focusing the search for biosignatures on Mars: facies prediction with an example from Acidalia Planitia. In J. P. Grotzinger and R. E. Milliken (Eds.), *Sedimentary Geology of Mars, SEPM Special Publication 102*. Society for Sedimentary Geology, Tulsa, Oklahoma, pp. 183–194.

Oró, J. and Holzer, G. (1979). The photolytic degradation and oxidation of organic compounds under simulated Martian conditions. *Journal of Molecular Evolution*, 14, 153–160.

Parnell, J. and Lindgren, P. (2006). Survival of reactive carbon through meteorite impact melting. *Geology*, 34, 1029–1032.

Pavlov, A. A., Vasilyev, G., Ostryakov, V. M., Pavlov, A. K., and Mahaffy, P. (2012). Degradation of the organic molecules in the shallow subsurface of Mars due to irradiation by cosmic rays. *Geophysical Research Letters*, 39, L13202.

Poch, O., Jaber, M., Stalport, F., Nowak, S., Georgelin, T., Lambert, J.-F., Szopa, C., and Coll, P. (2015). Effect of Nontronite Smectite Clay on the Chemical Evolution of Several Organic Molecules under Simulated Martian Surface Ultraviolet Radiation Conditions. *Astrobiology*, 15, 221–237.

Poch, O., Kaci, S., Stalport, F., Szopa, C., and Coll, P. (2014). Laboratory insights into the chemical and kinetic evolution of several organic molecules under simulated Mars surface UV radiation conditions. *Icarus*, 242, 50–63.

Poulet, F., Bibring, J.-P., Mustard, J. F., Gendrin, A., Mangold, N., Langevin, Y., Arvidson, R. E., Gondet, B., Gomez, C., and Team, T. O. (2005). Phyllosilicates on Mars and implications for early martian climate. *Nature*, 438, 623–627.

Price, L. C. (1983). Geologic time as a parameter in organic metamorphism and vitrinite reflectance as an absolute paleogeothermometer. *Journal of Petroleum Geology*, 6, 5–37.

Price, L. C. (1993). Thermal stability of hydrocarbons in nature: Limits, evidence, characteristics, and possible controls. *Geochimica et Cosmochimica Acta*, 57, 3261–3280.

Quantin, C., Carter, J., Thollot, P., Broyer, J., Lozach, L., Davis, J., Grindrod, P., Pajola, M., Baratti, E., and Rossato, S. (2016). Oxia Planum, the landing site for ExoMars 2018. In *47th Lunar and Planetary Science Conference Abstracts, #2863*.

Shkrob, I. A., Chemerisov, S. D., and Marin, T. W. (2010). Photocatalytic Decomposition of Carboxylated Molecules on Light-Exposed Martian Regolith and Its Relation to Methane Production on Mars. *Astrobiology*, 10, 425–436.

Stalport, F., Coll, P., Szopa, C., Cottin, H., and Raulin, F. (2009). Investigating the Photostability of Carboxylic Acids Exposed to Mars Surface Ultraviolet Radiation Conditions. *Astrobiology*, 9, 543–549.

Steininger, H., Goesmann, F., and Goetz, W. (2012). Influence of magnesium perchlorate on the pyrolysis of organic compounds in Mars analogue soils. *Planetary and Space Science*, 71, 9–17.

Summons, R. E., Amend, J. P., Bish, D., Buick, R., Cody, G. D., Des Marais, D. J., Dromart, G., Eigenbrode, J. L., Knoll, A. H., and Sumner, D. Y. (2011). Preservation of Martian Organic and Environmental Records: Final Report of the Mars Biosignature Working Group. *Astrobiology*, 11, 157–181.

Tissot, B. P. and Welte, D. H. (1984). *Petroleum Formation and Occurrence*. 2. edition, Springer, Berlin, Heidelberg.

Vago, J. L., Lorenzoni, L., Calantropio, F., and Zashchirinskiy, A. M. (2015). Selecting a landing site for the ExoMars 2018 mission. *Solar System Research*, 49, 538–542.

Vago, J. L., Westall, F., Pasteur Instrument Teams, L. S. S. W. G., Other, C., Coates, A. J., Jaumann, R., Korablev, O., Ciarletti, V., Mitrofanov, I., Josset, J.-L., De Sanctis, M. C., Bibring, J.-P., Rull, F., Goesmann, F., Steininger, H., Goetz, W., Brinckerhoff, W., Szopa, C., Raulin, F., Edwards, H. G. M., Whyte, L. G., Fairén, A. G., Bridges, J., Hauber, E., Ori, G. G., Werner, S., Loizeau, D., Kuzmin, R. O., Williams, R. M. E., Flahaut, J., Forget, F., Rodionov, D., Svedhem, H., Sefton-Nash, E., Kminek, G., Lorenzoni, L., Joudrier, L., Mikhailov, V., Zashchirinskiy, A., Alexashkin, S., Calantropio, F., Merlo, A., Poulakis, P., Witasse, O., Bayle, O., Bayón, S., Meierhenrich, U., Carter, J., García-Ruiz, J. M., Baglioni, P., Haldemann, A., Ball, A. J., Debus, A., Lindner, R., Haessig, F., Monteiro, D., Trautner, R., Voland, C., Rebeyre, P., Goulty, D., Didot, F., Durrant, S., Zekri, E., Koschny, D., Toni, A., Visentin, G., Zwick, M., van Winnendael, M., Azkarate, M., Carreau, C., and the ExoMars Project Team (2017). Habitability on Early Mars and the Search for Biosignatures with the ExoMars Rover. *Astrobiology*, 17, 471–510.

van Thienen, P., Vlaar, N. J., and van den Berg, A. P. (2004). Plate tectonics on the terrestrial planets. *Physics of the Earth and Planetary Interiors*, 142, 61–74.

Waples, D. W. (2000). The kinetics of in-reservoir oil destruction and gas formation: constraints from experimental and empirical data, and from thermodynamics. *Organic Geochemistry*, 31, 553–575.

Westall, F., Foucher, F., Bost, N., Bertrand, M., Loizeau, D., Vago, J. L., Kminek, G., Gaboyer, F., Campbell, K. A., Bréhéret, J.-G., Gautret, P., and Cockell, C. S. (2015). Biosignatures on Mars: What, Where, and How? Implications for the Search for Martian Life. *Astrobiology*, 15, 998–1029.

Yen, A. S., Kim, S. S., Hecht, M. H., Frant, M. S., and Murray, B. (2000). Evidence That the Reactivity of the Martian Soil Is Due to Superoxide Ions. *Science*, 289, 1909–1912.

Summary, conclusions and outlook

8.1 Summary and conclusions

This thesis combines a series of mainly experimental studies which were aimed at (i) assessing the diversity of biomarker-like lipids from abiotic Fischer–Tropsch-type (FTT) synthesis, (ii) determining the impact of thermal stress on biologically and abiotically derived lipids, (iii) providing reference data to differentiate between biologically and abiotically synthesized lipids in sediments and rocks and (iv) identifying analytical limitations and potential pitfalls of MOMA gas chromatography–mass spectrometry (GC–MS) techniques.

In the first study, experimental maturation in gold capsules (300, 400 °C; 2 kbar; 2 – 2400 h) was performed on isolated kerogen from the Eocene Green River formation to determine the impact of thermal maturation on biological n-alkane distribution patterns and selected lipid biomarkers (pristane, phytane, steranes, hopanes, cheilanthanes; Chapter 2). The study revealed major differences in their thermal degradation behavior, directly influencing the applicability of corresponding biomarker ratios (e.g., pristane/phytane, steranes/hopanes). Hence, a careful evaluation of the thermal history of the sample is necessary before using these ratios for paleoreconstructions. Furthermore, it was demonstrated that n-alkane distribution patterns and respective biomarkers withstand thermal maturation at 300 °C for 2400 h while they quickly degrade at 400 °C (< 48 h, corresponding to 1.83% R_O).

The second study addressed FTT synthesis which yielded a variety of solvent extractable biomarker-like lipids (e.g., linear and methyl-branched alkanes and alkanols, n-alkanoic acids; Chapter 3). These showed a unimodal distribution of homologous compounds, in contrast to homolog/isomer preferences and uneven distributions which usually originate from biological sources. Thus, a discrimination of abiotically (FTT synthesis) and biologically derived lipids based on their primary distributions is principally possible. However, primary distributions change in the course of thermal maturation, which can complicate lipid source discrimination (see also Chapter 2). It should further be noted that analyses of the extraction residues from FTT reactions revealed the existence of a potential FTT derived polymer, but it is as yet unclear whether or not this could evolve into macromolecular kerogen-like material.

The third study (Chapter 4) comprised the investigation of kerogen from an Archean hydrothermal chert vein (3.5 Ga Dresser Formation, Pilbara Craton, Western Australia). The kerogen was embedded in a dense chert matrix without any disruptions or signs of external contamination which underlined its syngeneity. Organic matter cracked from the kerogen via catalytic hydropyrolysis showed n-alkane homologs with a distinct decrease $> n\text{-}C_{18}$. The same n-alkane pattern was observed in recent bacterial biomass from *Anabaena cylindrica*, whereas abiotically derived organics from FTT reactions exhibited unimodal distributions (see also Chapter 3). Based on these observations, a biological origin of the kerogen was inferred which is furthermore consistent with a low $\delta^{13}C_{TOC}$ value of -32.8 ± 0.3 ‰ and stable carbon isotope values of n-alkanes ranging from -29.4 ‰ to -33.3 ‰.

Moreover, case studies on a synthetic and a natural sample with and without Mg-perchlorate (0 wt%, 1 wt%, 10 wt%), using MOMA-like pyrolysis, in situ derivatization and thermochemolysis GC–MS techniques were performed (Section 5.7.5 and Chapter 6). The studies were aimed at evaluating the applicability of these techniques to different sample types, and assessing the impact of Mg-perchlorate on the analysis. Pyrolysis at 700 °C (10 s) provided a sufficient overview of the organic inventory of complex bulk samples. However, it is not suitable for the analysis of polar compounds, and led to the production of analytical by-products (e.g., aromatic, unsaturated compounds). Furthermore, the impact of perchlorate on pyrolysis was high, and resulted in partial or complete degradation of organics. In situ derivatization with *N*/*N*-methyl-tert-butyl-dimethylsilyltrifluoroacetamide/*N*/*N*-dimethylformamide (MTBSTFA/DMF; 250 °C, 10 min) facilitated the detection of polar organic compounds. On the other hand, this technique only revealed low abundances of *n*-alkanoic acids and no indication of organic compounds from the natural sample. In situ thermochemolysis with tetramethylammonium hydroxide (TMAH; 600 °C, 40 s) yielded the full organic inventory of both samples (polar and nonpolar compounds), showing some analytical by-products from thermal decomposition. Most importantly, this method was not affected by up to 10 wt% Mg-perchlorate. This underlines that perchlorates in martian soils do not necessarily hamper MOMA-like GC–MS analysis.

Lastly, it was demonstrated that the discrimination of biologically from abiotically derived organic materials is principally possible with MOMA-like GC–MS (Chapter 7). However, the applicability of each MOMA-like GC–MS technique depends upon sample type and character of the organic compounds. Hence, complementary analyses of a given sample using different techniques should be considered to minimize method dependent biases. Nonetheless, these studies emphasize that biomarkers in martian soil or rock samples can principally be detected by MOMA, and the obtained results will provide a reference for the interpretation of upcoming MOMA data.

8.2   Outlook

Ongoing work relating to this thesis includes the evaluation of results from experimental maturation of solvent extractable organic material derived from FTT synthesis (partially presented in Appendix D). The formation of abiotic kerogen-like materials during thermal alteration of solvent extractable FTT reaction products was not yet observed. Nonetheless, maturation data revealed, for example, that short chain *n*-alkanoic acids can be preserved for 2400 h at 300 °C.

Results from maturation experiments presented in this work mostly focused on the characterization of aliphatic hydrocarbon moieties (Chapter 2, Appendix D). Therefore, future investigations of maturation products should be extended to the evaluation of aromatic hydrocarbon fractions. This is to determine whether abiotically and biologically derived organic materials exhibit different aromatic hydrocarbon signatures that may allow their discrimination. Furthermore, future maturation experiments could encompass different pressure and temperature regimes as well as the addition of different matrix minerals. This may enable an estimate of the impact of these parameters on the preservation potential of biological distribution patterns and individual lipid biomarkers.

MOMA-like GC–MS studies using the flight analog system (FAS) provide the possibility to compile a comprehensive reference database for the ExoMars mission. Additional analog experiments to those presented in this study could include different substrates for synthetic samples and varying amounts of different oxychlorine compounds (e.g., Ca- and Mg-perchlorate mixtures). Furthermore, the analysis of experimentally maturated organic material would be helpful to evaluate potential limitations in distinguishing altered biologically and abiotically derived organic compounds via MOMA-like GC–MS. On the other hand, the analysis of fresh bacterial biomass can give insights in MOMA's capabilities to detect extant life.

Specific tests using the FAS should also assess potential limitations of the TMAH buffer. So far, it has been shown that TMAH buffers the reaction of up to 10 wt% Mg-perchlorate with organics in a natural and a synthetic sample (Chapter 6). Based on this, one of the next steps could be to analyze samples with Ca-, Mg-perchlorate and chlorate mixtures via MOMA-like thermochemolysis in order to determine whether or not different (mixtures of) oxychlorine compounds lead to other outcomes. Subsequently, the effectiveness of this method for analysis of Mars-like samples has to be tested. This could involve experiments using fine-grained basaltic material or clay minerals mixed with perchlorates as a substrate that is spiked with only a few ppm organics (e.g., standard mixtures containing short chain *n*-alkanes, *n*-alkanoic acids, *n*-alkanols, benzene, toluene). Finally, a series of tests using flight-like derivatization capsules should be conducted in order to verify that a flight-like release of TMAH to the sample (as it will be done by MOMA) still results in the same buffering reaction.

Appendices

Appendix A

Supplementary material

Assessing the diversity of lipids formed via Fischer–Tropsch-type reactions

Table A.1: Duration, analytical approaches and homolog ranges of individual Fischer–Tropsch-type (FTT) synthesis experiments.

	FTT 1	FTT 2	FTT 3	FTT 4	FTT 5	FTT 6	FTT 7	FTT 8
Duration [h]	66	74	73	71	74	71	71	70
GC–MS of total extract	X	X	X	X	X	X	X	X
GC–MS of hydrocarbon fraction (F1)	X	X						X
GC–MS of alcohol fraction (F2)	X	X						X
GC–MS of polar fraction (F3)	X							
Py-GC–MS of extraction residues	X	X						X
FTIR of extraction residues	X	X						
Combustion–infrared detection of extraction residues	X	X						
Homolog ranges								
n-Alkanes	$C_{11}-C_{40}$	$C_{11}-C_{39}$	$C_{11}-C_{41}$	$C_{11}-C_{36}$	$C_{11}-C_{38}$	$C_{11}-C_{35}$	$C_{11}-C_{36}$	$C_{11}-C_{39}$
Methylalkanes	$C_{12}-C_{36}$	$C_{12}-C_{35}$	n.d.	n.d.	n.d.	n.d.	n.d.	$C_{12}-C_{27}$
n-Alkan-1-ols	$C_{7}-C_{38}$	$C_{7}-C_{38}$	$C_{7}-C_{36}$	$C_{7}-C_{33}$	$C_{7}-C_{35}$	$C_{7}-C_{32}$	$C_{7}-C_{34}$	$C_{7}-C_{37}$
n-Alkan-2-ols	$C_{8}-C_{37}$	$C_{8}-C_{37}$	$C_{8}-C_{37}$	$C_{8}-C_{33}$	$C_{8}-C_{35}$	$C_{8}-C_{31}$	$C_{8}-C_{35}$	$C_{8}-C_{38}$
n-Alkan-3-ols	$C_{8}-C_{24}$	$C_{8}-C_{24}$	$C_{8}-C_{22}$	$C_{8}-C_{24}$	$C_{8}-C_{23}$	$C_{8}-C_{21}$	$C_{8}-C_{21}$	$C_{8}-C_{20}$
2-Methylalkan-1-ols	$C_{8}-C_{33}$	$C_{8}-C_{35}$	$C_{8}-C_{33}$	$C_{8}-C_{30}$	$C_{8}-C_{33}$	$C_{8}-C_{28}$	$C_{8}-C_{31}$	$C_{8}-C_{32}$
n-Alkanoic acids	$C_{7}-C_{26}$	$C_{7}-C_{26}$	$C_{7}-C_{24}$	$C_{7}-C_{24}$	$C_{7}-C_{24}$	$C_{7}-C_{23}$	$C_{7}-C_{25}$	$C_{7}-C_{24}$
n-Alkyl formates	$C_{8}-C_{30}$	$C_{8}-C_{30}$	$C_{8}-C_{31}$	$C_{8}-C_{27}$	$C_{8}-C_{29}$	$C_{8}-C_{26}$	$C_{8}-C_{24}$	$C_{8}-C_{25}$

X denotes conducted analyses. n.d., not determined; GC–MS, gas chromatographie–mass spectrometry; Py-GC–MS, pyrolysis-GC–MS; FTIR, Fourier transform infrared spectroscopy.
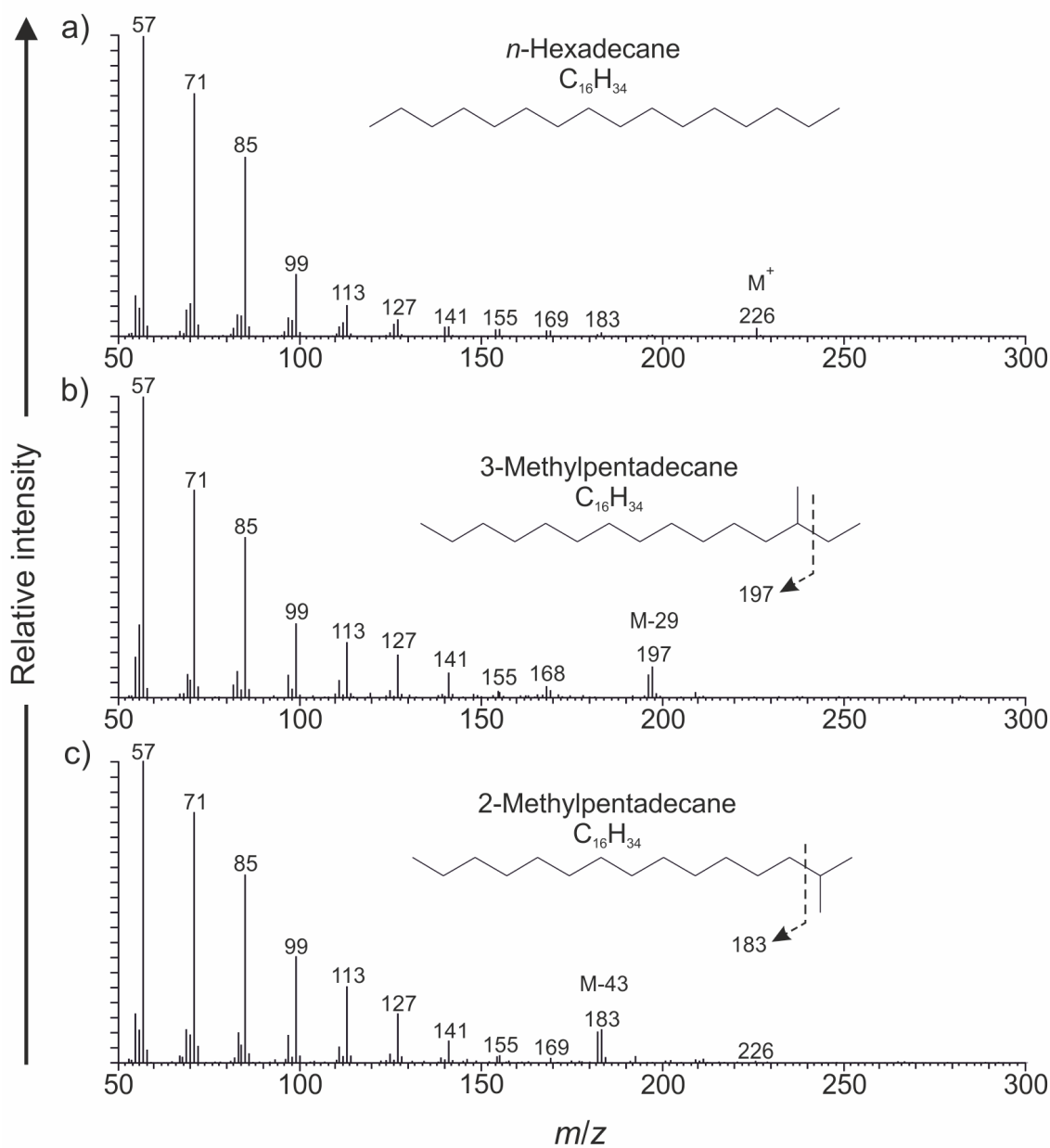
Figure A.1: Representative mass spectra of selected alkanes resulting from Fischer–Tropsch-type reactions. (**a**) *n*-hexadecane, (**b**) 3-methylpentadecane (*anteiso*-hexadecane), (**c**) 2-methylpentadecane (*iso*-hexadecane).
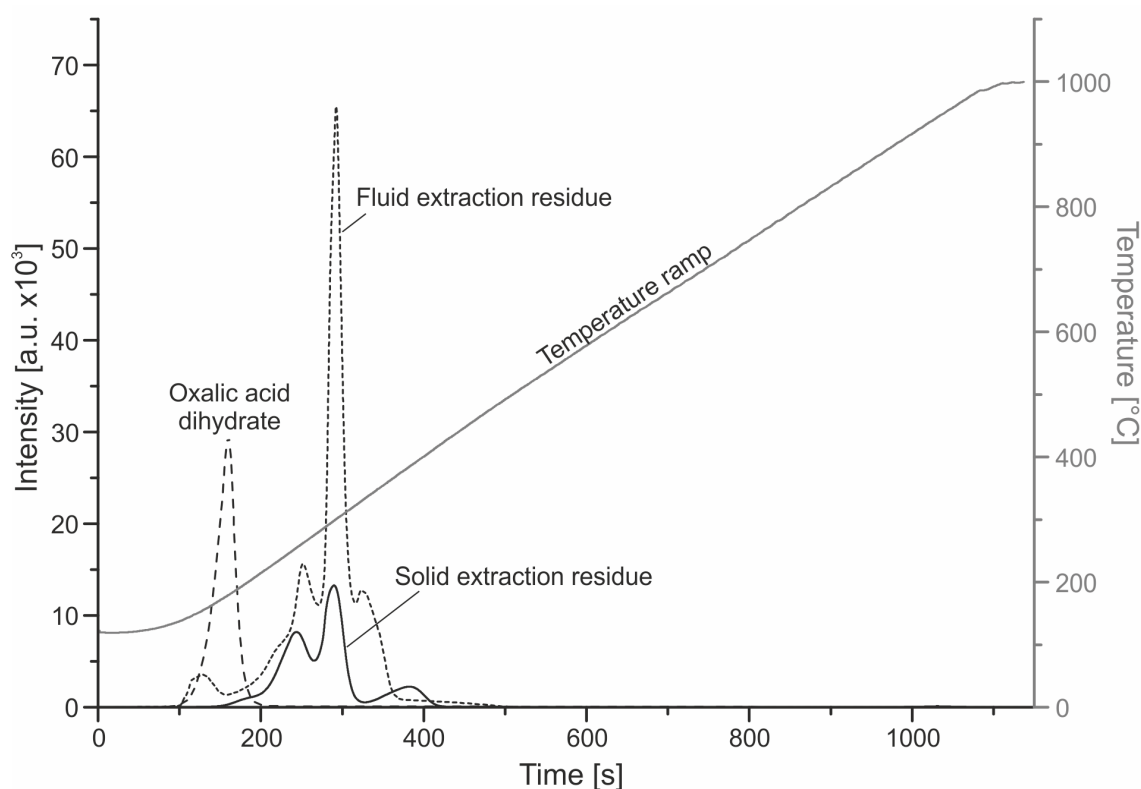
Figure A.2: Combustion–infrared detection data obtained from extraction residues of Fischer–Tropsch-type reaction products and oxalic acid dihydrate. The fluid extraction residue (dotted line) and the solid extraction residue (solid line) exhibit a major peak at 300 °C. Oxalic acid dihydrate (dashed line) shows only one peak at 183 °C. The temperature scale is referring to the temperature ramp of the combustion oven (plotted in grey).
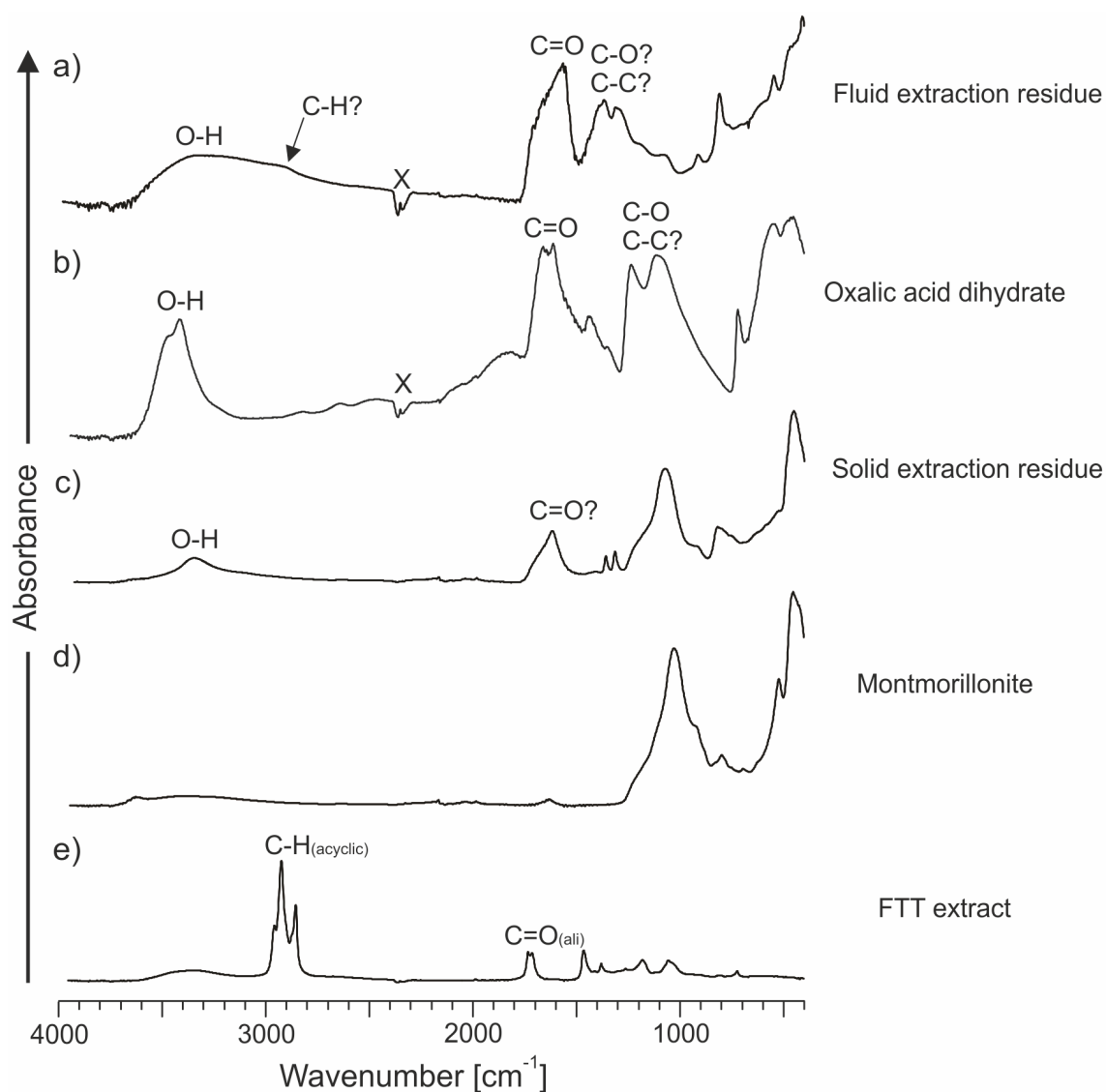
Figure A.3: Attenuated total reflectance Fourier transform infrared spectra of freeze dried extraction residues (**a**: fluid; **c**: solid), with (**b**) oxalic acid dihydrate, (**d**) montmorillonite, and (**e**) an organic extract (FTT extract) as references. Note the differences in O–H, C–H and C=O bonds between (**a**), (**b**), and (**e**). Furthermore, note the similarity between the strong bands (ca. $1050\ cm^{-1}$) in (**c**) and (**d**). X: negative bands due to interference with atmospheric CO_2; ali: aliphatic.
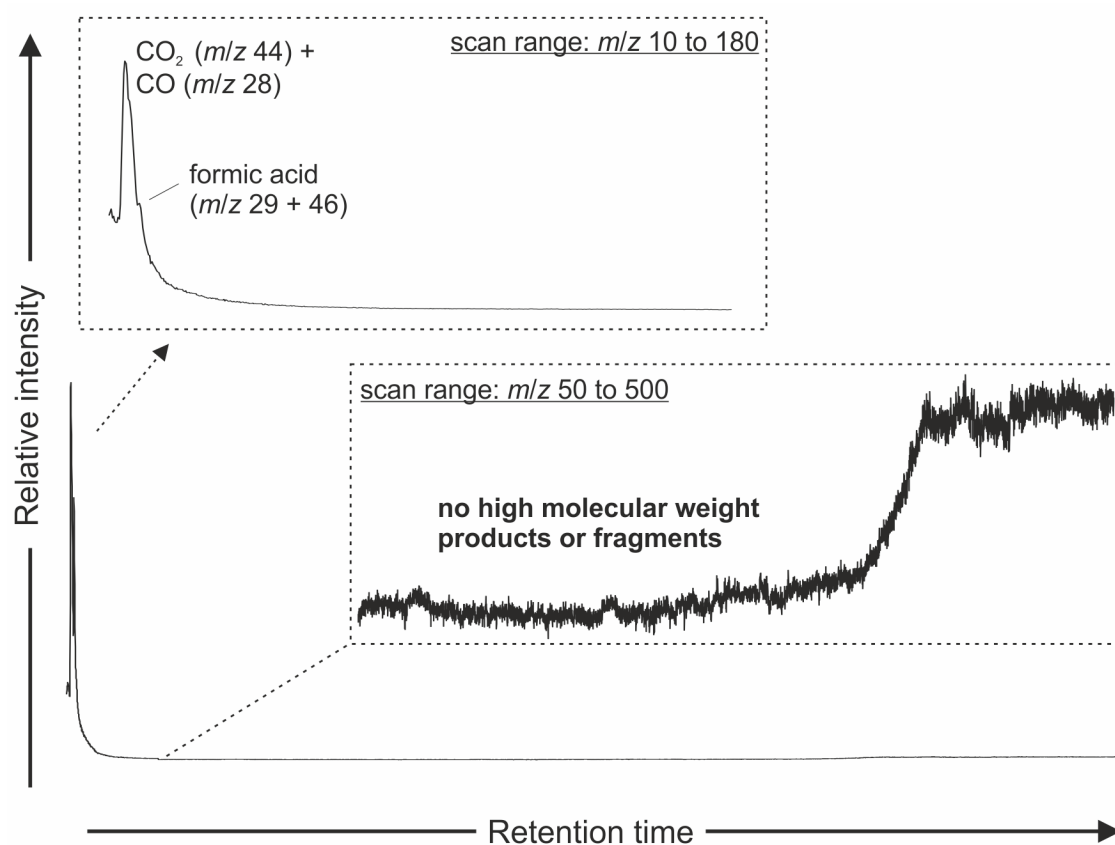
Figure A.4: Pyrolysis-GC–MS chromatograms (total ion current) of freeze dried fluid extraction residues (340 °C, 10 s). Note the presence of low molecular weight compounds (CO_2, CO and formic acid) and virtual absence of higher molecular weight organics.
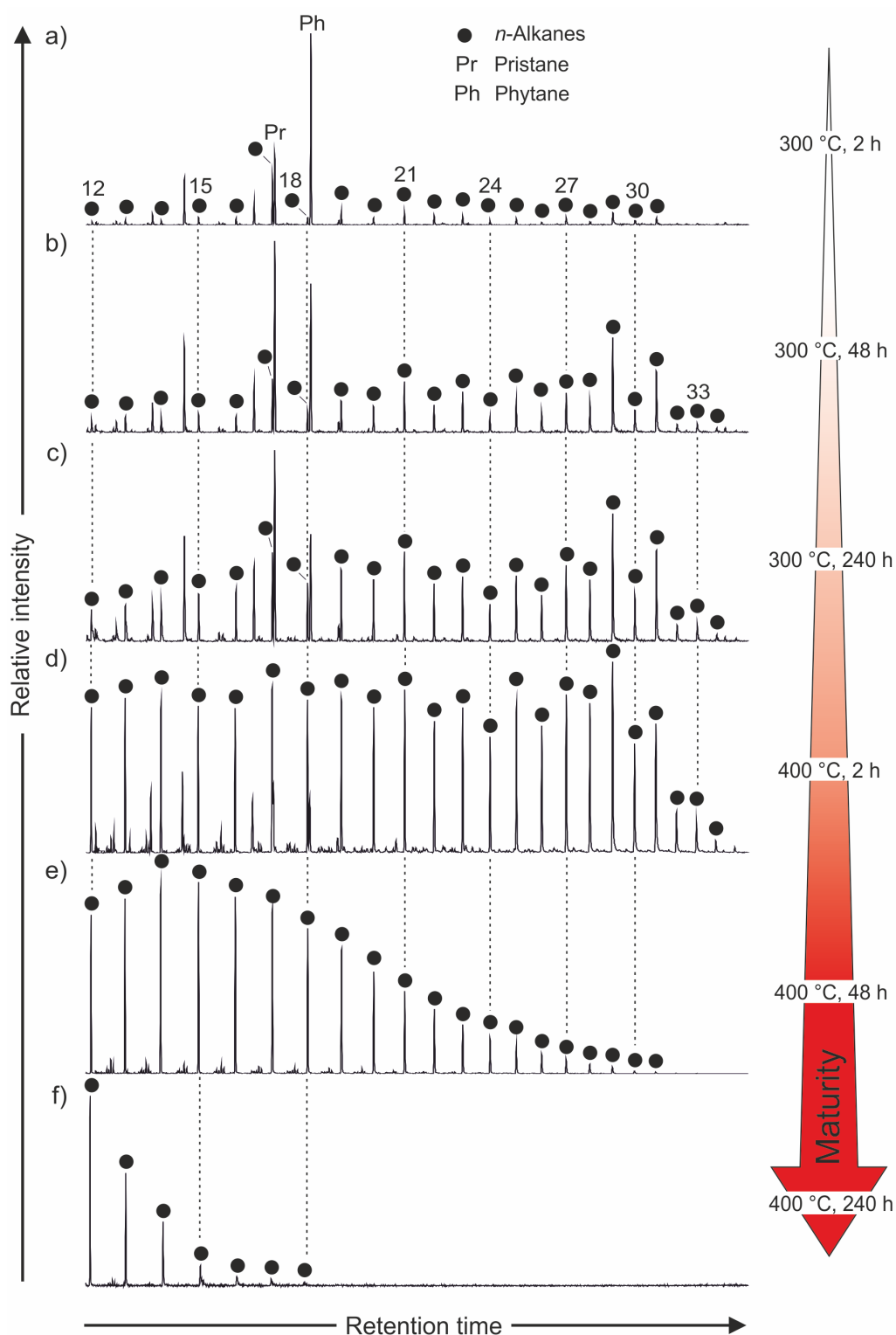
Figure A.5: Mass chromatograms (*m/z* 85) of the hydrocarbon fractions from experimentally matured Green River Shale kerogen (2 h at 300 °C to 240 h at 400 °C, **a**–**f**) demonstrating the evolution of *n*-alkane distributions during experimental maturation. Note that the odd-over-even predominance of *n*-alkanes is decreasing with increasing thermal maturity and is completely vanished after 48 h and 240 h (**e** and **f**, respectively). Furthermore, progressive thermal alteration caused a successive shift towards short-chain, low molecular weight *n*-alkanes (**e** to **f**).

Appendix B

Supplementary material

Ideas and perspectives: Hydrothermally driven redistribution and sequestration of early Archaean biomass —the "hydrothermal pump hypothesis"
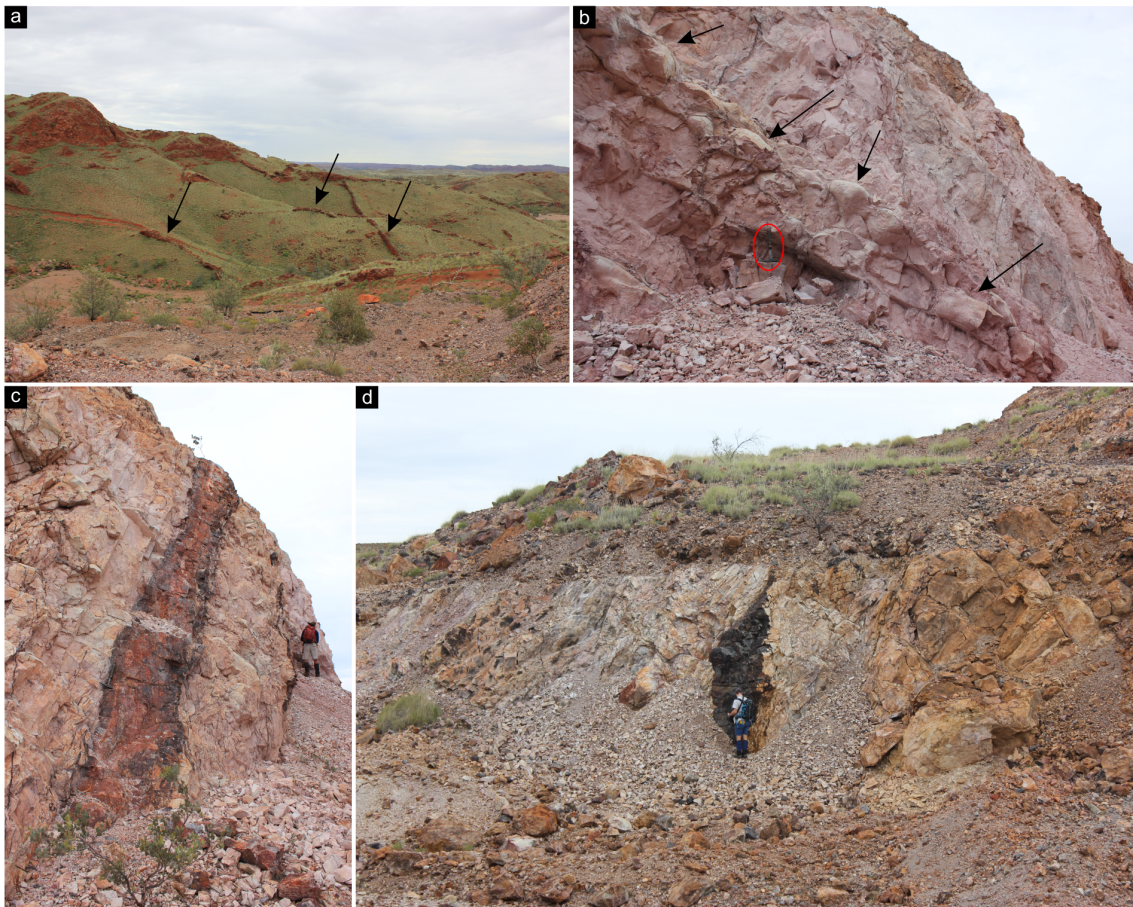
Figure B.1: Hydrothermal chert veins of the ca. 3.5 Ga Dresser Formation (Pilbara Craton, Western Australia). (**a**) Hydrothermal chert veins of the Dresser Formation (ridges, see arrows) forming large-scale networks in their host basalts. (**b**) Hydrothermally altered footwall basalts exhibiting pillow structures (arrows); hammer for scale (red circle). (**c** and **d**) Hydrothermal chert veins of the Dresser Formation penetrating komatiitic footwall basalts in a recent cut wall of the abandoned Dresser Mine (persons for scale). The analyzed hydrothermal chert vein occurs adjacent to the one shown in (**d**).
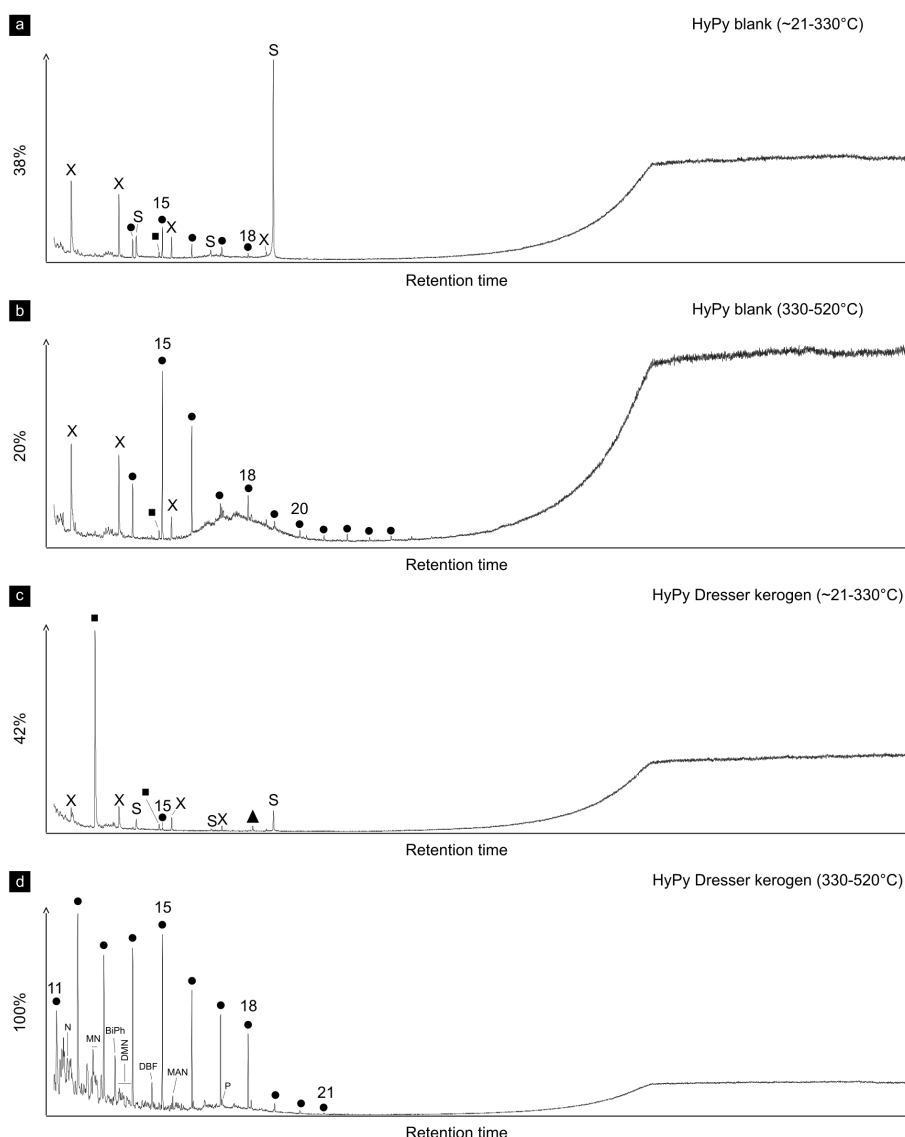
Figure B.2: Total ion current chromatograms. Low-temperature (**a**) and high-temperature (**b**) HyPy products of the analytical blank (combusted sea sand) obtained prior to HyPy of the Dresser kerogen. Low-temperature (**c**) and high-temperature (**d**) HyPy products of the Dresser kerogen. Compounds detected in (**a – c**) represent background contamination and/or artefacts. Note that high-temperature HyPy of the Dresser kerogen yielded significantly higher amounts of products with a distinctly different distribution pattern. Black dots: *n*-alkanes (numbers refer to carbon chain-lengths); triangle: phthalic acid; N: naphthalene; MN: methylnaphthalenes; BiPh: 1,1'-biphenyl; DMN: dimethylnaphthalenes; MAN: methylacenaphthenes; P: phenanthrene; crosses: siloxanes (GC column or septum bleeding); squares: phenols; S: sulphur.

Note: Percentage values given on the vertical axes of chromatograms (**a – c**) relate peak intensities to chromatogram (**d**) (HyPy Dresser kerogen, 330 – 520 °C).
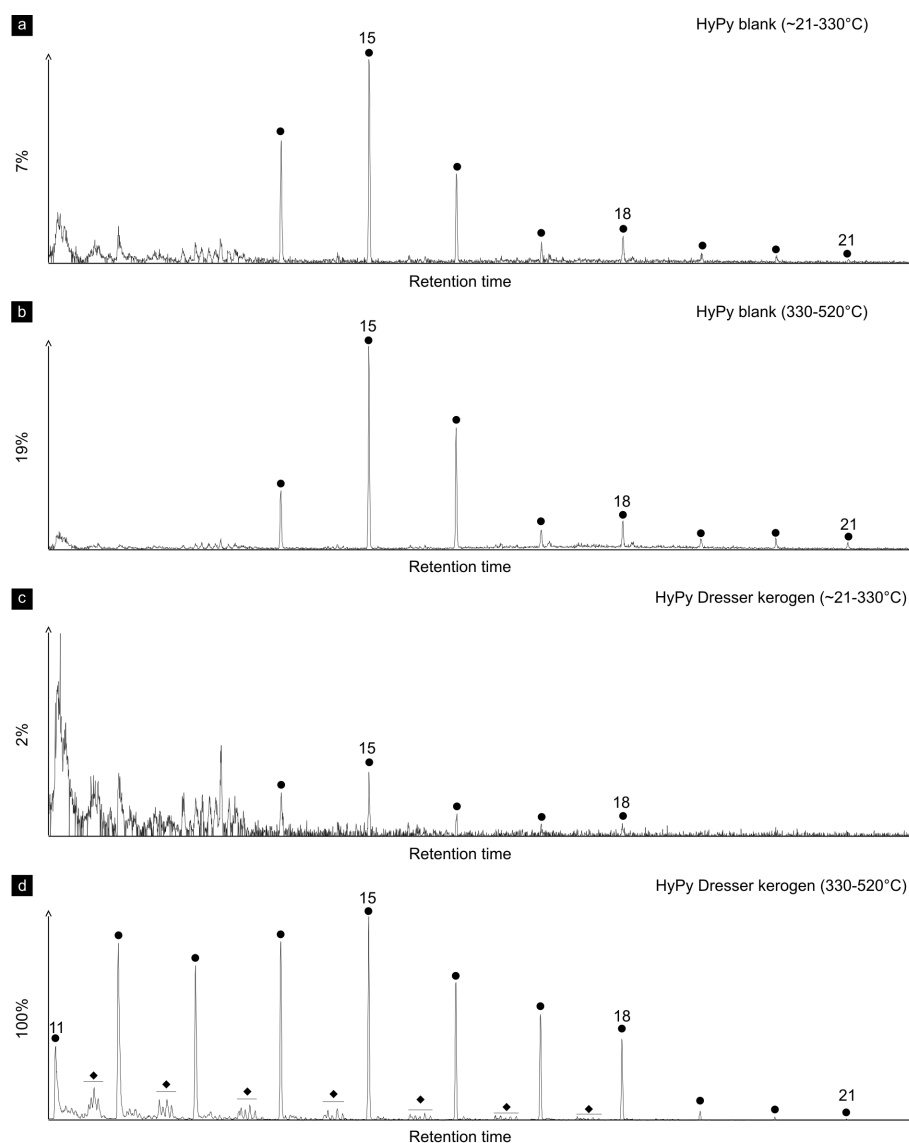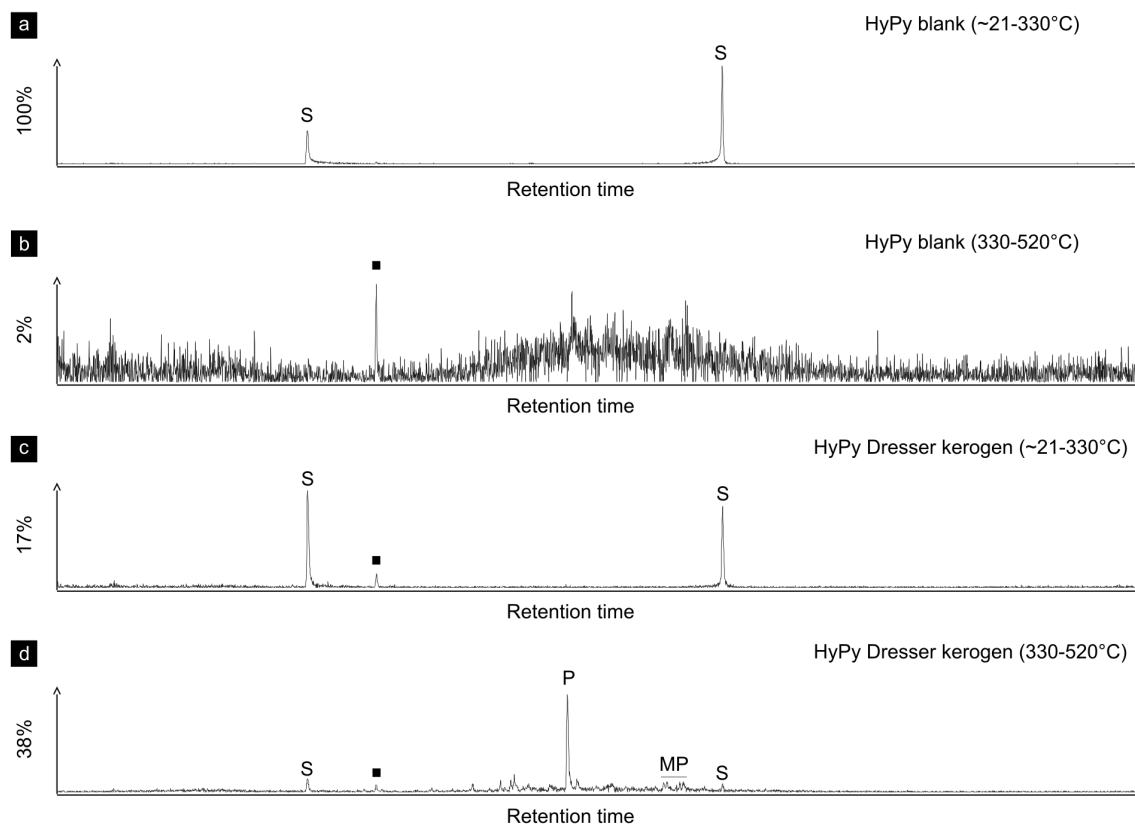
Figure B.3: Partial ion chromatograms selective for alkanes (*m/z* 85). Low-temperature (**a**) and high-temperature (**b**) HyPy products of the analytical blank (combusted sea sand) obtained prior to HyPy of the Dresser kerogen. Low-temperature (**c**) and high-temperature (**d**) HyPy products of the Dresser kerogen. High-temperature HyPy produced the highest yields of *n*-alkanes and minor clusters of isomeric monomethylalkanes (diamonds in **d**). The *n*-alkanes in the high-temperature pyrolysate of the Dresser kerogen (**d**) furthermore exhibit a distinct distribution different to those observed in (**a**–**c**). All compounds detected in (**a**–**c**) are considered to represent background contamination. Black dots: *n*-alkanes (numbers refer to carbon chain-lengths).

Note: Percentage values given on the vertical axes of chromatograms (**a**–**c**) relate peak intensities to chromatogram (**d**) (HyPy Dresser kerogen, 330–520 °C).
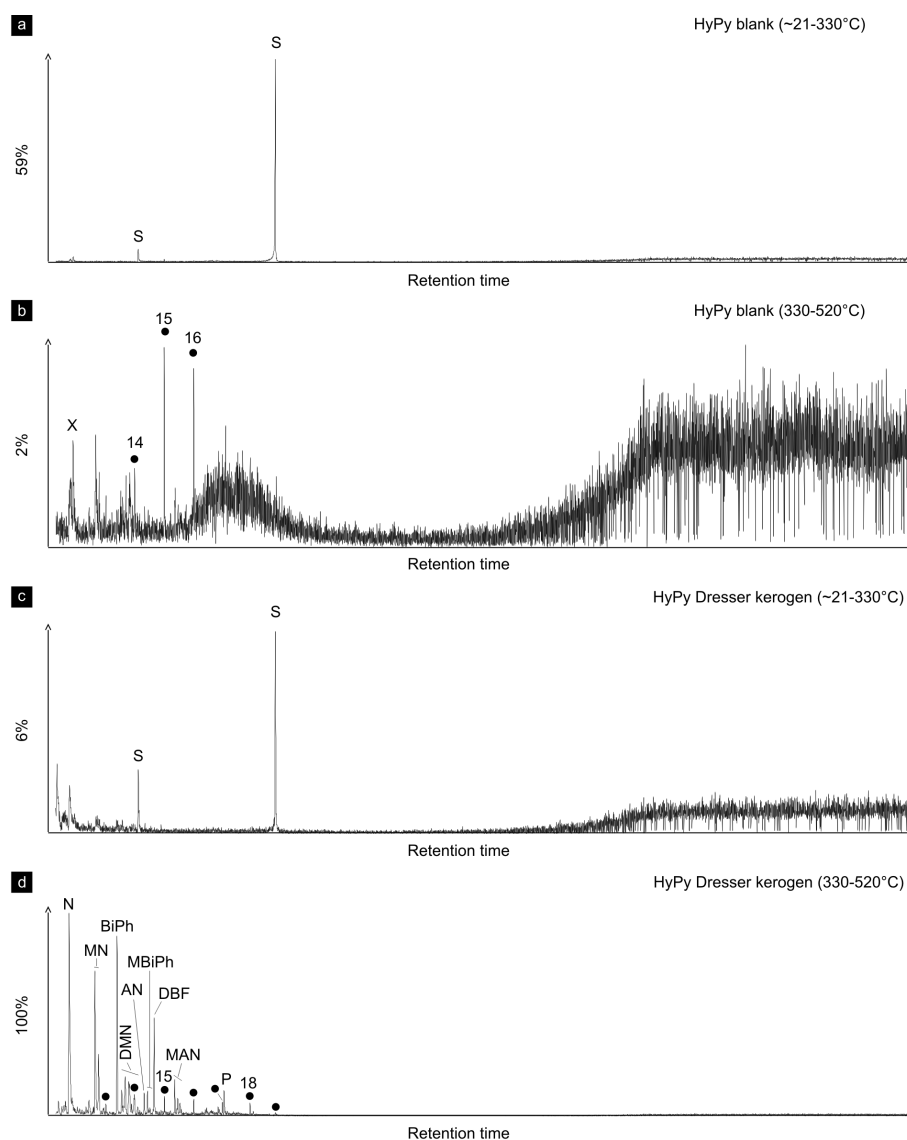
Figure B.4: Ion chromatograms selective for aromatic hydrocarbons (*m/z* 128, 142, 154, 156, 168, 178). Low-temperature (**a**) and high-temperature (**b**) HyPy products of analytical blank (combusted sea sand) obtained prior to HyPy of the Dresser kerogen. Low-temperature (**c**) and high-temperature (**d**) HyPy products of the Dresser kerogen. Note that high-temperature HyPy of the Dresser kerogen yielded a variety of aromatic hydrocarbons, which are orders of magnitudes lower or absent in all other pyrolysates. Black dots: *n*-alkanes (numbers refer to carbon chain-lengths); N: naphthalene; MN: methylnaphthalenes; BiPh: 1,1'-biphenyl; DMN: dimethylnaphthalenes; AN: acenaphthene; MBiPh: methylbiphenyls; DBF: dibenzofuran; MAN: methylacenaphthenes; P: phenanthrene; crosses: siloxanes (GC column or septum bleeding); S: elemental sulphur (likely derived from the sulfidic catalyst).

Note: Percentage values given on the vertical axes of chromatograms (**a – c**) relate peak intensities to chromatogram (**d**) (HyPy Dresser kerogen, $330 - 520$ °C).
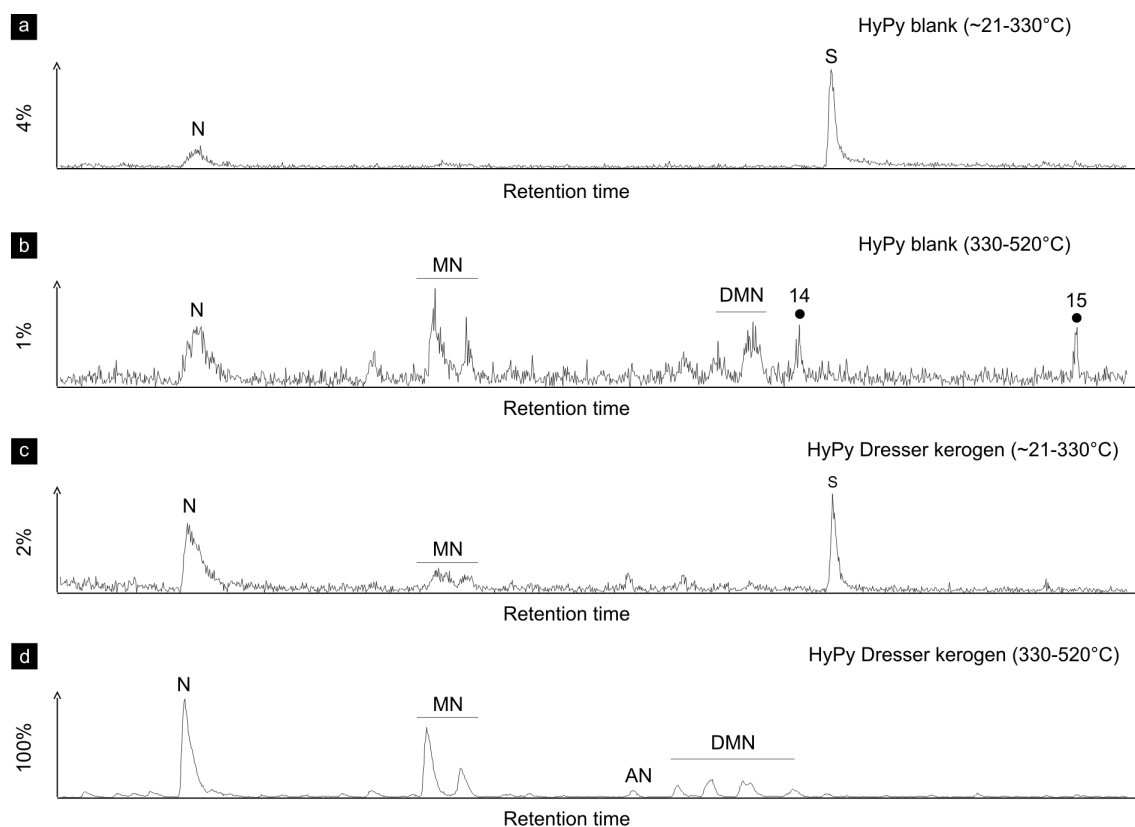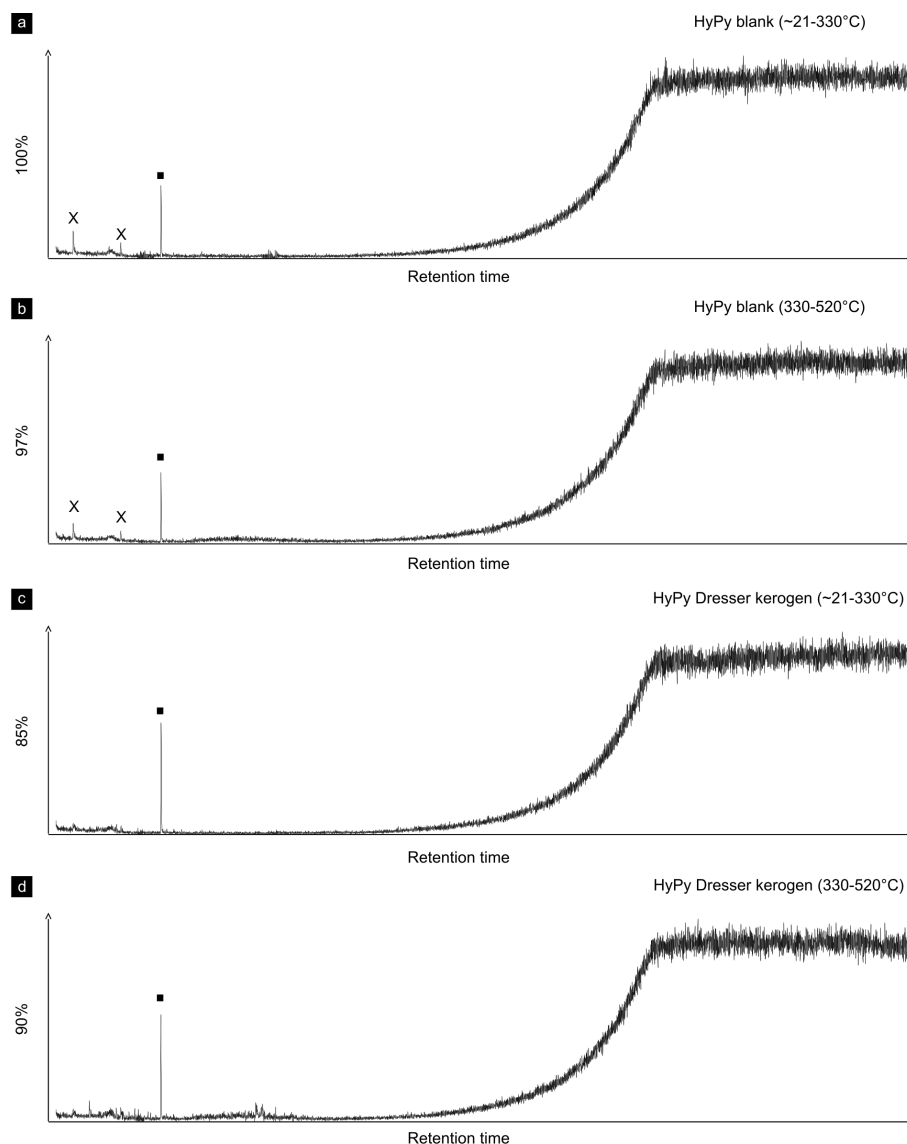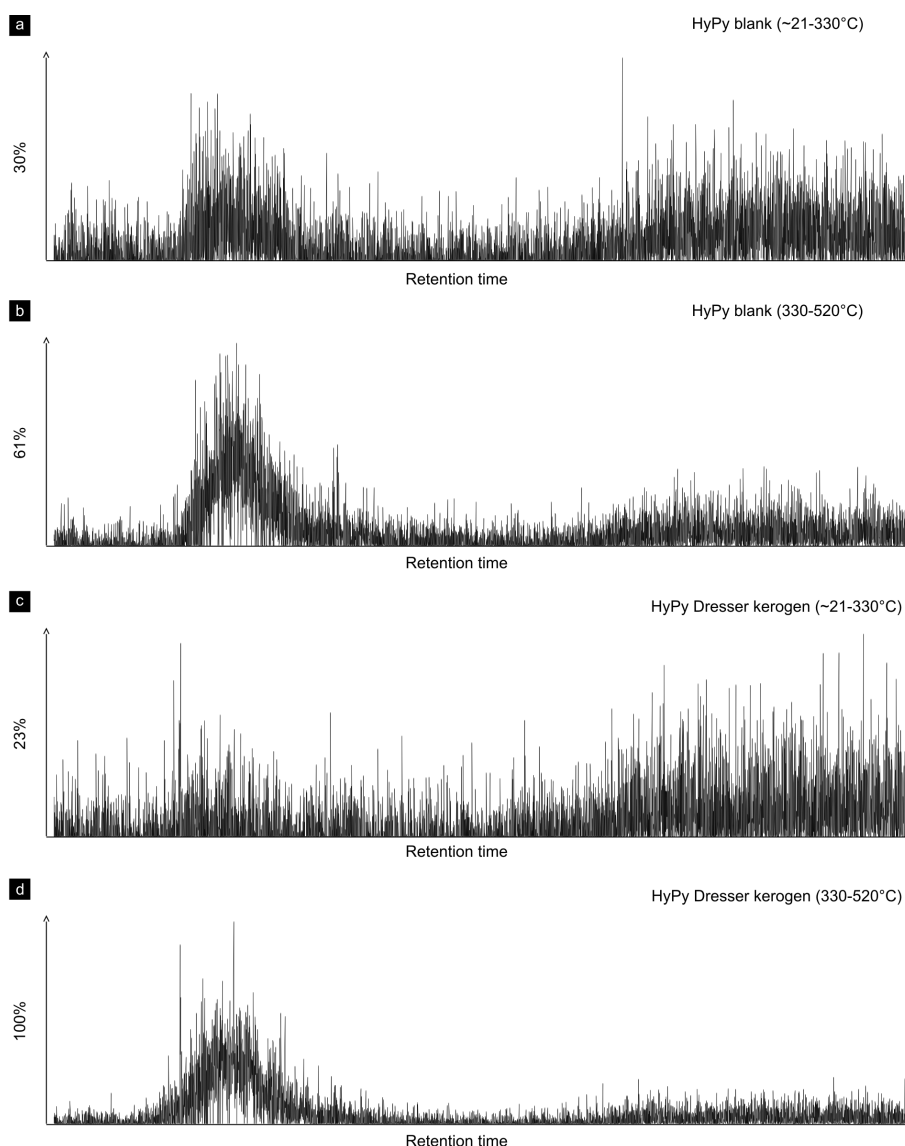
Figure B.5: Partial ion chromatograms selective for (dimethyl-, methyl-)naphthalenes (*m/z* 128, 142, 156). Low-temperature (**a**) and high-temperature (**b**) HyPy products of the analytical blank (combusted sea sand) obtained prior to HyPy of the Dresser kerogen. Low-temperature (**c**) and high-temperature (**d**) HyPy products of the Dresser kerogen. High-temperature HyPy of the Dresser kerogen yielded naphthalene (N), methylnaphthalenes (MN), dimethylnaphthalenes (DMN) and acenaphthene (AN), which are orders of magnitudes lower or absent in all other pyrolysates. Black dots: *n*-alkanes (numbers refer to carbon chain-lengths); S: elemental sulphur (likely derived from the sulfidic catalyst).

Note: Percentage values given on the vertical axes of chromatograms (**a**−**c**) relate peak intensities to chromatogram (**d**) (HyPy Dresser kerogen, 330−520 °C).

Figure B.6: Partial ion chromatograms selective for (methyl-)phenanthrenes (*m/z* 178, 192). Low-temperature (**a**) and high-temperature (**b**) HyPy products of the analytical blank (combusted sea sand) obtained prior to HyPy of the Dresser kerogen. Low-temperature (**c**) and high-temperature (**d**) HyPy products of the Dresser kerogen. Phenanthrene (P) and traces of methylphenanthrenes (MP) were only present in the high-temperature HyPy pyrolysate of the Dresser kerogen. Squares: phenols; S: elemental sulphur (likely derived from the sulfidic catalyst).
Note: Percentage values given on the vertical axes of chromatograms (**b** − **d**) relate peak intensities to chromatogram (**a**) (HyPy blank, ∼ 21 − 330 °C).
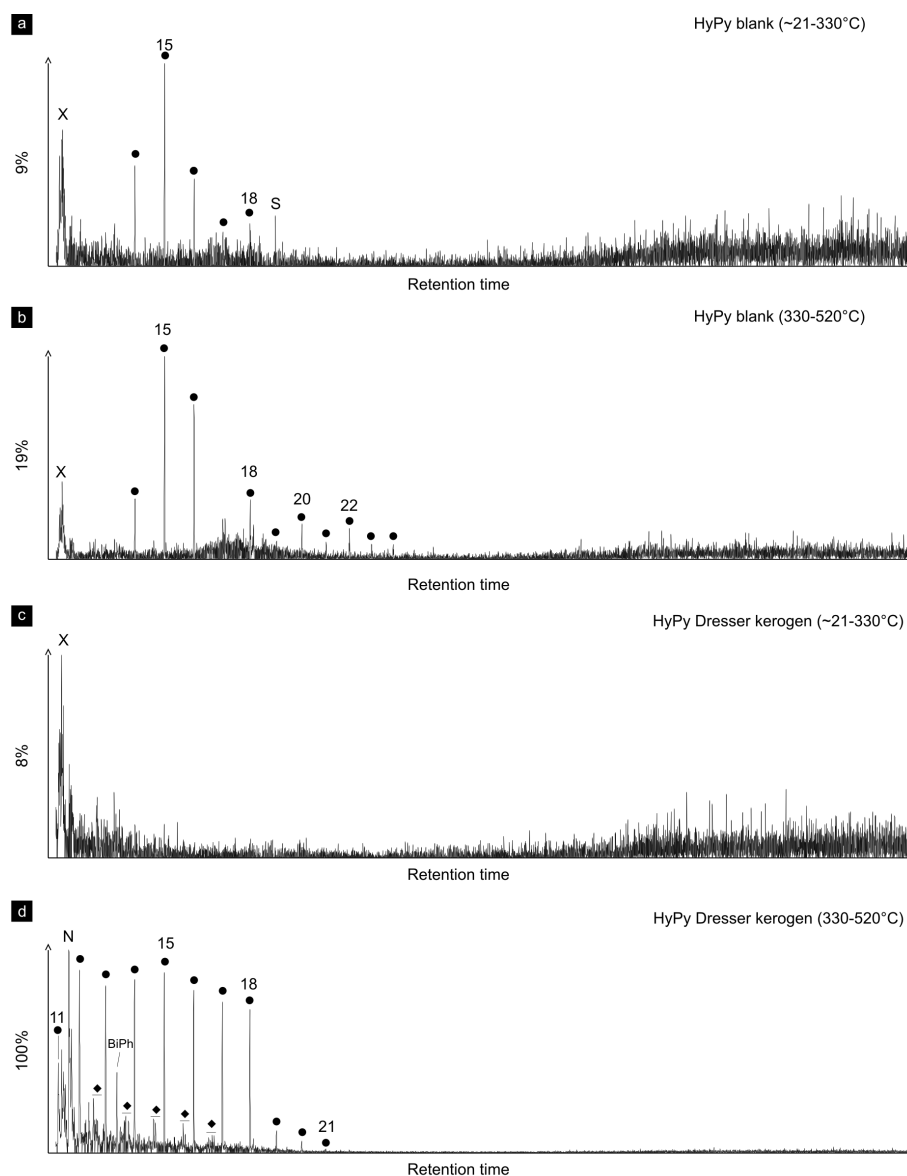
Figure B.7: Ion chromatograms selective for branched alkanes with quaternary carbon centres (BAQCs; *m/z* 127). Low-temperature (**a**) and high-temperature (**b**) HyPy products of the analytical blank (combusted sea sand) obtained prior to HyPy of the Dresser kerogen. Low-temperature (**c**) and high-temperature (**d**) HyPy products of the Dresser kerogen. Compounds detected in (**a − c**) represent background contamination and/or artefacts. Note the absence of BAQCs in all pyrolysates. Black dots: *n*-alkanes (numbers refer to carbon chain-lengths); diamonds: monomethylalkanes; N: naphthalene; BiPh: 1,1'-biphenyl; crosses: siloxanes (GC column or septum bleeding); S: elemental sulphur (likely derived from the sulfidic catalyst).
Note: Percentage values given on the vertical axes of chromatograms (**a − c**) relate peak intensities to chromatogram (**d**) (HyPy Dresser kerogen, 330 − 520 °C).

Figure B.8: Ion chromatograms selective for hopanes (*m/z* 191). Low-temperature (**a**) and high-temperature (**b**) HyPy products of the analytical blank (combusted sea sand) obtained prior to HyPy of the Dresser kerogen. Low-temperature (**c**) and high-temperature (**d**) HyPy products of the Dresser kerogen. All compounds in (**a–d**) represent background contamination and/or artefacts. Note the absence of hopanes in all pyrolysates. Crosses: siloxanes (GC column or septum bleeding); squares: phenols.

Note: Percentage values given on the vertical axes of chromatograms (**c – d**) relate peak intensities to chromatogram (**a**) (HyPy blank, ~ 21 – 330 °C).

Figure B.9: Ion chromatograms selective for steranes (*m/z* 217). Low-temperature (**a**) and high-temperature (**b**) HyPy chromatograms of the analytical blank (combusted sea sand) obtained prior to HyPy of the Dresser kerogen. Low-temperature (**c**) and high-temperature (**d**) HyPy products of the Dresser kerogen. Note the absence of steranes in all chromatograms.
Note: Percentage values given on the vertical axes of chromatograms (**a – c**) relate peak intensities to chromatogram (**d**) (HyPy Dresser kerogen, 330 – 520 °C).
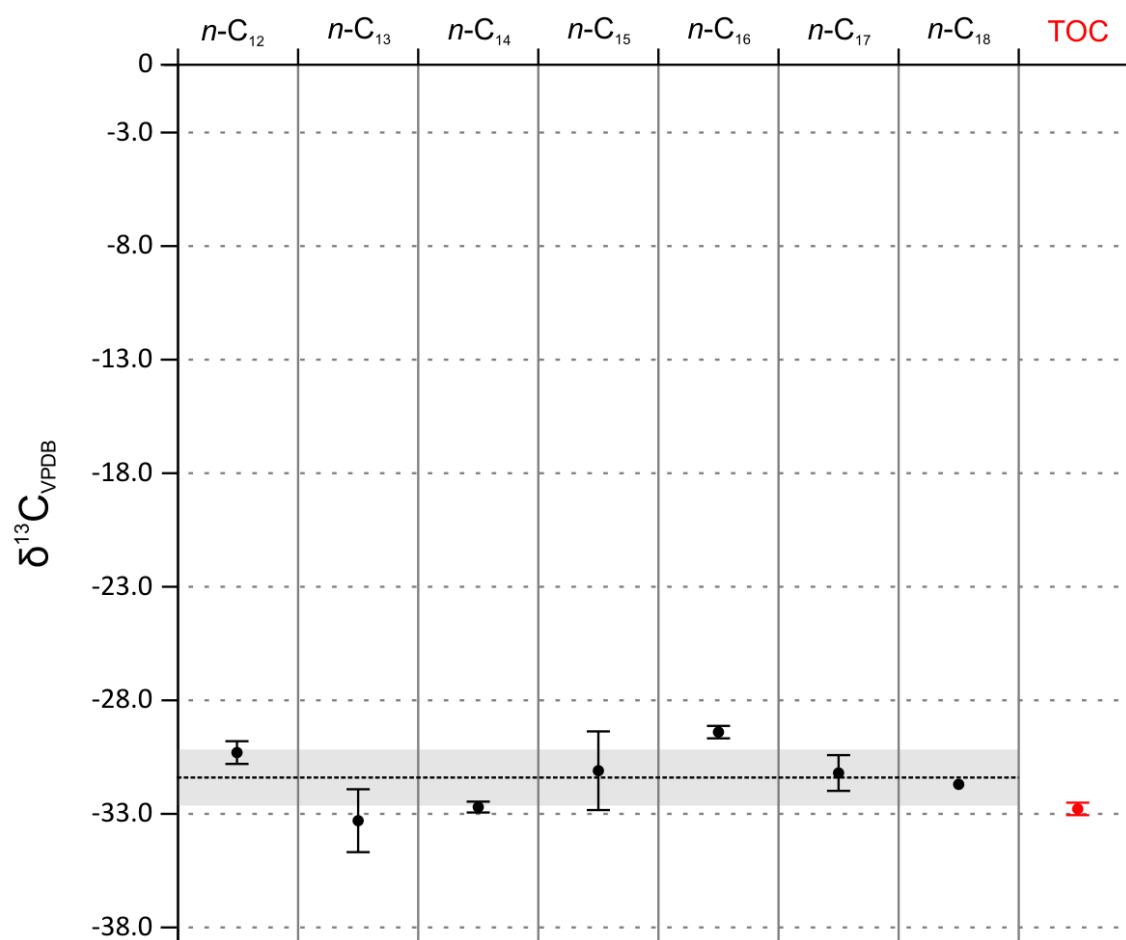
Figure B.10: Stable carbon isotope values (δ^{13}C) of *n*-alkanes released upon high-temperature HyPy and the total organic carbon (TOC). The isotopic similarity indicates that the *n*-alkanes (black dots) were generated from the kerogen (TOC, red dot). Vertical lines: Standard deviations of δ^{13}C values; dotted horizontal line: mean δ^{13}C value of *n*-alkanes (-31.4 ‰); shaded area: standard deviation of mean δ^{13}C value of *n*-alkanes (± 1.2 ‰).

Appendix C

Supplementary material

Investigating the effect of perchlorate on flight-like gas chromatography–mass spectrometry as performed by MOMA onboard the ExoMars 2020 rover
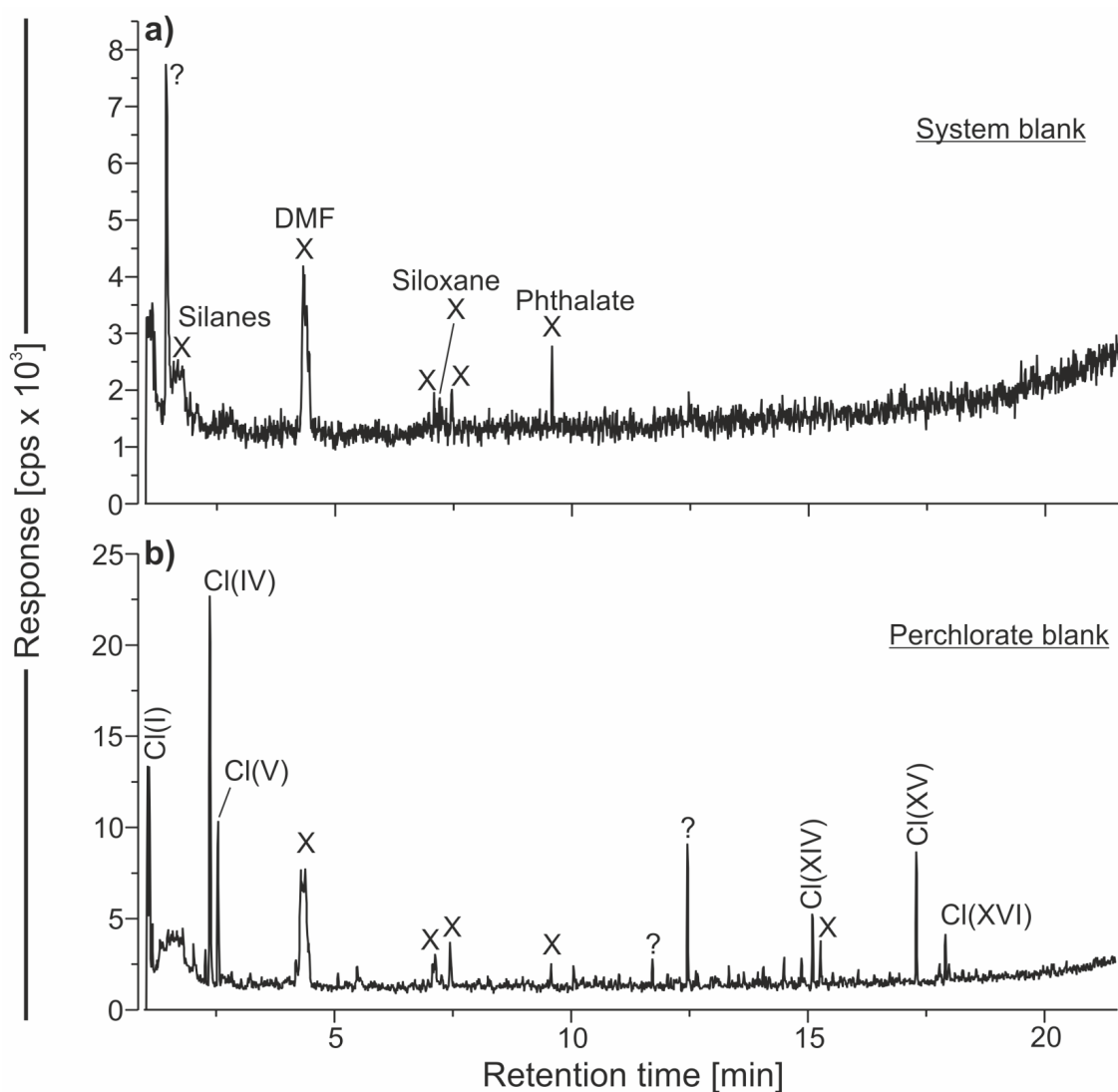
Figure C.1: GC–MS chromatograms (total ion current) of blank analysis (conducted in pyrolysis mode). (**a**) is showing the system blank without any sample (after cleaning), (**b**) is showing the perchlorate blank (SiO_2 with circa 5 wt% perchlorate). X signs indicate contamination. Signatures with roman numerals denote chlorinated compounds given in table C.1. cps, counts per second; DMF, N,N-dimethylformamide.

Table C.1: Aromatic hydrocarbons, chlorinated and N-bearing compounds from MOMA-like pyrolysis and in situ derivatization/thermochemolysis.

Peak label	Compound	Chemical formula
Aromatic hydrocarbons		
A(I)	Benzene	C_6H_6
A(II)	Toluene	C_7H_8
A(III)	Xylenes	C_8H_{10}
A(IV)	Trimethylbenzenes	C_9H_{12}
A(V)	1-Ethynyl-4-methyl-benzene	C_9H_8
A(VI)	Naphthalene	$C_{10}H_8$
A(VII)	Methylnaphthalenes	$C_{11}H_{10}$
A(VIII)	Dimethylnaphthalenes	$C_{12}H_{12}$
A(IX)	Acenaphthylene	$C_{12}H_8$
A(X)	Fluorene	$C_{13}H_{10}$
A(XI)	Phenanthrene	$C_{14}H_{10}$
Chlorinated compounds		
Cl(I)	Chloroethene	C_2H_3Cl
Cl(II)	Dichloromethane	CH_2Cl_2
Cl(III)	Trichloromethane	$CHCl_3$
Cl(IV)	Carbon tetrachloride	CCl_4
Cl(V)	Trichloroacetonitrile	C_2Cl_3N
Cl(VI)	Trichloroethylene	C_2HCl_3
Cl(VII)	Chloral hydrate	$C_2H_3Cl_3O_2$
Cl(VIII)	Tetrachloroethylene	C_2Cl_4
Cl(IX)	Chlorobenzene	C_6H_5Cl
Cl(X)	Benzoyl chloride	C_7H_5ClO
Cl(XI)	Chloroniconitrile	$C_6H_3ClN_2$
Cl(XII)	Trichlorobenzenes	$C_6H_3Cl_3$
Cl(XIII)	Tetrachlorobenzenes	$C_6H_2Cl_4$
Cl(XIV)	Pentachlorobenzene	C_6HCl_5
Cl(XV)	Hexachlorobenzene	C_6Cl_6
Cl(XVI)	Pentachlorobenzonitrile	C_7Cl_5N
N-bearing compounds		
N(I)	Benzonitrile	C_7H_5N
N(II)	Pyridinecarbonitrile	$C_6H_4N_2$
N(III)	1,5-Dicyano-2,4-dimethyl-2,4-diazapentane	$C_7H_{12}N_4$
N(IV)	Dimethylpyrazine	$C_6H_8N_2$
N(V)	1,3-Dimethyl-2,4,5-trioxoimidazolidine	$C_5H_6N_2O_3$
N(VI)	Naphthalenecarbonitrile	$C_{11}H_7N$
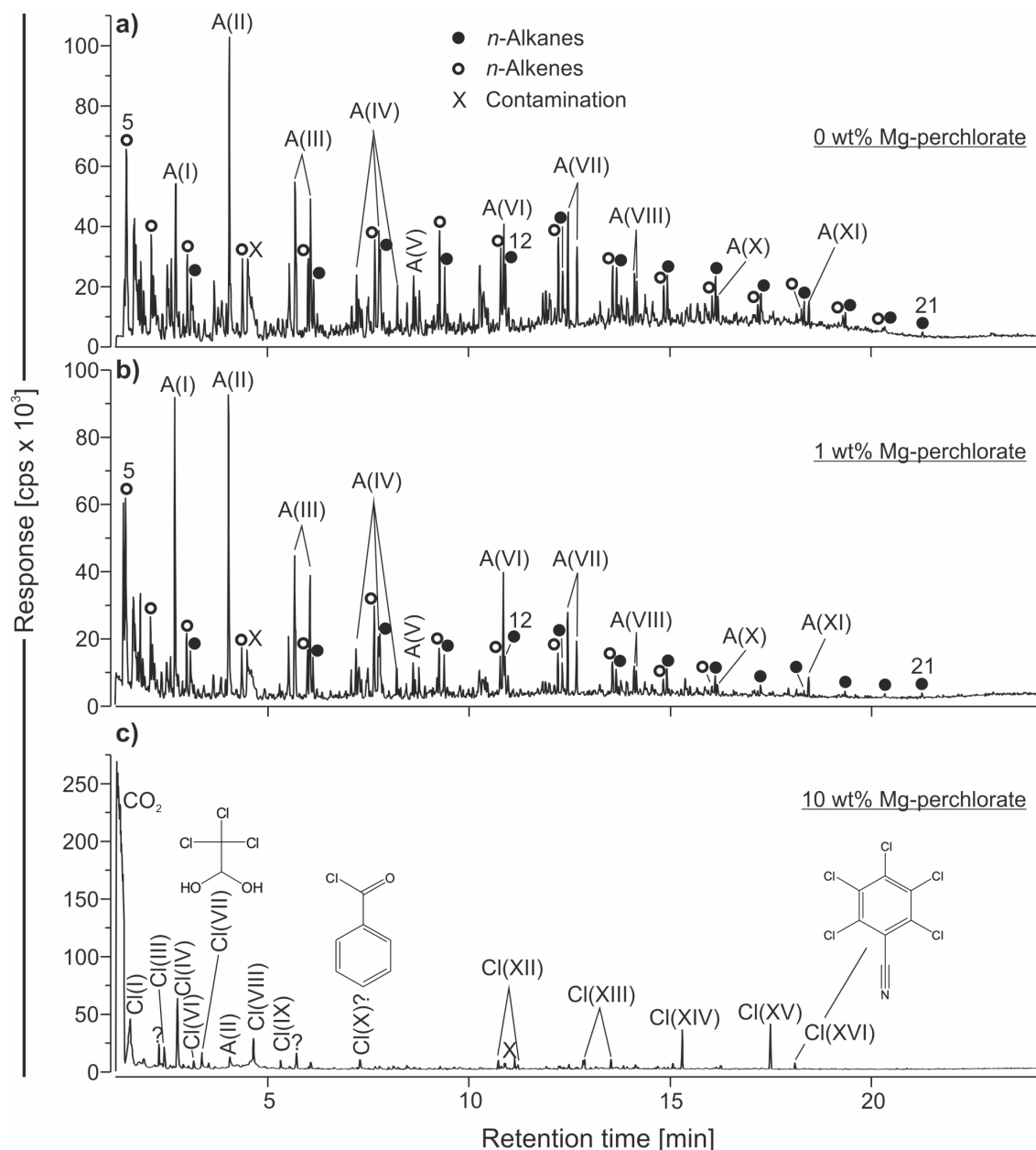
Figure C.2: GC–MS chromatograms (total ion current) of the pyrolysis analysis of the black chert with (**a**) 0 wt% Mg-perchlorate, (**b**) 1 wt% Mg-perchlorate and (**c**) 10 wt% Mg-perchlorate. Numbers indicate the carbon chain lengths of corresponding *n*-alkenes/*n*-alkanes. Signatures with roman numerals denote aromatic and chlorinated compounds given in table C.1. Note that degradation of organic compounds and formation of chlorinated species increase (**a** – **c**). cps, counts per second.
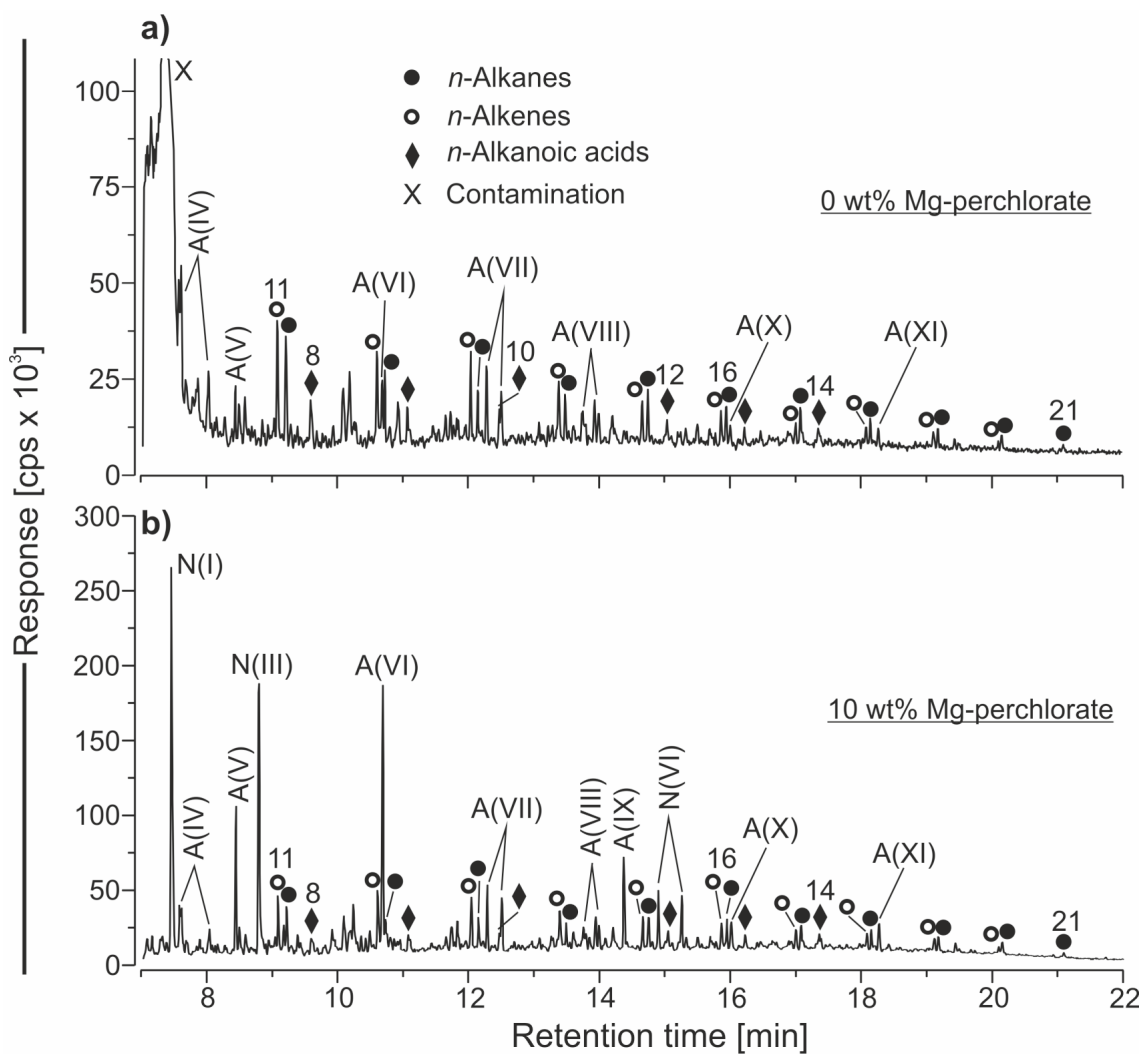
Figure C.3: GC–MS chromatograms (total ion current) of the in situ thermochemolysis with TMAH of the black chert with (**a**) 0 wt% Mg-perchlorate and (**b**) 10 wt% Mg-perchlorate. *n*-Alkanoic acids were analyzed as their methyl esters. Numbers indicate the carbon chain lengths of corresponding *n*-alkanoic acids and *n*-alkenes/*n*-alkanes. Signatures with roman numerals denote chlorinated and nitrogen-bearing compounds given in table C.1. Note that all compounds from (**a**) are still clearly identifiable in (**b**). cps, counts per second.

Appendix D

Experimental maturation of solvent extractable Fischer–Tropsch-type reaction products and a standard mix

Data presented here were obtained during a series of maturation experiments which are part of an ongoing study. Some objectives of this study are:

- To test whether or not thermal alteration of solvent extractable organics derived from Fischer–Tropsch-type (FTT) synthesis leads to formation of a kerogen-like material (see also Chapter 3)

- To determine the steadiness of abiotic n-alkane distribution patterns during experimental maturation

- To assess the preservation potential of functional organic molecules (e.g., n-alkanols and n-alkanoic acids) upon thermal stress

Samples and experimental procedure

Solvent extractable organic material from FTT synthesis (Chapter 3) and a standard mix containing n-$C_{11}-n$-C_{13} alkan-1-ols, n-C_{11} and n-C_{12} alkan-2-ols and n-$C_{11}-n$-C_{13} alkanoic acids (see also Chapter 6) were used for the experiments. Both were dissolved in dichloromethane (DCM).

40 μL of DCM solution containing either FTT synthesis derived organics or the standard mix were placed in a gold capsule (2.6 mm inner diameter, 15 mm length). The solvent was completely evaporated for ~ 3 h at room temperature and 40 μL ultraclean water were added. The capsule was closed using a Lampert™ tungsten inert gas impulse micro welding device. Experimental maturation was conducted at 300 °C and 2 kbar for time periods between 24 h and 4800 h. For details on the maturation procedure see also Chapter 2.

After the maturation, capsules were opened and extracted with DCM (4x, ultrasonication). Na_2SO_4 was added to the DCM extracts to withdraw remaining water. The extracts were derivatized with trimethylchlorosilane/N,O-bis(trimethylsilyl)trifluoroacetamide (TMCS/BSTFA, 0.5/9.5, V/V, Sigma Aldrich/Supelco) and analyzed by gas chromatography–mass spectrometry (GC–MS) as described in Section 3.2.

Summary of preliminary results

- presence of kerogen-like material was not yet observed

- n-alkane distribution patterns remained largely unchanged throughout thermal alteration periods (Fig. D.1)

- short-chain n-alkanols ($< C_{16}$) were quickly degraded while long chain moieties were partially preserved ≥ 240 h (Figs. D.2 and D.3)

- n-alkanoic acids ($\leq C_{13}$) were preserved for 2400 h (Figs. D.2 and D.3)
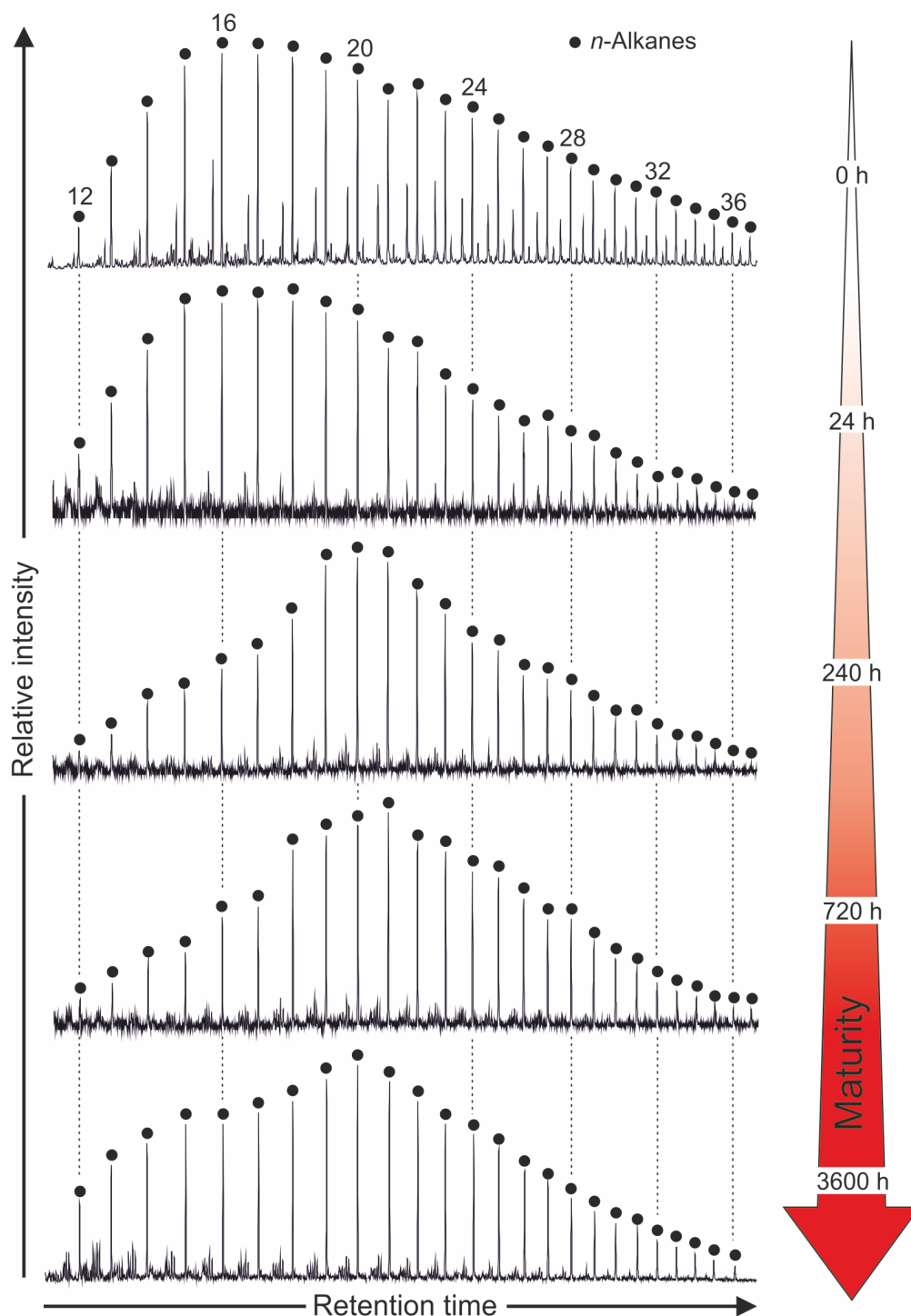
Figure D.1: Mass chromatograms (*m/z* 85, *n*-alkanes) of untreated (0 h, **a**) and experimentally maturated solvent extracted Fischer–Tropsch-type reaction products (24 h – 3600 h at 300 °C, **b** – **e**). Low abundances of *n*-alkanes at low retention times are at least partly due to evaporation loss during preparation. Note that the distribution patterns of *n*-alkanes remain largely unchanged during thermal maturation.
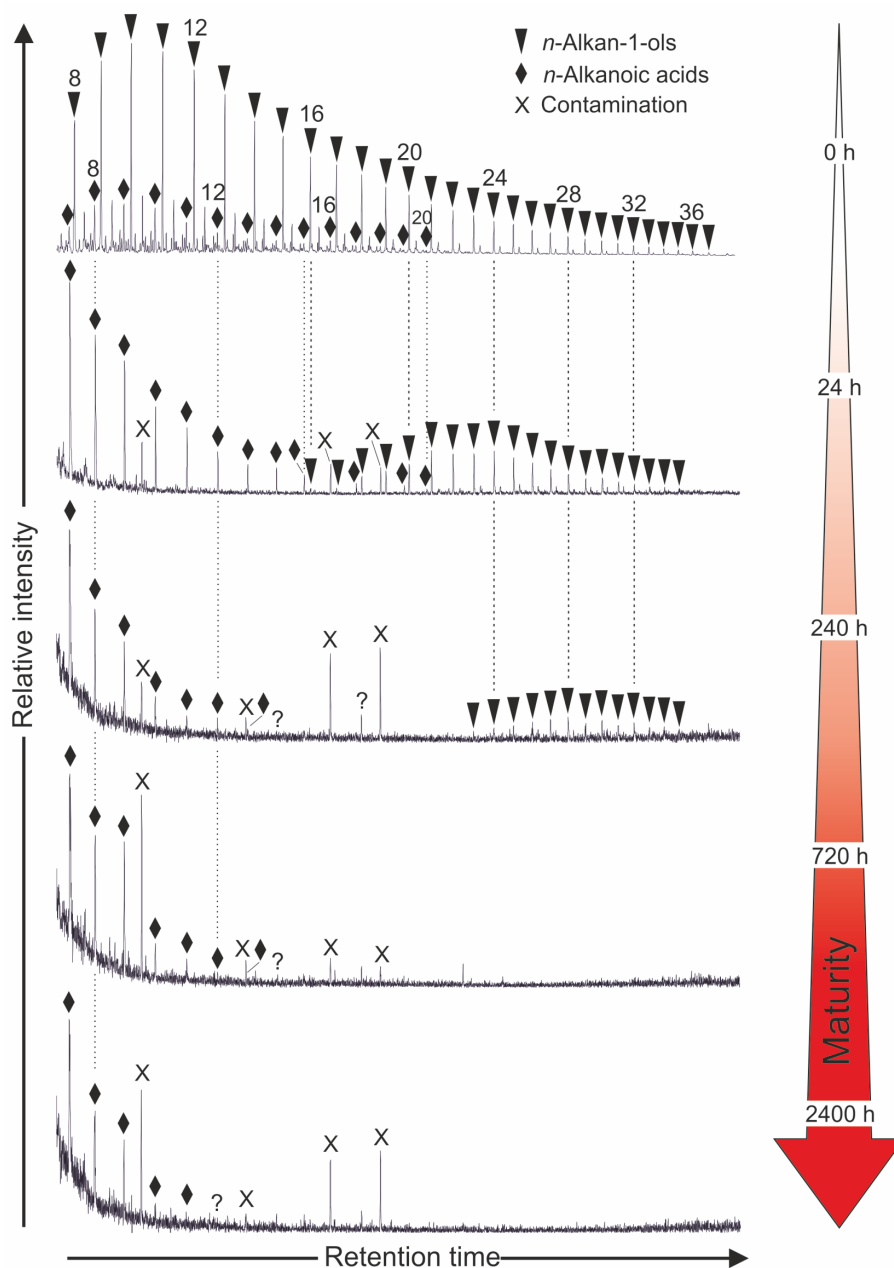
Figure D.2: Mass chromatograms (*m/z* 75) of untreated (0 h, **a**) and experimentally maturated solvent extracted Fischer–Tropsch-type reaction products (24 h – 2400 h at 300 °C, **b** – **e**). High abundances of *n*-C_{16} and *n*-C_{18} alkanoic acids are due to contamination from TMCS derivatization reagent. Note that *n*-alkanols $< C_{16}$ are more quickly degraded (< 24 h) than long chain moieties ($C_{16} - C_{33}$; > 24 h). Furthermore, *n*-Alkanoic acids $\leq C_{11}$ are preserved for 2400 h.
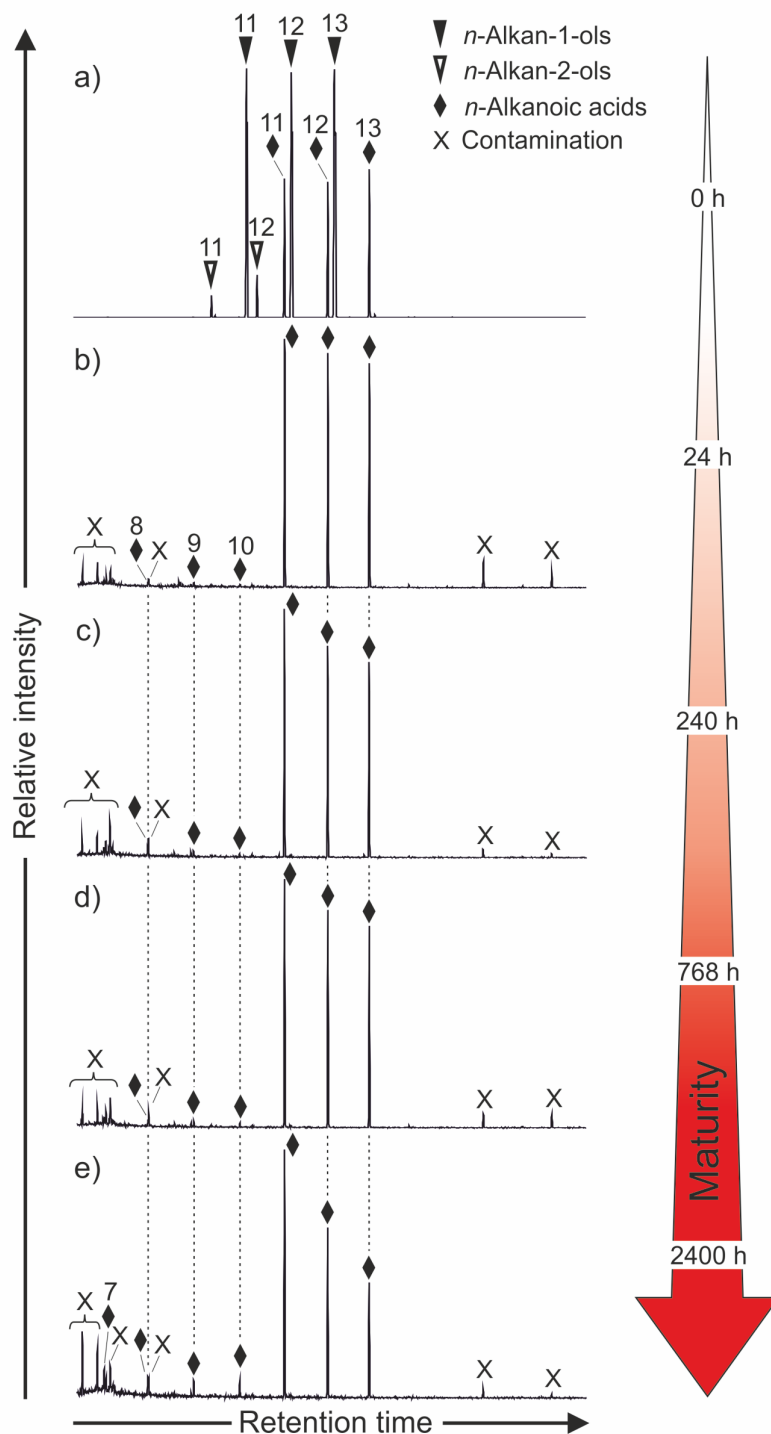
Figure D.3: Mass chromatograms (*m/z* 75) of untreated (0 h, **a**) and experimentally maturated (24 h – 2400 h at 300 °C, **b** – **e**) C_{11} – C_{13} *n*-alkan-1-ols, C_{11} – C_{12} *n*-alkan-2-ols and C_{11} – C_{13} *n*-alkanoic acids. Note that *n*-alkan-1-ols and *n*-alkan-2-ols are degraded in < 24 h. C_{11} – C_{13} *n*-alkanoic acids were preserved for 2400 h. Furthermore, < C_{11} *n*-alkanoic acid moieties were detected in maturation products.

Acknowledgements

Curriculum Vitae

Helge Mißbach
Date of birth: 10.10.1988
Place of birth: Salzgitter

Education

2015 – present   **Doctoral student** Geosciences, International Max Planck Research School for Solar System Science at the Max Planck Institute for Solar System Research, Georg-August-Universität Göttingen
Supervisors: Prof. Dr. Volker Thiel, PD Dr. Walter Goetz, Dr. Burkhard Schmidt

2012 – 2015   **Graduate student** (M.Sc. with honors) Geosciences, Georg-August-Universität Göttingen
Master's thesis: "Hydrochemistry and geomicrobiology of subterranean mine waters in the Kilianstollen near Marsberg" (written in German).
Supervisors: PD Dr. Gernot Arp, Dr. Andreas Reimer

2008 – 2012   **Undergraduate student** (B.Sc.) Geosciences, Georg-August-Universität Göttingen
Bachelor's thesis: "Stratigraphy and facies analysis of the Jena-Formation (Triassic, Anisian) in the Hildesheimer Wald exemplified by the Paßeiche stone pit" (written in German).
Supervisors: PD Dr. Frank Wiese, PD Dr. Gernot Arp

Grants and scholarships

2017   **Travel grant** (Göttingen International)

2016   **Travel grant** (SPP 1833 "Building a habitable earth"; University of Cologne)

2015   **PhD scholarship** (3 years; International Max Planck Research School for Solar System Science)

Invited Talks

2015   Working Group "Origin of Life", Göttingen Academy of Sciences and Humanities, Germany. Topic: "Formation and characterization of abiogenic vs. biogenic organic material"

Publications and conference contributions

Peer-reviewed journal articles (corresponding author marked with *)

Mißbach, H.*, Schmidt, B.C., Duda, J.-P., Lünsdorf, N.K., Goetz, W., Thiel, V. (2018). Assessing the diversity of lipids formed via Fischer–Tropsch-type reactions. *Organic Geochemistry* 119, 110–121.

Duda, J-P.*, Thiel, V., Bauersachs, T., Mißbach, H., Reinhardt, M., Schäfer, N., Van Kranendonk, M.J., Reitner, J. (2018). Ideas and perspectives: hydrothermally driven redistribution and sequestration of early Archaean biomass – the "hydrothermal pump hypothesis". *Biogeosciences* 15, 5, 1535–1548.

Goesmann, F., Brinckerhoff, W.B., Raulin, F., Goetz, W.*, Danell, R.M., Getty, S.A., Siljeström, S., Mißbach, H. et al. (2017) The Mars Organic Molecule Analyzer (MOMA) Instrument: Characterization of Organic Material in Martian Sediments. *Astrobiology* 17, 6–7, 655–685.

Mißbach, H.*, Duda, J.-P., Lünsdorf, N.K., Schmidt, B.C., Thiel, V. (2016). Testing the preservation of biomarkers during experimental maturation of an immature kerogen. *International Journal of Astrobiology* 15, 3, 165–175.

Conference contributions (own presentations only)

Mißbach, H., Duda, J.-P., Schmidt, B.C., Goetz, W., Lünsdorf, N.K., Thiel, V. (2017). Assessing the effects of thermal maturation on biogenic and abiogenic organic material. *28th International Meeting on Organic Geochemistry, Florence, Italy*. [Poster Presentation]

Mißbach, H., Duda, J.-P., Schmidt, B.C., Lünsdorf, N.K., Goetz, W., Reitner, J., Thiel, V. (2017). The fate of biogenic vs. abiogenic organic matter during thermal maturation. *SPP 1833 "Building a habitable Earth" General Meeting*, Jena, Germany. [Talk]

Mißbach, H., Steininger, H., Thiel, V., Goetz, W. (2017). Characterization of Organic Compounds in Martian Sediments: A Case Study imitating MOMA Pyrolysis & Derivatization onboard the ExoMars Rover. *48th Lunar and Planetary Science Conference*, The Woodlands, Texas, USA. [Poster presentation]

Mißbach, H., Thiel, V., Goetz, W., Schmidt, B.C. (2016). The Fate of Biogenic vs. Abiogenic Organic Matter during Thermal Maturation. *35th International Geological Congress*, Cape Town, South Africa. [Poster presentation]